AD-A086 008 PENNSYLVANIA STATE UNIV UNIVERSITY PARK APPLIED RESE--ETC F/G 20/1
A STUDY OF THE NEARFIELD OF AN EXCITED SPHERICAL SHELL.(U)
MAR 80 E WONG N00024-79-C-6043
UNCLASSIFIED ARL/PSU/TM-80-30 NL

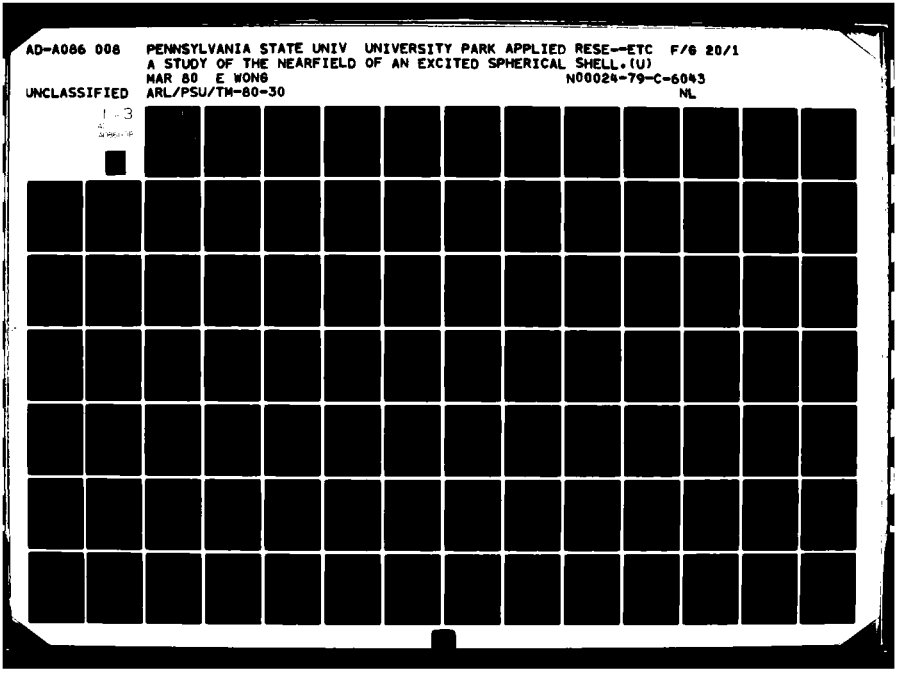

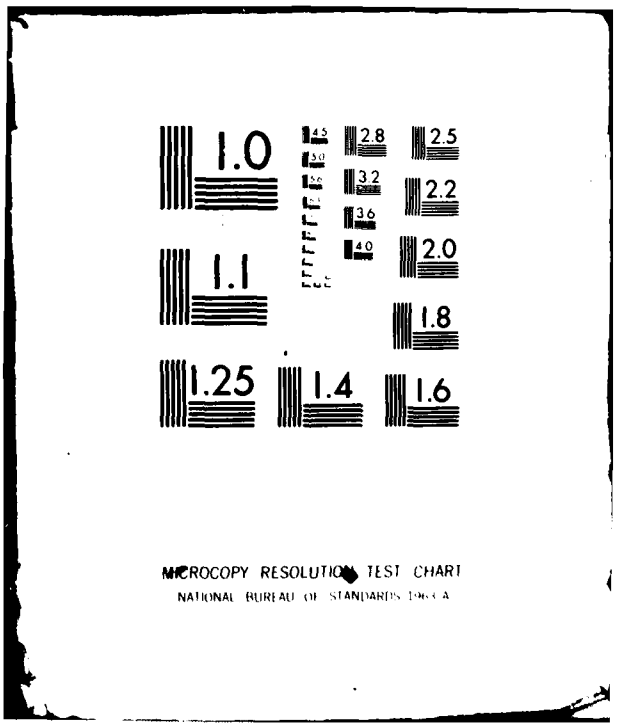
1.0
1.1
1.25
1.4
1.6
1.8
2.0
2.2
2.5
2.8
3.2
3.6
4.0
MICROCOPY RESOLUTION TEST CHART
NATIONAL BUREAU OF STANDARDS 1963 A

LEVEL II

12

A STUDY OF THE NEARFIELD OF AN EXCITED SPHERICAL SHELL

Edmond Wong

AD A086008

Technical Memorandum
File No. TM 80-30
March 17, 1980
Contract No. N00024-79-C-6043

Copy No. 5

DTIC
ELECTE
JUN 27 1980
S
D
C

The Pennsylvania State University
Institute for Science and Engineering
APPLIED RESEARCH LABORATORY
Post Office Box 30
State College, PA 16801

APPROVED FOR PUBLIC RELEASE
DISTRIBUTION UNLIMITED

DDC FILE COPY

NAVY DEPARTMENT

NAVAL SEA SYSTEMS COMMAND

80 6 26 033

(14) ARL/PSU/TM-80-30 (Doctoral thesis)

~~UNCLASSIFIED~~

SECURITY CLASSIFICATION OF THIS PAGE *(When Data Entered)*

REPORT DOCUMENTATION PAGE

READ INSTRUCTIONS BEFORE COMPLETING FORM

1. REPORT NUMBER: TM 80-30	2. GOVT ACCESSION NO.: AD-A086 008
3. RECIPIENT'S CATALOG NUMBER:	
4. TITLE *(and Subtitle)*: (6) A STUDY OF THE NEARFIELD OF AN EXCITED SPHERICAL SHELL	5. TYPE OF REPORT & PERIOD COVERED: PhD Thesis, May 1980
	6. PERFORMING ORG. REPORT NUMBER: TM 80-30
7. AUTHOR(s): (10) Edmond Wong	8. CONTRACT OR GRANT NUMBER(s): (15) N00024-79-C-6043
9. PERFORMING ORGANIZATION NAME AND ADDRESS: The Pennsylvania State University, Applied Research Laboratory, P. O. Box 30, State College, PA 16801	10. PROGRAM ELEMENT, PROJECT, TASK AREA & WORK UNIT NUMBERS: (11) 17 Mar
11. CONTROLLING OFFICE NAME AND ADDRESS: Naval Sea Systems Command, Department of the Navy, Washington, DC 20362 (12)	12. REPORT DATE: March 17, 1980
	13. NUMBER OF PAGES: 232 pages & figures
14. MONITORING AGENCY NAME & ADDRESS *(if different from Controlling Office)*	15. SECURITY CLASS. *(of this report)*: Unclassified, Unlimited
	15a. DECLASSIFICATION/DOWNGRADING SCHEDULE

16. DISTRIBUTION STATEMENT *(of this Report)*

Approved for public release, distribution unlimited, per NSSC (Naval Sea Systems Command), 4/9/80

17. DISTRIBUTION STATEMENT *(of the abstract entered in Block 20, if different from Report)*

18. SUPPLEMENTARY NOTES

19. KEY WORDS *(Continue on reverse side if necessary and identify by block number)*

acoustic, nearfield, spherical, shells, thesis

20. ABSTRACT *(Continue on reverse side if necessary and identify by block number)*

In this study, the acoustic near field of excited spherical shells is investigated. The interaction of the acoustic medium with the vibration response of an elastic spherical shell due to an excitation by a point force or an acoustic point source is investigated analytically and experimentally. Thus, only axisymmetric, nontorsional motion of the spherical sehll is considered, with a thin shell theory that includes extensional and bending deformation.

The elastic spherical sehll resonances were computed when in vacuo and when

DD FORM 1 JAN 73 1473 EDITION OF 1 NOV 65 IS OBSOLETE S/N 0102-LF-014-6601

UNCLASSIFIED

SECURITY CLASSIFICATION OF THIS PAGE *(When Data Entered)*

3/1(C)

20 ABSTRACT (continued)

submerged in light (air) and heavy (water) acoustic medium. These were verified experimentally by testing two duralumin shells, a = 8 inches in radius and wall thicknesses h = 0.0514 and 0.1069 inch. The measured resonance frequencies were within 5% of those predicted in air and in water for identified mode numbers up to 34. The measured mean-line driving point admittance also agreed well with the predicted ones to within 3 dB.

Also in this study, the exact wave harmonic series and the approximate Geometrical Theory of Diffraction (GTD) were used to predict the acoustic near field of an elastic spherical shell insonified by an acoustic point source. The predicted normalized, acoustic nearfield pressure computed by the exact solution agreed very well with the measured ones for frequencies up to ka = 30 . The nearfield acoustic pressure was also computed by the GTD method with a locally reacting impedance assumed for the spherical surface. The decayed diffracted rays were then computed and summed to give the total diffracted pressure spectra in the shadow zone. Various surface impedances were assumed and the resulting nearfield pressure was compared to the exact solution. The GTD solutions were generally 60 dB or more lower than the exact ones, even when one assumes the fairly hard characteristic impedance of duralumin to represent the impedance of the shell. The source of the discrepancy was traced to the structure-borne resonant vibration which is not accounted for in the GTD. This means that the predicted acoustic near field of general elastic structures as computed by the GTD method will not agree with the exact solution for such structures.

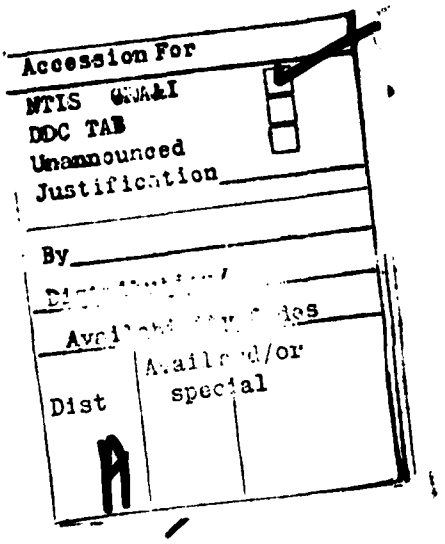

ABSTRACT

In this study, the acoustic near field of excited spherical shells is investigated. The interaction of the acoustic medium with the vibration response of an elastic spherical shell due to an excitation by a point force or an acoustic point source is investigated analytically and experimentally. Thus, only axisymmetric, nontorsional motion of the spherical shell is considered, with a thin shell theory that includes extensional and bending deformation.

The elastic spherical shell resonances were computed when in vacuo and when submerged in light (air) and heavy (water) acoustic medium. These were verified experimentally by testing two duralumin shells, a = 8 inches in radius and wall thicknesses h = 0.0514 and 0.1069 inch. The measured resonance frequencies were within 5% of those predicted in air and in water for identified mode numbers up to 34. The measured mean-line driving point admittance also agreed well with the predicted ones to within 3 dB.

Also in this study, the exact wave harmonic series and the approximate Geometrical Theory of Diffraction (GTD) were used to predict the acoustic near field of an elastic spherical shell insonified by an acoustic point source. The predicted normalized, acoustic nearfield pressure computed by the exact solution agreed very well with the measured ones for frequencies up to $ka = 30$. The nearfield acoustic pressure was also computed by the GTD method with a locally reacting impedance assumed for the spherical surface. The decayed diffracted rays were then computed and summed to give the

total diffracted pressure spectra in the shadow zone. Various surface impedances were assumed and the resulting nearfield pressure was compared to the exact solution. The GTD solutions were generally 60 dB or more lower than the exact ones, even when one assumes the fairly hard characteristic impedance of duralumin to represent the impedance of the shell. The source of the discrepancy was traced to the structure-borne resonant vibration which is not accounted for in the GTD. This means that the predicted acoustic near field of general elastic structures as computed by the GTD method will not agree with the exact solution for such structures.

TABLE OF CONTENTS

	Page
ABSTRACT	iii
LIST OF TABLES	vii
LIST OF FIGURES	ix
LIST OF SYMBOLS	xv
ACKNOWLEDGEMENTS	xix
I. BACKGROUND	1
1.1 Introduction	1
1.2 Statement of the Problem to be Studied and the Mathematical Model	2
II. FORMULATION OF THE THIN SPHERICAL SHELL'S EQUATION OF MOTION	7
2.1 Introduction	7
2.2 The Equations of Motion	8
2.3 The Natural Frequency, the Mechanical Impedance, and the Ratio U_n/W_n of the Shell in Vacuo	16
2.4 The Derivation of the Equations of Motion of a Spherical Shell in Terms of Generalized Coordinates	27
2.5 The Resonance Density of Spherical Shell	47
III. POINT FORCE AND SOURCE EXCITATION OF A SPHERICAL SHELL	55
3.1 Introduction	55
3.2 The Point Excited Vibration of a Shell	55
3.2.1 Numerical Analysis	58
3.3 A Spherical Thin Shell Insonified by an Acoustic Spherical Wave in a Fluid Medium	94
IV. THE GEOMETRICAL THEORY OF DIFFRACTION (GTD)	118
4.1 Introduction	118
4.2 The Watson Transformation	119
4.3 The Computation Method and Numerical Analysis	133
4.3.1 The Method of Computation	133
4.3.2 Numerical Analysis	136

TABLE OF CONTENTS (continued)

		Page
V.	EXPERIMENT	142
	5.1 Introduction	142
	5.2 General Experiment Approach	143
	5.3 Experimental Equipment	144
	5.4 Measurement of the Resonance Frequencies	148
	5.4.1 Measurements in Air	148
	5.4.2 Measurements in Water	149
	5.5 Measurement of the Directivity Pattern	151
	5.5.1 Measurement in Water	151
	5.5.2 Measurements in Air	152
	5.6 The Results of the Measurement of Resonance Frequency	155
	5.7 Measured Frequency Spectra of the Shell's Response	170
	5.8 The Results of the Directivity Pressure Field Measurement	170
VI.	SUMMARY AND CONCLUSIONS	193
	6.1 Introduction	193
	6.2 Point Excited Spherical Shells	194
	6.3 Acoustic Nearfield of a Point-Source Excited Spherical Shell	195
	6.4 Conclusions	196
	6.5 Suggested Future Research	197
REFERENCES		198
BIBLIOGRAPHY		201
APPENDIX A.	Derivation of the Shell's Equations of Motion	205
APPENDIX B.	Derivation of the Diffraction Factor	210

LIST OF TABLES

Table		Page
2.1	Resonance frequencies of a spherical duralumin membrane shell with thickness h = 0.1069" and radius a = 8" in vacuo - membrane theory	18
2.2	Resonance frequencies of a spherical duralumin classical shell with thickness h = 0.0514" and radius a = 8" in vacuo - classical theory	20
2.3	Resonance frequencies of a spherical duralumin classical shell with thickness h = 0.1069" and radius a = 8" in vacuo - classical theory	22
2.4	Resonance frequencies of a spherical duralumin classical shell with thickness h = 0.0514" and radius a = 8" in air - classical theory	35
2.5	Resonance frequencies of a spherical duralumin classical shell with thickness h = 0.1069" and radius a = 8" in air - classical theory	37
2.6	Resonance frequencies of a spherical duralumin classical shell with thickness h = 0.0514" and radius a = 8" in water	42
2.7	Resonance frequencies of a spherical duralumin classical shell with thickness h = 0.1069" and radius a = 8" in water	44
3.1	Physical properties of a spherical duralumin shell and acoustic media	59
3.2	Modal resonance impedance of a spherical duralumin shell with thickness h = 0.0514" in air for $\eta_E = 0$	61
3.3	Modal resonance impedance of a spherical duralumin shell with thickness h = 0.1069" in air for $\eta_E = 0$	62
3.4	Modal resonance impedance of a spherical duralumin shell with thickness h = 0.0514" in water for $\eta_E = 0$	63
3.5	Modal resonance impedance of a spherical duralumin shell with thickness h = 0.1069" in water for $\eta_E = 0$	65

LIST OF TABLES (continued)

Table		Page
3.6	Modal resonance impedance of a spherical duralumin shell with thickness h = 0.0514" in air for η_E = 0.0006	67
3.7	Modal resonance impedance of a spherical duralumin shell with thickness h = 0.1069" in air for η_E = 0.0006	68
3.8	Modal resonance impedance of a spherical duralumin shell with thickness h = 0.1069" in water for η_E = 0.0006	69
3.9	Modal resonance impedance of a spherical duralumin shell with thickness h = 0.1069" in water for η_E = 0.0006	71
5.1	Measured (f'_n) and calculated (f_n) resonance frequencies of a spherical shell (h = 0.0514") submerged in air and water	161
5.2	Measured (f'_n) and calculated (f_n) resonance frequencies of a spherical shell (h = 0.1069") submerged in air and water	162

LIST OF FIGURES

Figure		Page
1.1	Configuration of the spherical shell in the spherical coordinate system	5
2.1	Direction of the stresses σ_s acting on the middle surface of the shells. ρ_n , ρ_θ , ρ_ϕ are the orthogonal unit vectors	10
2.2	Orientation of the vectors of a spherical shell	12
2.3	Dimensionless frequency KA for various modes when spherical shells are excited in vacuo	24
2.4	Normalized acoustic resistance curves, Re $(Z_a)/\rho c$	33
2.5	Normalized acoustic reactance curves, IM $(Z_a)/\rho a$	34
2.6	Dimensionless frequency KA for various modes when spherical shells are submerged in air	39
2.7	Dimensionless frequency KA for various modes when spherical shells are submerged in water	40
2.8	Dimensionless frequency KA for various modes. Comparison of spherical shell in water with that in vacuo	46
2.9	Resonance density of a spherical shell, h = 0.1069", in vacuo	50
2.10	Resonance density of a spherical shell, h = 0.0514", in vacuo	51
2.11	Mean value of the driving point admittance of a spherical shell, h = 0.1069", in vacuo	53
3.1	Frequency response of modal mechanical resistance (r_{mn}), modal acoustic resistance (r_{an}), total modal resistance (r_n), and modal admittance (Y_{dn}) in air, normalized to $(\rho c)_{air}$	74
3.2	Frequency response of modal mechanical resistance (r_{mn}), modal acoustic resistance (r_{an}), total resistance (r_n), and modal admittance (Y_{dn}) in water, normalized to $(\rho c)_{water}$	76

LIST OF FIGURES (continued)

Figure		Page
3.3	DPA of a membrane shell with thickness h = 0.0514" in air	78
3.4	DPA of a membrane shell with thickness h = 0.1069" in air	79
3.5	DPA of a classical shell with thickness h = 0.0514" in air	80
3.6a	DPA of a classical shell with thickness h = 0.1069" in air, $0.01 \leq ka \leq 100$	81
3.6b	DPA of a classical shell with thickness h = 0.1069" in air, $10 \leq ka \leq 100$	82
3.7	DPA of a membrane shell with thickness h = 0.0514" in water	83
3.8	DPA of a membrane shell with thickness h = 0.1069" in water	84
3.9	DPA of a classical shell with thickness h = 0.0514" in water	85
3.10	DPA of a classical shell with thickness h = 0.1069" in water	86
3.11	Directivity pattern of a force excited classical shell with thickness h = 0.1069" for ka = 1.0307 , n = 2 in water	90
3.12	Directivity pattern of a force excited classical shell with thickness h = 0.1069" for ka = 10.659 , n = 2 in air	91
3.13	Directivity pattern of a force excited classical shell with thickness h = 0.1069" for ka = 15.745 , n = 4 in water	92
3.14	Directivity pattern of a force excited classical shell with thickness h = 0.1069" for ka = 14.886 , n = 29 in water	93
3.15	Frequency response of a membrane shell with thickness h = 0.1069" in air for r_o = 8.25" , r = 8.5" , and $\theta = 0°$	101

LIST OF FIGURES (continued)

Figure		Page
3.16	Frequency response of a classical shell with thickness h = 0.514" in air for r_o = 8.25", r = 8.5", and θ = 0°	102
3.17	Frequency response of a classical shell with thickness h = 0.1069" in air for r_o = 8.25", r = 8.5", and θ = 0°	103
3.18	Frequency response of a classical shell with thickness h = 0.0514" in water for r_o = 8.25", r = 8.5", and θ = 0°	104
3.19	Frequency response of a classical shell with thickness h = 0.1069" in water for r_o = 8.25", r = 8.5", and θ = 0°	105
3.20	Frequency response of a membrane shell with thickness h = 0.1069" in air for r_o = 8.25", r = 8.5", and θ = 180°	106
3.21	Frequency response of a classical shell with thickness h = 0.514" in air for r_o = 8.25", r = 8.5", and θ = 180°	108
3.22	Frequency response of a classical shell with thickness h = 0.1069" in air for r_o = 8.25", r = 8.5", and θ = 180°	109
3.23	Frequency response of a classical shell with thickness h = 0.0514" in water for r_o = 8.25", r = 8.5", and θ = 180°	110
3.24	Frequency response of a classical shell with thickness h = 0.1069" in water for r_o = 8.25", r = 8.5", and θ = 180°	111
3.25	Directivity pattern of a shell with thickness h = 0.1069" in air for n = 2	113
3.26	Directivity pattern of a shell with thickness h = 0.1069" in water for n = 2	114
3.27	Directivity pattern of a shell with thickness h = 0.1069" in air and water for ka = 0.2	115
3.28	Directivity pattern of a shell with thickness h = 0.1069" in air and water for ka = 14	117

LIST OF FIGURES (continued)

Figure		Page
4.1	Contour C's of integration in the complex s plane	121
4.2	Contour of the integral in Equation (4.6)	124
4.3	Frequency response of the pressure field of a GTD sphere in water for $r = 8.5"$, $r_o = 8.25"$, and $\theta = 180°$	138
4.4	Frequency response of the pressure field of a GTD sphere in water for $r = 8.5"$, $r_o = 8.25"$, and $\theta = 180°$	139
4.5	Frequency spectrum of an exact solution in water for $r = 8.5"$, $r_o = 8.25"$, and $\theta = 180°$	140
5.1	Geometrical configuration of a spherical shell and the location of its support system	146
5.2	Geometrical configuration of the holo-scanner	147
5.3	Operational set-up of the driving point inertance measurement	150
5.4	Set-up for measuring the sound directivity pattern in water	153
5.5	Set-up for measuring sound pressure in air	154
5.6	Set-up for measuring sound pressure in an anechoic chamber	156
5.7a	Measured driving point inertance of a duralumin spherical shell with thickness $h = 0.0514"$ in air	157
5.7b	Measured driving point inertance of a duralumin spherical shell with thickness $h = 0.0514"$ in air	158
5.8a	Measured driving point inertance of a duralumin spherical shell with thickness $h = 0.1069"$ in air	159
5.8b	Measured driving point inertance of a duralumin spherical shell with thickness $h = 0.1069"$ in air	160
5.9	Measured driving point inertance of a duralumin spherical shell with thickness $h = 0.0514"$ in water . . .	164
5.10	Measured driving point inertance of a duralumin spherical shell with thickness $h = 0.1069"$ in water . . .	165

LIST OF FIGURES (continued)

Figure		Page
5.11	Resonant frequencies of a duralumin spherical shell with thickness h = 0.0514" in air	166
5.12	Resonant frequencies of a duralumin spherical shell with thickness h = 0.1069" in air	167
5.13	Resonant frequencies of a duralumin spherical shell with thickness h = 0.0514" in water	168
5.14	Resonant frequencies of a duralumin spherical shell with thickness h = 0.1069" in water	169
5.15	Directivity pattern of a shell with thickness h = 0.1069" for ka = 4.4276 in water	171
5.16	Directivity pattern of a shell with thickness h = 0.1069" for ka = 8.398 in water	172
5.17	Directivity pattern of a shell with thickness h = 0.1069" for ka = 12.235 in water	173
5.18	Directivity pattern of a shell with thickness h = 0.1069" for ka = 22 in water	174
5.19	Directivity pattern of a shell with thickness h = 0.1069" for ka = 30 in water	175
5.20	2-D photographic experimental data of sound field near a shell with thickness h = 0.1069", insonified by a 1" diameter speaker for ka = 18 in air	177
5.21	3-D measured directivity pattern of a shell with thickness h = 0.1069" for ka = 18 in air	178
5.22	3-D predicted directivity pattern of a shell with thickness h = 0.1069" for ka = 18 in air	179
5.23	2-D measured directivity pattern of a shell with thickness h = 0.1069" for ka = 22 in air	181
5.24	3-D measured directivity pattern of a shell with thickness h = 0.1069" for ka = 22 in air	182
5.25	3-D predicted directivity pattern of a shell with thickness h = 0.1069" for ka = 22 in air	183
5.26	Measured phase pattern of a shell with thickness h = 0.1069" for ka = 6 in air	185

LIST OF FIGURES (continued)

Figure		Page
5.27	Measured phase pattern of a shell with thickness h = 0.1069" for ka = 10 in air	186
5.28	Measured phase pattern of a shell with thickness h = 0.1069" for ka = 14 in air	187
5.29	Measured phase pattern for a shell with thickness h = 0.1069" for ka = 18 in air	188
5.30	Measured phase pattern for a shell with thickness h = 0.1069" for ka = 22 in air	189
5.31	Measured phase pattern for a shell with thickness h = 0.1069" for ka = 26 in air	190
5.32	Measured phase pattern for a shell with thickness h = 0.1069" for ka = 30 in air	191

LIST OF SYMBOLS

a	radius of the spherical sehll
c	sound speed in the acoustic fluid
d	distance between the source and the receiver
h	thickness of the spherical shell
$h_n(x)[h_n^{(1)}(x)]$, $h_n^{(2)}(x)$	spherical Hankel function of the first and second kind and order n , respectively
$h'(x)$, $h_n^{(2)'}(x)$	derivative of spherical Hankel function with respect to the argument
i	$\sqrt{-1}$
j_n	spherical Bessel function of order n
k	wave number ω/c
ka	dimensionless frequency $\omega a/c$
p_i	*applied pressure*
p_d	pressure field of a submerged shell excited by a point force
p_h	rigid scattered pressure
p_r	radiated scattered or reactive pressure
p_s	scattered pressure
p	total pressure
q_n	roots of the Airy function
r,θ,ϕ	spherical coordinates
r	distance from the observer to the center of the spherical shell
r_o	distance from the source to the center of the spherical shell
r_{an}	acoustic resistance
r_{mn} (r_{sn})	mechanical resistance or structural resistance

t	time
u	tangential displacement
w	radial displacement
$\dot{u}$, $\dot{w}$	time derivative of u and w, respectively
$A(x)$	Airy function
$A'(x)$	derivative of $A(x)$ with respect to x
A_θ, A_ϕ	Lamé parameter
C_v	bar velocity
C_p	plate velocity
E	Young's modulus
E_n^{-1}	$= dn/d\Omega$, resonance density
$H_n^{(1)}(x)$, $H_n^{(2)}(x)$	cylindrical Hankel function of the first and second kind and order n, respectively
K_θ, K_ϕ	the changes in curvature due to bending of the deformed middle surface of a shell about the θ and ϕ coordinates, respectively
$K_{\theta\phi}$	parameter of torsional deformation
L_{an}	modal acoustic loss factor
L_{sn}	modal structural loss factor
$L_{uu}, L_{uw}, L_{wu}, L_{ww}$	differential operators
M	mass of the shell
M_{an}	fluid virtual mass
M_{mn}	mechanical reactance
M_n	modal mass of the shell
M_R	$= M_{an}/\bar{\mu}s_n$, mass loading factor
M_t	$= M_{an} + \bar{\mu}s_n$, total mass of the submerged shell
$P_n(\cos\theta)$	Legendre polynomial of degree n
Q	potential function

R_f	$= r_{a1} + r_{mn}$ resistance of the submerged shell
R_s	principal radius of curvature of the shell
R_θ, R_ϕ	principal radii of the curvature of the shell about θ and ϕ, respectively
S_n	mode shape factor of the shell
T	kinetic energy of the shell
$\overline{V}$	total strain energy of the shell
V_b	$= \alpha\omega^{1/2}$, bending velocity
Y_d	driving point admittance (DPA)
Y_c	mean value of the DPA
Z_{an}	$= r_{an} - i\omega M_{an}$, acoustic impedance
Z_{mn}	$= r_{mn} + iM_{mn}$, mechanical impedance
Z_a	$= Z_{mn}/\rho c$, normalized mechanical impedance
Z_n	$= Z_{an} + Z_{mn}$, total impedance of the submerged shell
α	$= [Eh^2/12\rho_s(1 - \nu^2)]^{1/4}$
α_n	decay factor for acoustic propagation
β	$= (h/a)^2/12$, bending factor
η	$= \cos\theta$
λ	wavelength
λ_n	$= n(n + 1)$
$\overline{\mu}$	$= \rho_s h$, surface density of the shell
μ_n	$= s_n + 1/2$, numerical variable
ν	Poisson ratio
ρ	mass density of the fluid
ρ_s	mass density of the shell
ρ_θ, ρ_ϕ, ρ_n	corresponding strains of σ_θ, σ_ϕ, σ_n
$\rho_{\theta\phi}$, $\rho_{\theta n}$, $\rho_{\phi n}$	corresponding shear strains of $\sigma_{\theta\phi}$, $\sigma_{\theta n}$, $\sigma_{\phi n}$

σ_θ, σ_ϕ, σ_n	normal stresses on three mutually perpendicular faces of an element of a shell
$\sigma_{\theta\phi}$, $\sigma_{\theta n}$, $\sigma_{\phi n}$	shear stresses
τ_n	$= q_n e^{i\pi/3}/6^{1/2}$
ω	angular frequency
ω_r	$= C_b/a$, ring frequency
Ω	$= \omega/\omega_r$, normalized frequency

ACKNOWLEDGEMENTS

The author wishes to express his sincere gratitude to the many individuals who contributed, directly and indirectly, to the successful completion of this thesis:

Professor Sabih I. Hayek, thesis advisor, for his constant inspiration throughout this work with his fresh enthusiasm; Professor Jiri Tichy, Professor Eugen J. Skudrzyk, Professor Robert W. Farwell, Dr. Alan D. Stuart, Dr. Walter King III, and Dr. Harold M. Frost for their constructive discussions and comments.

Thanks are due to Dr. Franklin Sun, Dr. Earl Williams, Mr. Ronald Fink, Mr. James Rishell, and Mr. Dale Sackrider for their technical assistance, and to Mrs. Dorothy Tindal for reading of the manuscript.

This research was supported by the Applied Research Laboratory of The Pennsylvania State University under contract with the Naval Sea Systems Command.

CHAPTER I

BACKGROUND

1.1 Introduction

The study of the vibration of a spherical shell submerged in an infinite acoustic fluid medium is the main objective of this thesis. The mechanical and acoustical energies are coupled by a fluid reaction [1]. The vibration of a spherical shell has been studied by many authors [2-8]. In a paper "On the Vibrations of a Spherical Shell," Lamb [2] has investigated a membrane spherical shell for axisymmetric vibration, and pointed out the existence of two infinite sets of normal modes. Baker [3] has expanded the work given by Lamb, and demonstrated experimentally the existence of normal modes predicted by the theory. Kalnins [4] studied the bending effects on the vibration of a spherical shell in vacuum, and labeled the lower branch as bending modes. Wilkinson [5] showed that there are three branches in the frequency spectrum when the equations of motion of closed spherical shells include the effects of transverse shear deformation and rotatory inertia.

Considering the vibration of a spherical shell submerged in fluid medium, Junger [1] examined the sound scattering of a membrane elastic spherical shell, insonified by a plane acoustic wave. He concluded that the scattering field of all elastic scatterers is the result of the rigid body scattering and radiation scattering. In another paper [6], he studied the same dynamic configuration but excited by a point force. He demonstrated the radiation loading on

an elastic shell. Hayek [7] studied the vibration of the forced, axisymmetric spherical shell in the light of the bending theory in an acoustic medium. He concluded that the resonance frequency is sensitive to the parameter (h/a), especially for large mode numbers n, and the resonance frequency increases as n increases, no matter how small is the ratio (h/a). Lauchle [8] extended the work of Junger, and demonstrated the interaction of a spherical acoustic wave with an elastic spherical shell in fluid media.

1.2 Statement of the Problem to be Studied and the Mathematical Model

In the present paper, the effects of fluid loading on elastic spherical shells are investigated experimentally and analytically. Mathematically, the shell is modeled using thin shell theory [9, 10], a theory considered valid for a large number of practical applications. Within the range of the thin shell theory, $(h/a) \leq 1/20$ [9], two different thickness ($h = 0.0514''$ and $h = 0.1069''$) duralumin elastic spherical shells of radii $a = 8''$ have been used for the experiments. In the thin shell theory, there are three approximations of different orders: (1) membrane theory [2]--this theory neglects all moments since the wall thickness of the shell is very small; (2) classical theory [7]--this theory includes the bending factor $(h/a)^2/12$; and (3) improved theory [5]--this theory includes the effects of transverse shear deformation and rotatory inertia. Investigation of the resonance frequencies of the shells showed that the classical thin shell theory is adequate. Due to the type of excitation of the shells, the basic

equations are limited to the axisymmetric nontorsional vibration of a spherical shell.

First, the equations of motion for the shells in this study are derived by applying Hamilton's variational principle. To investigate the effect of bending, the resonance frequencies are computed. The equation derived for the natural frequencies of a submerged shell is transcendental. The standard linear method was not useful for solving such an equation. Therefore, a new method was developed for the computation of the resonance frequencies. The new derivation also gives a deeper insight into physical interpretations of the results. This method, derived for the equations of motion of submerged cylindrical shells in terms of generalized coordinates, has been developed by Hayek [11] to compute the resonance frequencies of submerged shells. By applying this method to spherical shells, the resonance frequencies of a submerged spherical shell were obtained.

The second problem considered is the acoustic radiation from a point-force excited spherical shell. For a force-excited shell, consider a unit concentrated, harmonic force exciting the shell at $\theta = 0$. The shell is freely suspended in a fluid medium. The driving point admittance was computed for such a loading and measured experimentally. Furthermore, the expressions for the resonance density of the shell was derived for high and low frequencies. These were used in the characteristic admittance theory of Skudrzyk [12] to predict the meanline of the driving point admittance of a point-force excited spherical shell in vacuo.

The next problem considered is the acoustic point-source excited shell. The mathematical model for the shell motion is the same as that given above, but the shell is insonified by an acoustic spherical wave. The effect of the fluid loading on the shell is investigated for the near field analytically and experimentally. Furthermore, the radiated pressure due to the vibration of the shell responding to the pressure of the incident spherical wave will be examined analytically by use of wave harmonic functions. The internal damping is also considered in this problem.

Finally, the diffracted pressure field due to a point source in the vicinity of a spherical shell was re-evaluated by use of the Geometrical Theory of Diffraction (GTD) due to Keller [13-15]. This approach was taken because the wave harmonic function expansion would not be possible for shells that are not regularly shaped. The approach requires the knowledge of the impedance of the surface around which acoustic rays propagate. Comparison of the exact wave harmonic solution with the GTD method was made.

The model of the problems being studied consists of a spherical elastic thin shell excited by an acoustic spherical wave or a unit concentrated harmonic force. The shell is submerged in an infinite compressible acoustic medium having a mass density ρ, and the sound speed c. As shown in Figure 1.1, the shell has a radius a, and the thickness of its wall is h. The mass density of the shell is ρ_s, while Young's modulus and Poisson's ratio are E and ν, respectively. The shell is located at the origin of the spherical coordinate system. The source is located on the z-axis at the point

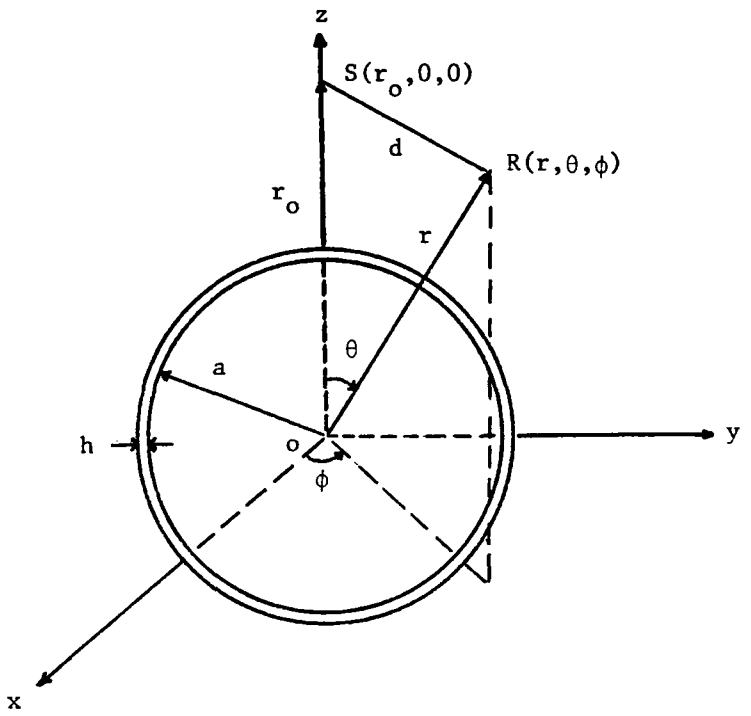

Figure 1.1 Configuration of the spherical shell in the spherical coordinate system

$S(r_o,0,0)$, a distance r_o from the center of the shell. The observer point is $R(r,\theta,\phi)$, where r is the observer distance from the center of the shell, and θ is the aspect angle. This arrangement will reduce the problem to the study of an axisymmetric vibration of a spherical shell as well as the pressure field.

CHAPTER II

FORMULATION OF THE THIN SPHERICAL SHELL'S EQUATION OF MOTION

2.1 Introduction

In this chapter, the equations of motion of a submerged spherical shell are derived by applying Hamilton's variational principle [16, 17]. For a better understanding of the dynamic interaction between a submerged spherical shell and the surrounding acoustic medium, the equations of motion are also derived in terms of generalized coordinates [11]. Generally, the analytic formulation is performed for idealized conditions. For thin elastic spherical shells submerged in a fluid medium, it is assumed that [9, 10]:

1. The material of the shell is linearly elastic, isotropic, and homogeneous--this means that the material of the shell obeys Hooke's law.
2. The ratio of the thickness to the radius is $(h/a) < 1/20$, so that the thin shell approximate theory can be used.
3. The displacement of the shell is small when compared to the thickness h .
4. The shell is freely suspended; straight fibers of the shell which are normal to its middle surface before deformation remain straight and normal to the deformed middle surface and do not suffer any extensions as suggested by Kirchhoff; and the normal

stresses acting on planes parallel to the shell middle surface are neglected as compared to the other stresses as introduced by Kirchhoff.

5. The acoustic pressure (disturbed pressure) has a linear relation with the condensation of the fluid.
6. The fluid is compressible and inviscid.

2.2 The Equations of Motion

In the present section, the dynamical response of an elastic body is considered where the applied forces, the displacements, etc., are time-dependent. To derive the equations of motion, Hamilton's variational principle is applied. The variational integral requires expressions for the kinetic energy T and the strain energy $\overline{V}$ of the system as well as the external forces as derived from a potential function Q. Hamilton's principle states that:

$$\delta \int_{t_1}^{t_2} (T - \overline{V} + Q)dt = 0 \quad , \tag{2.1}$$

where t_1 and t_2 are the initial and final time states, respectively, of the system. The symbol δ represents differential variation.

There are many different approaches to obtain an expression for the strain energy of a thin shell. In this study, the expression for the strain energy density of thin shells as developed in References [9] and [10] will be used. Generally, the expression for the strain energy for shells is defined by:

$$\bar{V} = \frac{1}{2}\int_v (\sigma_\theta\rho_\theta + \sigma_\phi\rho_\phi + \sigma_n\rho_n + \sigma_{\theta\phi}\rho_{\theta\phi} + \sigma_{\theta n}\rho_{\theta n} + \sigma_{\phi n}\rho_{\phi n})dv \quad , \tag{2.2}$$

where σ_θ, σ_ϕ, σ_n are the normal stresses on three mutually perpendicular faces of an element of the shell, ρ_θ, ρ_ϕ, ρ_n are the corresponding strains, $\sigma_{\theta\phi}$, $\sigma_{\theta n}$, $\sigma_{\phi n}$ are the shear stresses on these faces, $\rho_{\theta\phi}$, $\rho_{\theta n}$, $\rho_{\phi n}$ are the corresponding shear strains, and dv is the volume of the element. The stresses on the middle surface are shown in Figure 2.1.

By applying the assumptions of Kirchhoff in Section 2.1, the stress σ_n and the strains $\rho_{\theta n}$, $\rho_{\phi n}$ can be neglected as compared with the other stresses and strains, respectively. Therefore, Equation (2.2) may reduce to:

$$\bar{V} = \frac{1}{2}\int_v (\sigma_\theta\rho_\theta + \sigma_\phi\rho_\phi + \sigma_{\theta\phi}\rho_{\theta\phi})dv \quad . \tag{2.3}$$

Expressing all stresses in terms of strains, expanding the strain in a Taylor's series of (h/R_s), and neglecting terms of the order $(h/R_s)^3$ and higher, where R_s is the principal radius of curvature of the shell, one obtains an approximate expansion for the strain energy density:

$$\bar{V} = \frac{Eh}{2(1-\nu^2)}\int_s \left[(\rho_\theta + \rho_\phi)^2 - 2(1-\nu)(\rho_\theta\rho_\phi - \frac{\rho_{\theta\phi}^2}{4})\right]A_\theta A_\phi d\theta d\phi$$

$$+ \frac{Eh^3}{24(1-\nu^2)}\int_s \left[(K_\theta + K_\phi)^2 - 2(1-\nu)(K_\theta K_\phi - \frac{K_{\theta\phi}^2}{4})\right]A_\theta A_\phi d\theta d\phi, \tag{2.4}$$

where E is the Young's modulus, ν is the Poisson ratio, A_θ and A_ϕ are the Lamé parameters, K_θ and K_ϕ are the changes in curvature

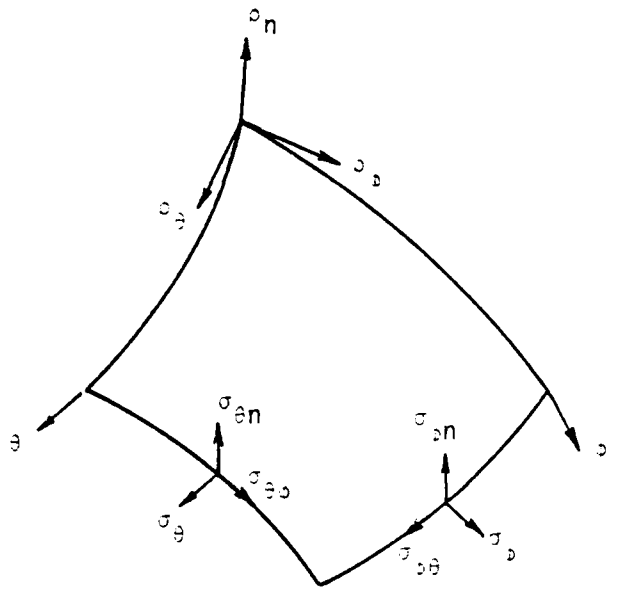

Figure 2.1 Direction of the stresses σ_s acting on the middle surface of the shells. ρ_n , ρ_0 , ρ_ϕ are the orthogonal unit vectors.

due to bending of the deformed middle surface of a shell about the θ and ϕ coordinates, respectively, and $K_{\theta\phi}$ is the parameter for torsional deformation. The integral in Equation (2.4) is the surface integral over the middle surface. It should be noted that the extensional and shear energy is represented by the first integral, and the second integral represents the bending and torsional energy.

For axisymmetric extensional and bending motion of the shell, Equation (2.4) can be further simplified because the shear and torsional factors vanish for axisymmetric motion. The variables in Equation (2.4) are, therefore, expressed as:

$$\rho_\theta = \frac{1}{A_\theta}\frac{\partial u}{\partial \theta} - \frac{w}{R_\theta} \quad ,$$

$$\rho_\phi = \frac{1}{A_\theta A_\phi}\frac{\partial A_\theta}{\partial \theta} u - \frac{w}{R_\phi} \quad ,$$

$$\rho_{\theta\phi} = 0 \quad ,$$

$$K_\theta = \frac{1}{A_\theta}\frac{\partial}{\partial \theta}\left(\frac{1}{A_\theta}\frac{\partial w}{\partial \theta} + \frac{u}{R_\theta}\right) + \frac{1}{A_\theta A_\phi}\frac{\partial A_\theta}{\partial \phi}\left(\frac{1}{A_\phi}\frac{\partial w}{\partial \phi}\right) \quad ,$$

$$K_\phi = \frac{1}{A_\theta A_\phi}\frac{\partial A_\phi}{\partial \theta}\left(\frac{1}{A_\theta}\frac{\partial w}{\partial \theta} + \frac{u}{R_\theta}\right)$$

and

$$K_{\theta\phi} = 0 \quad , \qquad (2.5)$$

where $u = u(\theta,t)$ and $w = w(\theta,t)$ are the tangential and radial displacements, respectively, and R_θ and R_ϕ are the radii of the curvature of the shell about θ and ϕ coordinates, respectively.

Consider the geometry of a spherical shell, then, $A_\theta = a$, $A_\phi = a \sin\theta$, and $R_\theta = R_\phi = a$. The geometric configuration is shown in Figure 2.2. Substituting the above relations into Equation (2.5),

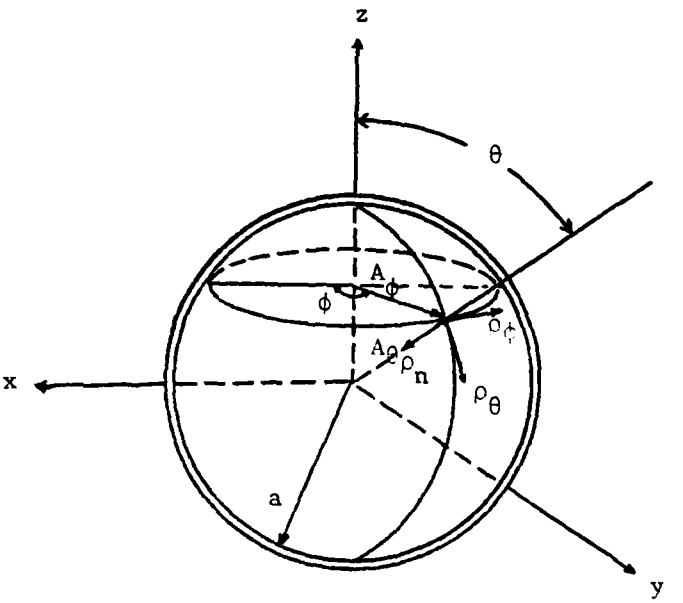

Figure 2.2 Orientation of the vectors of a spherical shell

one obtains expressions for a spherical shell:

$$\rho_\theta = \frac{1}{a}\left[\frac{\partial u}{\partial \theta} - w\right] ,$$

$$\rho_\phi = \frac{1}{a}\left[u \cot\theta - w\right] ,$$

$$\rho_{\theta\phi} = 0 ,$$

$$K_\theta = \frac{1}{a^2}\left[\frac{\partial^2 w}{\partial \theta^2} + \frac{\partial u}{\partial \theta}\right] ,$$

$$K_\phi = \frac{1}{a^2}\left[u + \frac{\partial w}{\partial \theta}\right] \cot\theta$$

and

$$K_{\theta\phi} = 0 . \qquad (2.6)$$

The total kinetic energy of the shell is:

$$T = \frac{1}{2}\rho_s \int_v (\dot{u}^2 + \dot{w}^2)dv$$

$$= \pi \rho_s h a^2 \int_0^\pi (\dot{u}^2 + \dot{w}^2) \sin\theta d\theta , \qquad (2.7)$$

where $\dot{u}$ and $\dot{w}$ are the time derivatives of u and w, respectively. The external forces of the considered problem are the normal component of applied surface forces, p_i (acoustical or mechanical forces), and the reactive normal surface force, p_r, due to the fluid loading. Therefore, the potential function due to these two force systems are:

$$Q = -\int_s (p_r + p_i)w ds$$

$$= -2\pi a^2 \int_0^\pi (p_r + p_i)w \sin\theta d\theta . \qquad (2.8)$$

Substituting the strain and kinetic energies and the potential function into Equation (2.1), one obtains the coupled equations of motion of a spherical shell in terms of displacements u and w :

$$(1 + \beta)\left[(\nu + \cot^2\theta)u - \cot\theta \frac{\partial u}{\partial \theta} - \frac{\partial^2 u}{\partial \theta^2}\right] + (\beta\cot^2\theta + 1 + \nu + \nu\beta) \frac{\partial w}{\partial \theta}$$

$$- \beta\cot\theta \frac{\partial^2 w}{\partial \theta^2} - \beta \frac{\partial^3 w}{\partial \theta^3} + \frac{1 - \nu^2}{E} \rho_s a^2 \frac{\partial^2 u}{\partial t^2} = 0 \qquad (2.9)$$

and

$$\beta \frac{\partial^3 u}{\partial \theta^3} + 2\beta\cot\theta \frac{\partial^2 u}{\partial \theta^2} - \left[(1 + \nu)(1 + \beta) + \beta\cot^2\theta\right] \frac{\partial u}{\partial \theta}$$

$$+ \left[\beta\cot^3\theta + 3\beta\cot\theta - (1 + \beta)(1 + \nu)\cot\theta\right]u$$

$$+ \beta\left[\frac{\partial^4 w}{\partial \theta^4} + 2\cot\theta \frac{\partial^3 w}{\partial \theta^3} - (1 + \nu + \cot^2\theta) \frac{\partial^2 w}{\partial \theta^2}\right.$$

$$\left. + (2\cot\theta + \cot^3\theta - \nu\cot\theta) \frac{\partial w}{\partial \theta}\right] + 2(1 + \nu)w$$

$$+ \frac{1 - \nu^2}{E} \rho_s a^2 \frac{\partial^2 w}{\partial t^2} + \frac{1 - \nu^2}{Eh} a^2(p_r + p_i) = 0 \quad , \qquad (2.10)$$

where $\beta = (h/a)^2/12$ is the bending factor.

By changing the variable θ in the foregoing equations to a new variable $\eta = \cos\theta$, and using a time harmonic variation for all variables:

$$u = U(\eta)e^{-i\omega t} \quad , \quad w = W(\eta)e^{-i\omega t} \quad ,$$

and

$$p_i = P_i(\eta)e^{-i\omega t} \quad , \quad p_r = P_r(\eta)e^{-i\omega t} \quad , \qquad (2.11)$$

Equations (2.9) and (2.10) can be rewritten in the following form:

$$L_{uu}U + L_{uw}W = (1 - \nu^2)\Omega^2 U \qquad (2.12)$$

and

$$L_{wu}U + L_{ww}W = (1 - \nu^2)\Omega^2 W - \frac{1 - \nu^2}{Eh} a^2(P_i + P_r) \quad , \quad (2.13)$$

where the operators L_{uu}, L_{uw}, L_{wu}, L_{ww} are given by:

$$L_{uu} = -(1 + \beta)[(1 - \eta^2)^{1/2} \frac{d^2}{d\eta^2} (1 - \eta^2)^{1/2} + (1 - \nu)] \quad , \quad (2.14)$$

$$L_{uw} = (1 - \eta^2)^{1/2}[\beta(1 - \nu) \frac{d}{d\eta} - (1 + \nu) \frac{d}{d\eta} + \beta \frac{d}{d\eta} \nabla^2] \quad , \quad (2.15)$$

$$L_{wu} = -\{[\beta(1 - \nu) - (1 + \nu)] \frac{d}{d\eta} (1 - \eta^2)^{1/2} + \beta\nabla^2 \frac{d}{d\eta} (1-\eta^2)^{1/2}\} \quad (2.16)$$

and

$$L_{ww} = \beta\nabla^4 + \beta(1 - \nu)\nabla^2 + 2(1 + \nu) \quad , \quad (2.17)$$

where

$$\nabla^2 = \frac{d}{d\eta} (1 - \eta^2) \frac{d}{d\eta}$$

$$\Omega^2 = \rho_s \omega^2 a^2 / E = \frac{\omega^2}{\omega_r^2} \quad \text{is the normalized frequency,}$$

$$\omega_r = \frac{C_b}{a} \quad \text{is the ring frequency}$$

and

$$C_b = \sqrt{\frac{E}{\rho_s}} \quad . \quad (2.18)$$

In Appendix A, a detailed derivation of the equations in this section is given.

For this problem, the tangential and radial displacements can be expressed in terms of Legendre polynomial of degree n as follows:

$$U(\eta) = \sum_{n=o}^{\infty} U_n (1 - \eta^2)^{1/2} \frac{dP_n(\eta)}{d\eta} \quad , \quad W(\eta) = \sum_{n=o}^{\infty} W_n P_n(\eta) \quad , \quad (2.19)$$

and

$$P_i = \sum_{n=o}^{\infty} p_{in} P_n(\eta) \quad , \quad P_r = \sum_{n=o}^{\infty} p_{rn} P_n(\eta) \quad . \qquad (2.20)$$

Then, on substitution of these two equations into Equations (2.12) and (2.13), one obtains two algebraic equations in terms of U_n and W_n :

$$\{(1 - \nu^2)\Omega^2 - (1 + \beta)[\lambda_n - (1 - \nu)]\}U_n$$

$$+ \{\beta[\lambda_n - (1 - \nu)] + (1 + \nu)\}W_n = 0 \qquad (2.21)$$

and

$$[\lambda_n \beta(1 - \nu) - (1 + \nu) - \beta\lambda_n^2]U_n + [\beta\lambda_n^2 - \beta(1 - \nu)\lambda_n$$

$$+ 2(1 + \nu) - (1 - \nu^2)\Omega^2]W_n = - \frac{1 - \nu^2}{Eh} a^2(p_{in} + p_{rn}) \quad , \qquad (2.22)$$

where $\lambda_n = n(n + 1)$.

2.3 The Natural Frequency, the Mechanical Impedance, and the Ratio U_n/W_n of the Shell in Vacuo

Before proceeding to present the solution to shell vibration excited by an acoustic point source, one should examine the free vibration of a spherical shell. For a freely vibrating shell, there exists no applied force, and the shell in vacuo is not subject to any reactive forces due to the fluid loading effect. It is evident that the foregoing Equations (2.21) and (2.22) become two homogeneous equations with two unknowns U_n and W_n . The determinant of the equations must vanish, which results in the frequency equation as follows:

$$(1 - \nu^2)^2\Omega^4 - [\beta\lambda_n^2 + (1 + \beta\nu)\lambda_n + (1 + 3\nu) - \beta(1 - \nu)](1 - \nu^2)\Omega^2$$

$$+ \beta\lambda_n^3 - 4\beta\lambda_n^2 + [\beta(5 - \nu^2) + (1 - \nu^2)]\lambda_n - 2(1 + \beta)(1 - \nu^2) = 0. \tag{2.23}$$

This is a quadratic equation in Ω^2 with only two distinct positive roots for each mode number n. The larger root of each mode belongs to the upper branch, and denoted by Ω_h. The smaller root, Ω_ℓ, belongs to the lower branch. The roots Ω_{hn} and $\Omega_{\ell n}$ are the natural frequencies of the spherical shell. For $n = 0$, there is only one positive real root:

$$\Omega_{ho}^2 \overset{\sim}{=} \frac{2}{1 - \nu} \quad .$$

This frequency represents purely radial motion, which is referred to as the "breathing mode." This mode's elastic energy is due to the extensional deformation only because the shell vibrates only in the radial direction, and the radius of curvature of the shell is constant. The natural frequencies of duralumin shells of radius $a = 8$ inches and thickness $h = 0.1069$ inch and $h = 0.0514$ inch were computed and tabulated in Tables 2.1, 2.2, and 2.3, respectively, and also plotted in Figure 2.3. It is clear that the natural frequencies of the lower branch for membrane theory, $\beta = 0$, are independent of the shell's thickness, while the natural frequencies of bending modes, for $\beta > 0$, vary with the thickness. However, the upper branch frequencies do not change significantly with β. For a thin shell, where the ratio h/a is very small such as the ratio 0.0064 shown in Figure 2.3, the membrane theory may be applicable at low frequencies

TABLE 2.1

RESONANCE FREQUENCIES OF A SPHERICAL DURALUMIN MEMBRANE SHELL
WITH THICKNESS h = 0.1069" AND RADIUS A = 8" IN VACUO - MEMBRANE THEORY

	N	ω	Ω	U_n/W_n	M_n/M
Lower	2	0.18021E+05	0.72866E+00	0.27449E+00	0.29041E+00
Branch	3	0.21413E+05	0.86580E+00	0.12512E+00	0.16969E+00
	4	0.22760E+05	0.92028E+00	0.71839E-01	0.12258E+00
	5	0.23427E+05	0.94722E+00	0.46779E-01	0.96877E-01
	6	0.23803E+05	0.96243E+00	0.32953E-01	0.80431E-01
	7	0.24037E+05	0.97189E+00	0.24497E-01	0.68907E-01
	8	0.24193E+05	0.97820E+00	0.18940E-01	0.60343E-01
	9	0.24301E+05	0.98258E+00	0.15089E-01	0.53710E-01
	10	0.24379E+05	0.98573E+00	0.12307E-01	0.48412E-01
	11	0.24439E+05	0.98813E+00	0.10232E-01	0.44079E-01
	12	0.24484E+05	0.98998E+00	0.86427E-02	0.40466E-01
	13	0.24520E+05	0.99142E+00	0.73977E-02	0.37406E-01
	14	0.24549E+05	0.99259E+00	0.64041E-02	0.34780E-01
	15	0.24571E+05	0.99348E+00	0.55985E-02	0.32501E-01
	16	0.24589E+05	0.99423E+00	0.49361E-02	0.30504E-01
	17	0.24606E+05	0.99492E+00	0.43849E-02	0.28740E-01
	18	0.24620E+05	0.99547E+00	0.39212E-02	0.27169E-01
	19	0.24630E+05	0.99588E+00	0.35275E-02	0.25762E-01
	20	0.24640E+05	0.99629E+00	0.31903E-02	0.24495E-01
	21	0.24649E+05	0.99663E+00	0.28993E-02	0.23346E-01
	22	0.24655E+05	0.99691E+00	0.26464E-02	0.22301E-01
	23	0.24662E+05	0.99718E+00	0.24253E-02	0.21346E-01
	24	0.24667E+05	0.99739E+00	0.22308E-02	0.20469E-01
	25	0.24672E+05	0.99759E+00	0.20588E-02	0.19662E-01
	26	0.24678E+05	0.99780E+00	0.19059E-02	0.18916E-01

TABLE 2.1 (continued)

	N	ω	Ω	U_n/W_n	M_n/M
	27	0.24681E+05	0.99793E+00	0.17695E-02	0.18225E-01
	28	0.24684E+05	0.99807E+00	0.16472E-02	0.17583E-01
	29	0.24688E+05	0.99821E+00	0.15372E-02	0.16984E-01
	30	0.24691E+05	0.99834E+00	0.14379E-02	0.16425E-01
	31	0.24693E+05	0.99841E+00	0.13479E-02	0.15902E-01
	32	0.24696E+05	0.99855E+00	0.12661E-02	0.15411E-01
	33	0.24698E+05	0.99862E+00	0.11915E-02	0.14949E-01
	34	0.24700E+05	0.99869E+00	0.11233E-02	0.14515E-01
	35	0.24701E+05	0.99876E+00	0.10608E-02	0.14104E-01
	36	0.24703E+05	0.99882E+00	0.10034E-02	0.13717E-01
	37	0.24705E+05	0.99889E+00	0.95055E-03	0.13350E-01
	38	0.24706E+05	0.99896E+00	0.90175E-03	0.13003E-01
	39	0.24708E+05	0.99903E+00	0.85662E-03	0.12673E-01
	40	0.24708E+05	0.99903E+00	0.81480E-03	0.12359E-01
	41	0.24710E+05	0.99910E+00	0.77596E-03	0.12061E-01
	42	0.24711E+05	0.99917E+00	0.73984E-03	0.11776E-01
	43	0.24711E+05	0.99917E+00	0.70618E-03	0.11505E-01
	44	0.24713E+05	0.99924E+00	0.67477E-03	0.11246E-01
	45	0.24713E+05	0.99924E+00	0.64541E-03	0.10998E-01
	46	0.24715E+05	0.99930E+00	0.61793E-03	0.10762E-01
	47	0.24715E+05	0.99930E+00	0.59216E-03	0.10535E-01
	48	0.24715E+05	0.99930E+00	0.56798E-03	0.10317E-01
	49	0.24716E+05	0.99937E+00	0.54524E-03	0.10108E-01
Upper Branch	0	0.42890E+05	0.17342E+01	-0.40030E+00	0.10000E+01
	1	0.52530E+05	0.21240E+01	-0.50000E+00	0.50000E+00
	2	0.72046E+05	0.29131E+01	-0.60720E+00	0.64243E+00
	3	0.95869E+05	0.38763E+01	-0.66601E+00	0.90326E+00
	4	0.12101E+06	0.48928E+01	-0.69600E+00	0.11876E+01
	5	0.14664E+06	0.59290E+01	-0.71257E+00	0.14757E+01
	6	0.17248E+06	0.69741E+01	-0.72254E+00	0.17636E+01
	7	0.19847E+06	0.80247E+01	-0.72895E+00	0.20504E+01

TABLE 2.2

RESONANCE FREQUENCIES OF A SPHERICAL DURALUMIN CLASSICAL SHELL
WITH THICKNESS h = 0.0154" AND RADIUS a = 8" IN VACUO - CLASSICAL THEORY

	N	ω	Ω	U_n/W_n	M_n/M
Lower Branch	2	0.18021E+05	0.72866E+00	0.27449E+00	0.29041E+00
	3	0.21418E+05	0.86600E+00	0.12513E+00	0.16970E+00
	4	0.22776E+05	0.92090E+00	0.71847E-01	0.12258E+00
	5	0.23464E+05	0.94873E+00	0.46787E-01	0.96879E-01
	6	0.23881E+05	0.96559E+00	0.32960E-01	0.80433E-01
	7	0.24177E+05	0.97758E+00	0.24505E-01	0.68909E-01
	8	0.24428E+05	0.98772E+00	0.18948E-01	0.60344E-01
	9	0.24671E+05	0.99752E+00	0.15096E-01	0.53711E-01
	10	0.24935E+05	0.10082E+01	0.12315E-01	0.48413E-01
	11	0.25239E+05	0.10205E+01	0.10240E-01	0.44080E-01
	12	0.25598E+05	0.10350E+01	0.86507E-02	0.40467E-01
	13	0.26028E+05	0.10524E+01	0.74056E-02	0.37407E-01
	14	0.26544E+05	0.10733E+01	0.64121E-02	0.34780E-01
	15	0.27154E+05	0.10979E+01	0.56064E-02	0.32501E-01
	16	0.27869E+05	0.11268E+01	0.49441E-02	0.30505E-01
	17	0.28700E+05	0.11604E+01	0.43929E-02	0.28740E-01
	18	0.29651E+05	0.11989E+01	0.39292E-02	0.27170E-01
	19	0.30729E+05	0.12425E+01	0.35355E-02	0.25763E-01
	20	0.31939E+05	0.12914E+01	0.31983E-02	0.24495E-01
	21	0.33285E+05	0.13458E+01	0.29073E-02	0.23347E-01
	22	0.34764E+05	0.14056E+01	0.26545E-02	0.22301E-01
	23	0.36383E+05	0.14711E+01	0.24333E-02	0.21346E-01
	24	0.38137E+05	0.15420E+01	0.22388E-02	0.20470E-01
	25	0.40027E+05	0.16184E+01	0.20668E-02	0.19662E-01
	26	0.42053E+05	0.17003E+01	0.19140E-02	0.18916E-01

TABLE 2.2 (continued)

	N	ω	Ω	U_n/W_n	M_n/M
	27	0.44211E+05	0.17876E+01	0.17775E-02	0.18225E-01
	28	0.46499E+05	0.18801E+01	0.16553E-02	0.17583E-01
	29	0.48918E+05	0.19779E+01	0.15453E-02	0.16984E-01
	30	0.51462E+05	0.20808E+01	0.14459E-02	0.16425E-01
	31	0.54130E+05	0.21887E+01	0.13559E-02	0.15902E-01
	32	0.56921E+05	0.23015E+01	0.12741E-02	0.15411E-01
	33	0.59833E+05	0.24193E+01	0.11995E-02	0.14949E-01
	34	0.62864E+05	0.25418E+01	0.11314E-02	0.14515E-01
	35	0.66013E+05	0.26692E+01	0.10689E-02	0.14105E-01
	36	0.69276E+05	0.28011E+01	0.10115E-02	0.13717E-01
	37	0.72654E+05	0.29377E+01	0.95861E-03	0.13351E-01
	38	0.76144E+05	0.30788E+01	0.90982E-03	0.13003E-01
	39	0.79746E+05	0.32244E+01	0.86469E-03	0.12673E-01
	40	0.83458E+05	0.33745E+01	0.82287E-03	0.12359E-01
	41	0.87281E+05	0.35291E+01	0.78403E-03	0.12061E-01
	42	0.91210E+05	0.36879E+01	0.74791E-03	0.11777E-01
	43	0.95247E+05	0.38512E+01	0.71426E-03	0.11505E-01
	44	0.99391E+05	0.40187E+01	0.68285E-03	0.11246E-01
	45	0.10364E+06	0.41906E+01	0.65350E-03	0.10999E-01
	46	0.10800E+06	0.43666E+01	0.62601E-03	0.10762E-01
	47	0.11246E+06	0.45470E+01	0.60025E-03	0.10535E-01
	48	0.11702E+06	0.47315E+01	0.57607E-03	0.10317E-01
	49	0.12169E+06	0.49202E+01	0.55334E-03	0.10109E-01
Upper	0	0.42890E+05	0.17342E+01	-0.40030E+00	0.10000E+01
Branch	1	0.52530E+05	0.21240E+01	-0.50000E+00	0.50000E+00
	2	0.72046E+05	0.29131E+01	-0.60718E+00	0.64240E+00
	3	0.95869E+05	0.38763E+01	-0.66597E+00	0.90317E+00
	4	0.12101E+06	0.48928E+01	-0.69593E+00	0.11874E+01
	5	0.14664E+06	0.59291E+01	-0.71246E+00	0.14753E+01
	6	0.17248E+06	0.69741E+01	-0.72237E+00	0.17628E+01
	7	0.19847E+06	0.80247E+01	-0.72872E+00	0.20492E+01

TABLE 2.3

RESONANCE FREQUENCIES OF A SPHERICAL DURALUMIN CLASSICAL SHELL
WITH THICKNESS h = 0.1069" AND RADIUS a = 8" IN VACUO - CLASSICAL THEORY

	N	ω	Ω	U_n/W_n	M_n/M
Lower Branch	2	0.18025E+05	0.72880E+00	0.27451E+00	0.29043E+00
	3	0.21435E+05	0.86669E+00	0.12515E+00	0.16971E+00
	4	0.22828E+05	0.92303E+00	0.71871E-01	0.12259E+00
	5	0.23589E+05	0.95380E+00	0.46812E-01	0.96886E-01
	6	0.24135E+05	0.97587E+00	0.32986E-01	0.80438E-01
	7	0.24639E+05	0.99622E+00	0.24531E-01	0.68913E-01
	8	0.25193E+05	0.10186E+01	0.18974E-01	0.60348E-01
	9	0.25862E+05	0.10457E+01	0.15123E-01	0.53715E-01
	10	0.26696E+05	0.10794E+01	0.12342E-01	0.48417E-01
	11	0.27730E+05	0.11212E+01	0.10267E-01	0.44083E-01
	12	0.28996E+05	0.11724E+01	0.86772E-02	0.40470E-01
	13	0.30517E+05	0.12339E+01	0.74322E-02	0.37409E-01
	14	0.32307E+05	0.13063E+01	0.64387E-02	0.34783E-01
	15	0.34375E+05	0.13899E+01	0.56331E-02	0.32504E-01
	16	0.36727E+05	0.14850E+01	0.49708E-02	0.30507E-01
	17	0.39361E+05	0.15915E+01	0.44196E-02	0.28742E-01
	18	0.42275E+05	0.17093E+01	0.39560E-02	0.27172E-01
	19	0.45465E+05	0.18383E+01	0.35623E-02	0.25765E-01
	20	0.48923E+05	0.19781E+01	0.32252E-02	0.24497E-01
	21	0.52643E+05	0.21285E+01	0.29342E-02	0.23348E-01
	22	0.56621E+05	0.22894E+01	0.26813E-02	0.22303E-01
	23	0.60850E+05	0.24604E+01	0.24602E-02	0.21348E-01
	24	0.65325E+05	0.26413E+01	0.22657E-02	0.20471E-01
	25	0.70041E+05	0.28320E+01	0.20938E-02	0.19664E-01
	26	0.74994E+05	0.30322E+01	0.19410E-02	0.18918E-01

TABLE 2.3 (continued)

	N	ω	Ω	U_n/W_n	M_n/M
	27	0.80177E+05	0.32418E+01	0.18046E-02	0.18227E-01
	28	0.85591E+05	0.34607E+01	0.16823E-02	0.17584E-01
	29	0.91230E+05	0.36887E+01	0.15724E-02	0.16986E-01
	30	0.97093E+05	0.39258E+01	0.14731E-02	0.16427E-01
	31	0.10318E+06	0.41718E+01	0.13831E-02	0.15903E-01
	32	0.10948E+06	0.44267E+01	0.13013E-02	0.15412E-01
	33	0.11600E+06	0.46903E+01	0.12268E-02	0.14951E-01
	34	0.12274E+06	0.49627E+01	0.11586E-02	0.14516E-01
	35	0.12969E+06	0.52437E+01	0.10962E-02	0.14106E-01
	36	0.13685E+06	0.55334E+01	0.10388E-02	0.13718E-01
	37	0.14423E+06	0.58316E+01	0.98600E-03	0.13352E-01
	38	0.15181E+06	0.61384E+01	0.93724E-03	0.13004E-01
	39	0.15961E+06	0.64536E+01	0.89216E-03	0.12674E-01
	40	0.16762E+06	0.67774E+01	0.85037E-03	0.12360E-01
	41	0.17584E+06	0.71098E+01	0.81159E-03	0.12062E-01
	42	0.18426E+06	0.74504E+01	0.77551E-03	0.11777E-01
	43	0.19289E+06	0.77992E+01	0.74190E-03	0.11506E-01
	44	0.20174E+06	0.81570E+01	0.71054E-03	0.11247E-01
	45	0.21077E+06	0.85223E+01	0.68123E-03	0.11000E-01
	46	0.22003E+06	0.88965E+01	0.65380E-03	0.10763E-01
	47	0.22949E+06	0.92789E+01	0.62809E-03	0.10536E-01
	48	0.23916E+06	0.96702E+01	0.60396E-03	0.10318E-01
	49	0.24903E+06	0.10069E+02	0.58128E-03	0.10109E-01
Upper	0	0.42890E+05	0.17342E+01	-0.40030E+00	0.10000E+01
Branch	1	0.52530E+05	0.21240E+01	-0.50000E+00	0.50000E+00
	2	0.72048E+05	0.29131E+01	-0.60715E+00	0.64236E+00
	3	0.95873E+05	0.38765E+01	-0.66585E+00	0.90290E+00
	4	0.12101E+06	0.48930E+01	-0.69569E+00	0.11866E+01
	5	0.14664E+06	0.59293E+01	-0.71207E+00	0.14738E+01
	6	0.17250E+06	0.69748E+01	-0.72180E+00	0.17601E+01
	7	0.19847E+06	0.80247E+01	-0.72795E+00	0.20450E+01

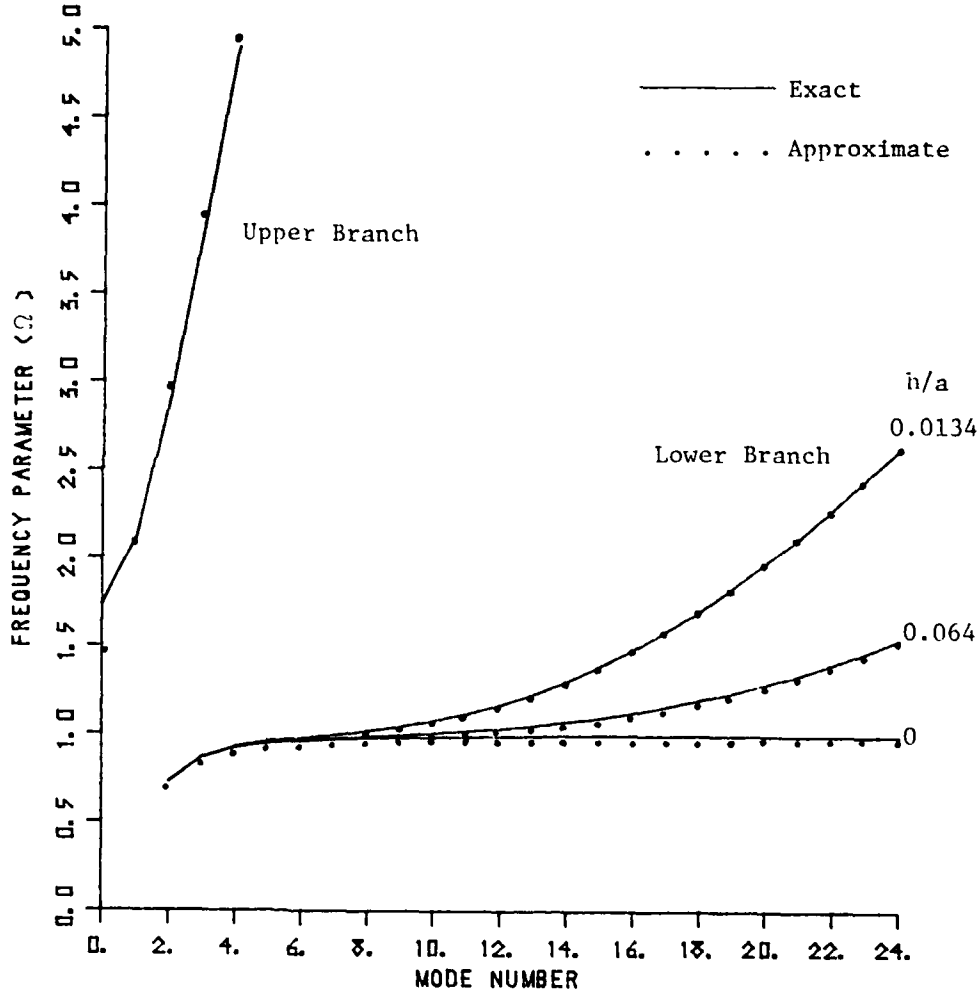

Figure 2.3 Dimensionless frequency Ω for various modes when spherical shells are excited in vacuo

or for small values of the mode number. It is interesting to note that Ω approaches unity when the mode number goes to infinity for $\beta = 0$. Different asymptotic approximations to the roots of Equation (2.23) can be obtained as follows:

$$\Omega_{\ell n}^2 \approx \frac{\lambda_n - 2}{\lambda_n + 1 + 3\nu} , \quad \Omega < 1 , \tag{2.25a}$$

$$\Omega_{\ell n}^2 \approx \frac{\beta\lambda_n^2}{1 - \nu^2} + 1 , \quad \Omega > 1 \tag{2.25b}$$

and

$$\Omega_{hn}^2 \approx \frac{\lambda_n + 1 + 3\nu}{1 - \nu^2} , \quad n \geq 0 . \tag{2.25c}$$

For a thick shell (h = 0.1069") or thin shell (h = 0.0514"), Equation (2.25b) and (2.25c) predicts the natural frequencies with 10% accuracy for $n \geq 6$ for the lower branch and $n \geq 3$ for the upper branch. These approximations are better than those given by Feit and Junger [18] which eliminates the unity in Equation (2.25b). The unity in the formula for the lower branch represents the membrane energy and the first term represents the bending energy. Thus, neglecting this factor, the 10% accuracy can only be obtained for $n \geq 20$ for the lower branch. If n is large enough, the unity can be neglected and the shell resonances approach those of a plate of equivalent surface, i.e., the shell resonances fall in the so-called "plate range," where the curvature effects are no longer important. When $\Omega < 1$, the lower branch roots given by Equation (2.25a) are within 5% for $n \leq 10$. These frequencies are shown in Figure 2.3.

The modal mechanical impedance of a spherical shell is independent of the type of excitation. It just indicates how the shell

itself responds to a modal force. In order to determine the modal mechanical impedance of a shell, the problem of the forced vibration of a shell in vacuo shall be considered. Since the structure is in vacuo, there is no fluid pressure acting on the shell. The modal fluid pressure p_{rn} in Equation (2.22) should be set to zero. Then, solving the equations of motion in Equations (2.21) and (2.22), one obtains the modal mechanical impedance of the spherical shell:

$$Z_{mn} = \frac{p_{in}}{\dot{W}_n} = \frac{p_{in}}{-i\omega W_n} = -\frac{iEh}{(1-\nu^2)\omega a}\frac{N_n}{D_n} \quad , \qquad (2.26)$$

where

$$N_n = (1-\nu^2)^2\Omega^4 - [\beta\lambda_n^2 + (1+\beta\nu)\lambda_n + 1 + 3\nu - \beta(1-\nu)](1-\nu^2)\Omega^2$$

$$+ \beta\lambda_n^3 - 4\beta\lambda_n^2 + [\beta(5-\nu^2) + (1-\nu^2)]\lambda_n - 2(1+\beta)(1-\nu^2),$$

and

$$D_n = -(1+\beta)\lambda_n + (1-\nu)(1+\beta) + (1-\nu^2)\Omega^2 \quad .$$

When $\beta = 0$, Z_{mn} reduces to the modal mechanical impedance of a membrane shell [8]. The modal ratio of the tangential to radial displacement amplitude U_n/W_n is obtained from Equation (2.21) as follows:

$$\frac{U_n}{W_n} = \frac{\beta[\lambda_n - (1-\nu)] + (1+\nu)}{(1+\beta)[\lambda_n - (1-\nu)] - (1-\nu^2)\Omega^2} \quad . \qquad (2.27)$$

The modal ratio depends on the excitation frequency Ω . The modal ratio for two duralumin spherical shells at the natural frequencies is shown in Tables 2.1, 2.2, and 2.3. It decreases with increasing n (and natural frequency) for the lower branch, while it is fairly constant for the upper branch.

2.4 The Derivation of the Equations of Motion of a Spherical Shell in Terms of Generalized Coordinates

Although the equations of motion of a spherical shell have been derived, the derivation of the dynamic equation in terms of generalized coordinates is also necessary. Equations (2.21) and (2.22) in terms of the tangential and the radial displacements cannot, in some ways, provide a clear-cut mathematical model from which one can immediately identify physical properties. However, when the dynamic equations are expressed in the form of a differential equation in terms of generalized coordinates, the model is mathematically identical to that of a single oscillator system.

A derivation of the shell's dynamic equations is accomplished by applying Hamilton's principle as presented in Section 2.2. The displacements u and w are expressed in terms of generalized coordinates as follows:

$$u = \sum \bar{U}_n(\theta) q_n(t) \tag{2.28}$$

and

$$w = \sum \bar{W}_n(\theta) q_n(t) \quad , \tag{2.29}$$

where $\bar{U}_n$ and $\bar{W}_n$ are the mode shapes of the tangential and the radial component of the displacement as defined in Section 2.2, and $q_n(t)$ are the generalized coordinates.

Following the preceding derivation, the variation of the kinetic energy and the potential function of external forces are:

$$\delta T = \bar{\mu} (\bar{U}_n^2 + \bar{W}_n^2) \ddot{q}_n \delta q_n \tag{2.30}$$

and

$$\delta Q = -(P_u \bar{U}_n + P_w \bar{W}_n)\delta q_n \quad , \tag{2.31}$$

where $\bar{\mu} = \rho_s h$ is the surface density of the shell, P_u and P_w are the external forces on the surface of the shell in tangential and radial directions, respectively, and $\ddot{q}_n$ represents the acceleration.

For the free vibration of the shell, $\delta Q = 0$, and $q_n(t) = \exp(-i\omega t)$, where ω is the natural frequency root of Equation (2.23), then, from Hamilton's variational principle, one obtains the strain energy:

$$\int \delta \bar{V} ds = \int \delta T ds$$

$$= -\bar{\mu}\omega_n^2 q_n \delta q_n \int_s (\bar{U}_n^2 + \bar{W}_n^2) ds \quad , \tag{2.32}$$

where ω_n is the natural frequency of the n^{th} mode.

For the forced vibration, one has the equation of motion expressed in terms of generalized coordinates:

$$\ddot{q}_n + \omega_n^2 q_n = \frac{F_n(t)}{M_n} \quad , \tag{2.33}$$

where the generalized force is:

$$F_n(t) = \int_s (P_u \bar{U}_n + P_w \bar{W}_n) ds \quad , \tag{2.34}$$

and the generalized mass (modal mass) is:

$$M_n = \bar{\mu} \int_s (\bar{U}_n^2 + \bar{W}_n^2) ds \quad . \tag{2.35}$$

For a spherical shell:

$$M_n = \bar{\mu} \int_0^{2\pi} \int_0^{\pi} (\bar{U}_n^2 + \bar{W}_n^2) a^2 \sin\theta \, d\theta d\phi$$

$$= 2\pi a^2 \bar{\mu} \int_{-1}^{+1} \left[\frac{U_n^2}{W_n^2} (1 - \eta^2) \left(\frac{dP_n(\eta)}{d\eta} \right)^2 + P_n^2(\eta) \right] d\eta, \quad (2.36)$$

where

$$\bar{U}_n(\eta) = \frac{U_n}{W_n} \sqrt{1 - \eta^2} \frac{dP_n}{d\eta}$$

and

$$\bar{W}_n(\eta) = P_n(\eta) \quad . \quad (2.37)$$

Using the following integrals:

$$\int_{-1}^{+1} (1 - \eta^2) \left(\frac{dP_n(\eta)}{d\eta} \right)^2 d\eta = \frac{2n(n+1)}{2n+1}$$

and

$$\int_{-1}^{+1} P_n^2(\eta) d\eta = \frac{2}{2n+1} \quad ,$$

one has:

$$M_n = \frac{4\pi a^2 \bar{\mu}}{2n+1} \left[\lambda_n \left(\frac{U_n}{W_n} \right)^2 + 1 \right] = \frac{M}{2n+1} S_n \quad , \quad (2.38)$$

where $S_n = \lambda_n (U_n/W_n)^2 + 1$ is the mode shape factor of the shell, M is the total mass of the shell.

Three kinds of forces will be considered, namely, the excitation force, the reactive acoustic pressure, and the internal structural damping force of the system. The generalized applied force, acting normally on the surface, is given by:

$$F_{1n} = \int_s P_{w1} \bar{W}_n \, ds$$

$$= 2\pi a^2 \int_{-1}^{+1} \bar{W}_n \, p_{in} \, d\eta \quad , \tag{2.39}$$

and the acoustic pressure on the surface of an axisymmetric shell is:

$$p_{rn} = - Z_{an} \dot{\bar{W}}_n = - Z_{an} \bar{W}_n \dot{q}_n \quad , \tag{2.40}$$

where the acoustic impedance is:

$$Z_{an} = i\rho c \frac{h_n^{(1)}(ka)}{h_n^{(1)\prime}(ka)} = r_{an} - i\omega M_{an} \quad , \tag{2.41}$$

where r_{an} and M_{an} represent the modal acoustic resistance and reactance (virtual mass), respectively. Substituting Equation (2.40) into Equation (2.34), one has the generalized acoustic pressure:

$$F_{2n} = - Z_{an} \dot{q}_n \int_s \bar{W}_n^2 \, ds \quad . \tag{2.42}$$

By applying Equation (2.37), F_{2n} becomes:

$$F_{2n} = - \frac{4\pi a^2}{2n+1} [r_{an} \dot{q}_n + M_{an} \ddot{q}_n] \quad . \tag{2.43}$$

In order to derive the structural damping force, consider the damping force to be proportional to the velocity, and the generalized force thus becomes:

$$F_{3n} = - K\dot{q}_n \int_0^{2\pi} \int_{-1}^{+1} \left(\frac{\bar{U}_n^2}{\bar{W}_n^2} + 1 \right) \bar{W}_n^2 \, a^2 \, d\eta d\phi \quad , \tag{2.44}$$

where K is a proportional constant. By using the result of Equation (2.38), one obtains:

$$F_{3n} = - M_n K \dot{q}_n \quad . \tag{2.45}$$

Replacing the generalized forces in Equation (2.33), the modal dynamic equation of the shell becomes:

$$(M_{an} + \bar{\mu}S_n)\ddot{q}_n + (r_{an} + r_{sn})\dot{q}_n + \omega_n^2 \bar{\mu} S_n q_n = f_n \quad , \tag{2.46}$$

where $r_{sn} = KS_n$, and $f_n = \frac{2n+1}{2} \int_{-1}^{+1} \bar{W}_n \, p_{in} d\eta$.

It is evident that the differential Equation (2.46) is similar to that of a damped single oscillator [12]. The coefficient of $\ddot{q}_n$ represents the total mass, M_t, of the system which is the sum of the modal mass, M_n, of the shell and the accelerated fluid virtual mass [12] due to the fluid loading. The coefficient of $\dot{q}_n$, consisting of the radiation resistance, r_{an}, and the structural resistance, r_{sn}, corresponds to the resistance factor, R_f. The coefficient of q_n corresponds to the stiffness of the shell's elasticity.

Rewriting Equation (2.46), one obtains:

$$\ddot{q}_n + \frac{\frac{K}{\bar{\mu}} + \frac{r_n}{\bar{\mu}S_n}}{1 + \frac{M_{an}}{\bar{\mu}S_n}} \dot{q}_n + \frac{\omega_n^2}{1 + \frac{M_{an}}{\bar{\mu}S_n}} q_n = \frac{\int_{-1}^{+1} \bar{W}_n p_{in} d\eta}{\left(1 + \frac{M_{an}}{\bar{\mu}S_n}\right)\left(\frac{2}{2n+1}\right)\bar{\mu}S_n} \quad . \tag{2.47}$$

For a freely vibrating shell in an acoustic medium, let $q_n = A_n \exp(-i\bar{\omega}_n t)$, where the natural frequency of the submerged shell $\bar{\omega}_n$, Equation (2.47) gives an expression for $\bar{\omega}_n$ as:

$$\bar{\omega}_n^2 = \frac{\omega_n^2}{1 + \frac{M_{an}}{\bar{\mu}S_n}} = \frac{\omega_n^2}{1 + M_R} \quad , \tag{2.48}$$

where ω_n is the natural frequency in vacuo, and the factor, $M_R = M_{an}/\bar{\mu}S_n$, represents the ratio of the additional fluid virtual mass to the unloaded shell modal mass.

It is evident from Equation (2.48) that the resonant frequency of a submerged shell is affected by the virtual mass, M_{an}, and the modal mass, $M_n = \bar{\mu}S_n$. In other words, it is determined by the mass loading factor, M_R. The virtual mass, which is a function of the frequency, adds to the inertia of the shell. The contribution of this mass to the total mass of the system depends on the acoustic characteristic impedance ρc. The modal normalized acoustic resistance, $r_{an}/\rho c$, and reactance, $M_{an}/\rho a$, are computed from Equation (2.40) and plotted in Figures 2.4 and 2.5, vs the nondimensional frequency ka, respectively. The modal reactance increases with frequency and then decreases rapidly toward zero as the frequency increases. It means that the virtual mass is low at high frequencies. The normalized modal acoustic resistance increases from zero to peak value before it reaches its asymptotic value of unity for high frequencies.

The natural frequencies of a submerged shell $\bar{\omega}_n$ are obtained from Equation (2.48) by use of an iteration technique, since the natural frequencies in vacuo, ω_n, are already known. These are tabulated in Tables 2.4 and 2.5 for the two shells and plotted in Figures 2.6 and 2.7. It is evident that the submerged shell natural frequencies of the lower branch are lower than those for a shell in vacuo. However, the submerged shell natural frequencies of the lower branch approach those for a shell in vacuo at high frequencies. This is evident when one examines Equation (2.48) since M_{an} vanishes for high frequencies. However, for a shell vibrating in air, the natural frequencies are the

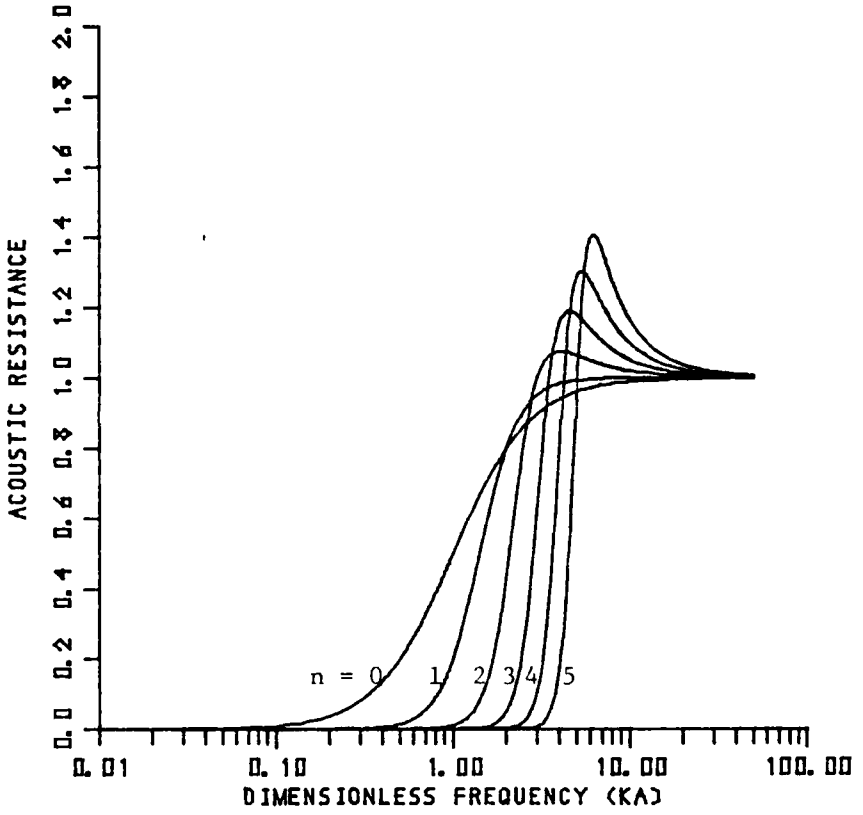

Figure 2.4 Normalized acoustic resistance curves, $Re(Z_a)/\rho c$

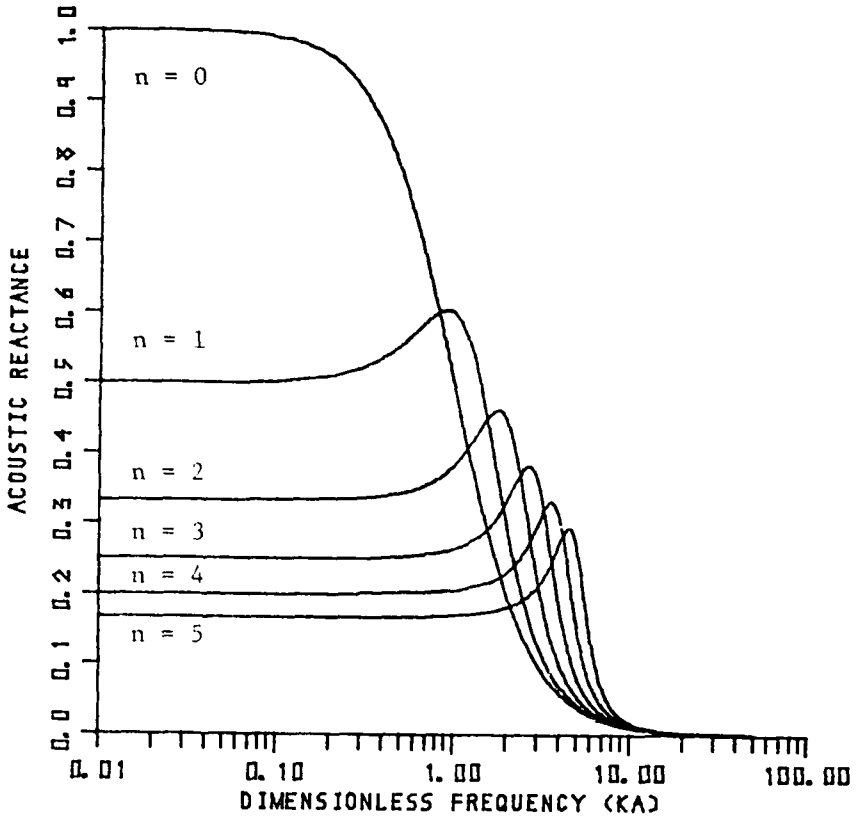

Figure 2.5 Normalized acoustic reactance curves, $\mathrm{Im}(Z_a)/\rho a$

TABLE 2.4

RESONANCE FREQUENCIES OF A SPHERICAL DURALUMIN CLASSICAL SHELL
WITH THICKNESS h = 0.0514" AND RADIUS a = 8" IN AIR - CLASSICAL THEORY

	N	Ω	U_n/W_n	Loss	M_R	M_n/M	$\overline{\mu S}_n$	M_{an}
Lower Branch	2	0.729E+00	0.275E+00	0.214E-02	0.212E-03	0.291E+00	0.411E-04	0.873E-08
	3	0.867E+00	0.125E+00	0.223E-02	0.191E-03	0.170E+00	0.336E-04	0.642E-08
	4	0.923E+00	0.719E-01	0.230E-02	0.192E-03	0.123E+00	0.312E-04	0.600E-08
	5	0.954E+00	0.468E-01	0.236E-02	0.201E-03	0.969E-01	0.302E-04	0.607E-08
	6	0.976E+00	0.330E-01	0.243E-02	0.216E-03	0.804E-01	0.296E-04	0.638E-08
	7	0.996E+00	0.245E-01	0.249E-02	0.235E-03	0.689E-01	0.293E-04	0.687E-08
	8	0.102E+01	0.190E-01	0.256E-02	0.258E-03	0.604E-01	0.291E-04	0.749E-08
	9	0.105E+01	0.151E-01	0.262E-02	0.284E-03	0.537E-01	0.289E-04	0.820E-08
	10	0.108E+01	0.123E-01	0.267E-02	0.310E-03	0.484E-01	0.288E-04	0.893E-08
	11	0.112E+01	0.103E-01	0.269E-02	0.333E-03	0.441E-01	0.287E-04	0.955E-08
	12	0.117E+01	0.868E-02	0.268E-02	0.346E-03	0.405E-01	0.287E-04	0.991E-08
	13	0.123E+01	0.743E-02	0.262E-02	0.345E-03	0.374E-01	0.286E-04	0.988E-08
	14	0.131E+01	0.644E-02	0.253E-02	0.329E-03	0.348E-01	0.286E-04	0.939E-08
	15	0.139E+01	0.563E-02	0.240E-02	0.299E-03	0.325E-01	0.285E-04	0.852E-08
	16	0.148E+01	0.497E-02	0.225E-02	0.260E-03	0.305E-01	0.285E-04	0.741E-08
	17	0.159E+01	0.442E-02	0.208E-02	0.218E-03	0.287E-01	0.285E-04	0.622E-08
	18	0.171E+01	0.396E-02	0.190E-02	0.179E-03	0.272E-01	0.285E-04	0.509E-08
	19	0.184E+01	0.356E-02	0.174E-02	0.144E-03	0.258E-01	0.285E-04	0.411E-08
	20	0.198E+01	0.323E-02	0.158E-02	0.116E-03	0.245E-01	0.284E-04	0.329E-08
	21	0.213E+01	0.293E-02	0.143E-02	0.925E-04	0.233E-01	0.284E-04	0.263E-08
	22	0.229E+01	0.268E-02	0.130E-02	0.742E-04	0.223E-01	0.284E-04	0.211E-08
	23	0.246E+01	0.246E-02	0.119E-02	0.599E-04	0.213E-01	0.284E-04	0.170E-08
	24	0.264E+01	0.227E-02	0.109E-02	0.487E-04	0.205E-01	0.284E-04	0.138E-08
	25	0.283E+01	0.209E-02	0.994E-03	0.399E-04	0.197E-01	0.284E-04	0.113E-08
	26	0.303E+01	0.194E-02	0.913E-03	0.329E-04	0.189E-01	0.284E-04	0.934E-09

TABLE 2.4 (continued)

	N	Ω	U_n/W_n	Loss	M_R	M_n/M	$\overline{\mu S}_n$	M_{an}
	27	0.324E+01	0.180E-02	0.841E-03	0.274E-04	0.182E-01	0.284E-04	0.777E-09
	28	0.346E+01	0.168E-02	0.777E-03	0.230E-04	0.176E-01	0.284E-04	0.652E-09
	29	0.369E+01	0.157E-02	0.719E-03	0.194E-04	0.170E-01	0.284E-04	0.550E-09
	30	0.393E+01	0.147E-02	0.668E-03	0.165E-04	0.164E-01	0.284E-04	0.468E-09
	31	0.417E+01	0.138E-02	0.622E-03	0.141E-04	0.159E-01	0.284E-04	0.401E-09
	32	0.443E+01	0.130E-02	0.581E-03	0.122E-04	0.154E-01	0.284E-04	0.345E-09
	33	0.469E+01	0.123E-02	0.543E-03	0.105E-04	0.150E-01	0.284E-04	0.299E-09
	34	0.496E+01	0.116E-02	0.509E-03	0.917E-05	0.145E-01	0.284E-04	0.260E-09
	35	0.524E+01	0.110E-02	0.478E-03	0.803E-05	0.141E-01	0.284E-04	0.228E-09
	36	0.553E+01	0.104E-02	0.450E-03	0.705E-05	0.137E-01	0.284E-04	0.200E-09
	37	0.583E+01	0.986E-03	0.425E-03	0.623E-05	0.134E-01	0.284E-04	0.177E-09
	38	0.614E+01	0.937E-03	0.401E-03	0.552E-05	0.130E-01	0.284E-04	0.157E-09
	39	0.645E+01	0.892E-03	0.380E-03	0.491E-05	0.127E-01	0.284E-04	0.139E-09
	40	0.678E+01	0.850E-03	0.360E-03	0.439E-05	0.124E-01	0.284E-04	0.124E-09
	41	0.711E+01	0.812E-03	0.341E-03	0.393E-05	0.121E-01	0.283E-04	0.111E-09
	42	0.745E+01	0.776E-03	0.324E-03	0.353E-05	0.118E-01	0.283E-04	0.100E-09
	43	0.780E+01	0.742E-03	0.309E-03	0.319E-05	0.115E-01	0.283E-04	0.903E-10
	44	0.816E+01	0.711E-03	0.294E-03	0.288E-05	0.112E-01	0.283E-04	0.816E-10
	45	0.852E+01	0.681E-03	0.280E-03	0.261E-05	0.110E-01	0.283E-04	0.740E-10
	46	0.890E+01	0.654E-03	0.268E-03	0.237E-05	0.108E-01	0.283E-04	0.672E-10
	47	0.928E+01	0.628E-03	0.256E-03	0.216E-05	0.105E-01	0.283E-04	0.612E-10
	48	0.967E+01	0.604E-03	0.245E-03	0.197E-05	0.103E-01	0.283E-04	0.559E-10
	49	0.101E+02	0.581E-03	0.235E-03	0.180E-05	0.101E-01	0.283E-04	0.512E-10
Upper	0	0.173E+01	-0.400E+00	0.128E-02	0.507E-04	0.100E+01	0.283E-04	0.143E-08
Branch	1	0.212E+01	-0.500E+00	0.699E-03	0.226E-04	0.500E+00	0.425E-04	0.960E-09
	2	0.291E+01	-0.607E+00	0.238E-03	0.562E-05	0.642E+00	0.910E-04	0.511E-09
	3	0.388E+01	-0.666E+00	0.910E-04	0.162E-05	0.903E+00	0.179E-03	0.289E-09
	4	0.489E+01	-0.696E+00	0.427E-04	0.600E-06	0.119E+01	0.303E-03	0.182E-09
	5	0.593E+01	-0.712E+00	0.232E-04	0.269E-06	0.147E+01	0.459E-03	0.124E-09
	6	0.697E+01	-0.721E+00	0.140E-04	0.138E-06	0.176E+01	0.647E-03	0.894E-10
	7	0.802E+01	-0.728E+00	0.905E-05	0.776E-07	0.205E+01	0.870E-03	0.675E-10

TABLE 2.5

RESONANCE FREQUENCIES OF A SPHERICAL DURALUMIN CLASSICAL SHELL
WITH THICKNESS h = 0.1069" AND RADIUS a = 8" IN AIR - CLASSICAL THEORY

	N	Ω	U_n/W_n	Loss	M_R	M_n/M	$\overline{\mu S}_n$	M_{an}
Lower Branch	2	0.729E+00	0.274E+00	0.445E-02	0.442E-03	0.290E+00	0.198E-04	0.874E-08
	3	0.866E+00	0.125E+00	0.464E-02	0.397E-03	0.170E+00	0.162E-04	0.643E-08
	4	0.921E+00	0.718E-01	0.480E-02	0.402E-03	0.123E+00	0.150E-04	0.603E-08
	5	0.949E+00	0.468E-01	0.495E-02	0.424E-03	0.969E-01	0.145E-04	0.615E-08
	6	0.965E+00	0.330E-01	0.512E-02	0.462E-03	0.804E-01	0.142E-04	0.658E-08
	7	0.977E+00	0.245E-01	0.532E-02	0.517E-03	0.689E-01	0.141E-04	0.728E-08
	8	0.987E+00	0.189E-01	0.557E-02	0.597E-03	0.603E-01	0.140E-04	0.834E-08
	9	0.997E+00	0.151E-01	0.587E-02	0.713E-03	0.537E-01	0.139E-04	0.990E-08
	10	0.101E+01	0.123E-01	0.625E-02	0.883E-03	0.484E-01	0.138E-04	0.122E-07
	11	0.102E+01	0.102E-01	0.671E-02	0.114E-02	0.441E-01	0.138E-04	0.158E-07
	12	0.103E+01	0.865E-02	0.726E-02	0.155E-02	0.405E-01	0.138E-04	0.213E-07
	13	0.105E+01	0.741E-02	0.789E-02	0.220E-02	0.374E-01	0.138E-04	0.302E-07
	14	0.107E+01	0.641E-02	0.850E-02	0.322E-02	0.348E-01	0.137E-04	0.443E-07
	15	0.110E+01	0.561E-02	0.884E-02	0.473E-02	0.325E-01	0.137E-04	0.649E-07
	16	0.112E+01	0.494E-02	0.850E-02	0.658E-02	0.305E-01	0.137E-04	0.901E-07
	17	0.116E+01	0.439E-02	0.730E-02	0.817E-02	0.287E-01	0.137E-04	0.112E-06
	18	0.119E+01	0.393E-02	0.568E-02	0.897E-02	0.272E-01	0.137E-04	0.123E-06
	19	0.124E+01	0.354E-02	0.425E-02	0.904E-02	0.258E-01	0.137E-04	0.124E-06
	20	0.129E+01	0.320E-02	0.325E-02	0.875E-02	0.245E-01	0.137E-04	0.120E-06
	21	0.134E+01	0.291E-02	0.264E-02	0.838E-02	0.233E-01	0.137E-04	0.115E-06
	22	0.140E+01	0.265E-02	0.232E-02	0.806E-02	0.223E-01	0.137E-04	0.110E-06
	23	0.147E+01	0.243E-02	0.223E-02	0.783E-02	0.213E-01	0.137E-04	0.107E-06
	24	0.154E+01	0.224E-02	0.233E-02	0.768E-02	0.205E-01	0.137E-04	0.105E-06
	25	0.161E+01	0.207E-02	0.262E-02	0.758E-02	0.197E-01	0.137E-04	0.103E-06
	26	0.169E+01	0.191E-02	0.313E-02	0.746E-02	0.189E-01	0.137E-04	0.102E-06

TABLE 2.5 (continued)

	N	Ω	U_n/W_n	Loss	M_R	M_n/M	$\bar{\mu}S_n$	M_{an}
	27	0.178E+01	0.178E-02	0.384E-02	0.721E-02	0.182E-01	0.136E-04	0.984E-07
	28	0.187E+01	0.166E-02	0.470E-02	0.666E-02	0.176E-01	0.136E-04	0.909E-07
	29	0.197E+01	0.155E-02	0.549E-02	0.571E-02	0.170E-01	0.136E-04	0.779E-07
	30	0.208E+01	0.145E-02	0.591E-02	0.445E-02	0.164E-01	0.136E-04	0.607E-07
	31	0.219E+01	0.136E-02	0.585E-02	0.320E-02	0.159E-01	0.136E-04	0.436E-07
	32	0.230E+01	0.127E-02	0.546E-02	0.219E-02	0.154E-01	0.136E-04	0.299E-07
	33	0.242E+01	0.120E-02	0.493E-02	0.148E-02	0.149E-01	0.136E-04	0.202E-07
	34	0.254E+01	0.113E-02	0.440E-02	0.101E-02	0.145E-01	0.136E-04	0.138E-07
	35	0.267E+01	0.107E-02	0.392E-02	0.705E-03	0.141E-01	0.136E-04	0.961E-08
	36	0.280E+01	0.101E-02	0.351E-02	0.505E-03	0.137E-01	0.136E-04	0.688E-08
	37	0.294E+01	0.959E-03	0.316E-02	0.371E-03	0.134E-01	0.136E-04	0.506E-08
	38	0.308E+01	0.910E-03	0.286E-02	0.280E-03	0.130E-01	0.136E-04	0.382E-08
	39	0.322E+01	0.865E-03	0.260E-02	0.216E-03	0.127E-01	0.136E-04	0.295E-08
	40	0.337E+01	0.823E-03	0.239E-02	0.170E-03	0.124E-01	0.136E-04	0.232E-08
	41	0.353E+01	0.784E-03	0.220E-02	0.137E-03	0.121E-01	0.136E-04	0.186E-08
	42	0.369E+01	0.748E-03	0.203E-02	0.111E-03	0.118E-01	0.136E-04	0.152E-08
	43	0.385E+01	0.714E-03	0.189E-02	0.920E-04	0.115E-01	0.136E-04	0.125E-08
	44	0.402E+01	0.683E-03	0.176E-02	0.770E-04	0.112E-01	0.136E-04	0.105E-08
	45	0.419E+01	0.653E-03	0.165E-02	0.651E-04	0.110E-01	0.136E-04	0.887E-09
	46	0.437E+01	0.626E-03	0.155E-02	0.555E-04	0.108E-01	0.136E-04	0.757E-09
	47	0.455E+01	0.600E-03	0.145E-02	0.478E-04	0.105E-01	0.136E-04	0.651E-09
	48	0.473E+01	0.576E-03	0.137E-02	0.414E-04	0.103E-01	0.136E-04	0.565E-09
	49	0.492E+01	0.553E-03	0.130E-02	0.362E-04	0.101E-01	0.136E-04	0.493E-09
Upper Branch	0	0.173E+01	-0.400E+00	0.267E-02	0.105E-03	0.100E+01	0.136E-04	0.143E-08
	1	0.212E+01	-0.500E+00	0.145E-02	0.470E-04	0.500E+00	0.204E-04	0.960E-09
	2	0.291E+01	-0.607E+00	0.495E-03	0.117E-04	0.642E+00	0.437E-04	0.511E-09
	3	0.388E+01	-0.666E+00	0.189E-03	0.336E-05	0.903E+00	0.861E-04	0.289E-09
	4	0.489E+01	-0.696E+00	0.887E-04	0.125E-05	0.119E+01	0.146E-03	0.182E-09
	5	0.593E+01	-0.713E+00	0.482E-04	0.560E-06	0.148E+01	0.221E-03	0.124E-09
	6	0.697E+01	-0.724E+00	0.289E-04	0.285E-06	0.177E+01	0.313E-03	0.894E-10
	7	0.802E+01	-0.728E+00	0.189E-04	0.162E-06	0.205E+01	0.418E-03	0.675E-10

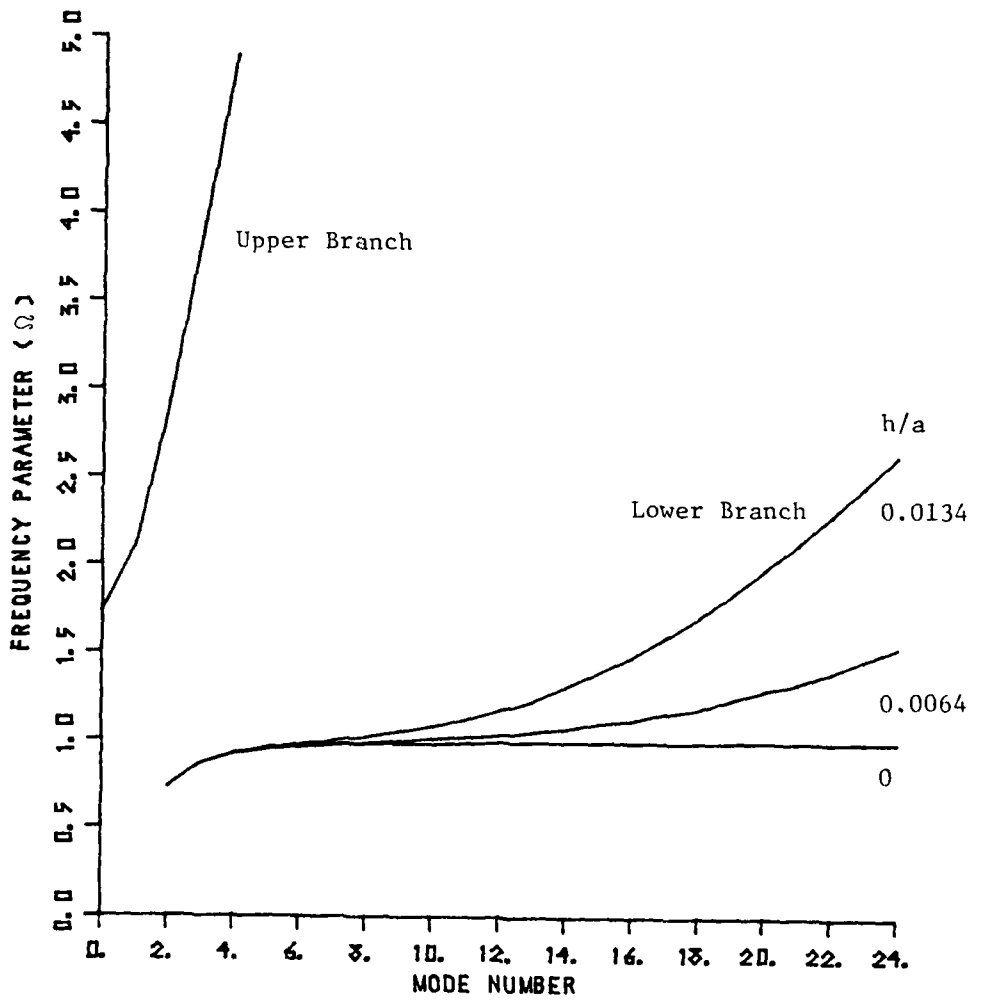

Figure 2.6 Dimensionless frequency Ω for various modes when spherical shells are submerged in air

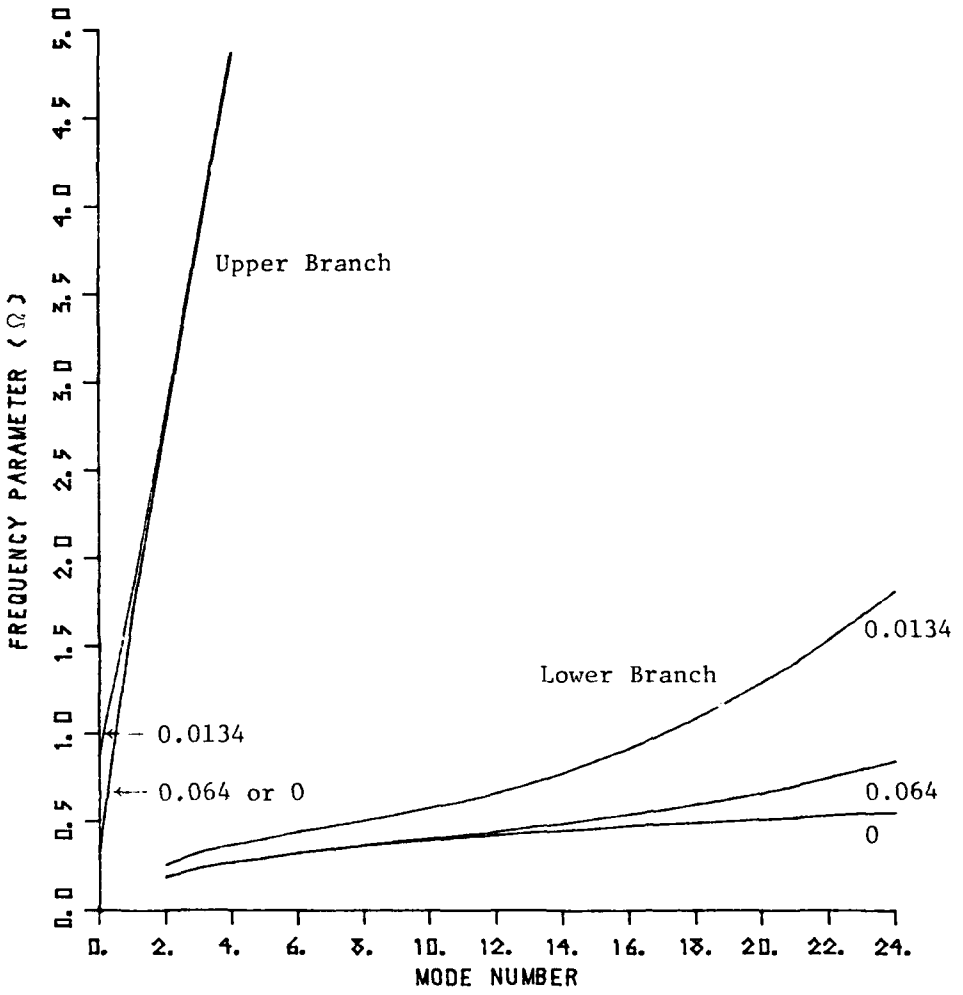

Figure 2.7 Dimensionless frequency Ω for various modes when spherical shells are submerged in water

same as those for a shell in vacuo for both branches (see Figures 2.3 and 2.6) because of the light acoustic loading.

For a shell submerged in water (heavy fluid loading), the factor M_R for the lower branch is significant when compared to unity as shown in Tables 2.6 and 2.7. The resonant frequency for a submerged shell is thus lower than the natural frequency in vacuo as shown in Figures 2.7 and 2.8. The mass loading factor, M_R, increases up to four times the mass of the shell for the mode shapes of the primarily radial modes of the lower branch $(U_n/W_n) << 1$ (strong fluid coupling) except that $(U_n/W_n) = 1$ $(\Omega_1 = 0)$ for the first mode. Thus, the natural frequencies in water are reduced significantly for the lower branch at low mode numbers. However, when M_R decreases to less than unity for high mode orders of the lower branch (higher frequencies), the natural frequencies in water are slightly decreased from those in air. For the mode shapes of the upper branch, which are primarily tangential $(U_n/W_n) < 1$ (weak fluid coupling), the virtual mass of the accelerated fluid is negligible when one examines M_R for the higher branch in Tables 2.4, 2.5, 2.6, and 2.7. In other words, the heavy fluid loading significantly influences the branch having a strong coupling (lower branch) and slightly alters the frequencies of the first few modes of the upper branch only (weak coupling).

The modal acoustical and structural loss factors, L_{an} and L_{sn}, respectively, can be defined from the modal single oscillator modal in Equation (2.46) as follows:

$$L_{an} = \frac{r_{an}}{\omega_n (M_{an} + \bar{\mu} S_n)} \quad , \tag{2.49}$$

TABLE 2.6

RESONANCE FREQUENCIES OF A SPHERICAL DURALUMIN CLASSICAL SHELL
WITH THICKNESS h = 0.0514" AND RADIUS a = 8" IN WATER

	N	Ω	U_n/W_n	Loss	M_R	M_n/M	$\overline{\mu S}_n$	M_{an}
Lower	2	0.186E+00	0.252E+00	0.276E-02	0.143E+02	0.276E+00	0.188E-04	0.270E-03
Branch	3	0.235E+00	0.118E+00	0.160E-03	0.125E+02	0.167E+00	0.159E-04	0.199E-03
	4	0.270E+00	0.693E-01	0.540E-05	0.106E+02	0.122E+00	0.149E-04	0.158E-03
	5	0.299E+00	0.456E-01	0.132E-06	0.906E+01	0.966E-01	0.145E-04	0.131E-03
	6	0.324E+00	0.324E-01	0.255E-08	0.787E+01	0.803E-01	0.142E-04	0.112E-03
	7	0.347E+00	0.242E-01	0.408E-10	0.695E+01	0.689E-01	0.141E-04	0.977E-04
	8	0.368E+00	0.187E-01	0.567E-12	0.621E+01	0.603E-01	0.140E-04	0.867E-04
	9	0.388E+00	0.150E-01	0.704E-14	0.561E+01	0.537E-01	0.139E-04	0.779E-04
	10	0.408E+00	0.122E-01	0.811E-16	0.511E+01	0.484E-01	0.138E-04	0.708E-04
	11	0.427E+00	0.102E-01	0.890E-18	0.470E+01	0.441E-01	0.138E-04	0.648E-04
	12	0.448E+00	0.861E-02	0.961E-20	0.434E+01	0.405E-01	0.138E-04	0.598E-04
	13	0.469E+00	0.737E-02	0.105E-21	0.404E+01	0.374E-01	0.138E-04	0.555E-04
	14	0.491E+00	0.639E-02	0.121E-23	0.377E+01	0.348E-01	0.137E-04	0.518E-04
	15	0.514E+00	0.559E-02	0.149E-25	0.354E+01	0.325E-01	0.137E-04	0.485E-04
	16	0.540E+00	0.493E-02	0.203E-27	0.333E+01	0.305E-01	0.137E-04	0.457E-04
	17	0.567E+00	0.438E-02	0.317E-29	0.315E+01	0.287E-01	0.137E-04	0.431E-04
	18	0.598E+00	0.392E-02	0.586E-31	0.298E+01	0.272E-01	0.137E-04	0.409E-04
	19	0.631E+00	0.353E-02	0.130E-32	0.284E+01	0.258E-01	0.137E-04	0.388E-04
	20	0.668E+00	0.319E-02	0.352E-34	0.270E+01	0.245E-01	0.137E-04	0.370E-04
	21	0.708E+00	0.290E-02	0.116E-35	0.258E+01	0.233E-01	0.137E-04	0.353E-04
	22	0.751E+00	0.265E-02	0.462E-37	0.247E+01	0.223E-01	0.137E-04	0.338E-04
	23	0.798E+00	0.243E-02	0.225E-38	0.237E+01	0.213E-01	0.137E-04	0.324E-04
	24	0.849E+00	0.223E-02	0.133E-39	0.228E+01	0.205E-01	0.137E-04	0.311E-04
	25	0.903E+00	0.206E-02	0.951E-41	0.219E+01	0.197E-01	0.137E-04	0.299E-04
	26	0.961E+00	0.191E-02	0.817E-42	0.211E+01	0.189E-01	0.137E-04	0.288E-04

TABLE 2.6 (continued)

	N	Ω	U_n/W_n	Loss	M_R	M_n/M	$\overline{\mu S}_n$	M_{an}
	27	0.102E+01	0.177E-02	0.838E-43	0.203E+01	0.182E-01	0.136E-04	0.278E-04
	28	0.109E+01	0.165E-02	0.102E-43	0.197E+01	0.176E-01	0.136E-04	0.268E-04
	29	0.116E+01	0.154E-02	0.149E-44	0.190E+01	0.170E-01	0.136E-04	0.259E-04
	30	0.123E+01	0.144E-02	0.253E-45	0.184E+01	0.164E-01	0.136E-04	0.251E-04
	31	0.131E+01	0.135E-02	0.494E-46	0.178E+01	0.159E-01	0.136E-04	0.243E-04
	32	0.139E+01	0.127E-02	0.110E-46	0.173E+01	0.154E-01	0.136E-04	0.236E-04
	33	0.148E+01	0.120E-02	0.273E-47	0.168E+01	0.149E-01	0.136E-04	0.229E-04
	34	0.157E+01	0.113E-02	0.756E-48	0.164E+01	0.145E-01	0.136E-04	0.223E-04
	35	0.166E+01	0.107E-02	0.233E-48	0.159E+01	0.141E-01	0.136E-04	0.217E-04
	36	0.175E+01	0.101E-02	0.790E-49	0.155E+01	0.137E-01	0.136E-04	0.211E-04
	37	0.185E+01	0.955E-03	0.294E-49	0.151E+01	0.134E-01	0.136E-04	0.206E-04
	38	0.196E+01	0.907E-03	0.120E-49	0.147E+01	0.130E-01	0.136E-04	0.201E-04
	39	0.207E+01	0.862E-03	0.532E-50	0.144E+01	0.127E-01	0.136E-04	0.196E-04
	40	0.218E+01	0.820E-03	0.255E-50	0.140E+01	0.124E-01	0.136E-04	0.191E-04
	41	0.229E+01	0.781E-03	0.132E-50	0.137E+01	0.121E-01	0.136E-04	0.187E-04
	42	0.241E+01	0.745E-03	0.736E-51	0.134E+01	0.118E-01	0.136E-04	0.183E-04
	43	0.253E+01	0.711E-03	0.438E-51	0.131E+01	0.115E-01	0.136E-04	0.179E-04
	44	0.266E+01	0.680E-03	0.279E-51	0.128E+01	0.112E-01	0.136E-04	0.175E-04
	45	0.279E+01	0.651E-03	0.189E-51	0.126E+01	0.110E-01	0.136E-04	0.171E-04
	46	0.292E+01	0.623E-03	0.136E-51	0.123E+01	0.108E-01	0.136E-04	0.168E-04
	47	0.306E+01	0.598E-03	0.103E-51	0.121E+01	0.105E-01	0.136E-04	0.165E-04
	48	0.320E+01	0.573E-03	0.828E-52	0.118E+01	0.103E-01	0.136E-04	0.161E-04
	49	0.335E+01	0.551E-03	0.701E-52	0.116E+01	0.101E-01	0.136E-04	0.158E-04
Upper	0	0.339E+00	-0.174E+01	0.107E+01	0.252E+02	0.100E+01	0.136E-04	0.343E-03
Branch	1	0.170E+01	-0.109E+01	0.190E+01	0.566E+00	0.113E+01	0.461E-04	0.261E-04
	2	0.276E+01	-0.950E+00	0.889E+00	0.118E+00	0.128E+01	0.874E-04	0.103E-04
	3	0.380E+01	-0.885E+00	0.432E+00	0.387E-01	0.149E+01	0.142E-03	0.548E-05
	4	0.485E+01	-0.846E+00	0.236E+00	0.162E-01	0.170E+01	0.208E-03	0.339E-05
	5	0.591E+01	-0.820E+00	0.142E+00	0.796E-02	0.192E+01	0.289E-03	0.230E-05
	6	0.696E+01	-0.805E+00	0.907E-01	0.431E-02	0.217E+01	0.384E-03	0.166E-05
	7	0.801E+01	-0.791E+00	0.618E-01	0.255E-02	0.240E+01	0.490E-03	0.125E-05

TABLE 2.7

RESONANCE FREQUENCIES OF A SPHERICAL DURALUMIN CLASSICAL SHELL
WITH THICKNESS h = 0.1069" AND RADIUS a = 8" IN WATER

	N	Ω	U_n/W_n	Loss	M_R	M_n/M	$\overline{\mu S}_n$	M_{an}
Lower Branch	2	0.254E+00	0.253E+00	0.115E-01	0.720E+01	0.277E+00	0.392E-04	0.282E-03
	3	0.323E+00	0.119E+00	0.124E-02	0.621E+01	0.167E+00	0.331E-04	0.206E-03
	4	0.371E+00	0.695E-01	0.778E-04	0.520E+01	0.122E+00	0.311E-04	0.162E-03
	5	0.409E+00	0.458E-01	0.349E-05	0.443E+01	0.966E-01	0.301E-04	0.133E-03
	6	0.444E+00	0.324E-01	0.125E-06	0.384E+01	0.803E-01	0.296E-04	0.113E-03
	7	0.476E+00	0.242E-01	0.387E-08	0.338E+01	0.689E-01	0.292E-04	0.988E-04
	8	0.508E+00	0.188E-01	0.112E-09	0.302E+01	0.603E-01	0.290E-04	0.876E-04
	9	0.542E+00	0.150E-01	0.321E-11	0.272E+01	0.537E-01	0.289E-04	0.787E-04
	10	0.579E+00	0.123E-01	0.987E-13	0.248E+01	0.484E-01	0.288E-04	0.714E-04
	11	0.619E+00	0.102E-01	0.344E-14	0.228E+01	0.441E-01	0.287E-04	0.654E-04
	12	0.665E+00	0.863E-02	0.145E-15	0.211E+01	0.405E-01	0.286E-04	0.603E-04
	13	0.717E+00	0.740E-02	0.763E-17	0.196E+01	0.374E-01	0.286E-04	0.560E-04
	14	0.776E+00	0.641E-02	0.519E-18	0.183E+01	0.348E-01	0.286E-04	0.523E-04
	15	0.843E+00	0.561E-02	0.463E-19	0.172E+01	0.325E-01	0.285E-04	0.490E-04
	16	0.917E+00	0.495E-02	0.544E-20	0.162E+01	0.305E-01	0.285E-04	0.462E-04
	17	0.100E+01	0.440E-02	0.835E-21	0.153E+01	0.287E-01	0.285E-04	0.437E-04
	18	0.109E+01	0.394E-02	0.166E-21	0.146E+01	0.272E-01	0.285E-04	0.414E-04
	19	0.119E+01	0.355E-02	0.419E-22	0.139E+01	0.258E-01	0.285E-04	0.394E-04
	20	0.130E+01	0.321E-02	0.132E-22	0.132E+01	0.245E-01	0.284E-04	0.376E-04
	21	0.141E+01	0.292E-02	0.507E-23	0.126E+01	0.233E-01	0.284E-04	0.360E-04
	22	0.154E+01	0.267E-02	0.235E-23	0.121E+01	0.223E-01	0.284E-04	0.345E-04
	23	0.167E+01	0.245E-02	0.128E-23	0.116E+01	0.213E-01	0.284E-04	0.331E-04
	24	0.181E+01	0.225E-02	0.815E-24	0.112E+01	0.205E-01	0.284E-04	0.319E-04
	25	0.196E+01	0.208E-02	0.594E-24	0.108E+01	0.197E-01	0.284E-04	0.307E-04
	26	0.212E+01	0.193E-02	0.491E-24	0.104E+01	0.189E-01	0.284E-04	0.297E-04

TABLE 2.7 (continued)

	N	Ω	U_n/W_n	Loss	M_R	M_n/M	$\overline{\mu S}_n$	M_{an}
	27	0.229E+01	0.179E-02	0.454E-24	0.101E+01	0.182E-01	0.284E-04	0.287E-04
	28	0.246E+01	0.167E-02	0.467E-24	0.979E+00	0.176E-01	0.284E-04	0.278E-04
	29	0.264E+01	0.156E-02	0.527E-24	0.950E+00	0.170E-01	0.284E-04	0.269E-04
	30	0.283E+01	0.146E-02	0.649E-24	0.922E+00	0.164E-01	0.284E-04	0.262E-04
	31	0.303E+01	0.137E-02	0.866E-24	0.897E+00	0.159E-01	0.284E-04	0.255E-04
	32	0.323E+01	0.129E-02	0.124E-23	0.874E+00	0.154E-01	0.284E-04	0.248E-04
	33	0.345E+01	0.122E-02	0.191E-23	0.852E+00	0.150E-01	0.284E-04	0.242E-04
	34	0.367E+01	0.115E-02	0.313E-23	0.831E+00	0.145E-01	0.284E-04	0.236E-04
	35	0.390E+01	0.109E-02	0.544E-23	0.812E+00	0.141E-01	0.284E-04	0.230E-04
	36	0.413E+01	0.103E-02	0.996E-23	0.794E+00	0.137E-01	0.284E-04	0.225E-04
	37	0.437E+01	0.977E-03	0.192E-22	0.777E+00	0.134E-01	0.284E-04	0.220E-04
	38	0.463E+01	0.928E-03	0.387E-22	0.761E+00	0.130E-01	0.284E-04	0.216E-04
	39	0.488E+01	0.883E-03	0.814E-22	0.746E+00	0.127E-01	0.284E-04	0.212E-04
	40	0.515E+01	0.841E-03	0.178E-21	0.732E+00	0.124E-01	0.284E-04	0.208E-04
	41	0.542E+01	0.803E-03	0.406E-21	0.719E+00	0.121E-01	0.283E-04	0.204E-04
	42	0.570E+01	0.767E-03	0.956E-21	0.707E+00	0.118E-01	0.283E-04	0.200E-04
	43	0.599E+01	0.733E-03	0.232E-20	0.696E+00	0.115E-01	0.283E-04	0.197E-04
	44	0.628E+01	0.702E-03	0.580E-20	0.685E+00	0.112E-01	0.283E-04	0.194E-04
	45	0.659E+01	0.673E-03	0.148E-19	0.675E+00	0.110E-01	0.283E-04	0.191E-04
	46	0.689E+01	0.645E-03	0.390E-19	0.666E+00	0.108E-01	0.283E-04	0.189E-04
	47	0.721E+01	0.619E-03	0.105E-18	0.657E+00	0.105E-01	0.283E-04	0.186E-04
	48	0.753E+01	0.595E-03	0.288E-18	0.649E+00	0.103E-01	0.283E-04	0.184E-04
	49	0.786E+01	0.573E-03	0.801E-18	0.641E+00	0.101E-01	0.283E-04	0.182E-04
Upper	0	0.877E+00	-0.991E+00	0.215E+01	0.291E+01	0.100E+01	0.283E-04	0.824E-04
Branch	1	0.183E+01	-0.807E+00	0.146E+01	0.340E+00	0.767E+00	0.652E-04	0.222E-04
	2	0.281E+01	-0.792E+00	0.588E+00	0.730E-01	0.953E+00	0.135E-03	0.985E-05
	3	0.383E+01	-0.782E+00	0.261E+00	0.228E-01	0.119E+01	0.236E-03	0.539E-05
	4	0.487E+01	-0.773E+00	0.134E+00	0.915E-02	0.144E+01	0.367E-03	0.336E-05
	5	0.592E+01	-0.767E+00	0.774E-01	0.433E-02	0.170E+01	0.528E-03	0.229E-05
	6	0.697E+01	-0.762E+00	0.485E-01	0.230E-02	0.195E+01	0.718E-03	0.165E-05
	7	0.802E+01	-0.760E+00	0.321E-01	0.132E-02	0.222E+01	0.944E-03	0.125E-05

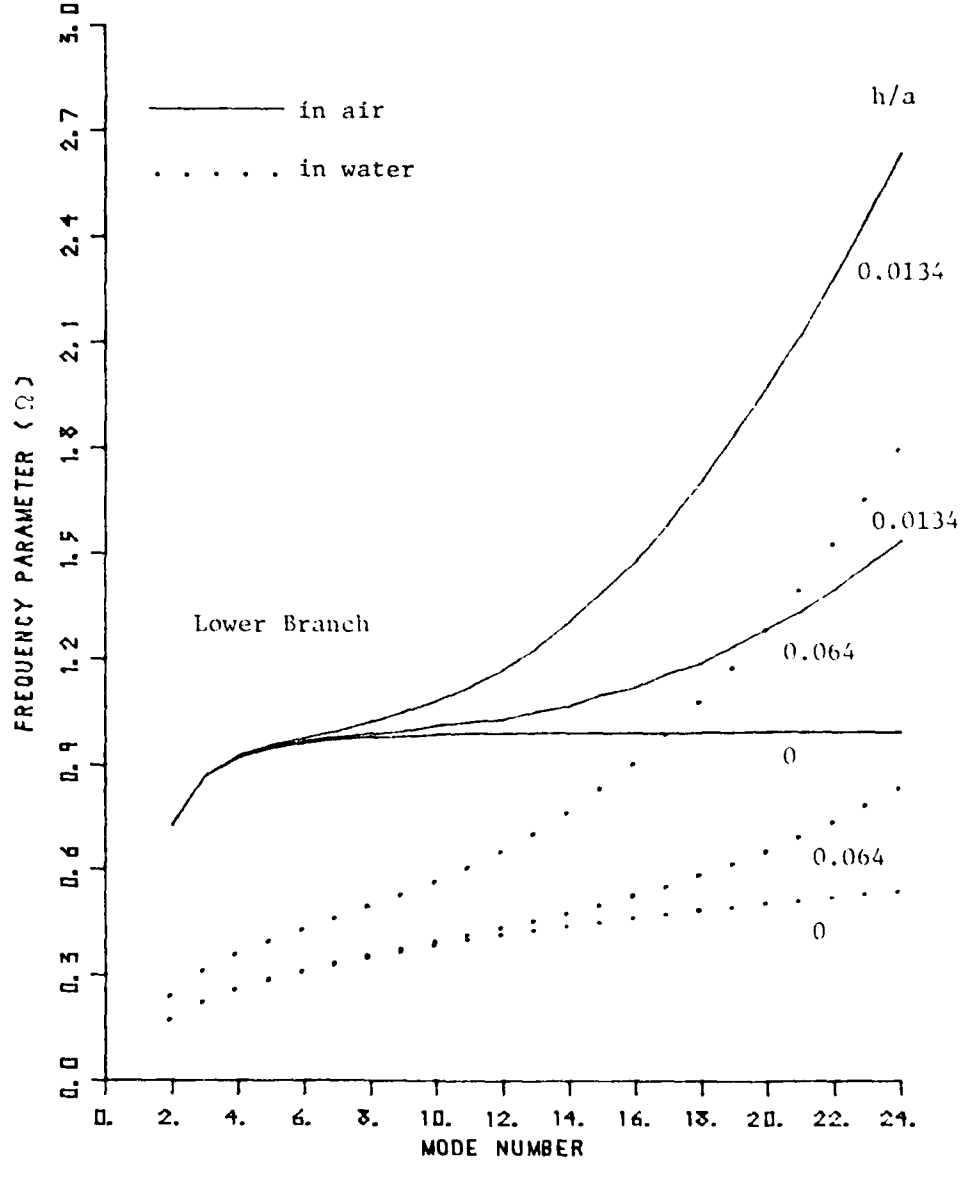

Figure 2.8 Dimensionless frequency Ω for various modes. Comparison of spherical shell in water with that in vacuo

and

$$L_{sn} = \frac{r_{sn}}{\omega_n \bar{\mu} S_n} \quad . \tag{2.50}$$

The loss factor, L_{rn}, is tabulated in Tables 2.4 and 2.5 for air and in Tables 2.6 and 2.7 for water. The total impedance is defined as:

$$Z_n = Z_{an} + Z_{mn} \quad , \tag{2.51}$$

where the acoustic impedance, Z_{an}, is given in Equation (2.41) and the mechanical impedance, Z_{mn}, is given in Equation (2.26). At resonance, the reactive part of Z_n must vanish, i.e., $Im(Z_n) = 0$. Thus, the modal impedance of the submerged shell is purely resistive at resonance. The total resistance of the submerged shell is the sum of the structural and acoustic loss factors.

2.5 The Resonance Density of Spherical Shell

In order to obtain an approximation of the shell's characteristic admittance, a study of the spherical shell's resonance density is necessary. The resonance density [12] is defined as:

$$\frac{1}{E_n} = \frac{dn}{d\omega}$$

$$= \frac{a}{C_b} \frac{dn}{d\Omega} \quad , \tag{2.52}$$

where ω is the resonant angular frequency and $C_b = (E/\rho_s)^{1/2}$. By differentiating Equation (2.23) with respect to mode number n , the resonance density is expressed as:

$$\frac{dn}{d\Omega} \cong \Omega \frac{4(1 - \nu^2)\Omega^2 - 2c_n}{a_n \Omega^2 - b_n} \quad , \tag{2.53}$$

where

$$a_n = (2n + 1)(1 + \nu\beta + 2\beta\lambda_n) \quad ,$$

$$b_n = \frac{(2n + 1)[3\beta\lambda_n^2 - 8\beta\lambda_n + \beta(5 - \nu^2) + (1 - \nu^2)]}{(1 - \nu^2)}$$

$$c_n = 1 + 3\nu - \beta(1 - \nu) + \lambda_n(1 + \nu\beta) + \beta\lambda_n^2 \quad .$$

At low frequency or in the membrane range $\Omega < 1$, the parameters in Equation (2.53) can be approximated as follows:

$$a_n \approx (2n + 1) \quad ,$$

$$b_n \approx (2n + 1)$$

and

$$c_n \approx (1 + 3\nu + \lambda_n) \quad . \tag{2.54}$$

Then, Equation (2.54) with n and λ_n substituted for Equation (2.25a) can be expressed approximately as:

$$\frac{dn}{d\Omega} \approx \frac{2\sqrt{2}\,\Omega}{(1 - \Omega^2)\sqrt{1 - \Omega^4}} \quad , \quad \Omega < 1 \quad , \tag{2.55}$$

which is independent of the shell thickness, because this is in the membrane range. In the membrane range, the resonance density increases as Ω increases [see Equation (2.55)]. The resonance density reaches a maximum [see Equations (2.53) and (2.54)] when Ω is given by:

$$\Omega^2 \approx \frac{3\beta\lambda_n^2}{1 - \nu^2} + 1 \quad . \tag{2.56}$$

Thus, the maximum resonance density is given by:

$$\frac{dn}{d\Omega} \approx 0.433/\beta^{1/2} \quad .$$

It is quite clear that, in general, the maximum point is not at $\Omega = 1$ except for a membrane maximum, when $\beta = 0$. Due to introduction of the term $\beta\lambda_n^2$, the maximum occurs at $\Omega > 1$. Actually, the resonance density is an inverse slope of the frequency curves shown in Figures 2.6 and 2.7. Thick shells' natural frequencies leave the membrane mode at higher frequency when compared to thin shells. The take-off point from the membrane curve in Figure 2.8 is the maximum point of the resonance density. Therefore, it is expected that the maximum point of the resonance density is closer to unity as the thickness of the shell decreases and that the peak becomes higher (see Figures 2.9 and 2.10). For frequencies above $\Omega = 1$, the resonance density decreases slowly with frequency.

At high frequency, $\Omega >> 1$, as the resonances approach the plate range, it is convenient to use the asymptotic form. By differentiating Equation (2.25a), the resonance density for the spherical shell becomes:

$$\frac{dn}{d\Omega} \approx \frac{1}{2}\left(\frac{1-\nu^2}{\beta}\right)^{1/4} \frac{1}{\Omega^{1/2}\left[1-\frac{1}{\Omega^2}\right]^{3/4}} \quad \text{for} \quad \Omega > 1 \ , \tag{2.57a}$$

and, in the plate range, becomes:

$$\frac{dn}{d\Omega} \approx \frac{1}{2}\left(\frac{1-\nu^2}{\beta}\right)^{1/4} \frac{1}{\Omega^{1/2}} \quad \text{for} \quad \Omega >> 1 \ , \tag{2.57b}$$

with a maximum value given by:

$$\frac{dn}{d\Omega} \approx 0.433/\beta^{1/2} \ . \tag{2.57c}$$

Figures 2.9 and 2.10 show the resonance density of the two spherical shells in vacuo. Curves (1), (2), (3), and (4) represent,

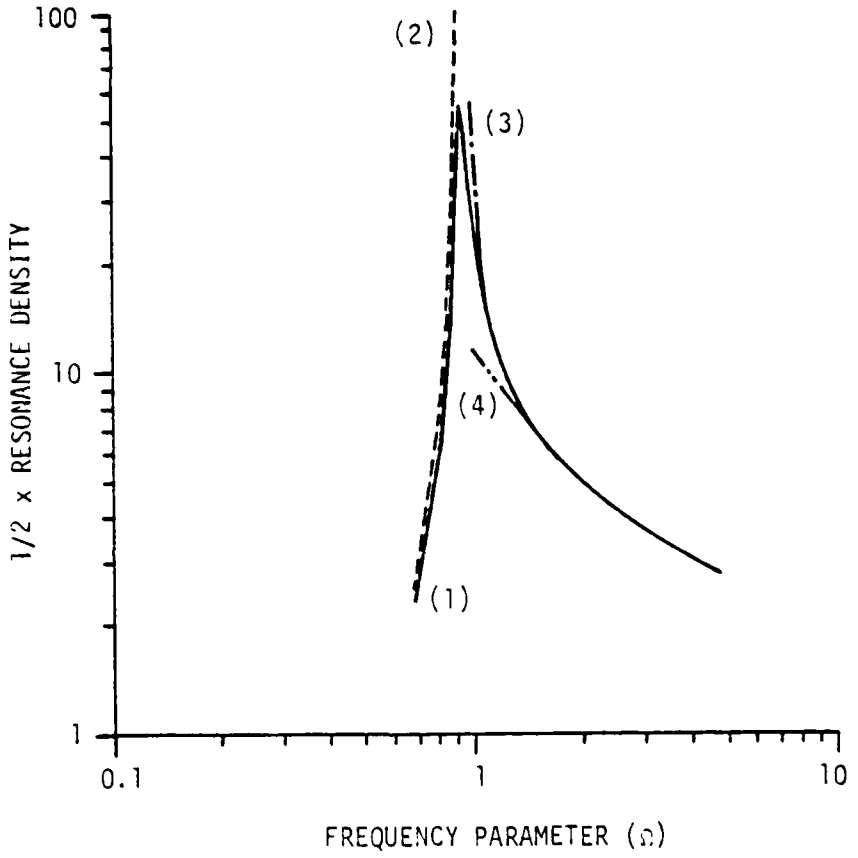

Figure 2.9 Resonance density of a spherical shell, h = 0.1069", in vacuo

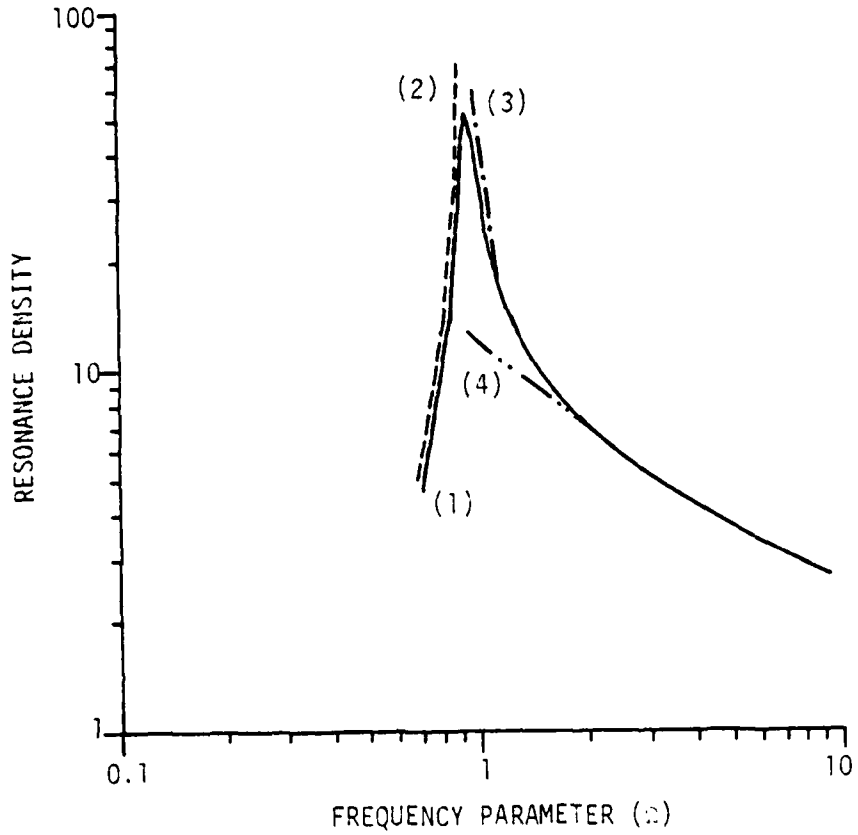

Figure 2.10 Resonance density of a spherical shell, h = 0.0514", in vacuo

respectively, the resonance density for the exact [Equation (2.53)], the low frequency approximation [Equation (2.55)], the density for midrange frequencies' approximation [Equation (2.57a)], and the high frequency plate range [Equation (2.57b)]. The maximum point in the resonance density spectrum separates the resonances into membrane range and plate range. Resonances between those two ranges are in the so-called "coupling range." The segment of Curve (1) for $\Omega > 1.5$ matches with that of Curve (4) for the plate range, and Curve (3) matches Curve (1) down to $\Omega \tilde{\sim} 1$. Curve (2) matches with Curve (1) up to $\Omega = 1.0$. In the membrane range, both shells have the same resonance density [see Equation (2.55)]. The higher resonance density of the thin shell implies that it has a higher response when one considers the driving point admittance (DPA) because the mean value of the DPA [12] is:

$$Y_c = \frac{\pi}{2E_n M_n} \quad , \tag{2.58}$$

where M_n is the modal mass of the spherical shell [Equation (2.38)]. Figure 2.11 shows the mean value of the DPA of the shells. For $\Omega > 1$,

$$Y_c = \frac{\pi a}{4C_b M_n} \frac{\left(\frac{1-\nu^2}{\beta}\right)^{1/4}}{\Omega^{1/2}\left[1-\frac{1}{\Omega^2}\right]^{3/4}} \tag{2.59}$$

and

$$Y_c \tilde{\sim} (8\alpha^2 \rho_s h)^{-1} \quad \text{for} \quad \Omega >> 1 \quad . \tag{2.60}$$

When $\Omega < 1$, E_n in Equation (2.58) is replaced by $\Delta\omega$ because the shell does not have many modes in the membrane range, and also, a 3 dB is added to Equation (2.59) due to the imaginary part of the mean value of the DPA (see Reference 12). Thus,

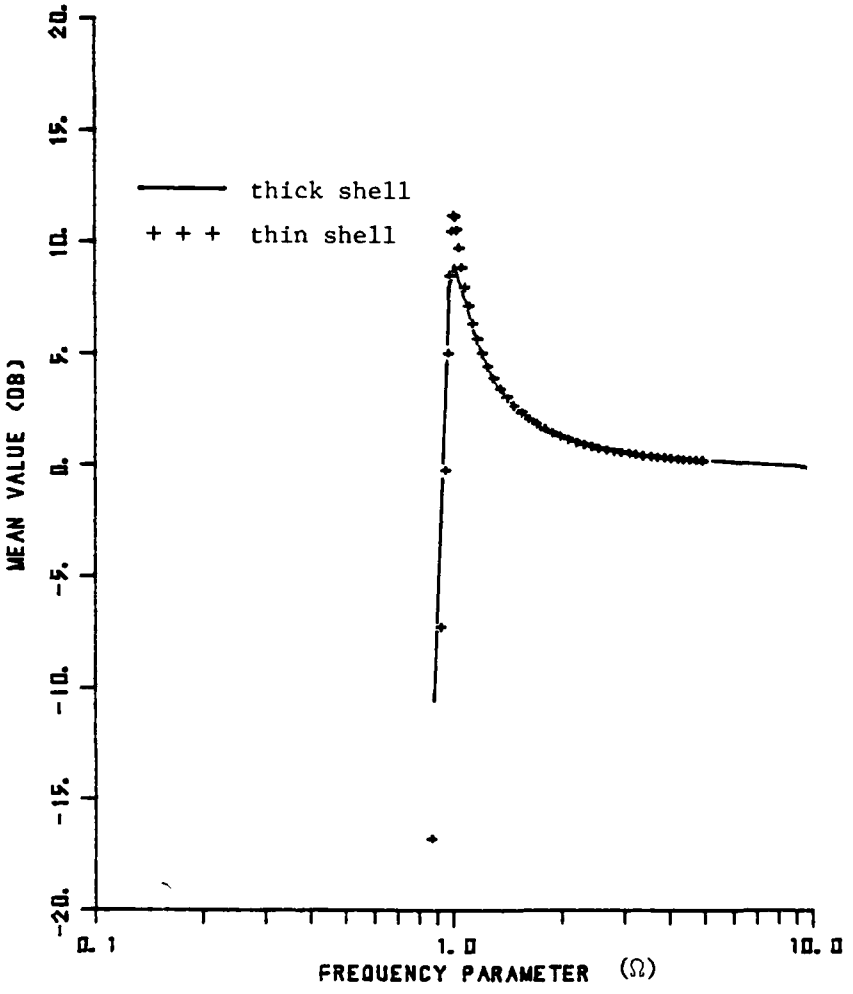

Figure 2.11 Mean value of the driving point admittance of a spherical shell, h = 0.1069" , in vacuo

$$Y_c = \frac{2(n+1)}{8\alpha^2 \rho_s h \sqrt{3(1-\nu^2)}\ \Delta\Omega} \quad , \quad \Omega < 1 \ , \tag{2.61}$$

where $\Delta\Omega = (\omega_{n+1} - \omega_n) \ / \ \omega_r$

and $\alpha^4 = \dfrac{Eh^2}{12\rho_s(1-\nu^2)}$.

CHAPTER III

POINT FORCE AND SOURCE EXCITATION OF A SPHERICAL SHELL

3.1 Introduction

In this chapter, the problem of the forced vibration of the shell in an acoustic medium is presented. The two significant factors which affect the response of the excited shell are the mechanical and the acoustical impedances. The mechanical impedance is due to the response of the shell in vacuo, and the acoustical impedance is due to the fluid loading.

3.2 The Point Excited Vibration of a Shell

The response of a point excited shell in an acoustic medium is analyzed in this section. The fluid pressure p_{rn} in Equation (2.22) is no longer assumed to be zero. Since the radiated acoustic pressure p_{rn} is an outgoing wave, it can be expressed in terms of the spherical Hankel function of first kind and order n. Therefore,

$$p_{rn} = C_n h_n(kr) \tag{3.1}$$

or

$$p_r = \sum_{n=o}^{\infty} C_n h_n(kr) P_n(\eta) \quad ,$$

where C_n is a modal acoustic amplitude, and k is the wave number ω/c.

The inertial force of the shell balances the acoustic force due to the fluid reaction at the boundary of the shell $r = a$. Then, by applying Euler's equation, one obtains the coefficient:

$$C_n = i\rho c\dot{W}_n/h_n'(ka) \quad . \tag{3.2}$$

Substituting C_n into Equation (3.1), one has:

$$P_r(r,\eta) = \sum_{n=o}^{\infty} i\rho c[h_n(kr)/h_n'(ka)]\dot{W}_n P_n(\eta)$$

$$= \sum_{n=o}^{\infty} Z_{an}[h_n(kr)/h_n(ka)]\dot{W}_n P_n(\eta) \quad , \tag{3.3}$$

where $Z_{an} = i\rho c[h_n(ka)/h_n'(ka)]$ is defined as the acoustic radiation impedance.

The radial displacement of the submerged shell is obtained by solving the two simultaneous Equations (2.21) and (2.22) at the boundary. The radial displacement is:

$$W_n = -(p_{in} + p_{rn})/i\omega Z_{mn} \quad \text{at} \quad r = a \quad , \tag{3.4}$$

and the radial velocity is given by:

$$\dot{W}_n = (p_{in} + p_{rn})/Z_{mn} \quad . \tag{3.5}$$

The fluid pressure on the surface of the shell is deduced from Equation (3.3) to be:

$$p_{rn}(a) = -Z_{an}\dot{W}_n \quad , \tag{3.6}$$

where the negative sign denotes the outward pressure.

The radial velocity and the radial displacement as expressed in terms of the applied force and the total impedance of the shell by combining Equations (3.5) and (3.6) are, respectively:

$$\dot{W}_n = p_{in}/Z_n \quad , \tag{3.7}$$

where Z_n is the modal impedance of a submerged shell, and

$$W_n = ip_{in}/\omega Z_n \quad . \tag{3.8}$$

The impedance of the system is no longer solely the mechanical impedance, but the sum of the mechanical and the acoustic impedances. This impedance will cause a change in the displacement and the resonance frequency from those in vacuo.

The driving point admittance and the response pressure field are examined first. Consider a unit concentrated force which can be described by:

$$p_i = (1/4\pi a^2) \sum_{n=o}^{\infty} (2n + 1)P_n(\eta)$$

$$= \sum_{n=o}^{\infty} p_{in}P_n(\eta) \quad . \tag{3.9}$$

From Equation (3.7), the modal velocity of the shell in an acoustic medium is given by:

$$\dot{W}_n = \frac{2n + 1}{4\pi a^2 Z_n} \quad . \tag{3.10}$$

The radial velocity of the submerged shell is given:

$$\dot{W} = \sum_{n=o}^{\infty} (2n + 1)P_n(\eta)/(4\pi a^2 Z_n) \quad . \tag{3.11}$$

When $Z_{an} = 0$ in the above equations, the structure is vibrating in vacuo.

The driving point admittance (DPA) is defined as the ratio of the radial velocity of the shell to the applied force at that particular point. The DPA is obtained directly by setting $\eta = 1$ $[P_n(1) = 1]$ in

Equations (3.9) and (3.11) and taking the ratio,

$$Y_d = \frac{\sum_{n=o}^{\infty} \frac{2n+1}{Z_n}}{4\pi a^2} \quad . \tag{3.12}$$

Finally, substituting Equation (3.10) for $\dot{W}_n$ into Equation (3.3), the pressure field of a submerged shell is:

$$p_d(r,\eta) = \frac{1}{4\pi a^2} \sum (2n+1) \frac{Z_{an}}{Z_n} \frac{h_n(kr)}{h_n'(ka)} P_n(\eta) \quad . \tag{3.13}$$

At resonance, the imaginary part of the total impedance Z_n is equal to zero. Then, Z_n reduces to the sum of the internal damping r_{sn} of the shell and the acoustic resistance r_{an}, where $r_{an} = \text{Real}[i\rho c h_n(ka)/h_n'(ka)]$. The modal impedance of a submerged shell is expressed conveniently as:

$$Z_n(\omega) = Z_{an} + Z_{mn}$$

$$= [r_{mn} + r_{an}(\omega)] + i[M_{mn}(\omega) - \omega M_{an}(\omega)] \quad ,$$

where $Z_{mn} = r_{mn} + iM_{mn}$ and $Z_{an} = r_{an} - i\omega M_{an}$, for mode number $n = 0, 1, 2, \ldots j-1, j, j+1, \ldots$.

3.2.1 Numerical Analysis. Calculations are made for two different duralumin spherical shells when submerged in air and water. The physical properties of the shell material, fluid, and the dimensions of the shellsare listed in Table 3.1. The computation was performed on an IBM 36/72 digital computer.

Before proceeding to examine the behavior of the DPA of the shells, an understanding of the physical role the mechanical and the acoustic impedance play in the DPA, and the relationship between them,

TABLE 3.1

PHYSICAL PROPERTIES OF A DURALUMIN

SPHERICAL SHELL AND ACOUSTIC MEDIA

Thickness (h)	0.0514", 0.1069"
Radius (a)	8"
Young's Modulus (E)	1.037×10^{7} psi
Poisson's Ratio (ν)	0.335
Mass Density of the Shell (ρ_s)	2.649×10^{-4} lb. sec.^{2}/in.^{4}
Mass Density of Air (ρ)	1.15×10^{-7} lb. sec.^{2}/in.^{4}
Mass Density of Water (ρ)	9.645×10^{-5} lb. sec./in.^{4}
Velocity of Sound in Air (c)	1.356×10^{4} in./sec.
Velocity of Sound in Water (c)	6×10^{4} in./sec.
$(ka)_{air}$	$0.3033 \times \Omega$
$(ka)_{water}$	$6.85 \times 10^{-2} \times \Omega$
$(\rho c)_{water}$	5.79 lb. sec./in.^{3}
$(\rho c)_{air}$	1.68×10^{-3} lb. sec./in.^{3}

is necessary. The resonant modal mechanical impedance Z_{mn}, the acoustic impedance Z_{an}, the total impedance Z_n, and the velocity $\dot{W}_n$ for an undamped shell, i.e., $\eta_E = 0$, are listed in Tables 3.2 and 3.3, and Tables 3.4 and 3.5 when submerged in air and water, respectively. For a damped shell, i.e., $\eta_E = 6 \times 10^{-4}$ [19], these values are listed in Tables 3.6 and 3.7, and Tables 3.8 and 3.9 when submerged in air and water, respectively. As mentioned in the previous section, the total reactance, i.e., the imaginary part of Z_n, is zero at resonance. But this is not true for calculation of the resonances to within 10^{-3}; hence, $I_m(Z_n)$ is not exactly zero.

Since the magnitudes of the mechanical and acoustical reactances are close, the error in their sum, when compared to the sum of the modal mechanical resistance r_{mn}, and the modal acoustic reactance r_{an}, can be significant. Thus, when evaluating the response at resonance, the sum of M_{mn} and M_{an} is set to zero to ensure that the response at resonance is dependent purely on the sum of r_{mn} and r_{an}.

In air, the resonances of both the lower and upper branches shown in Tables 3.2 and 3.3 are close to those in vacuo because the magnitude of the reactance $M_{an}(\omega_n)$ of the acoustic impedance $Z_{an}(\omega_n)$ is of the order of 10^{-3} in the lower branch and of the order of 10^{-4} in the upper branch. This means that the mass ratio factor M_R is negligibly small as compared with unity, and the resonances are nearly the same as those in vacuo. This was already shown in Figures 2.6 and 2.8. The DPA response of an undamped shell is dominated by the n^{th} mode near the n^{th} resonance frequency. The response is inversely proportional to the mode acoustic resistance at resonance. Since all the resonances in air occur for $ka > 10$, the modal acoustic resistance $r_{an}(\omega_n)$ approaches

TABLE 3.2

MODAL RESONANCE IMPEDANCE OF A SPHERICAL DURALUMIN SHELL WITH THICKNESS h = 0.0514" IN AIR FOR $\eta_E = 0$

	N	KA		Z_{mn}	Z_{an}		r_n	W_n
	2	10.6300	0.0	0.167E-03	0.159E-02	-0.157E-03	0.159E-02	0.392E+01
	3	12.6330	0.0	0.177E-03	0.161E-02	-0.138E-03	0.161E-02	0.541E+01
	4	13.4340	0.0	0.170E-03	0.164E-02	-0.137E-03	0.164E-02	0.682E+01
	5	13.8400	0.0	0.153E-03	0.168E-02	-0.144E-03	0.168E-02	0.812E+01
	6	14.0860	0.0	0.129E-03	0.174E-02	-0.157E-03	0.174E-02	0.929E+01
	7	14.2600	0.0	0.191E-03	0.181E-02	-0.176E-03	0.181E-02	0.103E+02
	8	14.4080	0.0	0.168E-03	0.190E-02	-0.204E-03	0.190E-02	0.111E+02
	9	14.5500	0.0	0.244E-03	0.201E-02	-0.244E-03	0.201E-02	0.117E+02
	10	14.7050	0.0	0.263E-03	0.216E-02	-0.305E-03	0.216E-02	0.121E+02
	11	14.8820	0.0	0.359E-03	0.234E-02	-0.398E-03	0.234E-02	0.122E+02
	12	15.0900	0.0	0.566E-03	0.256E-02	-0.546E-03	0.256E-02	0.121E+02
	13	15.3390	0.0	0.812E-03	0.283E-02	-0.786E-03	0.283E-02	0.119E+02
	14	15.6350	0.0	0.117E-02	0.310E-02	-0.117E-02	0.310E-02	0.116E+02
	15	15.9820	0.0	0.178E-02	0.330E-02	-0.176E-02	0.330E-02	0.117E+02
	16	16.3880	0.0	0.253E-02	0.326E-02	-0.250E-02	0.326E-02	0.126E+02
	17	16.8630	0.0	0.321E-02	0.288E-02	-0.320E-02	0.288E-02	0.151E+02
	18	17.4150	0.0	0.364E-02	0.231E-02	-0.362E-02	0.231E-02	0.199E+02
	19	18.0480	0.0	0.379E-02	0.179E-02	-0.378E-02	0.179E-02	0.270E+02
	20	18.7610	0.0	0.383E-02	0.142E-02	-0.380E-02	0.142E-02	0.358E+02
	21	19.5550	0.0	0.379E-02	0.121E-02	-0.380E-02	0.121E-02	0.443E+02
	22	20.4280	0.0	0.382E-02	0.111E-02	-0.381E-02	0.111E-02	0.505E+02
	23	21.3810	0.0	0.389E-02	0.111E-02	-0.388E-02	0.111E-02	0.525E+02
	24	22.4140	0.0	0.399E-02	0.122E-02	-0.398E-02	0.122E-02	0.500E+02
	25	23.5260	0.0	0.414E-02	0.144E-02	-0.413E-02	0.144E-02	0.441E+02
	26	24.7180	0.0	0.427E-02	0.180E-02	-0.427E-02	0.180E-02	0.366E+02
*	0	25.3030	0.0	0.561E-04	0.156E-02	-0.615E-04	0.156E-02	0.799E+00
	27	25.9890	0.0	0.436E-02	0.233E-02	-0.433E-02	0.233E-02	0.294E+02
	28	27.3420	0.0	0.423E-02	0.300E-02	-0.421E-02	0.300E-02	0.237E+02
	29	28.7780	0.0	0.378E-02	0.367E-02	-0.380E-02	0.367E-02	0.200E+02

*Indicates upper branch modes.

TABLE 3.3

MODAL RESONANCE IMPEDANCE OF A SPHERICAL DURALUMIN SHELL
WITH THICKNESS $h = 0.1069"$ IN AIR FOR $\eta_E = 0$.

N	KA		Z_{mn}	Z_{an}		r_n	$\dot{W}_n$
2	10.6330	0.0	0.137E-03	0.159E-02	-0.157E-03	0.159E-02	0.392E+01
3	12.6450	0.0	0.849E-04	0.161E-02	-0.137E-03	0.161E-02	0.541E+01
4	13.4670	0.0	0.120E-03	0.164E-02	-0.137E-03	0.164E-02	0.682E+01
5	13.9160	0.0	0.129E-03	0.168E-02	-0.143E-03	0.168E-02	0.813E+01
6	14.2370	0.0	0.203E-03	0.174E-02	-0.154E-03	0.174E-02	0.932E+01
7	14.5340	0.0	0.173E-03	0.180E-02	-0.169E-03	0.180E-02	0.104E+02
8	14.8610	0.0	0.207E-03	0.187E-02	-0.189E-03	0.187E-02	0.113E+02
9	15.2560	0.0	0.233E-03	0.196E-02	-0.212E-03	0.196E-02	0.121E+02
10	15.7480	0.0	0.182E-03	0.205E-02	-0.238E-03	0.205E-02	0.127E+02
11	16.3570	0.0	0.305E-03	0.214E-02	-0.265E-03	0.214E-02	0.134E+02
12	17.1040	0.0	0.290E-03	0.222E-02	-0.287E-03	0.222E-02	0.140E+02
13	18.0010	0.0	0.270E-03	0.229E-02	-0.301E-03	0.229E-02	0.147E+02
14	19.0570	0.0	0.263E-03	0.233E-02	-0.303E-03	0.233E-02	0.154E+02
15	20.2770	0.0	0.314E-03	0.235E-02	-0.293E-03	0.235E-02	0.164E+02
16	21.6650	0.0	0.258E-03	0.235E-02	-0.272E-03	0.235E-02	0.175E+02
17	23.2190	0.0	0.281E-03	0.233E-02	-0.245E-03	0.233E-02	0.187E+02
18	24.9390	0.0	0.213E-03	0.229E-02	-0.215E-03	0.229E-02	0.201E+02
* 0	25.3030	0.0	0.117E-03	0.156E-02	-0.615E-04	0.156E-02	0.799E+00
19	26.8210	0.0	0.164E-03	0.225E-02	-0.187E-03	0.225E-02	0.216E+02
20	28.8610	0.0	0.190E-03	0.220E-02	-0.161E-03	0.220E-02	0.232E+02

*Indicates upper branch modes.

TABLE 3.4

MODAL RESONANCE IMPEDANCE OF A SPHERICAL DURALUMIN SHELL
WITH THICKNESS h = 0.0514" IN WATER FOR $\eta_E = 0$

N	KA	Z_{mn}	Z_{an}	r_n	$\dot{W}_n$
2	0.6130	0.0	0.127E+01 0.365E-02 -0.124E+01	0.365E-02	0.170E+01
3	0.7760	0.0	0.117E+01 0.199E-03 -0.116E+01	0.199E-03	0.437E+02
4	0.8920	0.0	0.106E+01 0.626E-05 -0.106E+01	0.626E-05	0.179E+04
5	0.9860	0.0	0.972E+00 0.141E-06 -0.969E+00	0.141E-06	0.967E+05
6	1.0690	0.0	0.898E+00 0.258E-08 -0.897E+00	0.258E-08	0.626E+07
* 0	1.1170	0.0	0.288E+01 0.321E+01 -0.288E+01	0.321E+01	0.387E-03
7	1.14	0.0	0.839E+00 0.390E-10 -0.837E+00	0.390E-10	0.479E+09
8	1.2150	0.0	0.789E+00 0.521E-12 -0.789E+00	0.521E-12	0.406E+11
9	1.2790	0.0	0.748E+00 0.619E-14 -0.747E+00	0.619E-14	0.382E+13
10	1.3440	0.0	0.714E+00 0.689E-16 -0.713E+00	0.689E-16	0.379E+15
11	1.4090	0.0	0.686E+00 0.736E-18 -0.685E+00	0.736E-18	0.388E+17
12	1.4760	0.0	0.663E+00 0.787E-20 -0.662E+00	0.787E-20	0.395E+19
13	1.5450	0.0	0.645E+00 0.849E-22 -0.643E+00	0.849E-22	0.396E+21
14	1.6180	0.0	0.631E+00 0.965E-24 -0.628E+00	0.965E-24	0.374E+23
15	1.6960	0.0	0.621E+00 0.119E-25 -0.617E+00	0.119E-25	0.325E+25
16	1.7800	0.0	0.614E+00 0.162E-27 -0.610E+00	0.162E-27	0.253E+27
17	1.8710	0.0	0.612E+00 0.253E-29 -0.605E+00	0.253E-29	0.172E+29
18	1.9720	0.0	0.611E+00 0.475E-31 -0.604E+00	0.475E-31	0.968E+30
19	2.0820	0.0	0.614E+00 0.106E-32 -0.606E+00	0.106E-32	0.457E+32
20	2.2030	0.0	0.618E+00 0.292E-34 -0.611E+00	0.292E-34	0.174E+34
21	2.3350	0.0	0.625E+00 0.987E-36 -0.618E+00	0.987E-36	0.542E+35
22	2.4780	0.0	0.635E+00 0.406E-37 -0.627E+00	0.406E-37	0.138E+37
23	2.6330	0.0	0.646E+00 0.206E-38 -0.639E+00	0.206E-38	0.284E+38
24	2.7990	0.0	0.660E+00 0.125E-39 -0.652E+00	0.125E-39	0.487E+39
25	2.9770	0.0	0.675E+00 0.918E-41 -0.667E+00	0.918E-41	0.690E+40
26	3.1680	0.0	0.692E+00 0.821E-42 -0.684E+00	0.821E-42	0.803E+41

*Indicates upper branch modes.

TABLE 3.4 (continued)

	N	KA		Z_{mn}		Z_{an}	r_n	$\dot{W}_n$
	27	3.3720	0.0	0.710E+00	0.883E-43	-0.702E+00	0.883E-43	0.774E+42
	28	3.5880	0.0	0.729E+00	0.111E-43	-0.722E+00	0.111E-43	0.637E+43
	29	3.8180	0.0	0.749E+00	0.168E-44	-0.743E+00	0.168E-44	0.437E+44
	30	4.0620	0.0	0.770E+00	0.300E-45	-0.765E+00	0.300E-45	0.253E+45
	31	4.3180	0.0	0.792E+00	0.608E-46	-0.788E+00	0.608E-46	0.129E+46
	32	4.5870	0.0	0.815E+00	0.141E-46	-0.813E+00	0.141E-46	0.573E+46
	33	4.8680	0.0	0.839E+00	0.366E-47	-0.838E+00	0.366E-47	0.228E+47
	34	5.1610	0.0	0.864E+00	0.106E-47	-0.863E+00	0.106E-47	0.812E+47
	35	5.4660	0.0	0.890E+00	0.337E-48	-0.889E+00	0.337E-48	0.262E+48
*	1	5.5970	0.0	0.677E+00	0.576E+01	-0.110E+01	0.576E+01	0.647E-03
	36	5.7840	0.0	0.917E+00	0.120E-48	-0.916E+00	0.120E-48	0.758E+48
	37	6.1140	0.0	0.944E+00	0.464E-49	-0.944E+00	0.464E-49	0.201E+49
	38	6.4560	0.0	0.972E+00	0.196E-49	-0.972E+00	0.196E-49	0.489E+49
	39	6.8110	0.0	0.100E+01	0.906E-50	-0.100E+01	0.906E-50	0.108E+50
	40	7.1780	0.0	0.103E+01	0.452E-50	-0.103E+01	0.452E-50	0.223E+50
	41	7.5570	0.0	0.106E+01	0.242E-50	-0.106E+01	0.242E-50	0.426E+50
	42	7.9490	0.0	0.109E+01	0.140E-50	-0.109E+01	0.140E-50	0.753E+50
	43	8.3530	0.0	0.112E+01	0.867E-51	-0.112E+01	0.867E-51	0.125E+51
	44	8.7690	0.0	0.115E+01	0.571E-51	-0.115E+01	0.571E-51	0.194E+51
*	2	9.0860	0.0	0.488E+00	0.592E+01	-0.702E+00	0.592E+01	0.105E-02
	45	9.1980	0.0	0.118E+01	0.402E-51	-0.118E+01	0.402E-51	0.281E+51
	46	9.6380	0.0	0.121E+01	0.297E-51	-0.121E+01	0.297E-51	0.389E+51
	47	10.0910	0.0	0.125E+01	0.234E-51	-0.125E+01	0.234E-51	0.505E+51
	48	10.5570	0.0	0.128E+01	0.196E-51	-0.128E+01	0.196E-51	0.616E+51
	49	11.0340	0.0	0.131E+01	0.171E-51	-0.131E+01	0.171E-51	0.722E+51
*	3	12.5420	0.0	0.401E+00	0.597E+01	-0.515E+00	0.597E+01	0.146E-02
*	4	16.0050	0.0	0.340E+00	0.600E+01	-0.406E+00	0.600E+01	0.187E-02
*	5	19.4740	0.0	0.295E+00	0.601E+01	-0.335E+00	0.601E+01	0.228E-02
*	6	22.9480	0.0	0.264E+00	0.602E+01	-0.285E+00	0.602E+01	0.269E-02
*	7	26.4290	0.0	0.223E+00	0.602E+01	-0.248E+00	0.602E+01	0.310E-02
*	8	29.9100	0.0	0.213E+00	0.603E+01	-0.219E+00	0.603E+01	0.351E-02

TABLE 3.5

MODAL RESONANCE IMPEDANCE OF A SPHERICAL DURALUMIN SHELL WITH THICKNESS h = 0.1069" IN WATER FOR $\eta_E = 0$

N	KA	Z_{mn}	Z_{an}		r_n	$\dot{W}_n$
2	0.8390	0.0	0.182E+01	0.233E-01 -0.178E+01	0.233E-01	0.267E+00
3	1.0640	0.0	0.165E+01	0.237E-02 -0.164E+01	0.237E-02	0.367E+01
4	1.2220	0.0	0.149E+01	0.137E-03 -0.148E+01	0.137E-03	0.815E+02
5	1.3500	0.0	0.135E+01	0.576E-05 -0.135E+01	0.576E-05	0.237E+04
6	1.4630	0.0	0.125E+01	0.196E-06 -0.124E+01	0.196E-06	0.826E+05
7	1.5700	0.0	0.116E+01	0.585E-08 -0.116E+01	0.585E-08	0.319E+07
8	1.6760	0.0	0.110E+01	0.164E-09 -0.110E+01	0.164E-09	0.129E+09
9	1.7870	0.0	0.105E+01	0.462E-11 -0.105E+01	0.462E-11	0.511E+10
10	1.9080	0.0	0.102E+01	0.142E-12 -0.102E+01	0.142E-12	0.184E+12
11	2.0420	0.0	0.100E+01	0.498E-14 -0.100E+01	0.498E-14	0.575E+13
12	2.1930	0.0	0.993E+00	0.211E-15 -0.992E+00	0.211E-15	0.147E+15
13	2.3650	0.0	0.994E+00	0.114E-16 -0.994E+00	0.114E-16	0.294E+16
14	2.5600	0.0	0.100E+01	0.808E-18 -0.100E+01	0.808E-18	0.446E+17
15	2.7790	0.0	0.102E+01	0.748E-19 -0.102E+01	0.748E-19	0.516E+18
* 0	2.8920	0.0	0.179E+01	0.517E+01 -0.179E+01	0.517E+01	0.241E-03
16	3.0250	0.0	0.105E+01	0.926E-20 -0.105E+01	0.926E-20	0.443E+19
17	3.2970	0.0	0.108E+01	0.149E-20 -0.108E+01	0.149E-20	0.292E+20
18	3.5970	0.0	0.112E+01	0.313E-21 -0.112E+01	0.313E-21	0.147E+21
19	3.9250	0.0	0.116E+01	0.837E-22 -0.116E+01	0.837E-22	0.579E+21
20	4.2810	0.0	0.121E+01	0.280E-22 -0.121E+01	0.280E-22	0.182E+22
21	4.6640	0.0	0.126E+01	0.114E-22 -0.126E+01	0.114E-22	0.469E+22
22	5.0750	0.0	0.131E+01	0.560E-23 -0.131E+01	0.560E-23	0.100E+23
23	5.5140	0.0	0.137E+01	0.326E-23 -0.137E+01	0.326E-23	0.179E+23
24	5.9800	0.0	0.143E+01	0.220E-23 -0.143E+01	0.220E-23	0.277E+23
* 1	6.0510	0.0	0.789E+00	0.577E+01 -0.101E+01	0.577E+01	0.647E-03
25	6.4730	0.0	0.149E+01	0.170E-23 -0.149E+01	0.170E-23	0.372E+23

*Indicates upper branch modes

TABLE 3.5 (continued)

	N	KA		Z_{mn}		Z_{an}		r_n	$\dot{W}_n$
	26	6.9930	0.0	0.156E+01	0.149E-23	-0.156E+01	0.149E-23	0.441E+23	
	27	7.5400	0.0	0.162E+01	0.147E-23	-0.162E+01	0.147E-23	0.465E+23	
	28	8.1130	0.0	0.169E+01	0.160E-23	-0.169E+01	0.160E-23	0.443E+23	
	29	8.7120	0.0	0.176E+01	0.191E-23	-0.176E+01	0.191E-23	0.384E+23	
*	2	9.2740	0.0	0.558E+00	0.592E+01	-0.685E+00	0.592E+01	0.105E-02	
	30	9.3370	0.0	0.183E+01	0.248E-23	-0.183E+01	0.248E-23	0.306E+23	
	31	9.9880	0.0	0.191E+01	0.349E-23	-0.191E+01	0.349E-23	0.224E+23	
	32	10.6650	0.0	0.198E+01	0.530E-23	-0.198E+01	0.530E-23	0.152E+23	
	33	11.3670	0.0	0.206E+01	0.858E-23	-0.206E+01	0.858E-23	0.971E+22	
	34	12.0940	0.0	0.214E+01	0.148E-22	-0.214E+01	0.148E-22	0.582E+22	
*	3	12.6400	0.0	0.442E+00	0.597E+01	-0.510E+00	0.597E+01	0.146E-02	
	35	12.8470	0.0	0.222E+01	0.270E-22	-0.222E+01	0.270E-22	0.327E+22	
	36	13.6240	0.0	0.230E+01	0.518E-22	-0.230E+01	0.518E-22	0.175E+22	
	37	14.4260	0.0	0.238E+01	0.104E-21	-0.238E+01	0.104E-21	0.893E+21	
	38	15.2530	0.0	0.247E+01	0.221E-21	-0.247E+01	0.221E-21	0.433E+21	
*	4	16.0620	0.0	0.366E+00	0.600E+01	-0.405E+00	0.600E+01	0.187E-02	
	39	16.1040	0.0	0.256E+01	0.487E-21	-0.256E+01	0.487E-21	0.202E+21	
	40	16.9800	0.0	0.264E+01	0.112E-20	-0.264E+01	0.112E-20	0.901E+20	
	41	17.8800	0.0	0.273E+01	0.266E-20	-0.273E+01	0.266E-20	0.388E+20	
	42	18.8030	0.0	0.283E+01	0.652E-20	-0.283E+01	0.652E-20	0.162E+20	
*	5	19.5100	0.0	0.313E+00	0.601E+01	-0.334E+00	0.601E+01	0.228E-02	
	43	19.7500	0.0	0.292E+01	0.165E-19	-0.292E+01	0.165E-19	0.656E+19	
	44	20.7220	0.0	0.302E+01	0.431E-19	-0.302E+01	0.431E-19	0.257E+19	
	45	21.7150	0.0	0.312E+01	0.115E-18	-0.312E+01	0.115E-18	0.986E+18	
	46	22.7320	0.0	0.322E+01	0.314E-18	-0.322E+01	0.314E-18	0.369E+18	
*	6	22.9740	0.0	0.260E+00	0.602E+01	-0.285E+00	0.602E+01	0.269E-02	
	47	23.7720	0.0	0.332E+01	0.877E-18	-0.332E+01	0.877E-18	0.135E+18	
	48	24.8360	0.0	0.342E+01	0.251E-17	-0.342E+01	0.251E-17	0.481E+17	
	49	25.9200	0.0	0.353E+01	0.724E-17	-0.353E+01	0.724E-17	0.170E+17	
*	7	26.4450	0.0	0.240E+00	0.602E+01	-0.248E+00	0.602E+01	0.310E-02	
*	8	29.9240	0.0	0.199E+00	0.603E+01	-0.219E+00	0.603E+01	0.351E-02	

TABLE 3.6

MODAL RESONANCE IMPEDANCE OF A SPHERICAL DURALUMIN SHELL WITH THICKNESS h = 0.0514" IN AIR FOR $\eta_E = 0$

N	KA	Z_{mn}		Z_{an}		r_n	$\dot{W}_n$
2	10.6300	0.214E-03	0.167E-03	0.159E-02	-0.157E-03	0.180E-02	0.345E+01
3	12.6330	0.208E-03	0.178E-03	0.161E-02	-0.138E-03	0.182E-02	0.479E+01
4	13.4340	0.205E-03	0.171E-03	0.164E-02	-0.137E-03	0.185E-02	0.606E+01
5	13.8400	0.204E-03	0.153E-03	0.168E-02	-0.144E-03	0.189E-02	0.724E+01
6	14.0860	0.204E-03	0.129E-03	0.174E-02	-0.157E-03	0.194E-02	0.832E+01
7	14.2600	0.204E-03	0.192E-03	0.181E-02	-0.176E-03	0.201E-02	0.926E+01
8	14.4080	0.205E-03	0.169E-03	0.190E-02	-0.204E-03	0.211E-02	0.100E+02
9	14.5500	0.206E-03	0.244E-03	0.201E-02	-0.244E-03	0.222E-02	0.106E+02
10	14.7050	0.207E-03	0.263E-03	0.216E-02	-0.305E-03	0.236E-02	0.110E+02
11	14.8820	0.209E-03	0.359E-03	0.234E-02	-0.398E-03	0.255E-02	0.112E+02
12	15.0900	0.211E-03	0.566E-03	0.256E-02	-0.546E-03	0.277E-02	0.112E+02
13	15.3390	0.215E-03	0.812E-03	0.283E-02	-0.786E-03	0.304E-02	0.110E+02
14	15.6350	0.218E-03	0.117E-02	0.310E-02	-0.117E-02	0.332E-02	0.109E+02
15	15.9820	0.223E-03	0.178E-02	0.330E-02	-0.176E-02	0.352E-02	0.109E+02
16	16.3880	0.228E-03	0.253E-02	0.326E-02	-0.250E-02	0.348E-02	0.118E+02
17	16.8630	0.235E-03	0.321E-02	0.288E-02	-0.320E-02	0.311E-02	0.140E+02
18	17.4150	0.242E-03	0.364E-02	0.231E-02	-0.362E-02	0.256E-02	0.180E+02
19	18.0480	0.251E-03	0.379E-02	0.179E-02	-0.378E-02	0.204E-02	0.237E+02
20	18.7610	0.261E-03	0.383E-02	0.142E-02	-0.380E-02	0.168E-02	0.303E+02
21	19.5550	0.272E-03	0.379E-02	0.121E-02	-0.380E-02	0.148E-02	0.362E+02
22	20.4280	0.284E-03	0.382E-02	0.111E-02	-0.381E-02	0.139E-02	0.402E+02
23	21.3810	0.297E-03	0.389E-02	0.111E-02	-0.388E-02	0.141E-02	0.415E+02
24	22.4140	0.311E-03	0.399E-02	0.122E-02	-0.398E-02	0.153E-02	0.398E+02
25	23.5260	0.327E-03	0.414E-02	0.144E-02	-0.413E-02	0.176E-02	0.359E+02
26	24.7180	0.343E-03	0.427E-02	0.180E-02	-0.427E-02	0.214E-02	0.307E+02
* 0	25.3030	0.350E-03	0.563E-04	0.156E-02	-0.615E-04	0.191E-02	0.652E+00
27	25.9890	0.361E-03	0.436E-02	0.233E-02	-0.433E-02	0.269E-02	0.254E+02
28	27.3420	0.379E-03	0.423E-02	0.300E-02	-0.421E-02	0.337E-02	0.210E+02
29	28.7780	0.399E-03	0.378E-02	0.367E-02	-0.380E-02	0.407E-02	0.180E+02

*Indicates upper branch modes.

TABLE 3.7

MODAL RESONANCE IMPEDANCE OF A SPHERICAL DURALUMIN SHELL WITH THICKNESS h = 0.1069" IN AIR FOR ϵ_E = 0.0006

N	KA	Z_{mn}		Z_{an}		r_n	$\dot{W}_n$
2	10.6330	0.445E-03	0.137E-03	0.159E-02	-0.157E-03	0.203E-02	0.306E+01
3	12.6450	0.433E-03	0.852E-04	0.161E-02	-0.137E-03	0.204E-02	0.426E+01
4	13.4670	0.428E-03	0.120E-03	0.164E-02	-0.137E-03	0.207E-02	0.541E+01
5	13.9160	0.427E-03	0.130E-03	0.168E-02	-0.143E-03	0.211E-02	0.648E+01
6	14.2370	0.429E-03	0.204E-03	0.174E-02	-0.154E-03	0.216E-02	0.747E+01
7	14.5340	0.433E-03	0.174E-03	0.180E-02	-0.169E-03	0.223E-02	0.836E+01
8	14.8610	0.439E-03	0.207E-03	0.187E-02	-0.189E-03	0.231E-02	0.914E+01
9	15.2560	0.448E-03	0.233E-03	0.196E-02	-0.212E-03	0.241E-02	0.981E+01
10	15.7480	0.461E-03	0.183E-03	0.205E-02	-0.238E-03	0.251E-02	0.104E+02
11	16.3570	0.478E-03	0.305E-03	0.214E-02	-0.265E-03	0.262E-02	0.109E+02
12	17.1040	0.498E-03	0.290E-03	0.222E-02	-0.287E-03	0.272E-02	0.114E+02
13	18.0010	0.524E-03	0.270E-03	0.229E-02	-0.301E-03	0.281E-02	0.119E+02
14	19.0570	0.554E-03	0.264E-03	0.233E-02	-0.303E-03	0.289E-02	0.125E+02
15	20.2770	0.588E-03	0.314E-03	0.235E-02	-0.293E-03	0.294E-02	0.131E+02
16	21.6650	0.628E-03	0.258E-03	0.235E-02	-0.272E-03	0.298E-02	0.138E+02
17	23.2190	0.673E-03	0.282E-03	0.233E-02	-0.245E-03	0.300E-02	0.145E+02
18	24.9390	0.722E-03	0.213E-03	0.229E-02	-0.215E-03	0.301E-02	0.153E+02
* 0	25.3030	0.729E-03	0.117E-03	0.156E-02	-0.615E-04	0.229E-02	0.544E+00
19	26.8210	0.776E-03	0.164E-03	0.225E-02	-0.187E-03	0.302E-02	0.161E+02
20	28.8610	0.835E-03	0.191E-03	0.220E-02	-0.161E-03	0.303E-02	0.168E+02

*Indicates upper branch modes.

TABLE 3.8

MODAL RESONANCE IMPEDANCE OF A SPHERICAL DURALUMIN SHELL
WITH THICKNESS h = 0.0514" IN WATER FOR η_E = 0.0006

	N	KA	Z_{mn}		Z_{an}		r_n	$\dot{W}_n$
	2	0.6130	0.518E-04	0.127E+01	0.365E-02	-0.124E+01	0.370E-02	0.168E+01
	3	0.7760	0.555E-04	0.117E+01	0.199E-03	-0.116E+01	0.255E-03	0.342E+02
	4	0.8920	0.599E-04	0.106E+01	0.626E-05	-0.106E+01	0.662E-04	0.169E+03
	5	0.9860	0.642E-04	0.972E+00	0.141E-06	-0.969E+00	0.643E-04	0.213E+03
	6	1.0690	0.684E-04	0.898E+00	0.258E-08	-0.897E+00	0.684E-04	0.236E+03
*	0	1.1170	0.684E-04	0.288E+01	0.321E+01	-0.288E+01	0.321E+01	0.387E-03
	7	1.1430	0.723E-04	0.839E+00	0.390E-10	-0.837E+00	0.723E-04	0.258E+03
	8	1.2130	0.762E-04	0.789E+00	0.521E-12	-0.789E+00	0.762E-04	0.277E+03
	9	1.2790	0.799E-04	0.748E+00	0.619E-14	-0.747E+00	0.799E-04	0.296E+03
	10	1.3440	0.837E-04	0.714E+00	0.689E-16	-0.713E+00	0.837E-04	0.312E+03
	11	1.4090	0.875E-04	0.686E+00	0.736E-18	-0.685E+00	0.875E-04	0.327E+03
	12	1.4760	0.915E-04	0.663E+00	0.787E-20	-0.662E+00	0.915E-04	0.340E+03
	13	1.5450	0.956E-04	0.645E+00	0.849E-22	-0.643E+00	0.956E-04	0.351E+03
	14	1.6180	0.100E-03	0.631E+00	0.965E-24	-0.628E+00	0.100E-03	0.361E+03
	15	1.6960	0.105E-03	0.621E+00	0.119E-25	-0.617E+00	0.105E-03	0.368E+03
	16	1.7800	0.110E-03	0.614E+00	0.162E-27	-0.610E+00	0.110E-03	0.374E+03
	17	1.8710	0.115E-03	0.612E+00	0.253E-29	-0.605E+00	0.115E-03	0.377E+03
	18	1.9720	0.121E-03	0.611E+00	0.475E-31	-0.604E+00	0.121E-03	0.379E+03
	19	2.0820	0.128E-03	0.614E+00	0.106E-32	-0.606E+00	0.128E-03	0.378E+03
	20	2.2030	0.136E-03	0.618E+00	0.292E-34	-0.611E+00	0.136E-03	0.376E+03
	21	2.3350	0.144E-03	0.625E+00	0.987E-36	-0.618E+00	0.144E-03	0.372E+03
	22	2.4780	0.152E-03	0.635E+00	0.406E-37	-0.627E+00	0.152E-03	0.367E+03
	23	2.6330	0.162E-03	0.646E+00	0.206E-38	-0.639E+00	0.162E-03	0.361E+03
	24	2.7990	0.172E-03	0.660E+00	0.125E-39	-0.652E+00	0.172E-03	0.354E+03
	25	2.9770	0.183E-03	0.675E+00	0.918E-41	-0.667E+00	0.183E-03	0.347E+03
	26	3.1680	0.195E-03	0.692E+00	0.821E-42	-0.684E+00	0.195E-03	0.339E+03

*Indicates upper branch modes.

TABLE 3.8 (continued)

	N	KA	Z_{mn}		Z_{an}		r_n	$\dot{W}_n$
	27	3.3720	0.207E-03	0.710E+00	0.883E-43	-0.702E+00	0.207E-03	0.330E+03
	28	3.5880	0.220E-03	0.729E+00	0.111E-43	-0.722E+00	0.220E-03	0.322E+03
	29	3.8180	0.234E-03	0.749E+00	0.168E-44	-0.743E+00	0.234E-03	0.313E+03
	30	4.0620	0.249E-03	0.770E+00	0.300E-45	-0.765E+00	0.249E-03	0.304E+03
	31	4.3180	0.265E-03	0.792E+00	0.608E-46	-0.788E+00	0.265E-03	0.296E+03
	32	4.5870	0.282E-03	0.815E+00	0.141E-46	-0.813E+00	0.282E-03	0.287E+03
	33	4.8680	0.299E-03	0.839E+00	0.366E-47	-0.838E+00	0.299E-03	0.279E+03
	34	5.1610	0.317E-03	0.864E+00	0.106E-47	-0.863E+00	0.317E-03	0.271E+03
	35	5.4660	0.335E-03	0.890E+00	0.337E-48	-0.889E+00	0.335E-03	0.263E+03
*	1	5.5970	0.116E-02	0.677E+00	0.576E+01	-0.110E+01	0.576E+01	0.647E-03
	36	5.7840	0.355E-03	0.917E+00	0.120E-48	-0.916E+00	0.355E-03	0.256E+03
	37	6.1140	0.375E-03	0.944E+00	0.464E-49	-0.944E+00	0.375E-03	0.249E+03
	38	6.4560	0.396E-03	0.972E+00	0.196E-49	-0.972E+00	0.396E-03	0.242E+03
	39	6.8110	0.418E-03	0.100E+01	0.906E-50	-0.100E+01	0.418E-03	0.235E+03
	40	7.1780	0.440E-03	0.103E+01	0.452E-50	-0.103E+01	0.440E-03	0.229E+03
	41	7.5570	0.464E-03	0.106E+01	0.242E-50	-0.106E+01	0.464E-03	0.223E+03
	42	7.9490	0.488E-03	0.109E+01	0.140E-50	-0.109E+01	0.488E-03	0.217E+03
	43	8.3530	0.512E-03	0.112E+01	0.867E-51	-0.112E+01	0.512E-03	0.211E+03
	44	8.7690	0.538E-03	0.115E+01	0.571E-51	-0.115E+01	0.538E-03	0.206E+03
*	2	9.0860	0.357E-02	0.488E+00	0.592E+01	-0.702E+00	0.593E+01	0.105E-02
	45	9.1980	0.564E-03	0.118E+01	0.402E-51	-0.118E+01	0.564E-03	0.201E+03
	46	9.6380	0.591E-03	0.121E+01	0.297E-51	-0.121E+01	0.591E-03	0.196E+03
	47	10.0910	0.619E-03	0.125E+01	0.234E-51	-0.125E+01	0.619E-03	0.191E+03
	48	10.5570	0.647E-03	0.128E+01	0.196E-51	-0.128E+01	0.647E-03	0.186E+03
	49	11.0340	0.677E-03	0.131E+01	0.171E-51	-0.131E+01	0.677E-03	0.182E+03
*	3	12.5420	0.800E-02	0.401E+00	0.597E+01	-0.515E+00	0.598E+01	0.145E-02
*	4	16.0050	0.150E-01	0.340E+00	0.600E+01	-0.406E+00	0.601E+01	0.186E-02
*	5	19.4740	0.253E-01	0.295E+00	0.601E+01	-0.335E+00	0.604E+01	0.227E-02
*	6	22.9480	0.397E-01	0.263E+00	0.602E+01	-0.285E+00	0.606E+01	0.267E-02
*	7	26.4290	0.582E-01	0.222E+00	0.602E+01	-0.248E+00	0.608E+01	0.307E-02
*	8	29.9100	0.830E-01	0.211E+00	0.603E+01	-0.219E+00	0.611E+01	0.346E-02

TABLE 3.9

MODAL RESONANCE IMPEDANCE OF A SPHERICAL DURALUMIN SHELL
WITH THICKNESS h = 0.1069" IN WATER FOR η_E = 0.0006

N	KA	Z_{mn}		Z_{an}		r_n	$\dot{W}_n$
2	0.8390	0.148E-03	0.182E+01	0.233E-01	-0.178E+01	0.234E-01	0.265E+00
3	1.0640	0.159E-03	0.165E+01	0.237E-02	-0.164E+01	0.253E-02	0.344E+01
4	1.2220	0.171E-03	0.149E+01	0.137E-03	-0.148E+01	0.308E-03	0.363E+02
5	1.3500	0.183E-03	0.135E+01	0.576E-05	-0.135E+01	0.189E-03	0.725E+02
6	1.4630	0.195E-03	0.125E+01	0.196E-06	-0.124E+01	0.195E-03	0.829E+02
7	1.5700	0.207E-03	0.116E+01	0.585E-08	-0.116E+01	0.207E-03	0.903E+02
8	1.6760	0.219E-03	0.110E+01	0.164E-09	-0.110E+01	0.219E-03	0.965E+02
9	1.7870	0.232E-03	0.105E+01	0.462E-11	-0.105E+01	0.232E-03	0.102E+03
10	1.9080	0.247E-03	0.102E+01	0.142E-12	-0.102E+01	0.247E-03	0.106E+03
11	2.0420	0.264E-03	0.100E+01	0.498E-14	-0.100E+01	0.264E-03	0.108E+03
12	2.1930	0.283E-03	0.993E+00	0.211E-15	-0.992E+00	0.283E-03	0.110E+03
13	2.3650	0.304E-03	0.994E+00	0.114E-16	-0.994E+00	0.304E-03	0.110E+03
14	2.5600	0.329E-03	0.100E+01	0.808E-18	-0.100E+01	0.329E-03	0.110E+03
15	2.7790	0.357E-03	0.102E+01	0.748E-19	-0.102E+01	0.357E-03	0.108E+03
* 0	2.8920	0.369E-03	0.179E+01	0.517E+01	-0.179E+01	0.517E+01	0.241E-03
16	3.0250	0.388E-03	0.105E+01	0.926E-20	-0.105E+01	0.388E-03	0.106E+03
17	3.2970	0.423E-03	0.108E+01	0.149E-20	-0.108E+01	0.423E-03	0.103E+03
18	3.5970	0.461E-03	0.112E+01	0.313E-21	-0.112E+01	0.461E-03	0.998E+02
19	3.9250	0.503E-03	0.116E+01	0.837E-22	-0.116E+01	0.503E-03	0.965E+02
20	4.2810	0.548E-03	0.121E+01	0.280E-22	-0.121E+01	0.548E-03	0.930E+02
21	4.6640	0.597E-03	0.126E+01	0.114E-22	-0.126E+01	0.597E-03	0.896E+02
22	5.0750	0.649E-03	0.131E+01	0.560E-23	-0.131E+01	0.649E-03	0.862E+02
23	5.5140	0.705E-03	0.137E+01	0.326E-23	-0.137E+01	0.705E-03	0.829E+02
24	5.9800	0.764E-03	0.143E+01	0.220E-23	-0.143E+01	0.764E-03	0.797E+02
* 1	6.0510	0.178E-02	0.789E+00	0.577E+01	-0.101E+01	0.577E+01	0.646E-03
25	6.4730	0.827E-03	0.149E+01	0.170E-23	-0.149E+01	0.827E-03	0.767E+02

*Indicates upper branch modes.

TABLE 3.9 (continued)

	N	KA	Z_{mn}		Z_{an}		r_n	$\dot{W}_n$
	26	6.9930	0.893E-03	0.156E+01	0.149E-23	-0.156E+01	0.893E-03	0.738E+02
	27	7.5400	0.963E-03	0.162E+01	0.147E-23	-0.162E+01	0.963E-03	0.710E+02
	28	8.1130	0.104E-02	0.169E+01	0.160E-23	-0.169E+01	0.104E-02	0.684E+02
	29	8.7120	0.111E-02	0.176E+01	0.191E-23	-0.176E+01	0.111E-02	0.659E+02
*	2	9.2740	0.562E-02	0.558E+00	0.592E+01	-0.685E+00	0.592E+01	0.105E-02
	30	9.3370	0.119E-02	0.183E+01	0.248E-23	-0.183E+01	0.119E-02	0.636E+02
	31	9.9880	0.128E-02	0.191E+01	0.349E-23	-0.191E+01	0.128E-02	0.614E+02
	32	10.6650	0.136E-02	0.198E+01	0.530E-23	-0.198E+01	0.136E-02	0.594E+02
	33	11.3670	0.145E-02	0.206E+01	0.858E-23	-0.206E+01	0.145E-02	0.574E+02
	34	12.0940	0.154E-02	0.214E+01	0.148E-22	-0.214E+01	0.154E-02	0.556E+02
*	3	12.6400	0.134E-01	0.442E+00	0.597E+01	-0.510E+00	0.598E+01	0.145E-02
	35	12.8470	0.164E-02	0.222E+01	0.270E-22	-0.222E+01	0.164E-02	0.538E+02
	36	13.6240	0.174E-02	0.230E+01	0.518E-22	-0.230E+01	0.174E-02	0.522E+02
	37	14.4260	0.184E-02	0.238E+01	0.104E-21	-0.238E+01	0.184E-02	0.507E+02
	38	15.2530	0.195E-02	0.247E+01	0.221E-21	-0.247E+01	0.195E-02	0.492E+02
*	4	16.0620	0.265E-01	0.366E+00	0.600E+01	-0.405E+00	0.602E+01	0.186E-02
	39	16.1040	0.205E-02	0.256E+01	0.487E-21	-0.256E+01	0.205E-02	0.478E+02
	40	16.9800	0.217E-02	0.264E+01	0.112E-20	-0.264E+01	0.217E-02	0.465E+02
	41	17.8800	0.228E-02	0.273E+01	0.266E-20	-0.273E+01	0.228E-02	0.452E+02
	42	18.8030	0.240E-02	0.283E+01	0.652E-20	-0.283E+01	0.240E-02	0.441E+02
*	5	19.5100	0.464E-01	0.313E+00	0.601E+01	-0.334E+00	0.606E+01	0.226E-02
	43	19.7500	0.252E-02	0.292E+01	0.165E-19	-0.292E+01	0.252E-02	0.429E+02
	44	20.7220	0.264E-02	0.302E+01	0.431E-19	-0.302E+01	0.264E-02	0.419E+02
	45	21.7150	0.277E-02	0.312E+01	0.115E-18	-0.312E+01	0.277E-02	0.409E+02
	46	22.7320	0.290E-02	0.322E+01	0.314E-18	-0.322E+01	0.290E-02	0.399E+02
*	6	22.9740	0.741E-01	0.259E+00	0.602E+01	-0.285E+00	0.609E+01	0.265E-02
	47	23.7720	0.303E-02	0.332E+01	0.877E-18	-0.332E+01	0.303E-02	0.390E+02
	48	24.8360	0.317E-02	0.342E+01	0.251E-17	-0.342E+01	0.317E-02	0.381E+02
	49	25.9200	0.331E-02	0.353E+01	0.724E-17	-0.353E+01	0.331E-02	0.372E+02
*	7	26.4450	0.112E+00	0.237E+00	0.602E+01	-0.248E+00	0.613E+01	0.304E-02
*	8	29.9240	0.160E+00	0.195E+00	0.603E+01	-0.219E+00	0.619E+01	0.342E-02

the characteristic impedance $(\rho c)_{air} = 0.168 \times 10^{-3}$. Thus, the amplitude of the modal admittance, theoretically, is approximately the level of $1/(\rho c)_{air}$. For a damped shell with a structural loss factor of $\eta_E = 6 \times 10^{-4}$ for duralumin, the structural modal resistance $r_{mn}(\omega_n)$ at resonance has a very small value (see Tables 3.6 and 3.7). Since $r_{mn}(\omega_n)$ is smaller than the acoustic modal resistance $r_{an}(\omega_n)$, the DPA is not significantly changed by the inclusion of a small structural damping. Figure 3.1 shows the modal mechanical and acoustic resistance of the duralumin spherical shell in air at resonance. It is evident that the modal acoustic resistance dominates over the mechanical resistance, because the latter is due to the small structural damping. The minimum at $ka = 25.303$ in the curves is due to the fundamental membrane resonance $n = 0$ of the upper branch. The modal admittance at that frequency is almost 30 dB below that of the lower branch resonance in the neighborhood. This is not because of the total modal resistance r_n , but because of the low mode number ($n = 0$). As seen from Curve (3) of Figure 3.1, the response is considered flat within 3 dB. For the driving point modal admittance, the mode factor $(2n + 1)$ in Equation (3.12) amplifies the differences between the upper and lower branch modal response.

When in water, this situation changes completely. First, the lower branch resonances remain within the lower frequency range for high mode numbers up to $n = 43$, as shown in Tables 3.8 and 3.9, because the acoustic modal mass $M_{an}(\omega_n)$ are comparably large. The upper branch resonances are, of course, in the high frequency range except for the first few resonances. Second, the acoustic modal

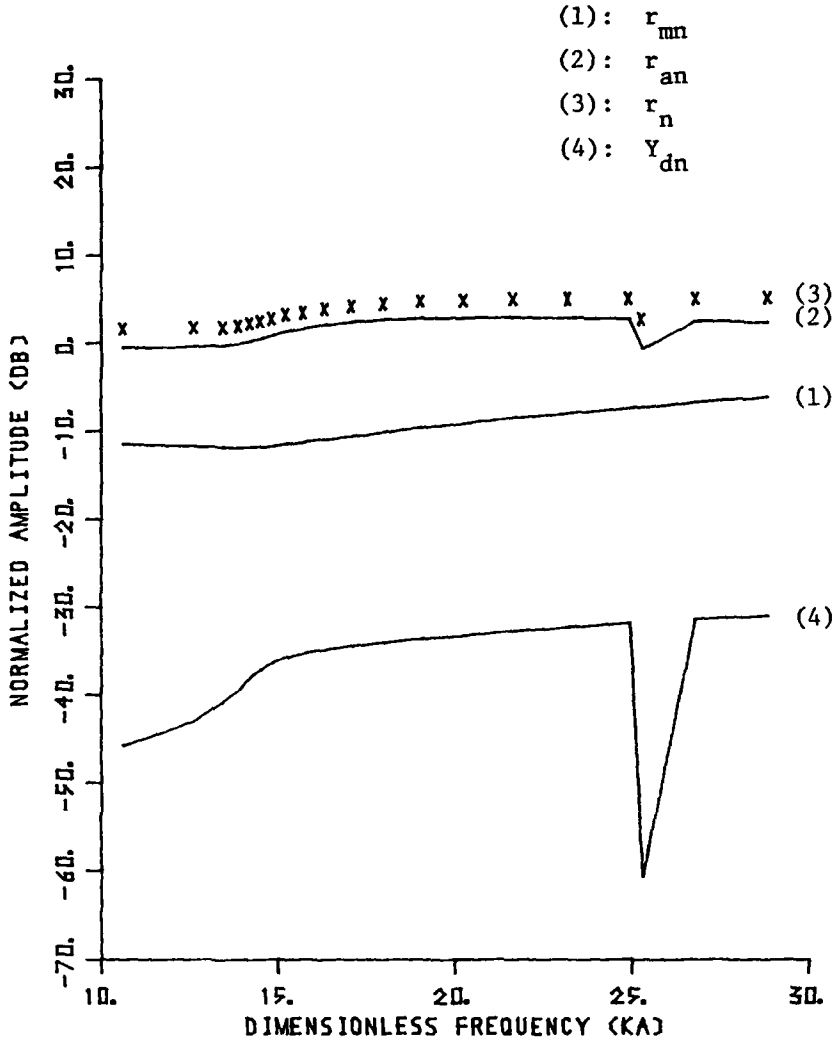

Figure 3.1 Frequency response of modal mechanical resistance (r_{mn}), modal acoustic resistance (r_{an}, total modal resistance (r_n), and modal admittance (Y_{dn}) in air, normalized to $(\rho c)_{air}$

resistance $r_{an}(\omega_n)$ is much smaller than the characteristic impedance $(\rho c)_{water} = 5.79$, and decreases with increasing mode number (see Figure 2.4) while it is near the characteristic impedance at the frequencies of the upper branch. This means that the modal admittance increases as the mode number and natural frequency increase. However, modes of the upper branch may not show up as sharply. The contribution of the resonant modal term of the lower branch to the DPA is larger than that of the upper branch. Finally, the internal damping will cause the admittance to drop, but not significantly. Figure 3.2 shows the resonant response of the modal structural resistance, acoustic resistance, total resistance, and admittance in water. The modal mechanical resistance r_{mn} increases slightly with increasing resonance frequency. The modal acoustic resistance r_{an} initially decreases sharply with increasing resonance frequency, which corresponds to the lower branch resonances, but eventually increases to ρc as the mode number and the natural frequency increases. All the upper branch resonances have modal resistance of ρc because the normalized resonances of the upper branch $(k_n a)$ are larger than n (see Figure 2.4). The resonant modal admittance is thus mechanically controlled except for the first few lower branch resonances and all of the upper branch resonances. The resonant modal resistance and admittance for a shell vibrating in water are much higher than those in air except for the first two modes as shown in Figure 3.1. Again, the factor $(2n + 1)$ accounts for the difference. For example, the first resonance in air occurs at $ka = 10.633$, for $n = 2$, and the modal admittance is 13.1 dB, while for $ka = 10.665$, corresponding to the $n = 32$ mode when the shell is submerged in water, it has a modal admittance of

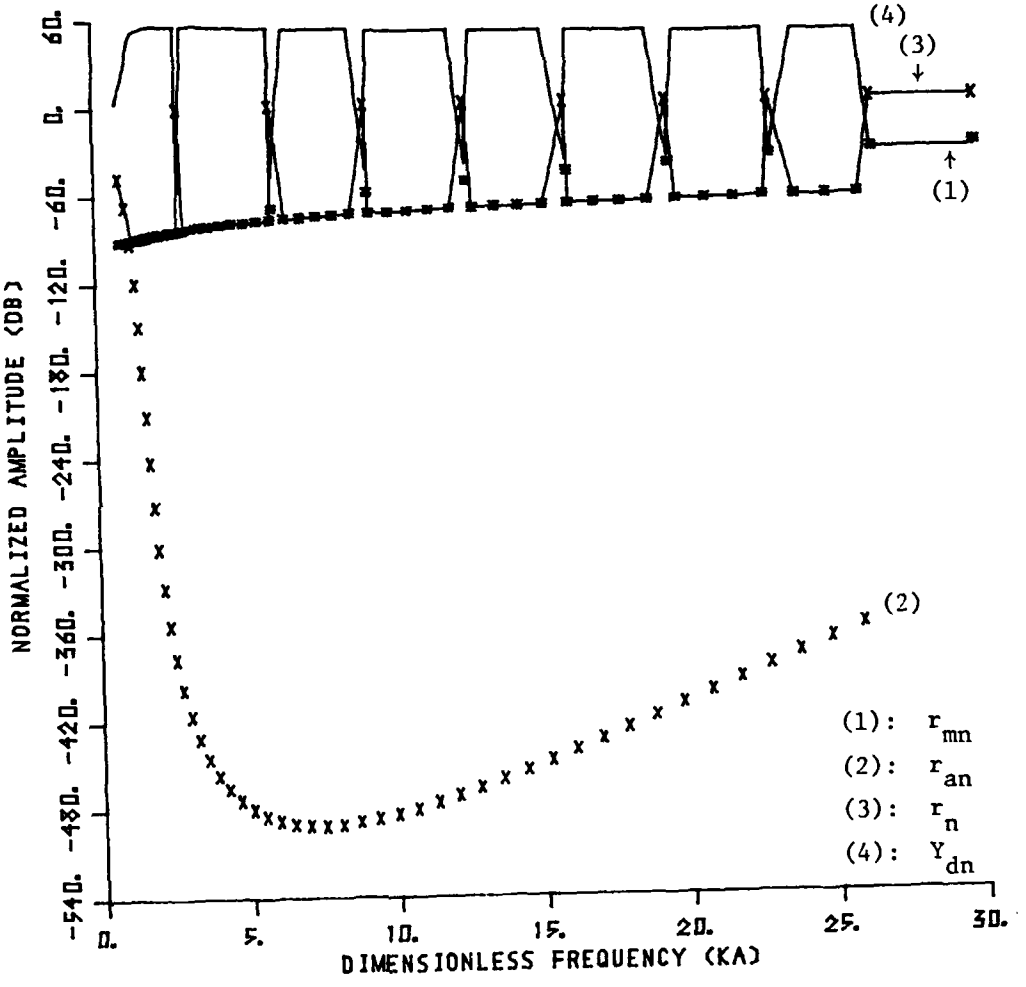

Figure 3.2 Frequency response of modal mechanical resistance (r_{mn}), modal acoustic resistance (r_{an}), total resistance (r_n), and modal admittance (Y_{dn}) in water, normalized to $(\rho c)_{water}$

AD-A086 008 PENNSYLVANIA STATE UNIV UNIVERSITY PARK APPLIED RESE--ETC F/G 20/1
A STUDY OF THE NEARFIELD OF AN EXCITED SPHERICAL SHELL.(U)
MAR 80 E WONG N00024-79-C-6043
UNCLASSIFIED ARL/PSU/TM-80-30 NL

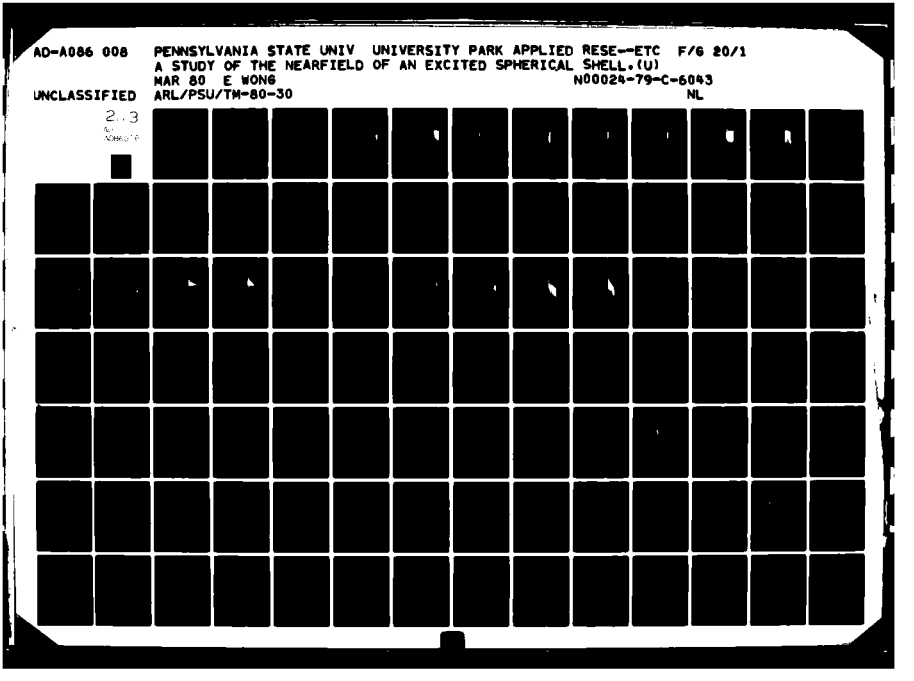

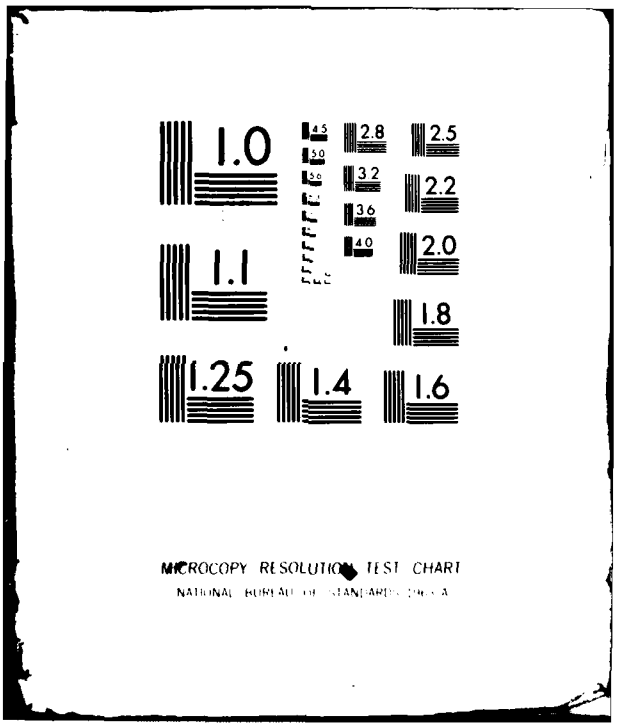
1.0
1.1
1.25
1.4
1.6
1.8
2.0
2.2
2.5
2.8
3.2
3.6
4.0
4.5
5.0
MICROCOPY RESOLUTION TEST CHART
NATIONAL BUREAU OF STANDARDS-1963-A

38.8 dB. However, if one were to compute the modal admittance for much higher mode order (and resonance), the modal resistance in water would be much higher than that for air, and the modal admittance in air would be much higher than that in water.

Theoretically, the largest contribution to the lower branch resonance comes from the resonant modal term of the lower branch, while the resonant modal term of the upper branch is dominated by the adjoining resonant modal terms of the lower branch. Summation of all modal terms gives a resultant DPA as in Equation (3.12), which should include the resonant modal term. This also applies to the pressure field in Equation (3.13), although the Hankel function converges well when $n \geq ka$.

The magnitude of the DPA is shown as a function of ka in Figures 3.3 through 3.10 for two shells which are submerged in both air and water when both membrane and classical theories are considered. In air, Figures 3.3 and 3.4 show that the DPA of shells, h = 0.0514" and 0.1069", are not significantly different for a membrane shell theory (whenever the membrane or classical theory is employed, they are conveniently called membrane or classical shell, respectively). The main feature of these two curves is that the resonances are so clustered together (high resonant density), as shown in Figure 2.6, that the curves exhibit no distinct resonant response except at $ka = 14.59$. This is the frequency limit of the lower branch of the membrane theory. Thus, there is an infinite number of modes near this frequency. This explains the large peak at that frequency, because the energy in the shell is concentrated near that frequency. Since all the resonances are close to this frequency, even for the first

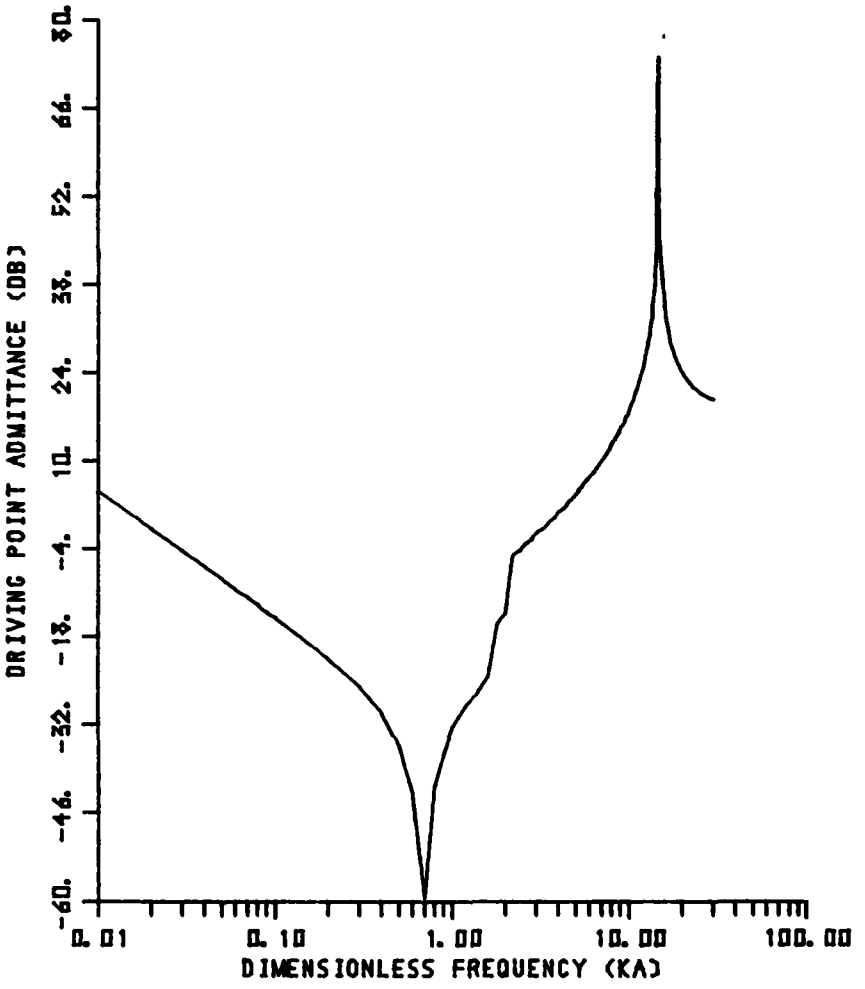

Figure 3.3 DPA of a membrane shell with thickness h = 0.0514" in air

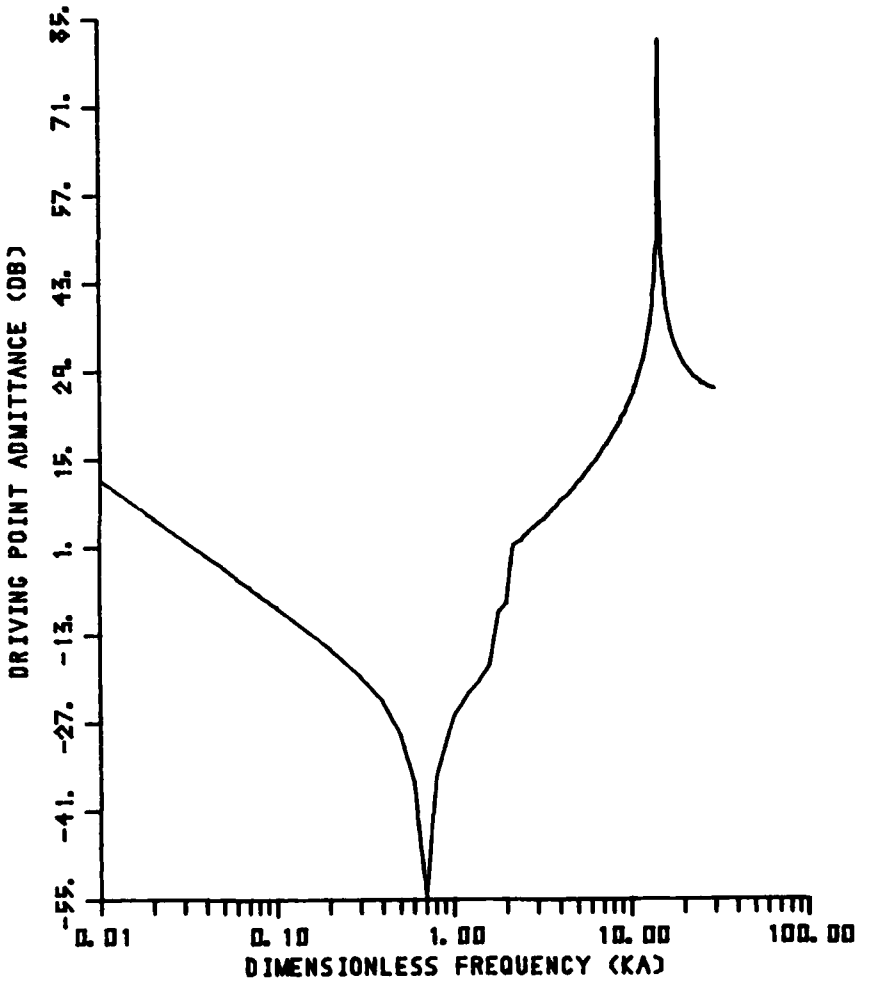

Figure 3.4 DPA of a membrane shell with thickness h = 0.1069" in air

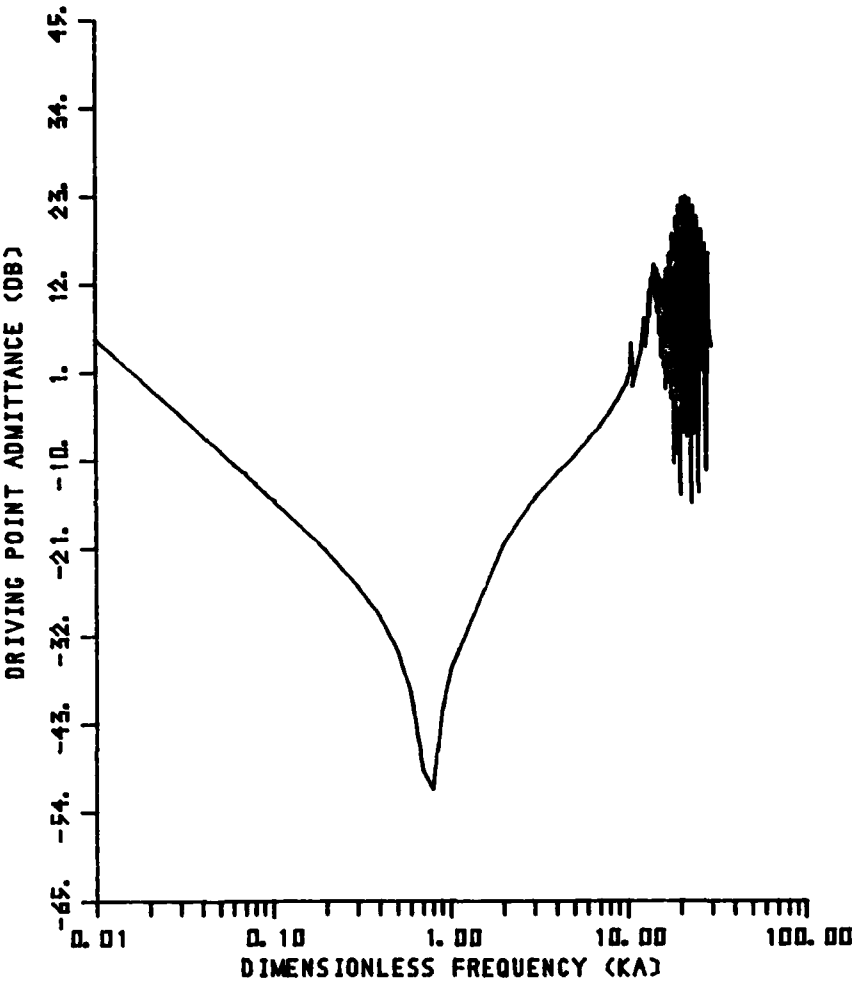

Figure 3.5 DPA of a classical shell with thickness h = 0.0514" in air

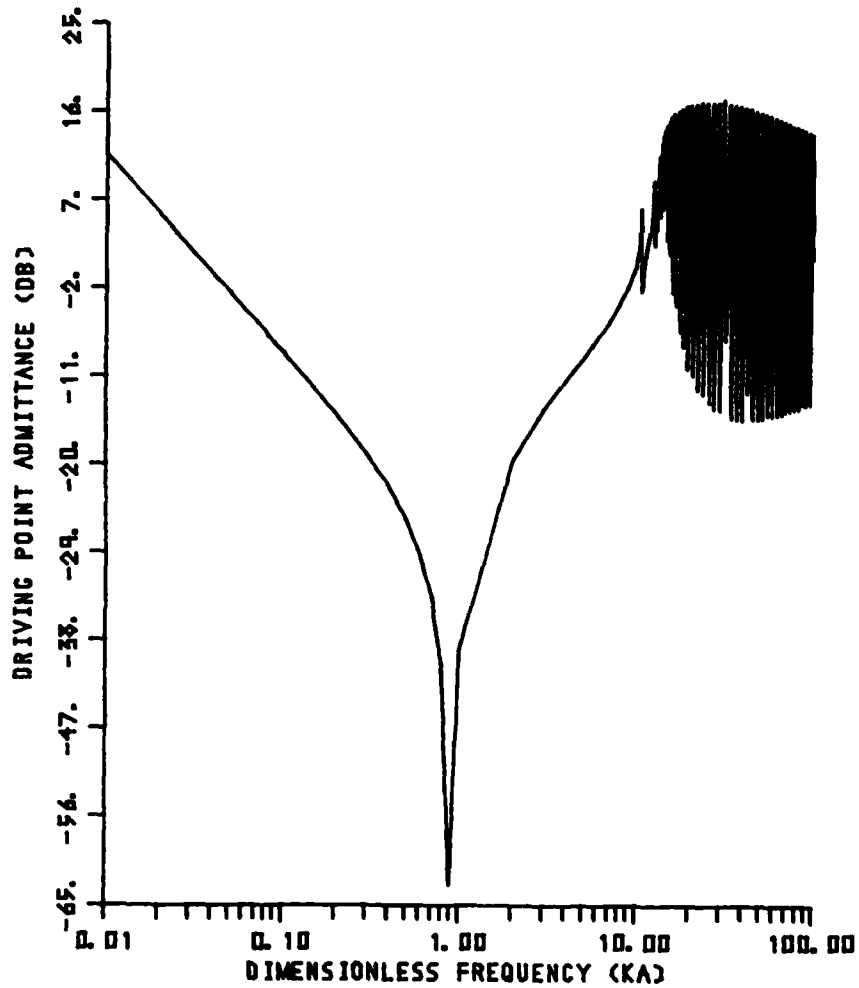

Figure 3.6a DPA of a classical shell with thickness h = 0.1069" in air, $0.01 \leq ka \leq 100$

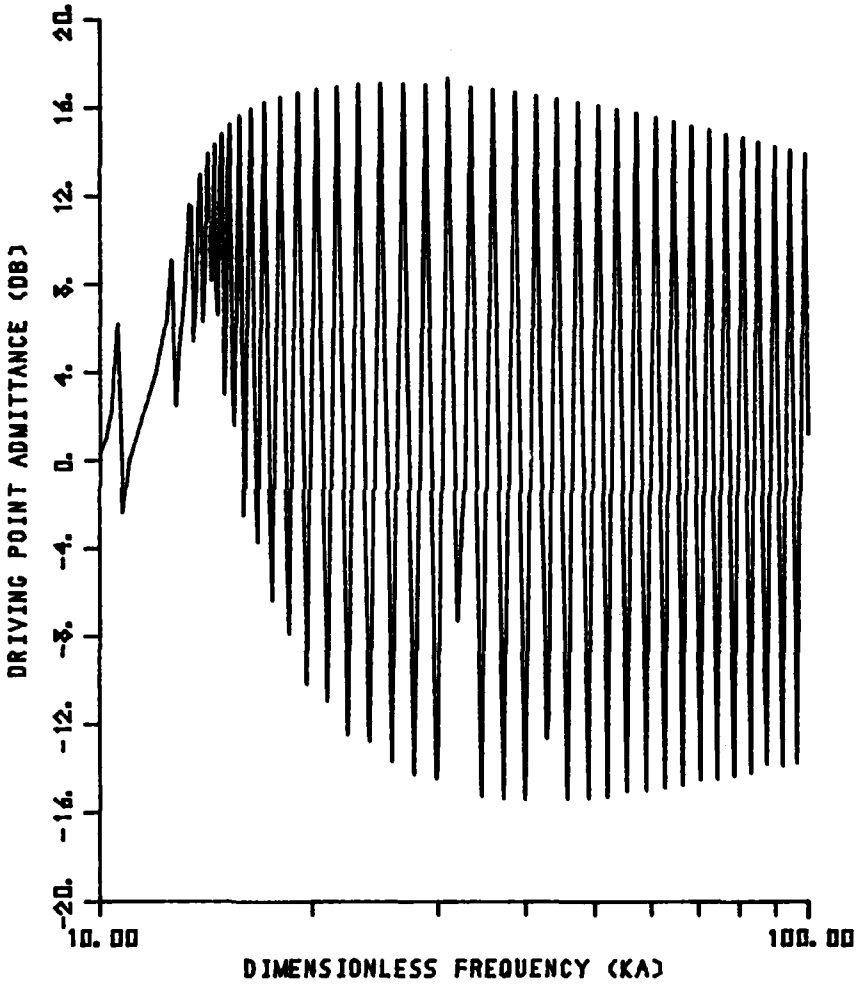

Figure 3.6b DPA of a classical shell with thickness h = 0.1069" in air, $10 \leq ka \leq 100$

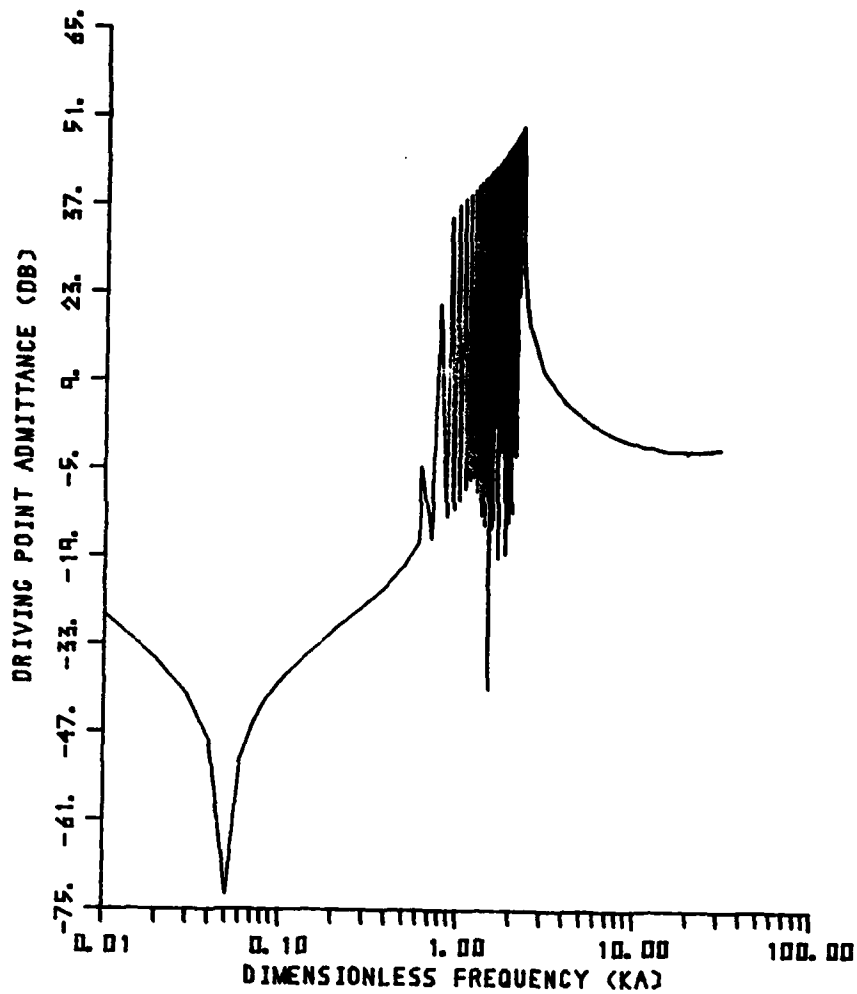

Figure 3.7 DPA of a membrane shell with thickness h = 0.0514" in water

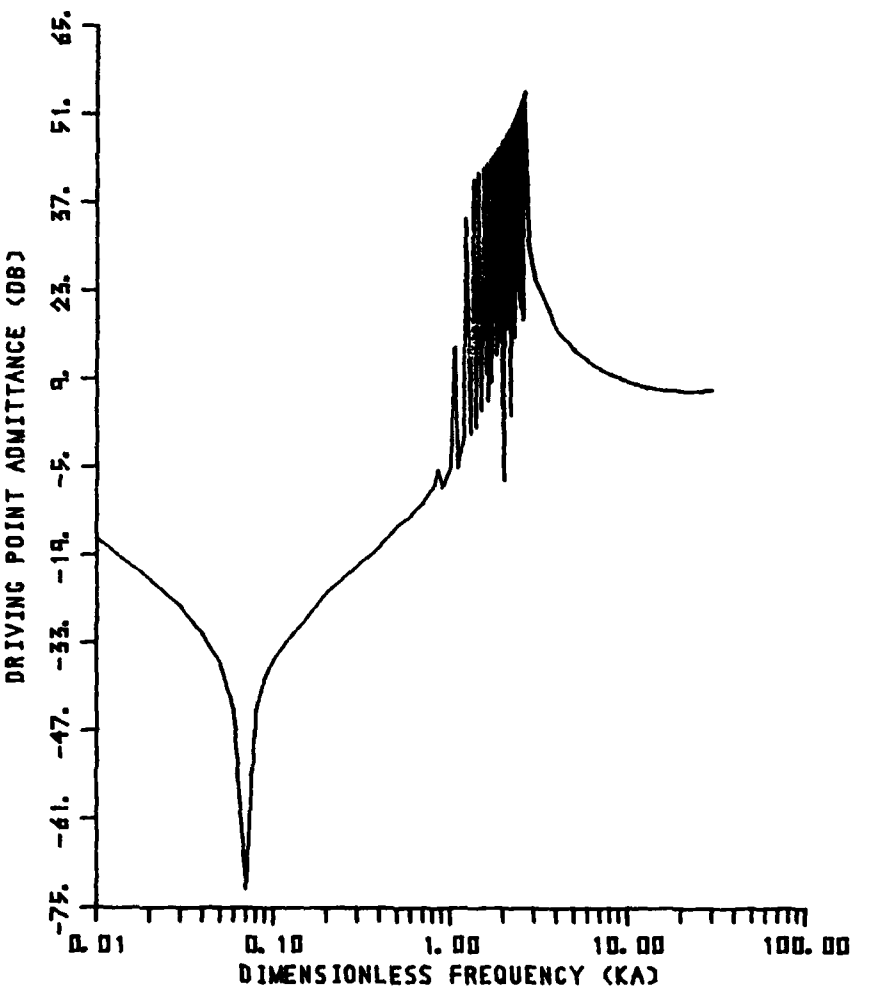

Figure 3.8 DPA of a membrane shell with thickness h = 0.1069" in water

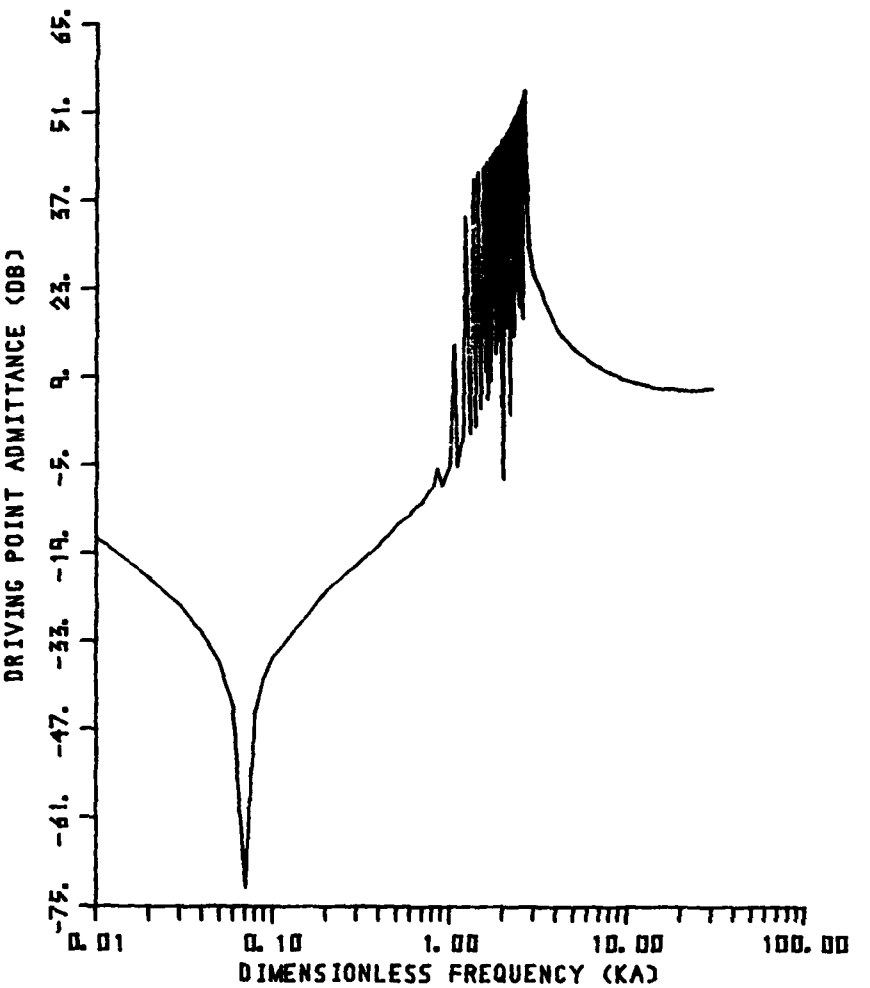

Figure 3.8 DPA of a membrane shell with thickness h = 0.1069" in water

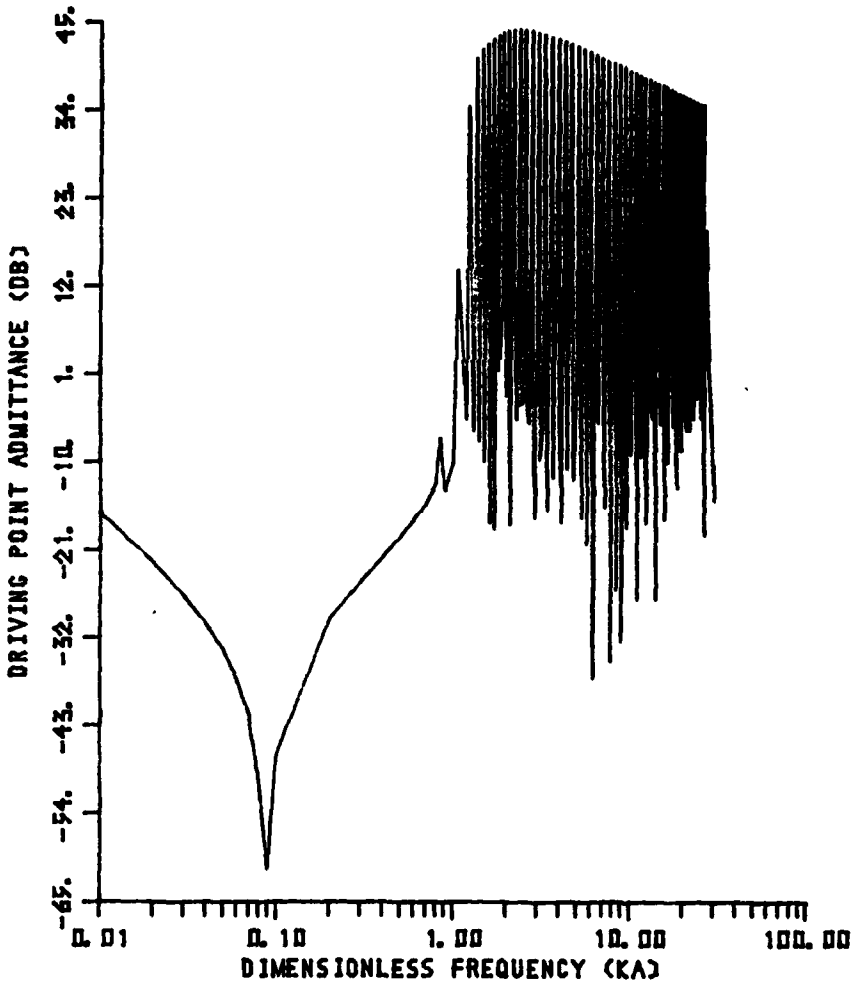

Figure 3.9 DPA of a classical shell with thickness h = 0.0514" in water

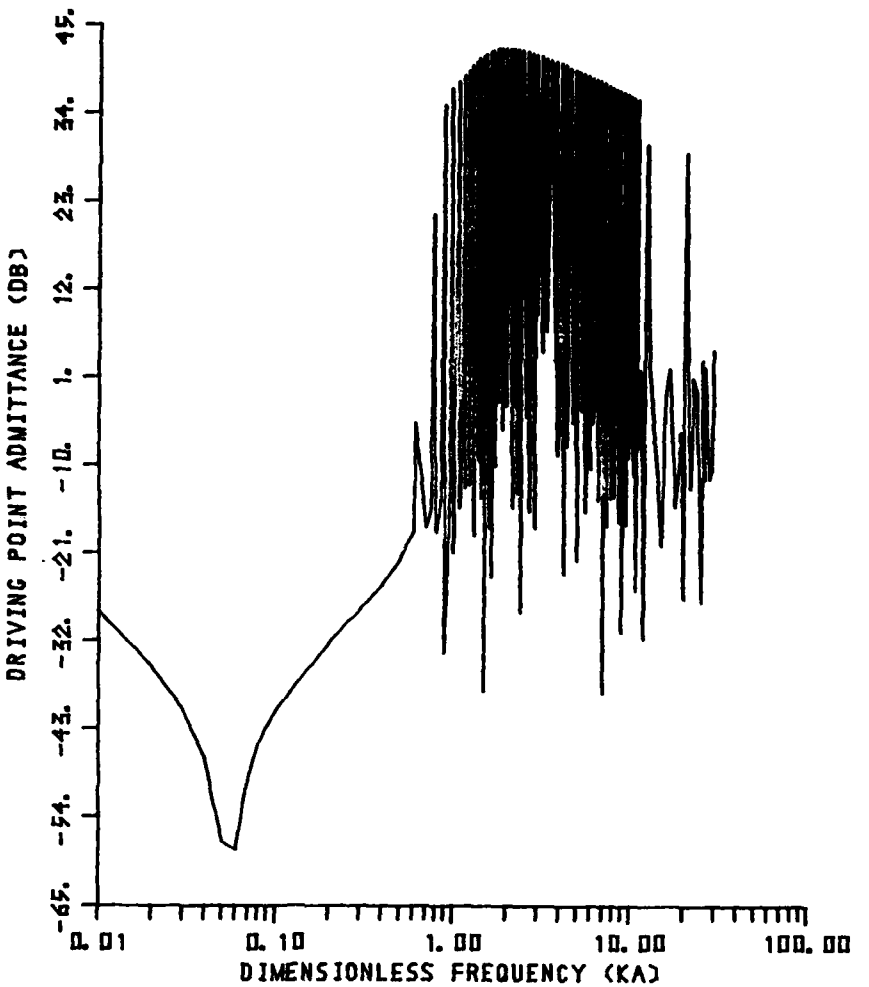

Figure 3.10 DPA of a classical shell with thickness h = 0.1069" in water

resonance, no distinct resonance response can be observed. The non-normalized thin shell admittance is approximately 6 dB higher than that for the thick shell because the mechanical impedance of the thin shell is approximately half of that for the thick shell, see Equation (2.26). However, the normalized thick shell response in Figure 3.4 is 6 dB higher than that for the thin shell response because the ratio of the normalization factors used for the shells is approximately equal to 4, which accounts for the 12 dB difference. The minimum response at frequencies less than the first resonance corresponds to the first anti-resonance between the rigid body frequency ($\Omega_1 = 0$) and the first resonance (Ω_2). Thus, for frequencies below the first anti-resonance, the motion at the center of gravity of the freely suspended shell is governed by a term $Y_o = 1/Z_o = 1/i\omega M$, where M is the total mass of the shell. Therefore, the slope of the response is 6 dB per octave. For classical shells, the resonances are well-spaced, and the resonant response shows distinct peaks in Figures 3.5, 3.6A, and 3.6B.

When the shells are submerged in water, the DPA curve is quite different from that in air. For a membrane shell, the resonance increases slowly with the increasing mode number as shown in Figures 3.7 and 3.8, while the peaks at the resonances are distinct for resonances up to $ka = 3.3$. All the remaining resonances are located close to this frequency, which means that the energy is concentrated near this frequency. Thus, no distinct resonance response is observed above this frequency. The upper branch modes have a low admittance, so that they do not produce peak response at their resonances, which occur mostly above $ka = 3.3$. However, since the lowest mode ($n = 2$) resonance is less than $ka = 1$, the resonance peaks are distinct since

they occur at frequencies far enough below $ka = 3.3$. The resonant response increases monotonically up to $ka = 3.3$ due to the factor $(2n + 1)$ in the expression for the admittance. The curves for classical shells are shown in Figures 3.9 and 3.10.

Generally, the height of the DPA response in air is higher than that in water below the first resonance. This is explained by the fact that the virtual mass of the displaced acoustic medium at low frequencies is negligible in air when compared to the mass of the shell but is much higher than the mass of the shell vibrating in water. Thus, since the admittance below the first resonance is $1/\omega M$, M being the total mass being vibrated, the admittance in air is much higher than that in water. However, the admittance of the shell at resonances is lower in air than in water because of the previously explained behavior of the modal admittances in air and in water.

The minimum point in Figures 3.3 through 3.10 corresponds to anti-resonance between the rigid body motion frequency $(\Omega_1 = 0)$ and the first resonance. It will shift due to the position of the first resonance. The position of the first resonance of the shell in air is the same for all shell thickness, so that the anti-resonance does not shift. However, the first resonance of the shells submerged in water is almost one-tenth of that in air, so that the location of the anti-resonance shifts down accordingly.

In vacuo or air, the mean value of the DPA for a shell will approach the value of the characteristic impedance of an infinite plate. The result is shown in Figure 3.6B. The line MN in the resonant spectrum is the predicted mean value computed by Equation (2.58). The resonant mean value is in excellent agreement with the

line MN , but the predicted mean value in the first few modes of the membrane range fails to agree. This is because there are so few resonances in the membrane range.

The mean value method can also be used to predict the mean value of the DPA of a shell in water. However, it has to overcome the difficulty due to the introduction of the virtual mass in the equation of motion. At very high frequency, the mean value of the DPA of a submerged shell again approaches the unloaded plate value.

As previously discussed, the fluid loading is so important that it affects the frequency spectrum. The role it plays in the directivity pattern is to change the amplitude of the pattern but not the shape. Figures 3.11 and 3.12 are the directivity plots of the 2^{nd} mode at their resonances, $ka = 1.0307$ in water and $ka = 10.659$ in air, of a shell with thickness $h = 0.1069"$. All the peaks shown in Figures 3.3 through 3.10 represent resonances of the lower branch. Figures 3.13 and 3.14 show the modal shapes for the resonance of the 4^{th} mode of the upper branch, and at $ka = 14.886$ for the resonance of the 29^{th} mode of the lower branch for a shell with thickness $h = 0.1069"$ in water. Close examination of these two mode shapes show that the 29^{th} mode of the lower branch predominates the shell vibration response at $ka = 15.745$ which should have exhibited a 4^{th} ordered mode.

The pressure field in water is higher than that in air since the acoustic resistance in air is much larger than that in water. The symmetrical resonant shape, and the mode number of a directivity pattern are information to be used to properly identify a resonance experimentally.

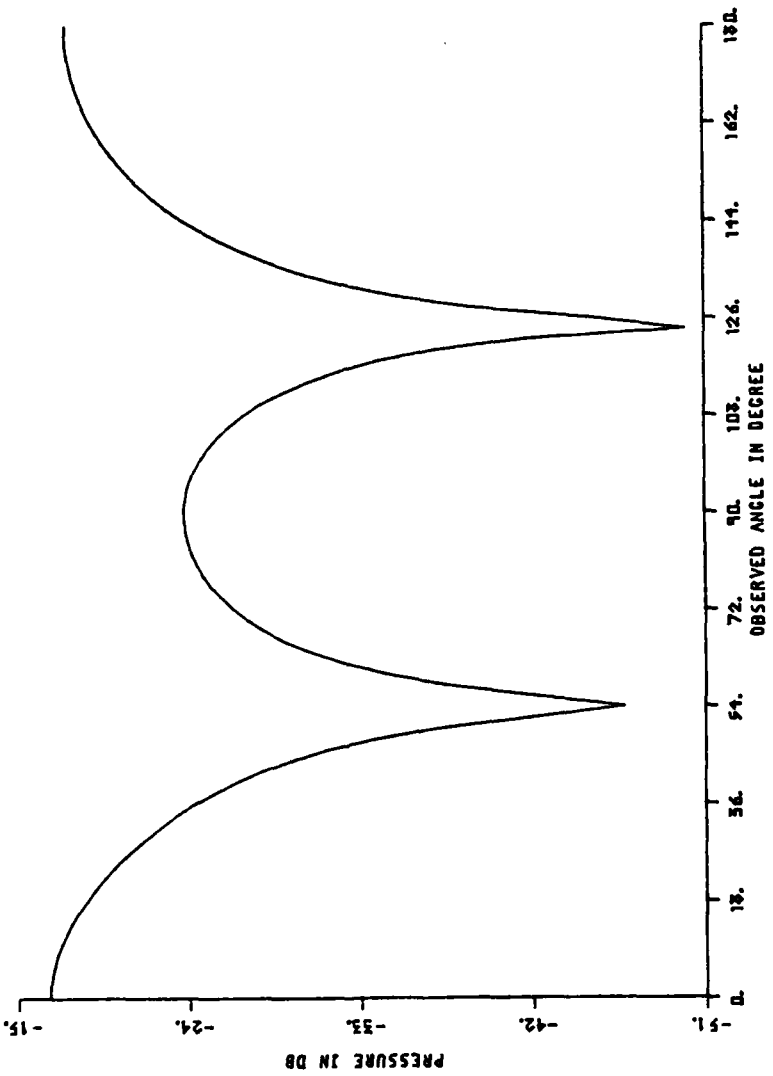

Figure 3.11 Directivity pattern of a force excited classical shell with thickness h = 0.1069" for ka = 1.0307 , n = 2 in water

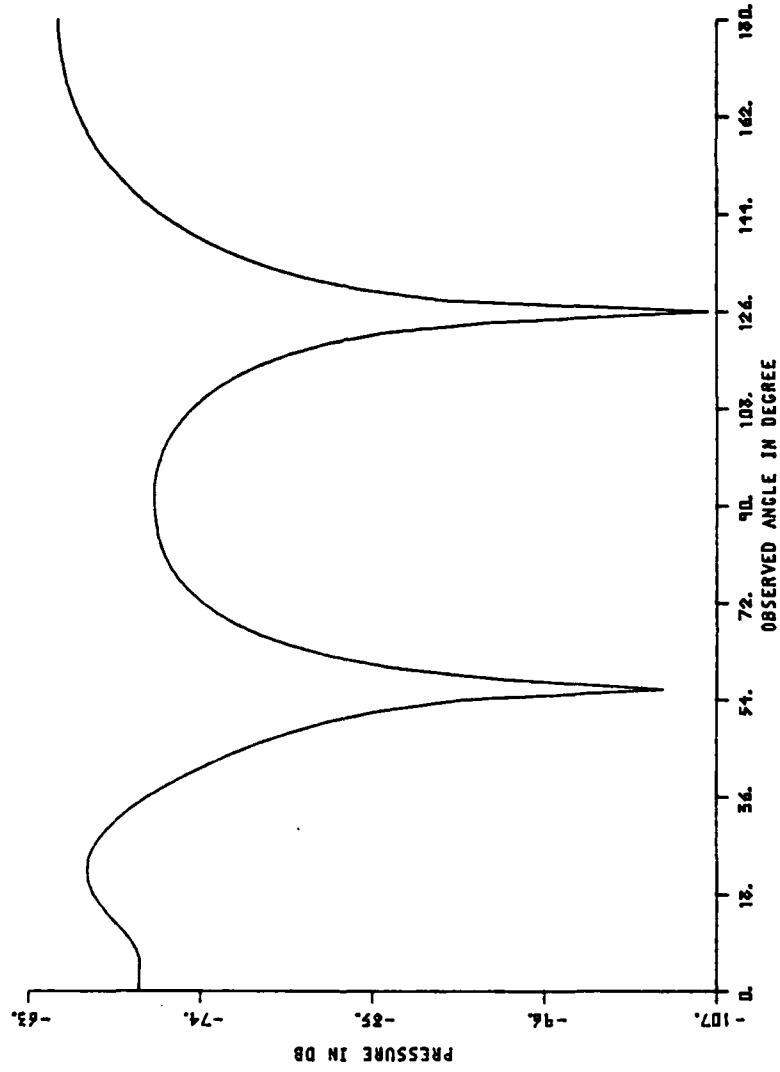

Figure 3.12 Directivity pattern of a force excited classical shell with thickness h = 0.1069" for ka = 10.659, n = 2 in air

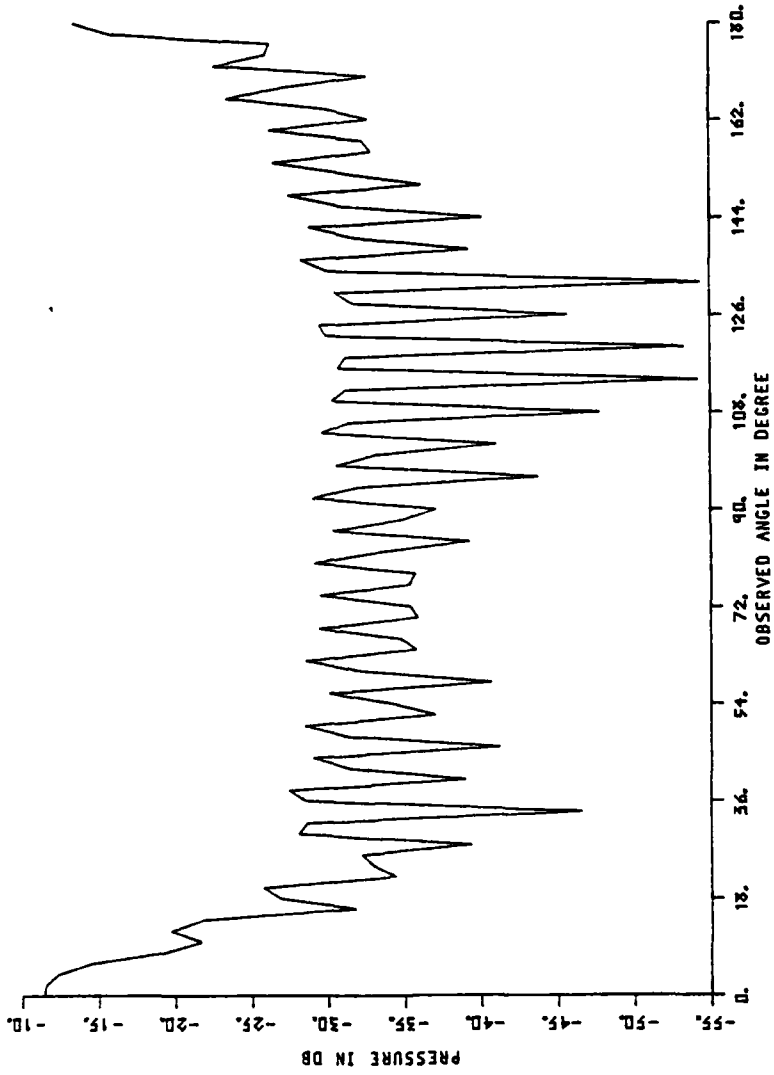

Figure 3.13 Directivity pattern of a force excited classical shell with thickness h = 0.1069" for ka = 15.745 , n = 4 in water

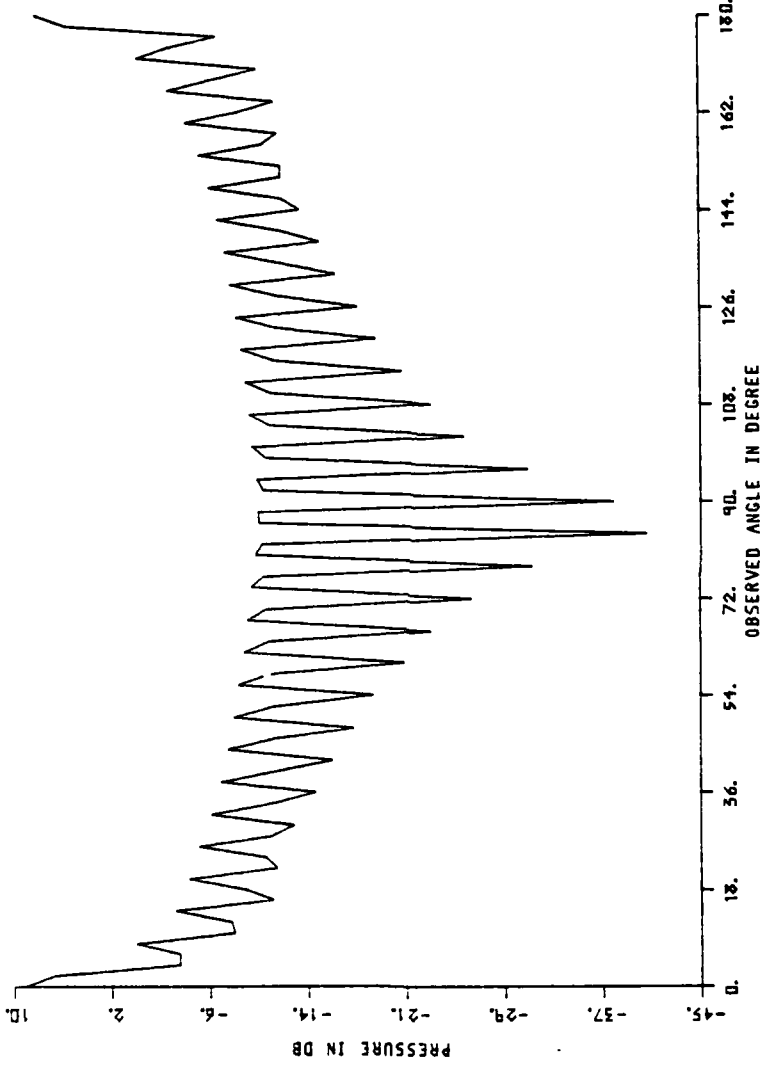

Figure 3.14 Directivity pattern of a force excited classical shell with thickness h = 0.1069" for ka = 14.886, n = 29 in water

3.3 A Spherical Thin Shell Insonified by an Acoustic Spherical Wave in a Fluid Medium

In order to have a better understanding of the elastic scattering response of an elastic spherical shell as being insonified by a spherical acoustic source, a discussion of the rigid and the radiated scattering of a scattered field is given first. For an elastic structure, the observed pressure field is not only the sum of the incident pressure $p_i(r,\theta)$ and the blocked (rigid) scattered pressure $p_h(r,\theta)$ as scattered by the boundary of the structure, but must also include the radiated scattered pressure due to the response of the vibration of the structure generated by the incident wave. The resultant pressure is, therefore,

$$p = p_i + p_s \quad , \tag{3.14}$$

where the scattered pressure is:

$$p_s = p_h + p_r \quad .$$

The geometrical configuration of the system is shown in Figure 1.1. The source is located at a point S on the positive z-axis, at a distance r_o from the shell's center. The observer point is located at a distance r from the center and θ degree off the z-axis. The system is assumed to be axisymmetric. Expanding the spherical acoustic source $p_i = e^{ikd}/(4\pi d)$ in terms of Legendre function $P_n(\eta)$ in the spherical coordinates [20], one has:

$$p_i = e^{ikd}/(4\pi d)$$

$$= (ik/2\pi)h_o(kd)$$

$$= (ik/4\pi)\sum_{n=o}^{\infty}(2n+1)P_n(\eta)\begin{cases} j_n(kr_o)h_n(kr) & r \geq r_o \\ j_n(kr)h_n(kr_o) & r \leq r_o \end{cases},$$

(3.15)

where $k = \omega/c$, j_n and h_n are, respectively, spherical Bessel and Hankel functions of the first kind and of order n.

First, the scattering by a rigid sphere will be evaluated. The rigid scattered pressure p_h is the pressure field from the surface of the shell considered as a rigid sphere. It can be written in the following form:

$$p_h = \sum_{n=o}^{\infty} D_n h_n(kr)P_n(\eta) \quad , \tag{3.16}$$

where D_n is an undetermined coefficient. Therefore, the resultant pressure p_{ih} due to the boundary reflection and the incident pressure p_i is:

$$p_{ih} = p_i + p_h \quad . \tag{3.17}$$

On the surface of the shell $r = a$, the resultant particle velocity must vanish at the radial direction

$$\dot{W}_{ih} = 0 \quad . \tag{3.18}$$

The continuity condition on the spherical surface requires that the radial component of the shell velocity equals the particle velocity at the boundary as follows:

$$\rho \frac{\partial \dot{W}_{ih}}{\partial t} = - \frac{\partial p_{ih}}{\partial r} \quad , \quad \text{at} \quad r = a \quad . \tag{3.19}$$

Applying the boundary condition, one has:

$$\frac{\partial p_i}{\partial r} + \frac{\partial p_h}{\partial r} = 0 \quad , \quad \text{at} \quad r = a \quad .$$

Substituting p_i and p_h from Equations (3.15) and (3.16), the undetermined coefficient D_n is obtained as:

$$D_n = - (ik/4\pi)(2n + 1) \frac{j_n'(ka)}{h_n'(ka)} h_n(kr_o) \quad ,$$

where j_n' and h_n' are the spatial derivative of j_n and h_n along the radial direction, respectively. Substituting D_n into Equation (3.16), this gives the scattered pressure field from a rigid sphere:

$$p_h = - \frac{ik}{4\pi} \sum_{n=o}^{\infty} (2n + 1) P_n(\eta) j_n(ka) h_n(kr) \frac{h_n(kr)}{h_n'(ka)} \, . \tag{3.20}$$

For the scattered pressure from an elastic spherical shell, the radiated scattered pressure of the shell p_r can also be expressed as harmonic outgoing waves in the form of Equation (3.16):

$$p_r = \sum_{n=o}^{\infty} B_n h_n(kr) P_n(\eta) \quad , \tag{3.21}$$

where B_n is the expansion coefficient to be determined. The radiated pressure must satisfy Euler's equation on the surface (r = a) as:

$$\frac{\partial p_r}{\partial r} = - \rho \frac{\partial \dot{W}}{\partial t} \quad . \tag{3.22}$$

The response velocity $\dot{W}$ on the surface of a submerged shell is equal to the ratio of the resultant pressure on the surface to the mechanical

impedance. The ratio, given in the form of Equation (3.5), is:

$$\dot{W}_n = - \frac{p_{in} + p_{hn} + p_{rn}}{Z_{mn}} \quad ,$$

where the p_{in} , p_{hn} , and p_{rn} are the modal terms of the p_i , p_h , and p_r , respectively. And $p_{rn} = Z_{an}\dot{W}_n$ is obtained from Equation (3.6). Thus,

$$\dot{W}_n = - \frac{p_{in} + p_{hn}}{Z_{an} + Z_{mn}} \quad . \tag{3.23}$$

Substituting Equation (3.23) into Equation (3.22), one has:

$$\frac{\partial p_{rn}}{\partial r} = - i\rho\omega \frac{p_{in} + p_{hn}}{Z_n} \quad . \tag{3.24}$$

Finally, substituting Equations (3.14), (3.20), and (3.21) into Equation (3.23), one obtains the coefficient as:

$$B_n = i \frac{\rho c}{4\pi a^2 k} (2n + 1) \frac{h_n(kr_o)}{(Z_{an} + Z_{mn})[h_n'(ka)]^2} \quad .$$

From Equation (3.17), the radiated pressure field becomes:

$$p_r = i \frac{\rho c}{4\pi a^2 k} \sum_{n=o}^{\infty} (2n + 1) P_n(\eta) \frac{h_n(kr_o) h_n(kr)}{Z_n [h_n'(ka)]^2} \quad . \tag{3.25}$$

Substituting Equations (3.20) and (3.25) for p_h and p_r into Equation (3.14), the total scattered pressure is expressed as:

$$p_s = -\frac{ik}{4\pi}\sum_{n=o}^{\infty}(2n+1)P_n(\eta)\frac{h_n(kr_o)h_n(kr)}{h_n'(ka)}$$

$$\times\left[j_n'(ka) - \frac{\rho c}{(ka)^2 h_n'(ka) Z_n}\right]$$

$$= -\frac{ik}{4\pi}\sum_{n=o}^{\infty}(2n+1)P_n(\eta)h_n(kr_o)h_n(kr)$$

$$\times\left[\frac{j_n(ka) - i\frac{Z_{mn}}{\rho c}j_n'(ka)}{h_n(ka) - i\frac{Z_{mn}}{\rho c}h_n'(ka)}\right] \quad . \qquad (3.26)$$

From Equations (3.14), (3.15), and (3.26), the total pressure p of an elastic thin spherical shell driven by a spherical acoustic source is:

$$p = \frac{ik}{4\pi}\sum_{n=o}^{\infty}(2n+1)P_n(\eta)\begin{Bmatrix} h_n(kr) \\ h_n(kr_o)\end{Bmatrix}\begin{Bmatrix} j_n(kr_o) \\ j_n(kr)\end{Bmatrix}$$

$$-\begin{bmatrix} h_n(kr_o) \\ h_n(kr)\end{bmatrix}\begin{bmatrix} j_n(ka) - i\frac{Z_{mn}}{\rho c}j_n'(ka) \\ h_n(ka) - i\frac{Z_{mn}}{\rho c}h_n'(ka)\end{bmatrix}\begin{matrix} r \geq r_o \\ r \leq r_o\end{matrix} \quad . \qquad (3.27)$$

The result as given by Equation (3.27) can also be derived [8] by using the technique of Hamilton's variation principle. However, the result obtained by this technique does not give specific physical interpretation about the rigid scattering pressure, the radiated scattered pressure, or the relation between them. In contrast, the derivation previously given in this section can give a definitive physical insight of the contributions to the scattered pressure. For

a submerged, elastic spherical shell, the scattered pressure is the sum of the rigid and the radiated scattering as shown in Equation (3.26). The radiated scattering is a result of the characteristic of an elastic structure. It may be called "elastic scattering."

The characteristic of the elastic scattering is that the radiated scattered pressure p_r changes rapidly with resonant frequency. Since the $IM(Z_{an} + Z_{mn})$ varies rapidly near resonance in Equation (3.25) and vanishes at resonance while the factor of $(Z_{an} + Z_{mn})^{-1}$ changes slowly, the radiated pressure p_r is dominated by Z_n and fluctuates rapidly with frequency. The rapid fluctuation in the pressure is the result of the structural resonances as the reactance $M_{mn}(\omega_n)$ of the mechanical impedance is well-coupled to the ractance $M_{an}(\omega_n)$ of the acoustic impedance. The radiated pressure spectrum is similar to that of the DPA. Both the radiated pressure and DPA spectra are controlled by the total impedance Z_n. More precisely, these represent the response of the motion of the shell's surface to the incident pressure. However, the radiated pressure in Equation (3.25) is not only controlled by Z_n, but also by the characteristic impedance ρc. The frequency spectra of the pressure field of an elastic shell excited by an acoustic point-source were computed for two different shell thicknesses whether submerged in air and water, and the pressure evaluated at $\theta = 0°$ and $180°$.

In the illuminated zone, the total pressure is composed of the direct field, the reflected field, the diffracted field due to creeping waves around the shell, and the radiated field due to the vibration of the shell. The reflected and diffracted fields combine to generate

the blocked (rigid surface) scattering p_h . Thus, the first four fields are present in the scattering from a rigid sphere. The creeping waves of the diffracted field, which exists for $ka > 1$, are usually weak and thus are not noticable in the illuminated zone. However, since the creeping waves are the only waves existing in the shadow zone for a rigid sphere, they interfere destructively and constructively as a function of the acoustic wave number ka . If the radiated field, which is proportional to the characteristic impedance ρc of the medium, is high, then it predominates in the illuminated zone and the shadow zone, especially near resonance frequencies.

In air, the scattered pressure from an elastic shell in the illuminated zone $(\theta = 0°)$ is shown in Figures 3.15, 3.16, and 3.17. It can be seen that the rigid sphere is dominated by the direct and reflected waves; hence, no fluctuation in the frequency spectra are noticeable as was reasoned above. Since the characteristic impedance of air is low, the radiated pressure, even near resonances, is too low when compared to the scattered pressure from a rigid sphere. Hence, the total scattered pressure of a spherical shell in air resembles that of a rigid sphere in the illuminated zone.

In the shadow zone of a spherical shell in air, the scattered pressure in the low frequency range is that of long wavelength Rayleigh forward scattering $(ka << 1)$ which increases with frequency as can be easily seen in Figures 3.18, 3.19, and 3.20. In the high frequency range, the creeping waves are the only contributor to the field in the shadow zone of a rigid sphere. The constructive and destructive interference can be seen for a rigid sphere for $ka > 1$.

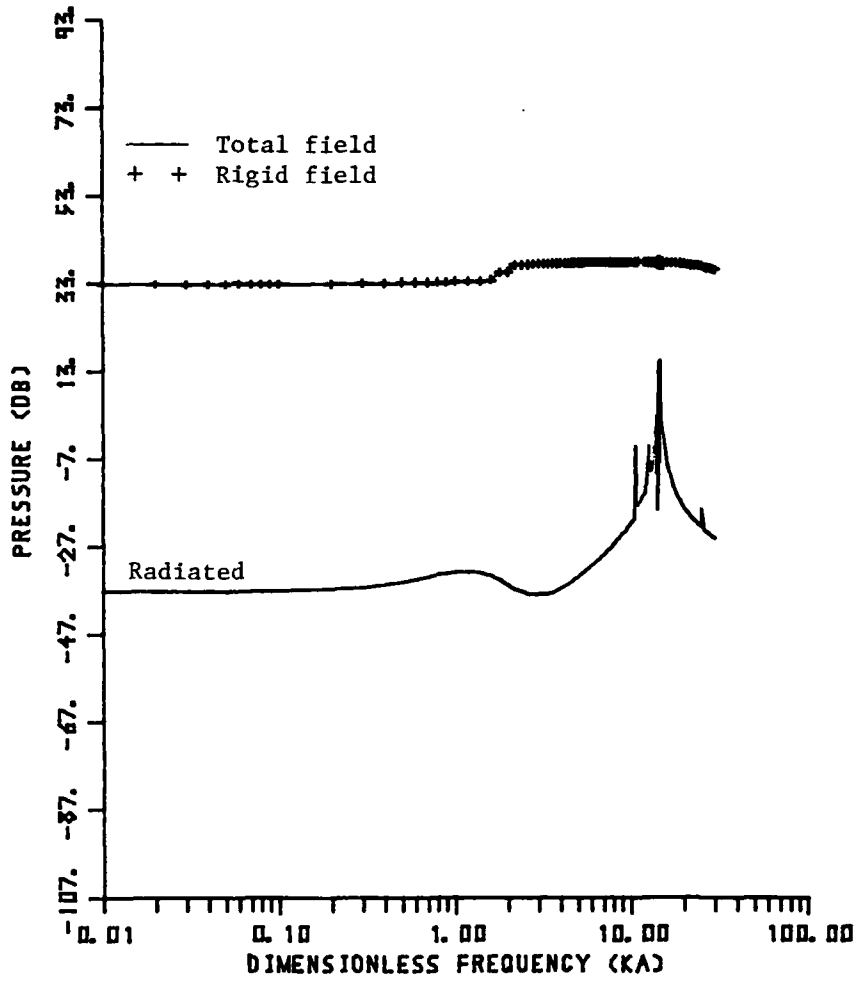

Figure 3.15 Frequency response of a membrane shell with thickness $h = 0.1069"$ in air for $r_o = 8.25"$, $r = 8.5"$, and $\theta = 0°$

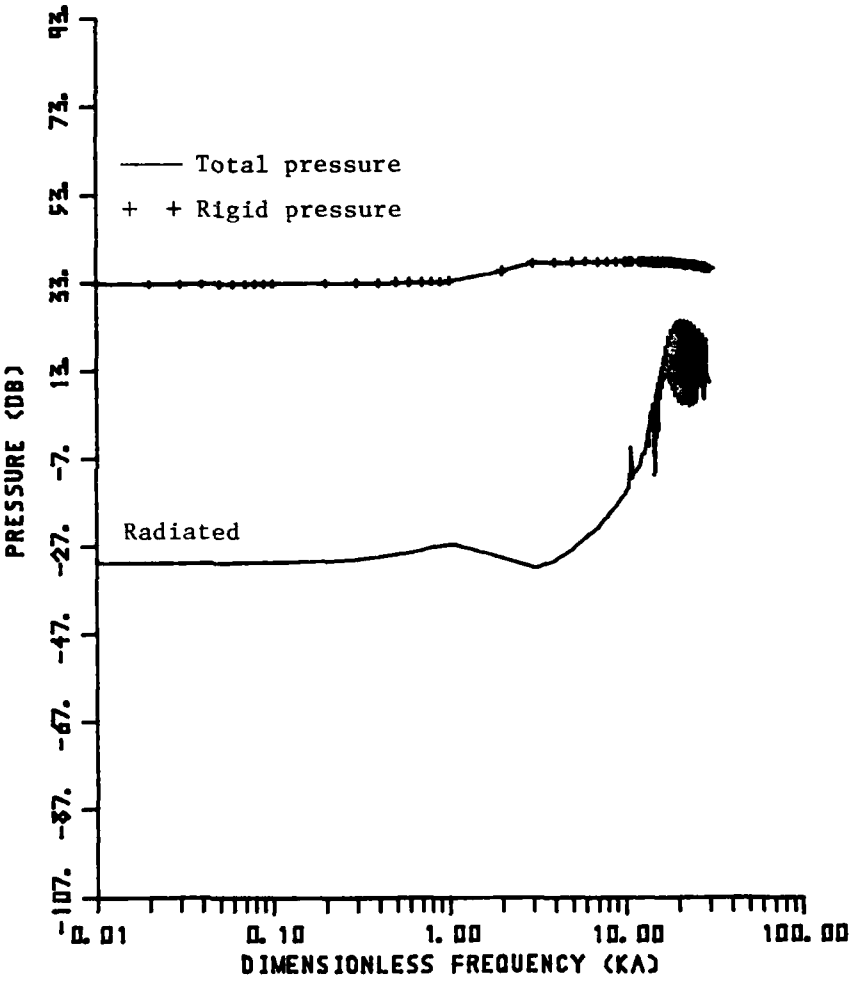

Figure 3.16 Frequency response of a classical shell with thickness $h = 0.0514"$ in air for $r_o = 8.25"$, $r = 8.5"$, and $\theta = 0°$

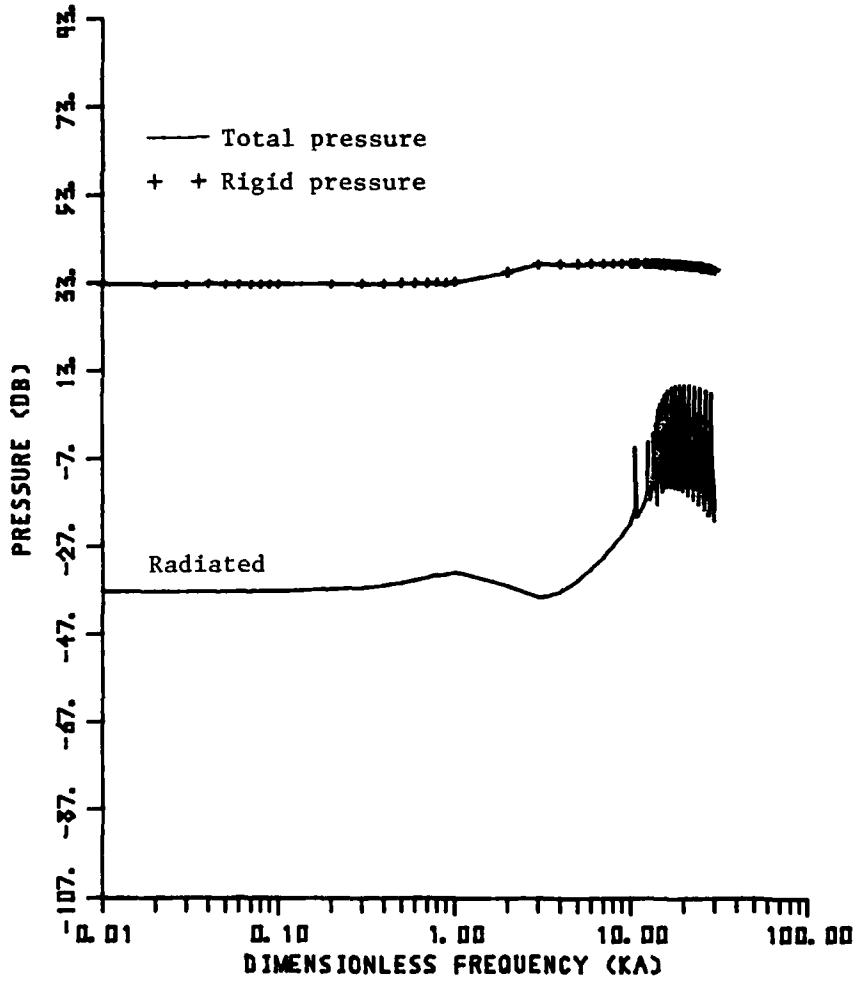

Figure 3.17 Frequency response of a classical shell with thickness $h = 0.1069"$ in air for $r_o = 8.25"$, $r = 8.5"$, and $\theta = 0°$

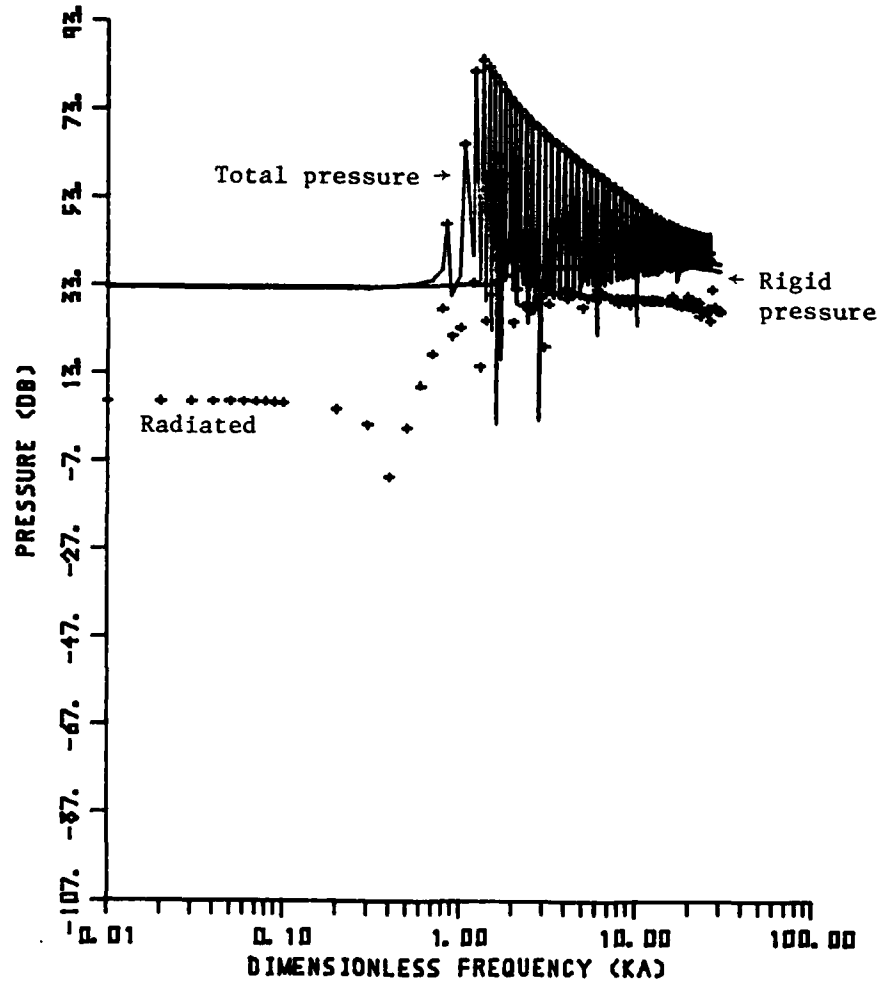

Figure 3.18 Frequency response of a classical shell with thickness $h = 0.0514"$ in water for $r_o = 8.25"$, $r = 8.5"$, and $\theta = 0°$

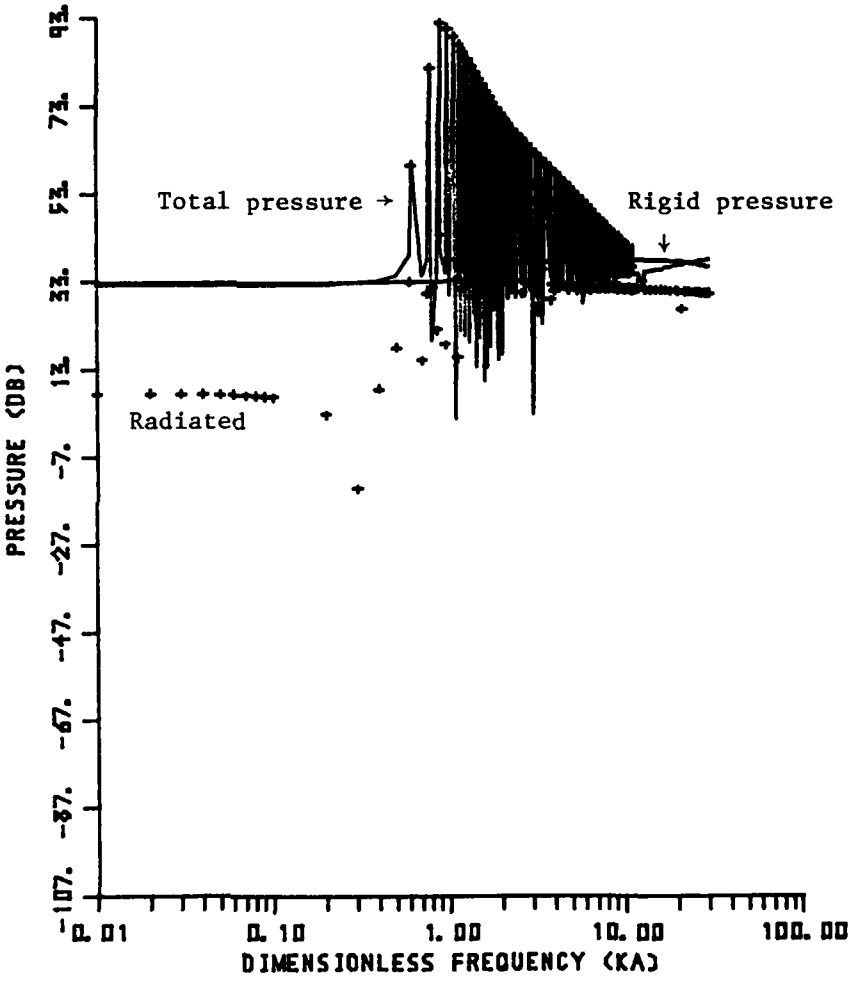

Figure 3.19 Frequency response of a classical shell with thickness $h = 0.1069"$ in water for $r_o = 8.25"$, $r = 8.5"$, and $\theta = 0°$

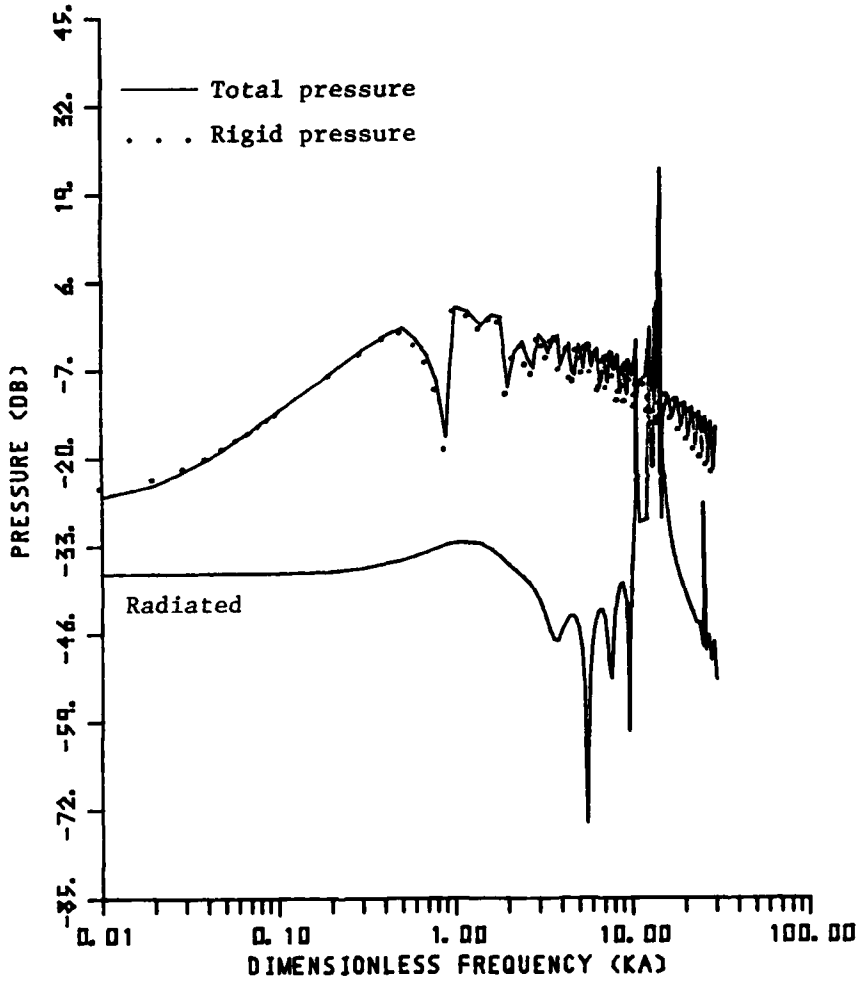

Figure 3.20 Frequency response of a membrane shell with thickness $h = 0.1069"$ in air for $r_o = 8.25"$, $r = 8.5"$, and $\theta = 180°$

However, the radiated field, while weak because of the characteristic impedance of air, is comparable and sometimes dominant over the weak creeping waves. This is clearly seen in Figures 3.8 through 3.20, where the resonant radiated field is dominant over the creeping waves for $ka > 10$, where all the resonances of the shell vibrating in air occur.

In water, the scattered pressure from an elastic shell in the illuminated zone ($\theta = 0°$) is shown in Figures 3.21 and 3.22. Here, the low frequency scattering below the first resonance of the shell is still dominated by rigid scattering. However, since the characteristic impedance of water is so much higher than air (+72 dB), the radiated pressure becomes dominant, even in the illuminated zones at the resonances of the submerged shell. This is more so when one examines the scattered pressure spectrum in the shadow zone ($\theta = 180°$) in Figures 3.23 and 3.24. The radiated pressure is higher than scattering by a rigid sphere by 30 dB in the low frequency, by 85 dB at resonance in the mid frequency range, and by 60 dB in the high frequency range.

In conclusion, the backscattered field (i.e., the illuminated zone) of a spherical shell in air can be represented by a rigid sphere. However, this is not true in water, where the resonant backscatter can be 60 - 85 dB higher than a rigid sphere for $ka > 1$. Thus, it can be stated emphatically that submerged elastic structures insonified in water can generate a much higher backscattered echo than a correspondingly sized rigid object. Furthermore, the elastic resonant scattering is even more pronounced in the shadow zone for structures insonified in air or in water. This means that structure-borne sound

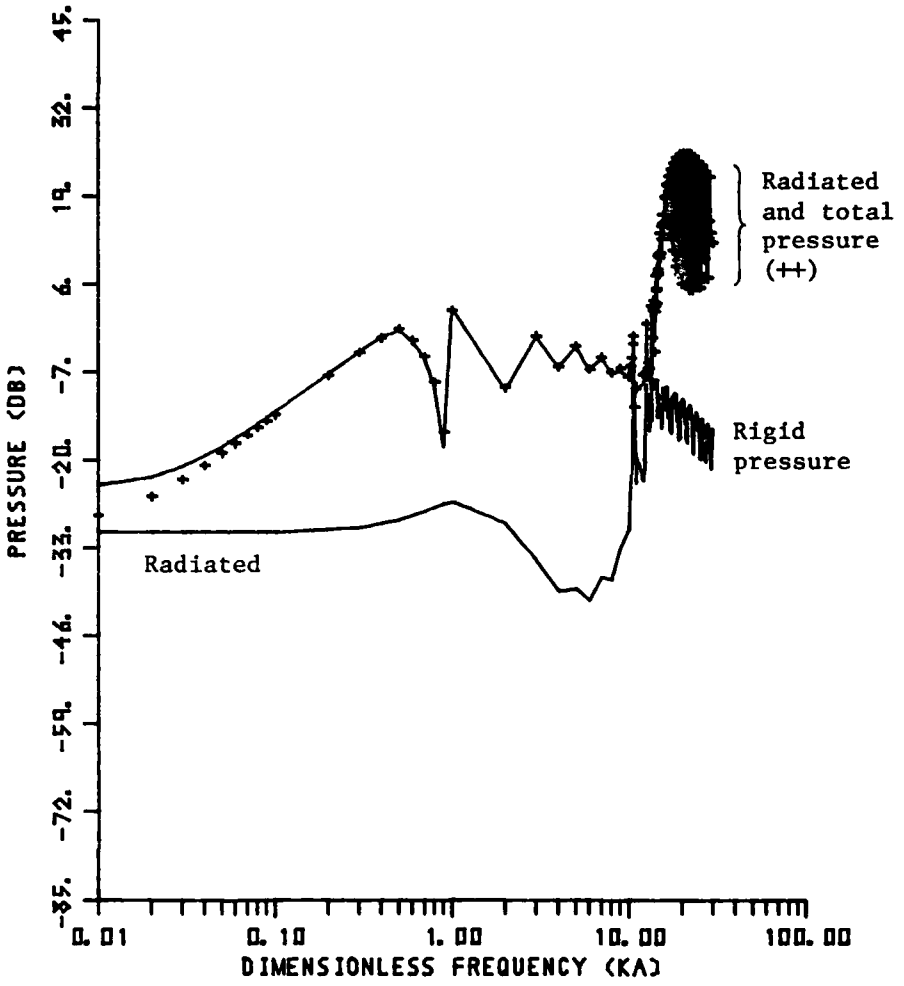

Figure 3.21 Frequency response of a classical shell with thickness $h = 0.0514"$ in air for $r_o = 8.25"$, $r = 8.5"$, and $\theta = 180°$

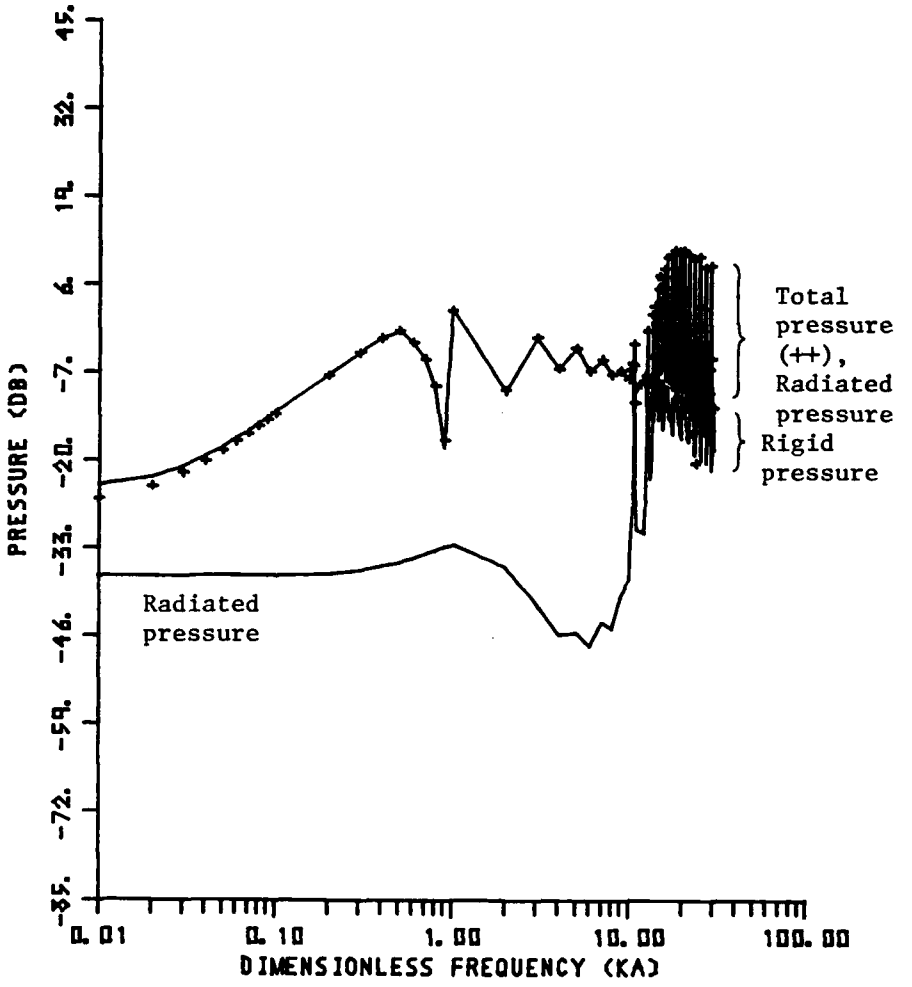

Figure 3.22 Frequency response of a classical shell with thickness $h = 0.1069"$ in air for $r_o = 8.25"$, $r = 8.5"$, and $\theta = 180°$

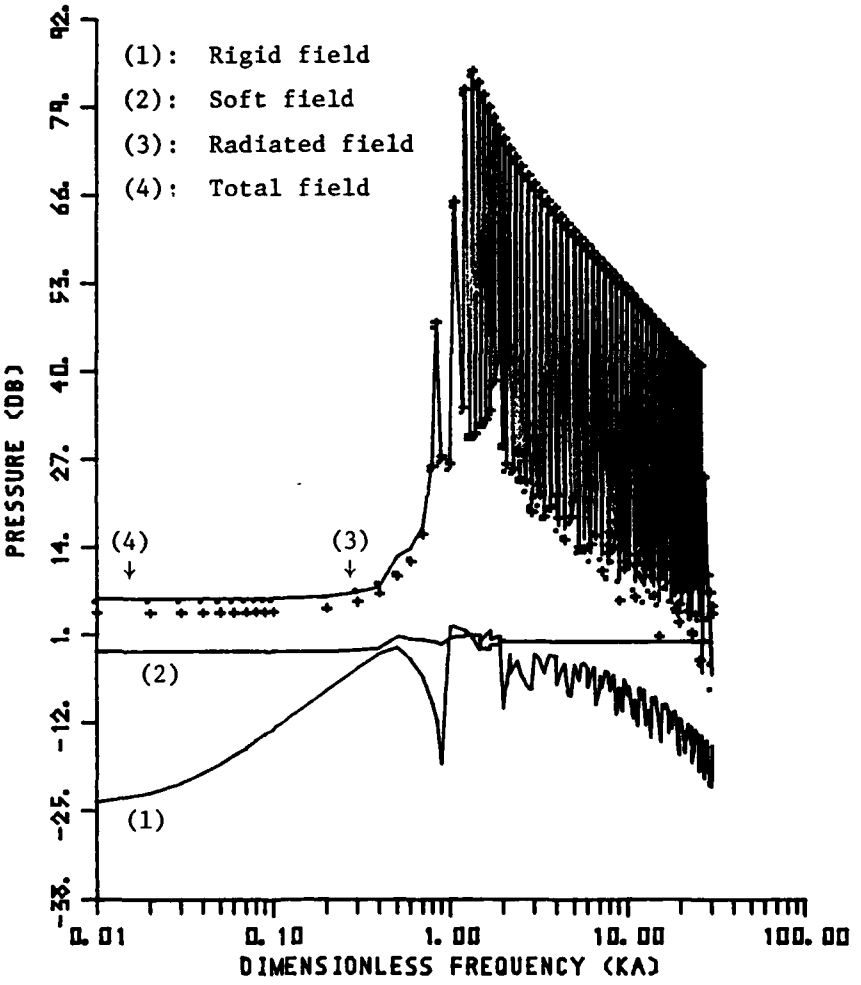

Figure 3.23 Frequency response of a classical shell with thickness $h = 0.0514"$ in water for $r_0 = 8.25"$, $r = 8.5"$, and $\theta = 180°$

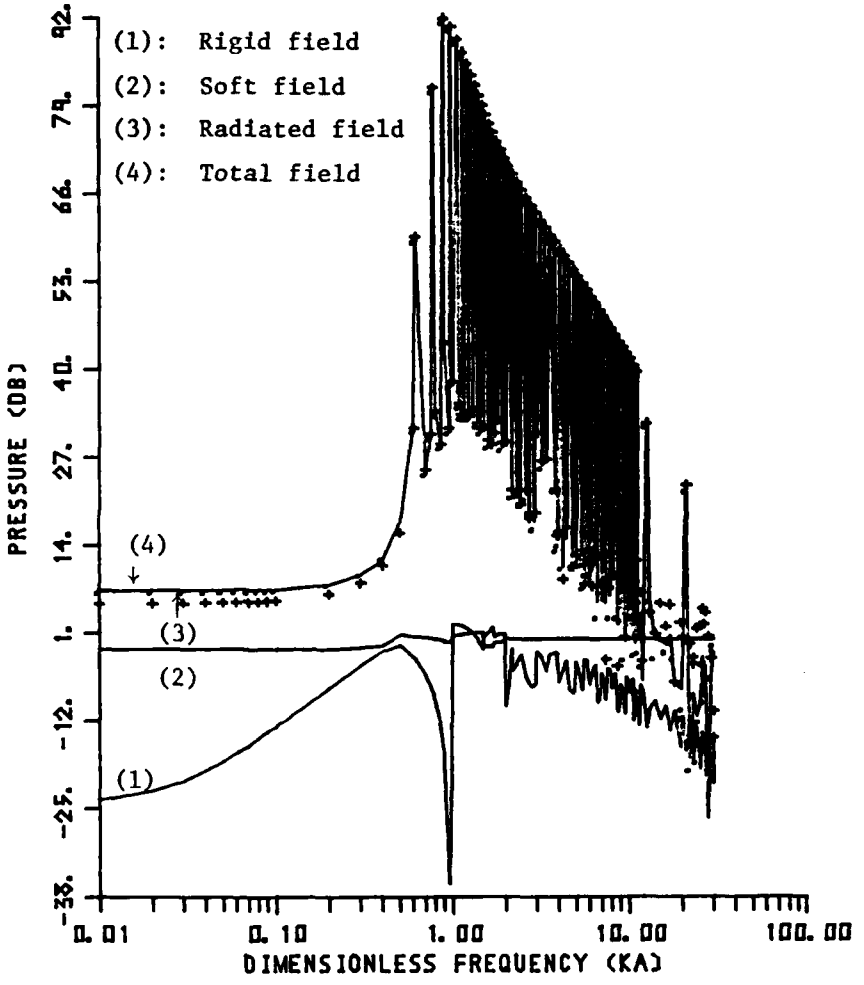

Figure 3.24 Frequency response of a classical shell with thickness $h = 0.1069"$ in water for $r_o = 8.25"$, $r = 8.5"$, and $\theta = 180°$

is predominant over rigid scattering in the shadow zone. This also means that measurement of the scattered pressure from an elastic structure in air cannot be used to predict the scattered pressure in water.

Figures 3.25 and 3.26 show the fluid loading effects on the directivity of the nearfield pressure. They both represent the resonant directivity patterns (n = 2) of the shell submerged in air and water, respectively. In air, due to the dominance of the blocked pressure over the radiated component, the pattern does not exhibit the n = 2 mode form. Instead, the pattern has fluctuations corresponding to the constructive and destructive interference of the creeping wave around a rigid sphere. In contrast, the directivity of shells in water gives the expected modal pattern n = 2 because the radiated pressure dominates the blocked component and has the expected number of nodes.

By examining the directivity pattern of the shells for extremely low, mid-range, and extremely high frequency, more information about the response of the elastic shells is obtained. For the case of a spherical source located at r_o = 8.25" and a field point located at r = 8.5" (both distances from the surface are less than one wavelength), the pattern of the submerged shell at extremely low frequency ka = 0.2 , which is below the first resonance, is shown in Figure 3.27, behaves like that of a rigid sphere in the illuminated zone. This is because the rigid component is much stronger than the radiated field at low frequencies below the first resonance. As the field point moves away from the source around the sphere, constructive and destructive interference occurs. The pattern in water is approximately

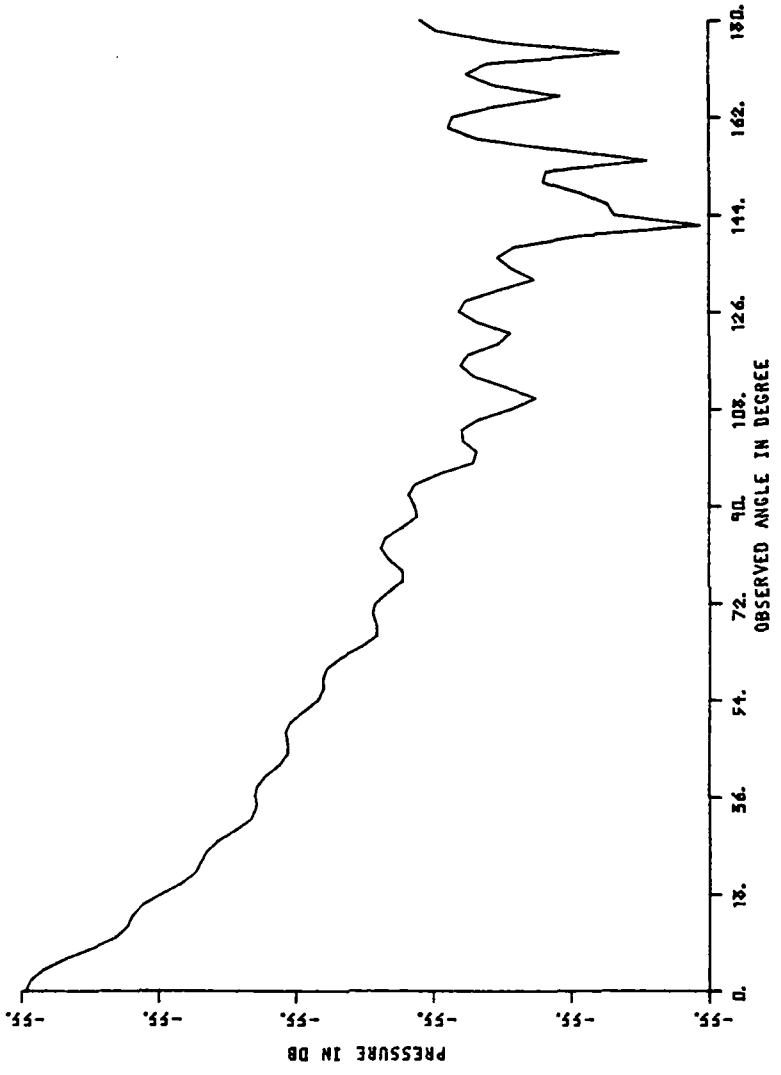

Figure 3.25 Directivity pattern of a shell with thickness h = 0.1069" in air for n = 2

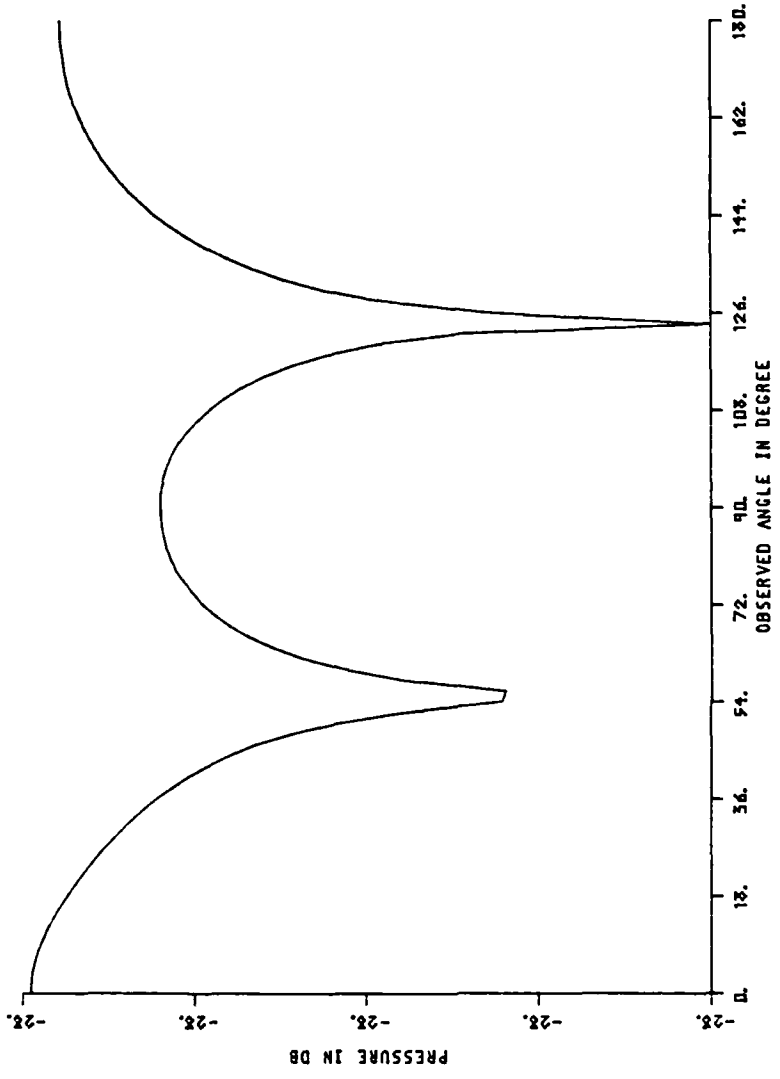

Figure 3.26 Directivity pattern of a shell with thickness h = 0.1069" in water for n = 2

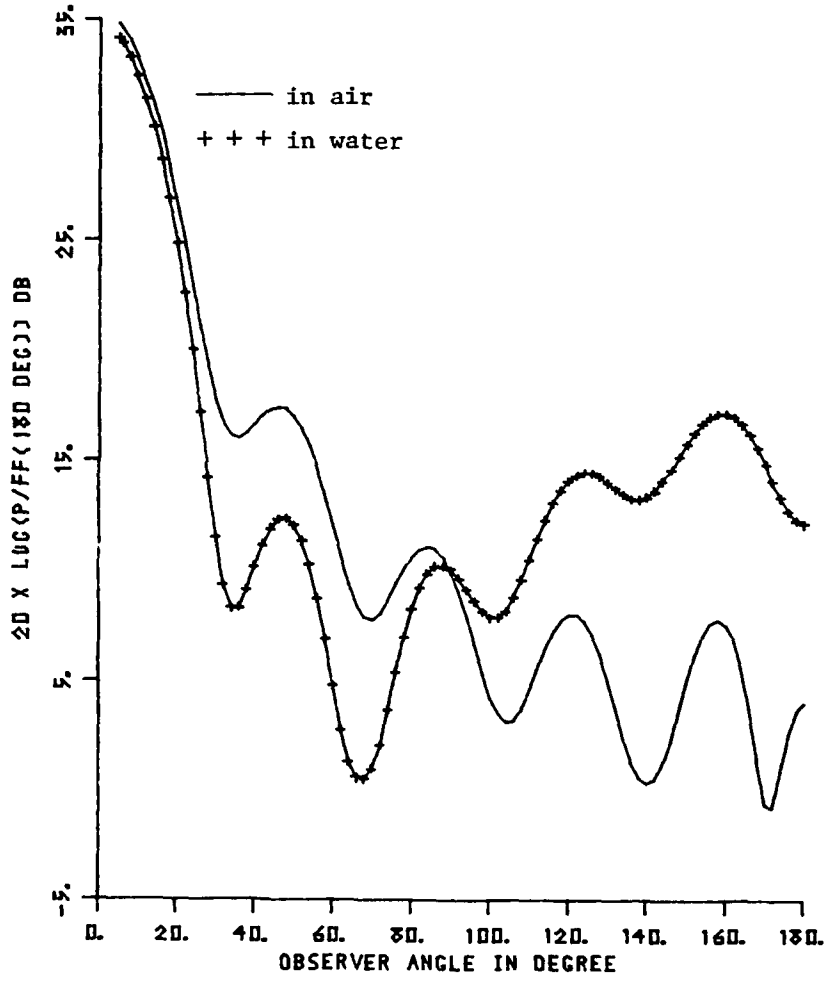

Figure 3.27 Directivity pattern of a shell with thickness h = 0.1069" in air and water for ka = 0.2

the same as that in air, although the former decreases in the illuminated zone and increases in the deep shadow zone. Near the ring frequency, e.g., for $ka = 14$, the observed field in water (see Figure 3.28) exhibits the $n = 29$ radiated resonant pressure pattern, while the observer field in air again exhibits a rigid diffraction pattern.

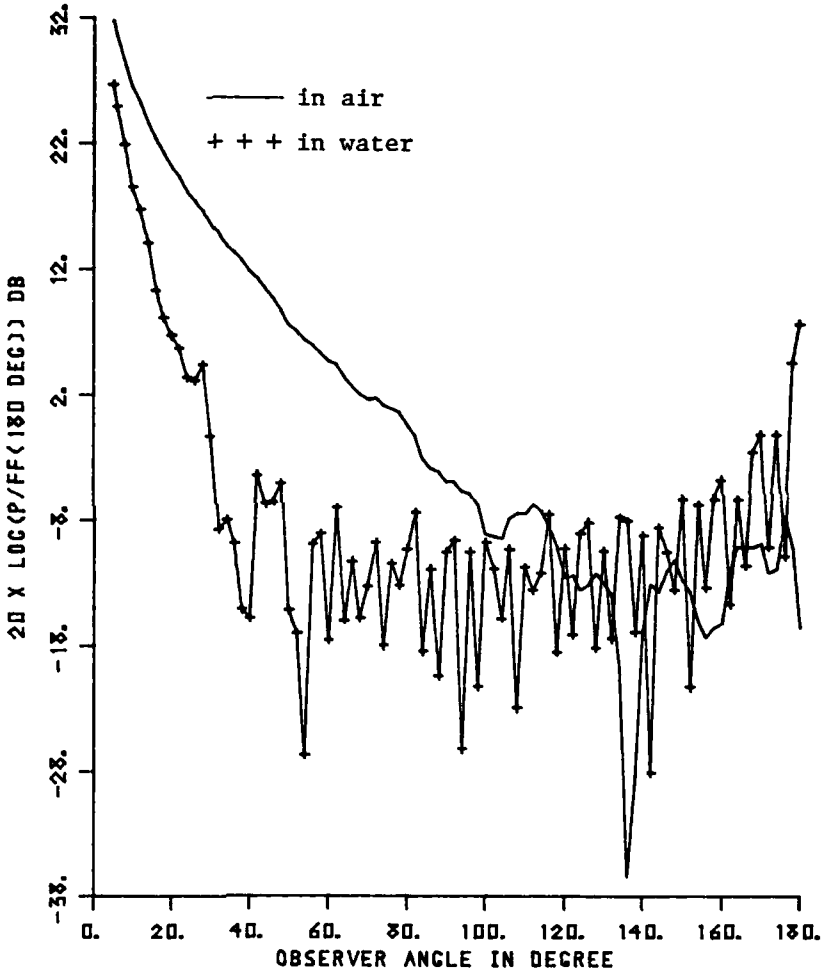

Figure 3.28 Directivity pattern of a shell with thickness h = 0.1069" in air and water for ka = 14

CHAPTER IV

THE GEOMETRICAL THEORY OF DIFFRACTION (GTD)

4.1 Introduction

In this chapter, a different approach is taken to solve the scattering problem of a submerged spherical shell at high frequencies. The procedure used is to compute the acoustic field for a sphere with an impedance boundary predicted by the GTD method and compare the levels with those determined from an exact solution.

In the previous chapter, the pressure field of a submerged spherical shell, insonified by a spherical wave, is expressed in the form of a wave harmonic series. If the wavelength is small when compared with the dimension of the shell (large ka), the sum of the modal terms are, therefore, poorly convergent. One may need as many as 2ka terms to attain reasonable accuracy. Because of the slow convergence, the wave-harmonic method is not practical at high frequencies. Therefore, asymptotic high-frequency approximations must be employed. One of these high-frequency approximate methods is the Geometrical Theory of Diffraction (GTD).

In the 1950's, Keller made a significant extension of the geometrical optics by including diffracted rays to describe the diffraction when the scatterer has edges, corners, or vertices, or when it has a smoothly curved surface. He has studied the spherical problem [13] by employing the GTD method. In this paper, the rays penetrate into the shadow zone and account for the non-zero field there, and also modify the illuminated field. The diffracted field

is obtained by multiplying the incident field at the diffracted point by a diffraction coefficient. This coefficient is derived from the exact solution. The GTD solution for a sphere is not adequate to predict the field at caustics. In order to have a valid solution near a caustic, the correct field is obtained by multiplying the GTD solution by correction factors [13].

Another high-frequency approximate technique is applied to evaluate the scattering field generated by those canonical shapes for which an exact solution is available. This technique was developed by Watson [21] about 60 years ago to solve the problem of radio wave diffracted into the shadow zone of the earth. He solved this problem by converting the slow convergent wave harmonic series into a complex integral. And solving the complex integral by residue method has led to a fast convergent series.

For large ka, both Keller's and Watson's method are adequate to solve the scattering field of a submerged spherical shell insonified by a spherical wave. For examining the problem of both the source and field point located near the surface, the Watson transformation will give a straight mathematical solution.

4.2 The Watson Transformation

Consider the forward scattering of a submerged elastic shell in Chapter III; the pressure field has the form:

$$f(n,\eta) = \sum_{n=o}^{\infty} (2n + 1) f(n) P_n(\eta) \quad , \tag{4.1}$$

where

$$f(n) = \frac{ik}{4\pi} h_n(kr) \left\{ j_n(kr_o) - \frac{\Omega j_n(ka)}{\Omega h_n(ka)} h_n(kr_o) \right\} , \quad r > r_o , \tag{4.2}$$

$$\Omega j_n = j_n(ka) - iZ_a j_n'(ka) ,$$

$$\Omega h_n = h_n(ka) - iZ_a h_n'(ka)$$

$$Z_a = Z_{mn}/\rho c ,$$

where the function $f(n)$ is assumed to be regular, and Z_a is a function of n and ka.

When converting the wave harmonic series into a contour integral, the integral of $P_n(\cos\theta)$ does not converge at $\theta = \pi$ for non-integer n because the integral has a line of logarithmic singularities along the line $\theta = \pi$ [22]. Thus, one can choose the spherical harmonic function $P_n(-\cos\theta)$, by using the relation:

$$P_n(-\cos\theta) = (-1)^n P_n(\cos\theta) , \tag{4.3}$$

which holds for integer n.

Taking a contour C enclosing the poles on the positive real axis in a complex s-plane (Figure 4.1), Equation (4.1) is transformed into such a complex contour integral:

$$\oint_{C_1} \frac{sf(s - \frac{1}{2}) P_{s-\frac{1}{2}}(-\cos\theta)}{\cos s\pi} ds = -2\pi i \sum R_i , \tag{4.4}$$

where $(-1)^n$ is proportional to $\cos(s\pi)$, $s = n + \frac{1}{2}$, $n = 0, 1, 2, \ldots$. The negative signs on the right-hand side of Equation (4.4) indicates the contour is clockwise.

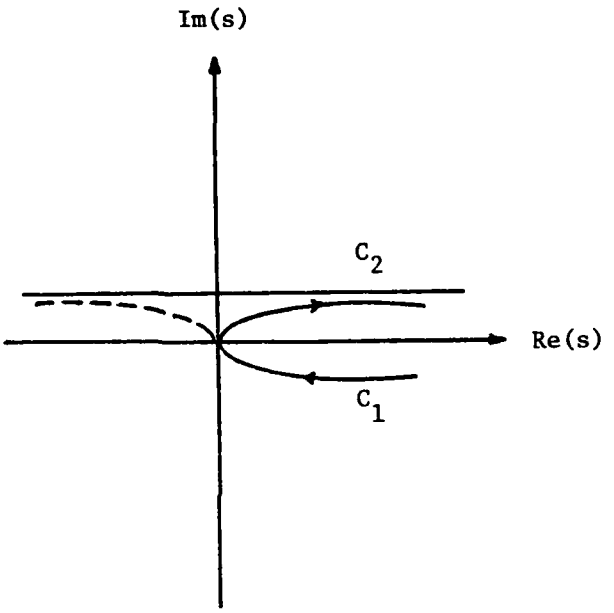

Figure 4.1 Contour C's of integration in the complex s plane

The residue R_n is expressed as:

$$R_n = \left. \frac{sf(s - \frac{1}{2})P^{(-\eta)}_{s-\frac{1}{2}}}{\frac{d}{ds}(\cos s\pi)} \right|_{s=s_n}$$

$$= s_n f(s_n - \tfrac{1}{2})P^{(-\eta)}_{s_n - 1/2}$$

$$= \tfrac{1}{2}(2n + 1)f(n)(-1)^n P_n(\eta) \; / \; [-\pi(-1)^n]$$

$$= \frac{1}{2}(2n + 1)f(n)P_n(\eta) \; / \; (-\pi) \quad . \qquad (4.5)$$

From Equations (4.4) and (4.5), one obtains the harmonic series in terms of the complex integral:

$$(2n + 1)f(n)P_n(\eta) = \frac{1}{i}\oint_{C_1} \frac{sf(s - \frac{1}{2})P^{(-\eta)}_{s-\frac{1}{2}}}{\cos(s\pi)}\, ds \quad . \qquad (4.6)$$

The next step of the Watson transformation is to deform the contour C_1 into C_2 which avoids the poles on the real axis, but includes the poles of $\Omega h_n(ka)$ [Equation (4.1)]. Replacing s by $-s$ in Equation (4.6), and by using the properties:

$$P_{s-1}(\cos\theta) = P_{-s-1}(\cos\theta) \quad ,$$

$$h_{s-1}(x) = e^{-is\pi} h_{-s-1}(x) \quad ,$$

$$h'_{s-1}(x) = e^{-is\pi} h'_{-s-1}(x) \quad , \quad x \gg 1 \quad ,$$

$$f(-s) = -f(s) \quad , \qquad (4.7)$$

and the integrand is an odd function. The lower half of contour C_1 is, therefore, deformed into an equivalent path shown as the broken line

in Figure 4.1. Thus, the contour C_1 may be replaced by a straight line C_2. The poles of the function $f(s - 1)$ are enclosed by the new contour of the integral formed by the path C_2 and the semicircle C_∞ as shown in Figure 4.2 (a detailed discussion of the choice C_∞ is given in Nussensveig's paper [23]). The contribution to be integral from C_2 is zero since the integrand is an odd function, and the integral vanishes along the path C_∞ as the radius of the semicircle approaches infinity (see Watson and Nussenzveig). The only contribution comes from the poles enclosed by C_2 and C_∞.

The poles are the zeros of the denominator $\Omega h_s(ka)$, which may be expanded in a Taylor series about the zeros s_n:

$$\Omega h_s(ka) = \Omega h_s(ka)\Big|_{s=s_n} + (s - s_n)\frac{\partial}{\partial s}[\Omega h_s(ka)]_{s=s_n} + \ldots . \tag{4.8}$$

It is obvious that at $s = s_n$:

$$\Omega h_{s_n}(ka) = 0$$

or

$$h_{s_n}(ka) \,/\, h'_{s_n}(ka) = iZ_a \quad , \tag{4.9}$$

where Z_a is assumed to be a function of ka only. This approximation of Z_a is to be used in this study henceforth. The residue is the coefficient b_1 of the term $(s - s_n)$:

$$b_1 = \frac{\partial}{\partial s}[\Omega h_s(ka)\Big|_{s=s_n} \tag{4.10}$$

because $\Omega h_s(ka)$ has simple poles only. Equation (4.9) is the boundary condition of the sphere. For a rigid sphere, Z_a approaches an infinite value. It implies that $h'_{s_n}(ka) = 0$. On the other hand, the sphere is called "soft" when Z_a or $h_{s_n}(ka)$ vanishes.

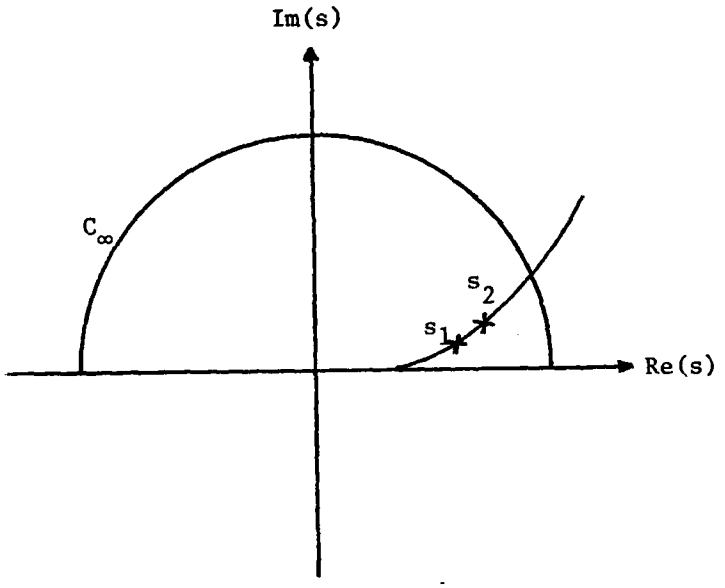

Figure 4.2 Contour of the integral in Equation (4.6)

By applying the residue theorem, the contour integral in Equation (4.6) may be expressed in terms of a residue series:

$$-\frac{1}{2i}\oint_{C_2+\infty}\frac{(2s+1)f(s)P_s(-\eta)}{\sin(\pi s)}\,ds = -\frac{2\pi i}{2i}\sum\frac{G(s_n)}{b_1}\,, \quad (4.11)$$

where

$$G(s_n) = \frac{ik}{4\pi}h_{s_n}(kr)\left\{j_{s_n}(kr_o)\Omega h_{s_n}(ka) - \Omega j_{s_n}(ka)h_{s_n}(kr_o)\right\} \times \frac{(2s_n+1(P_{s_n}(-\eta)}{\sin(\pi s_n)}\,.$$

The pressure field of the sphere is expressed as:

$$p = -\frac{ik}{4}\sum_{n=o}^{\infty} \times \frac{(2s_n+1)P_{s_n}(-\eta)h_{s_n}(kr)[j_{s_n}(kr_o)\Omega h_{s_n}(ka)-\Omega j_{s_n}(ka)h_{s_n}(kr_o)]}{\sin(s_n\pi)\frac{\partial}{\partial s}[\Omega h_s(ka)]_{s=s_n}} \quad (4.12)$$

By using the result in Equation (4.9) and

$$j_n(x) = \frac{1}{2}[h_n^{(1)}(x) + h_n^{(2)}(x)]\,,$$

one may reduce

$$j_{s_n}(kr_o)\Omega h_{s_n}(ka) - \Omega j_{s_n}h_{s_n}(kr_o) = -\frac{1}{2}h_{s_n}(kr_o)\Omega h_{s_n}^{(2)}(ka)\,. \quad (4.13)$$

Substituting the result in Equation (4.13) into Equation (4.12), one obtains:

$$p = \frac{ik}{8} \sum_{n=o}^{\infty} \frac{(2s_n+1)P_{s_n}(-\eta)}{\sin(\pi s_n)} h_{s_n}(kr) h_{s_n}(kr_o) \frac{\Omega h_{s_n}^{(2)}(ka)}{\frac{\partial}{\partial s}[\Omega h_s(ka)]_{s=s_n}}, \tag{4.14}$$

where

$$\frac{\Omega h_{s_n}^{(2)}(ka)}{\frac{\partial}{\partial s}[\Omega h_s(ka)]_{s=s_n}}$$

is proportional to the diffracted coefficient expressed in the GTD method [13].

At high frequencies, and $ka \tilde{=} s_n$, this term and Equation (4.9) can be expressed in terms of Airy function approximately (see Appendix B). The numerical computation is evaluated on the computer by applying the method derived by Bremmer [22]. The numerical evaluation will be discussed in the following section.

The pressure field expressed in Equation (4.14) is only valid in the shadow zone of the sphere because the choice of the spherical harmonic function [21, 22, 23, 24]. According to the geometrical optics, the shadow zone of a sphere is a zone in which there is no direct ray. Therefore, the zone is determined by the distance of the source from the surface and the location of the field point. Mathematically, the shadow zone, in terms of the observer angle θ, is:

$$\pi \leq \theta < \cos^{-1}\left(\frac{a}{r_o}\right) + \cos^{-1}\left(\frac{a}{r}\right) . \tag{4.15}$$

When the source and the field point are located near the surface of the sphere, the order of the Hankel function becomes comparable to the argument. For this case, the Hankel approximation of the Hankel

function will be employed [see Equation (B.4) in Appendix B]. Thus, the Hankel function in Equation (4.14) is expressed as:

$$h_{s_n}(kr) \sim \sqrt{\frac{2}{\pi kr}}\, e^{-i\frac{\pi}{3}} \left(\frac{6}{kr}\right)^{1/3} A[q_n^{(1)}]$$

and

$$h_{s_n}(kr_o) \sim \sqrt{\frac{2}{\pi kr_o}}\, e^{-i\frac{\pi}{3}} \left(\frac{6}{kr_o}\right)^{1/3} A[q_n^{(2)}] \quad , \qquad (4.16)$$

for $s_n \tilde{=} kr$ or kr_o, and large s_n, where $A[q_n^{(1)}]$ and $A[q_n^{(2)}]$ are the Airy function, and

$$q_n^{(1)} = [(ka - kr)(6)^{1/3} e^{-i\frac{\pi}{3}} + q_n(ka)^{1/3}](kr)^{-1/3}$$

and

$$q_n^{(2)} = [(ka - kr_o)(6)^{1/3} e^{-i\frac{\pi}{3}} + q_n(ka)^{1/3}](kr_o)^{-1/3} \quad , \qquad (4.17)$$

where $q_n = (6/ka)^{1/3} \cdot e^{-i\pi/3}(s_n - ka)$. As kr (or kr_o) $> |s_n|$, the Debye approximation [25] of the Hankel function is appropriate. The expansion is valid as the source and/or the field point is not located near the surface. The Debye approximation is expressed as:

$$h_{s_n}(kr) \tilde{=} (kr)^{-1/2} k^{-1/2} (a^2 - r^2)^{-1/4} e^{ik(r^2-a^2)^{1/2} - is_n \cos^{-1}(a/r)} \quad . \qquad (4.18)$$

The spherical harmonic function $P_{s_n}(-\cos\theta)$ is equal to unity at the antipode. At the other observer angle in the shadow zone, it is expressed as [22, 23]:

$$P_{s_n}(-\cos\theta) \simeq \sqrt{\frac{2}{\pi s_n \sin(\pi - \theta)}}\ \cos[s_n(\pi - \theta) - \frac{\pi}{4}]$$

$$\simeq \frac{e^{is_n(\pi-\theta)-i\frac{\pi}{4}} + e^{-is_n(\pi-\theta)+i\frac{\pi}{4}}}{\sqrt{2\pi\ ka\ \sin\theta}} \quad . \qquad (4.19)$$

The term $\sin(\pi s_n)$ can be expressed as:

$$\sin(\pi s_n) = -\cos(\pi\mu_n) = \frac{-e^{-i\mu_n\pi}(1 + e^{2i\mu_n\pi})}{2} \quad , \qquad (4.20)$$

where $\mu_n = s_n + \frac{1}{2}$, then $\mu_n = s_n$ for large ka .

Making use of the above relationships, the pressure field in Equation (4.14) gives:

(1) At the antipode, $\theta = \pi$

(A) As $(r - a)$ and $(r_o - a) > \lambda$ (wavelength)

$$p = -\frac{ae^{ik\sqrt{r^2-a^2} + ik\sqrt{r_o^2 - a^2}}}{2\sqrt{rr_o}\sqrt[4]{(r^2 - a^2)(r_o^2 - a^2)}} \sum_{n=o}^{\infty} \frac{e^{i\mu_n\pi}}{1 + e^{i2\mu_n\pi}}$$

$$\times e^{-i\mu_n\cos^{-1}(\frac{a}{r})-i\mu_n\cos^{-1}(\frac{a}{r_o})} \frac{\Omega H_{\mu_n}^{(2)}(ka)}{\frac{\partial}{\partial\mu}\left[\Omega H_{\mu}^{(1)}(ka)\right]_{\mu=\mu_n}} \quad .$$

(4.21)

(B) As $0 \leq (r - a)$ and $(r_o - a) \leq \lambda$

$$p = -\frac{i(6)^{2/3}\pi^{-1}k^{1/3}ae^{-i\frac{2\pi}{3}}}{(rr_o)^{5/6}} \sum_{n=o}^{\infty} \frac{e^{i\mu_n\pi}}{1 + e^{i2\mu_n\pi}} \times A[q_n^{(1)}]A[q_n^{(2)}] \frac{\Omega H_{\mu_n}^{(2)}(ka)}{\frac{\partial}{\partial\mu}[\Omega H_{\mu}^{(1)}(ka)]_{\mu=\mu_n}} . \tag{4.22}$$

(2) At an arbitrary observer angle in the shadow zone

(A) As $(r - a)$ and $(r_o - a) > \lambda$

$$p = -\frac{a^{1/2}e^{ik\left[\sqrt{r^2-a^2} + \sqrt{r_o^2-a^2}\right]}}{\sqrt{8\pi krr_o\sin\theta}\ \sqrt[4]{(r^2-a^2)(r_o^2-a^2)}} \times \sum_{n=o}^{\infty} \frac{e^{i\mu_n(2\pi-\theta)-i\frac{\pi}{4}} + e^{i\mu_n\theta+i\frac{\pi}{4}}}{1 + e^{i2\mu_n\pi}} \times e^{-i\mu_n[\cos^{-1}(\frac{a}{r})+\cos^{-1}(\frac{a}{r_o})]} \frac{\Omega H_{\mu_n}^{(2)}(ka)}{\frac{\partial}{\partial\mu}[\Omega H_{\mu}^{(1)}(ka)]_{\mu=\mu_n}} . \tag{4.23}$$

(B) As $0 \leq (r - a)$ and $(r_o - a) \leq \lambda$

$$p = \frac{-2\left(6^{2/3}a^{1/2}k^{1/3}\pi^{-1}e^{-i\frac{\pi}{6}}\right)}{\sqrt{8\pi krr_o\sin\theta}\,(rr_o)^{1/3}} \times \sum_{n=o}^{\infty} \frac{e^{i\mu_n(2\pi-\theta)-i\frac{\pi}{4}} + e^{i\mu_n\theta+i\frac{\pi}{4}}}{1 + e^{i2\mu_n\pi}} \times A[q_n^{(1)}]A[q_n^{(2)}] \frac{\Omega H_{\mu_n}^{(2)}(ka)}{\frac{\partial}{\partial\mu}[\Omega H_{\mu}^{(1)}(ka)]_{\mu=\mu_n}} ,$$

(4.24)

where

$$\frac{\Omega H_{\mu_n}^{(2)}(ka)}{\frac{\partial}{\partial\mu}[\Omega H_{\mu}^{(1)}(ka)]_{\mu=\mu_n}} \approx \frac{\Omega h_{s_n}^{(2)}(ka)}{\frac{\partial}{\partial s}[\Omega h_{s}^{(1)}(ka)]_{s=s_n}}$$

$$\approx \frac{\pi e^{i5\frac{\pi}{6}}}{6}\left(\frac{ka}{6}\right)^{1/3}\left[A'^2(q_n) + \frac{q_n}{3}A^2(q_n)\right]$$

as $s_n \approx \mu_n$ for large ka [see Equation (B.13) in Appendix B].

According to the GTD:

$$i\mu_n = (ik - \alpha_n)a \quad , \tag{4.25}$$

where α_n is a decay factor for acoustic propagation which depends on the local properties of the surface of the sphere. The term $\exp\{i\mu_n[\theta - \cos^{-1}(a/r) - \cos^{-1}(a/r_o)]\}$ in Equation (4.23) or $\exp\{i\mu_n[\pi - \cos^{-1}(a/r) - \cos^{-1}(a/r_o)]\}$ in Equation (4.21) is the combination of the phase change and the attenuation of the surface diffracted ray between the incident point on the surface and the

launch point. When both the source and the field point are located on the surface, the ray path on the surface increases such that the terms $\cos^{-1}(a/r)$ and $\cos^{-1}(a/r_o)$ vanish as $r = r_o = a$. The term $(1 + e^{i2\mu_n \pi})^{-1}$ represents the sum of the rays traveling along the surface n times, where n approaches infinity. Finally, $\Omega H^{(2)}_{\mu_n}(ka) \; / \; (\partial/\partial\mu)[\Omega H^{(1)}_{\mu}(ka)]_{\mu=\mu_n}$ is proportional to the diffraction coefficient.

For the case of the near field, the computation of the pressure field in Equations (4.22) and (4.24) takes a relatively longer computation time. Therefore, the tangent approximation of the Hankel function is used. For practical purposes, the tangent approximation is good enough for the accuracy.

The tangent approximation is expressed as:

$$h_\mu(z) \approx \frac{2e^{-i\frac{\pi}{4}}}{z^{5/6}\, 4\sqrt{2\tau}} \cos\left\{\frac{\pi}{4} + \frac{i}{3}(2\tau)^{3/2}\right\} \quad , \qquad (4.26)$$

where $\mu = z + z^{1/2}\tau$. For both the source and the field point located at a distance less than a wavelength from the surface of the shell, the τ in Equation (4.26) is a value corresponding to the arguments kr, kr_o, and ka. It is expressed as:

$$\mu = kr + (kr)^{1/3}\tau_1$$

or

$$\mu = kr_o + (kr_o)^{1/3}\tau_2 \quad . \qquad (4.27)$$

Also,

$$\mu = ka + (ka)^{1/3}\tau \quad . \qquad (4.28)$$

Combining Equations (4.27) and (4.28), τ_1 and τ_2 can be expressed approximately as:

$$\tau_1 \overset{\sim}{=} -(X_1 - 2\tau) / 2$$

and

$$\tau_2 \overset{\sim}{=} -(X_2 - 2\tau) / 2 , \qquad (4.29)$$

where $X_1 = (ka)^{2/3}(2h_1/a)$, $h_1 = r - a$

and $X_2 = (ka)^{2/3}(2h_2/a)$, $h_2 = r_o - a$.

Substituting Equation (4.29) into Equation (4.26), the tangent approximation of the Hankel function for the arguments kr and kr_o can be rewritten as:

$$h_\mu(kr) \sim \frac{2\cos[\frac{\pi}{4} + \frac{1}{3}(X_1 - 2\tau)^{3/2}]}{(kr)^{1/2}(ka)^{1/3}(X_1 - 2\tau)^{1/4}}$$

and

$$h_\mu(kr_o) \sim \frac{2\cos[\frac{\pi}{4} + \frac{1}{3}(X_2 - 2\tau)^{3/2}]}{(kr_o)^{1/2}(ka)^{1/3}(X_2 - 2\tau)^{1/4}} \quad . \qquad (4.30)$$

Following the procedure for deriving the near field and by applying the tangent approximation, Equation (4.30), the nearfield pressure is obtained from Equation (4.14) as:

$$p \overset{\sim}{=} \frac{i\pi(ka)^{2/3}e^{5\pi i/6}}{6^{1/3}a(kr)^{1/2}(kr_o)^{1/2}} \sum_{n=o}^{\infty} \frac{e^{i\mu_n\pi}}{1 + e^{2\pi i\mu_n}} \frac{\cos\theta_1\cos\theta_2}{(K_1K_2)^{1/4}}$$

$$\times \{3[A'(q_n)]^2 + q_nA^2(q_n)\}^{-1} \quad , \qquad (4.31)$$

where

$$\theta_1 = \frac{\pi}{4} + \frac{1}{3} K_1^{3/2} \quad ,$$

$$\theta_2 = \frac{\pi}{4} + \frac{1}{3} K_2^{3/2} \quad ,$$

$$K_1 = X_1 - 2\tau_n \quad ,$$

$$K_2 = X_2 - 2\tau_n \quad ,$$

$$\tau_n = q_n e^{i\frac{\pi}{3}} / 6^{1/3}$$

and

$$\mu_n = ka + (ka)^{1/3} \tau_n \quad .$$

4.3 The Method of Computation and Numerical Analysis

4.3.1 The Method of Computation. In order to evaluate numerically the pressure field in Section 4.2, the roots of the Airy function $A(q_n)$ have to be computed. The method used in this calculation was developed by Bremmer [22].

The boundary condition for the elastic sphere in Equation (4.9) is:

$$\frac{H_{s_n}^{(1)'}(ka)}{H_{s_n}^{(1)}(ka)} = - iZ_a^{-1} \quad . \tag{4.32}$$

As shown in Appendix B, this relation can be simplified by applying the Hankel approximation for $(s - ka)/ka < 1$, and Equation (4.32) becomes:

$$\frac{A'(q_n)}{A(q_n)} \simeq e^{i5\frac{\pi}{6}} \left(\frac{ka}{6}\right)^{1/3} Z_a^{-1} \quad , \tag{4.33}$$

where the Airy function is defined as:

$$A(q_n) = \int_0^\infty \cos(t^3 - qt)dt \quad ,$$

and $A'(q_n)$ is the derivative of $A(q_n)$. By making use of the tangent approximation of the Hankel function:

$$H_{s_n}(ka) \sim \frac{2^{5/4} e^{-i\frac{\pi}{4}}}{\pi^{1/2}(ka)^{1/4}(s_n - ka)^{1/4}} \cos[\tfrac{\pi}{4} + \tfrac{1}{3}(-2\tau_n)^{3/2}] \tag{4.34}$$

and

$$\frac{\partial H_{s_n}^{(1)}(ka)}{\partial(ka)} \sim -\frac{2^{5/4} e^{-i\frac{\pi}{4}}}{\pi^{1/2}(ka)(s_n - ka)^{1/4}} (-2\tau_n)^{1/2}(ka)^{1/3} \times \sin[\tfrac{\pi}{4} + \tfrac{1}{3}(-2\tau_n)^{3/2}] \quad , \tag{4.35}$$

Equation (4.32) becomes:

$$\tan[\tfrac{\pi}{4} + \tfrac{1}{3}(-2\tau_n)^{3/2}] = Z_a^{-1}(ka)^{1/3}(2\tau_n)^{-1/2} \quad . \tag{4.36}$$

This equation may be solved more easily than Equation (4.33) for the zeros τ_n, although it is less accurate than Equation (4.33). However, for $s_n >> 1$, the $A(q_n)$ and $A'(q_n)$ can be expressed as [24]:

$$A(q_n) \approx \frac{\sqrt{\pi}}{(3q_n)^{1/4}} \cos[2(\tfrac{q_n}{3})^{3/2} + \tfrac{\pi}{4}] \quad ,$$

$$A'(q_n) \approx -\frac{\sqrt{\pi}}{3}(3q_n)^{1/4} \sin[2(\tfrac{q_n}{3})^{3/2} + \tfrac{\pi}{4}]$$

or

$$\frac{A'(q_n)}{A(q_n)} \approx -(\tfrac{q_n}{3})^{1/2} \tan[2(\tfrac{q_n}{3})^{3/2} + \tfrac{\pi}{4}] \quad . \tag{4.37}$$

This equation does not provide an easy way to obtain the roots q_n for an arbitrary value Z_a, but it does show that the tangent approximation approaches the Hankel approximation as $Z_a \to \infty$ or $Z_a \to 0$. These two limiting cases will help evaluate τ_n for arbitrary values Z_a.

For Z_a approaching infinity, the zeros τ_n (s_n or q_n) is obtained from Equation (4.36):

$$\tau_{n,\infty} = \frac{1}{2}\left[3\pi\left(n + \frac{1}{4}\right)\right]^{2/3} e^{i\frac{\pi}{3}}$$

or

$$q_{n,\infty} = \frac{(6)^{1/3}}{2}\left[3\pi\left(n + \frac{1}{4}\right)\right]^{2/3}, \quad n = 0, 1, 2, \ldots \quad (4.38)$$

while for Z_a approaching zero:

$$\tau_{n,o} = \frac{1}{2}\left[3\pi\left(n + \frac{3}{4}\right)\right]^{2/3} e^{i\frac{\pi}{3}}$$

or

$$q_{n,o} = \frac{(6)^{1/3}}{2}\left[3\pi\left(n + \frac{3}{4}\right)\right]^{2/3} . \quad (4.39)$$

Bremmer [22] has developed a method to compute τ_n for arbitrary values of Z_a [$Z = -iZ_a(ka)^{-1}$] by expanding τ_n in terms of $\tau_{n,\infty}$ and Z or $\tau_{n,o}$ and Z. The two series are:

$$\tau_n = \tau_{n,o} - Z - \frac{2}{3}\tau_{n,o} Z^3 + \frac{1}{2} Z^4 - \frac{4}{5}\tau_{n,o} Z^5 \ldots , \quad (4.40)$$

for small Z, and

$$\tau_n = \tau_{n,\infty} - \frac{1}{2}\frac{1}{\tau_{n,\infty}}\frac{1}{Z} - \frac{1}{8}\frac{1}{\tau^3_{n,\infty}}\frac{1}{Z^2} - \frac{\left(1 + \frac{3}{4\tau^3_{n,\infty}}\right)}{12\,\tau^2_{n,\infty}}\frac{1}{Z^3} \cdots \quad (4.41)$$

for large Z.

On calculating q_n , the first few values of $\tau_{n,o}$ and $\tau_{n,\infty}$ are those obtained from the Hankel approximation; then, for $s_n >> 1$, the values of the tangent approximations in Equations (4.38) and (4.39) are used since both approximations are of the same order [see Equation (4.39)]. There is a criterion for determining when Equation (4.40) or Equation (4.41) will be employed for a given value of Z . If $Z^2\tau_n > 0.5$, Equation (4.41) for large Z will be used. Otherwise, Equation (4.40) will be applied.

4.3.2 Numerical Analysis. For this investigation, a spherical shell with an impedance boundary is being considered. Six different models for the elastic shell impedance have been used. They are listed as follows:

(1) Uniform Impedance

$$Z_1 = \rho_s C_p/\rho c \quad ,$$

where

$$C_p = [E\rho_s^{-1}(1 - \nu^2)^{-1}]^{1/2} \quad .$$

(2) Driving Point Impedance of an Infinite Plate

$$Z_2 = 8\alpha^2 \bar{\mu} / (2\pi a^2 \rho c) \ ,$$

where

$$\alpha^4 = h^2 E / 12(1 - \nu^2)\rho_s \quad .$$

(3) Wave Impedance of an Infinite Plate Excited by Normal Incident Plane Wave [26]

$$Z_3 = (\rho_s C_p/\rho c) / (c/C_p)(h/a)(ka) \quad .$$

(4) Bending Impedance of the Plate

$$Z_4 = \rho_s V_b / \rho c \quad ,$$

where $V_b = \alpha\omega^{1/2}$, bending velocity.

(5) Driving Point Impedance of a Spherical Shell Excited by a Uniform Force

$$Z_5 = \frac{1}{\rho c \sum_{n=o}^{\infty} \frac{F_n}{Z_{mn}}} \quad ,$$

where

$$F_n = \frac{2n+1}{4\pi a^2} \frac{\pi^{1/2} 2^{-2}}{\Gamma(1 + \frac{1}{2} - \frac{1}{2}n)\Gamma(\frac{1}{2} + \frac{3}{2} + \frac{1}{2}n)} \quad ,$$

$\Gamma(n)$ is a Gamma function.

(6) Driving Point Impedance of a Spherical Shell Excited by a Point Force [see Equation (3.12)]

$$Z_6 = \frac{4\pi a^2}{\rho c \sum_{n=o}^{\infty} \frac{(2n+1)}{Z_{mn}}} \quad .$$

The procedure of the computation is to calculate the τ_n for arbitrary values Z from Equations (4.40) or (4.41), then to calculate $A(q_n)$ and $A'(q_n)$, and finally, to compute the pressure field from Equation (4.31). The frequency spectra of the pressure field for spherical shells with the above six different impedances are shown in Figures 4.3, 4.4, and 4.5. The number marked on each curve indicates the frequency spectra of the shell with the marked number impedance as listed above.

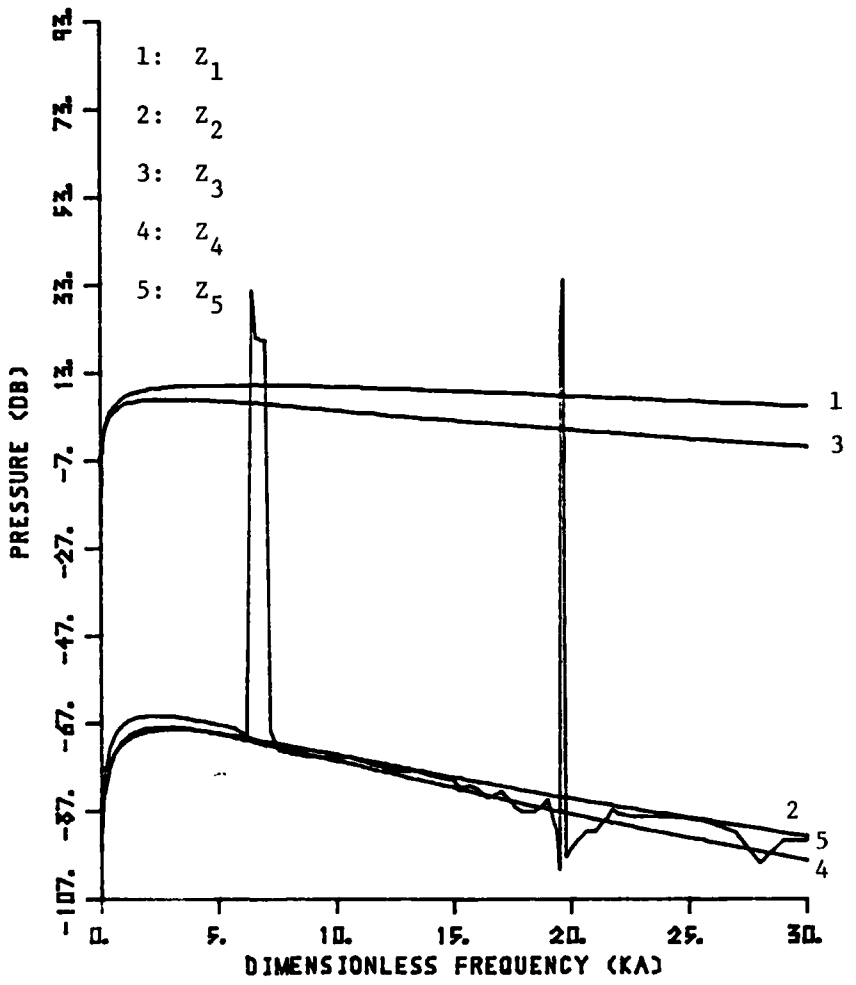

Figure 4.3 Frequency response of the pressure field of a GTD sphere in water for $r = 8.5"$, $r_o = 8.25"$, and $\theta = 180°$

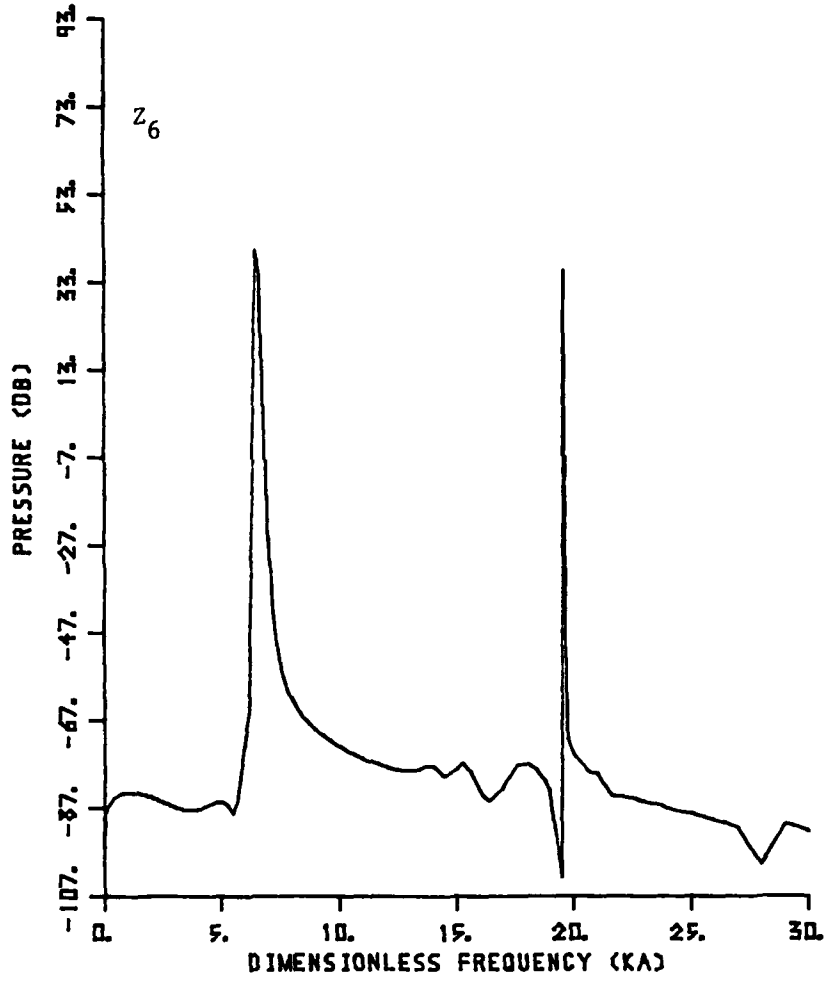

Figure 4.4 Frequency response of the pressure field of a GTD sphere in water for $r = 8.5"$, $r_o = 8.25"$, and $\theta = 180°$

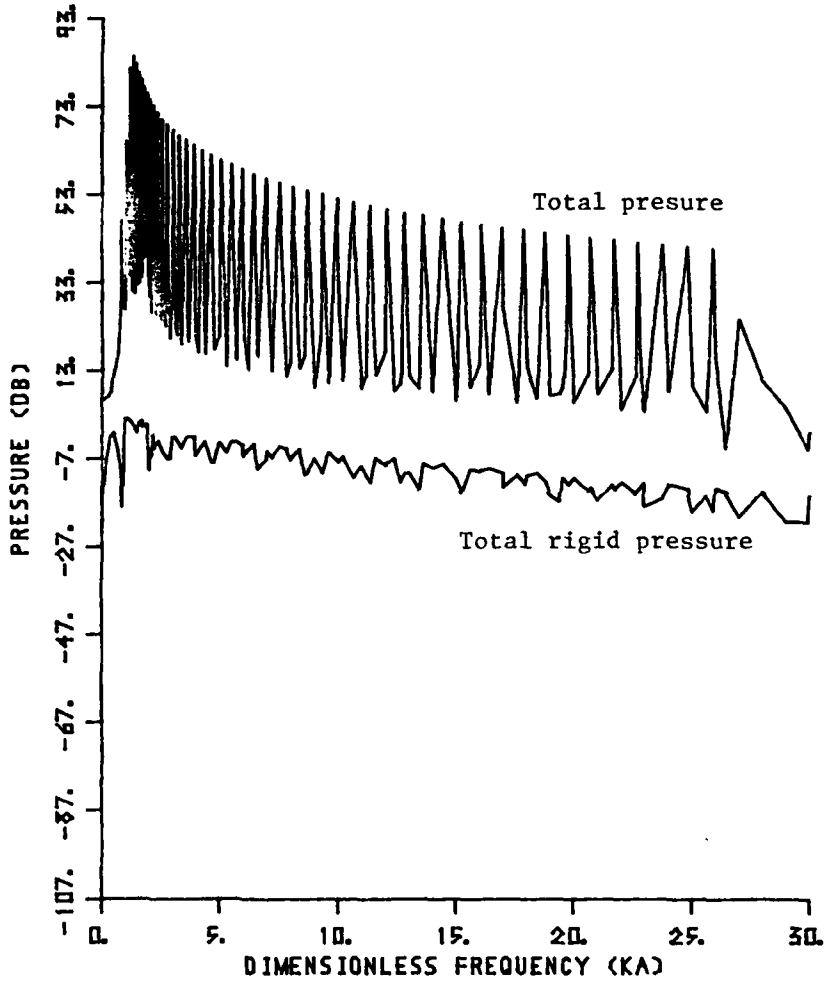

Figure 4.5 Frequency spectrum of an exact solution in water for r_o = 8.25" , r = 8.5" , and 0 = 180°

The uniform impedance Z_1 has a value of 55.6194, while the driving point impedance of an infinite plate is 0.0292. They are shown as Curves (1) and (2) in Figure 4.3.

Comparing Figures 4.3 and 4.4 with Figure 4.5, the frequency spectrum of the exact solution, the only GTD pressure field that is close to the exact solution is the pressure field of a shell with a uniform forced driving point impedance Z_1 [see Curve (1) in Figure 4.3]. According to Sachs's study [27], the GTD method gives a very accurate prediction for a rigid sphere in air. However, the calculation of an elastic sphere submerged in water is worse when compared with the exact solution.

The reason for the discrepancy between the GTD and the exact solution lies in the assumption that the impedance Z_a is purely a function of (ka) and not also dependent on the mode number n. This then allows for water-borne creeping waves around the impedance surface of the shell. But, it excludes the structure borne creeping waves, which were shown to be dominant in the illuminated and shadow zones of shells in water. Since the GTD was to be used for any shaped elastic shell where an exact expression for the shell impedance Z_a is not available, the method does not appear to be useful in predicting the near field of a general elastic structure in water when the shell impedance is approximated by any one of the six impedances given above.

CHAPTER V

EXPERIMENT

5.1 Introduction

The sound propagation near the surface of an elastic spherical thin shell vibrating in an acoustic medium due to a spherical sound source located at a point near the surface has been studied theoretically in the previous chapters. Both the wave harmonic and the geometrical theory diffraction methods have been employed in this study.

This chapter describes experimental techniques for vibration and sound measurement. These techniques were employed to determine the sound field near the surface of a spherical shell and the vibration field of the shell, and to provide experimental verification of the predictions of the theoretical analyses. The measurements were carried out into phases. When making experiments in the anechoic chamber located at the Garfield Thomas Water Tunnel Building of ARL of The Pennsylvania State University, the sound visualization technique was used. The results were expressed graphically in terms of the phase and directivity plots. When the shell was submerged in the anechoic water tank located in the Applied Research Laboratory at The Pennsylvania State University, the pressure directivity was measured and plotted. The resonance frequencies were also measured when the shell was submerged in air or water.

5.2 General Experimental Approach

The resonance frequency measurements were performed for both 14-gauge (actual thickness h = 0.0514 inch) and 8-gauge (actual thickness h = 0.1069 inch) thick spherical shells. The directivity pattern measurements were taken on an 8-gauge shell. Each of these shells is 16 inches in diameter and is constructed of duralumin material. The spherical shells were fabricated from two hemispherical shells welded at the equator and the welds ground smooth.

The experimental measurements were carried out in the anechoic chamber [29] at the Water Tunnel Building and the anechoic water tank [30] at the Applied Science Building. The anechoic chamber was built initially in support of this experimental program to investigate the fluid loading effects on elastic structures. It has internal dimensions of 11 x 12 x 18 feet. The sound absorbing walls are composed primarily of rock-wool fiberglass insulation, air voids, and wood frame members. It is considered as a semi-anechoic for frequencies less than 1 kHz and moderately anechoic for higher frequencies. The water-filled anechoic tank, which is 12 feet long, 4 feet wide, and 11 feet deep, is lined with Insulkrete wedges. Between 20 and 30 kHz, the tank is better than 90 percent absorbent. The absorption falls off rapidly below 20 kHz. The spherical shells were located near the center of the tank or the chamber. The source and receiver were placed on a horizontal plane through the center of the shell perpendicular to the walls of the tank or the chamber.

The resonances of spherical shells were measured by plotting the frequency response and the modal pattern. A continuous sinusoidal wave was applied to the shaker to excite the shell in both water and

air. In the case of the directivity pattern measurement, with the shell excited by an acoustic spherical source, a pulsed wave was used in water, while a C.W. source was used in air. The pulsed width was varied from 0.2 ms to 0.99 ms and the pulse was repeated every 102 ms to allow for the decay of the pulse in the tank. The total sound pressure was measured by a hydrophone rotated around the shell with a speed 0.69° per second. For measurements where both the source and the field points were located near the surface of the shell, the repetition rate assures that the receiver will adequately measure the signal before the arrival of the next pulse. Furthermore, in such a slow motion, the measured arm does not create any significant flow noise affecting the measurement of the acoustic pressure.

In the experiments to measure the directivity of the pressure field in air, the measured data was recorded on film, and was digitized by use of Vision and the Hybrid Computer at The Pennsylvania State University. The resulting data were represented in three dimensions with relief representing amplitude.

5.3 Experimental Equipment

The structures under investigation were two thin elastic duralumin spherical shells. The radius of both shells was 8 inches, and these shells have thicknesses of 0.1069 inch and 0.0514 inch, respectively. The former shell was suspended in water by four 40-lb fishing strings, 1/64 inch in diameter, attached to the shell by means of four eye-bolts, 1/8 inch in diameter, screwed to the surface. Three of them were located at the vertices of a one-inch equilateral triangle at the pole; the fourth was located at the center of the

triangle. All bolts were sealed with Silastic to prevent water from leaking into the shell and rust. The thinner shell was suspended in a similar manner, but with one eyebolt screwed on an aluminum adapter (1/2 inch in diameter, 1/4 inch thick) which was attached to the shell with epoxy resin. Both of the shells were anodized to prevent corrosion. The geometrical configuration is shown in Figure 5.1.

The holographic side scanner for recording the nearfield pressure was composed of a measuring arm, and a turntable as shown in Figure 5.2. The measuring arm was made of plexiglas because its characteristic impedance is approximately the same as that of water. The scanner has a 180-degree scanning range (the old one has a 350-degree scanning angle approximately). The receiver, which is attached to the measuring arm, could move away from the surface of the shell up to a distance of 6". The stepping distance of the receiver from the shell can be varied in steps by the use of a stepping motor. This flexibility will provide a method for recording the directivity of the pressure field of the shell at any distance from the surface in a 180° rotation.

For the measurements of the pressure field in the neighborhood of a spherical shell insonified by a spherical source in water, the Atlantic Research LC-32 hydrophone was used as a source (S), while the LC-10 was used as a receiver (R). These hydrophones are omnidirectional both as projector and receiver in the horizontal plane (the plane perpendicular to the axis of the hydrophone) over the frequency range used. The source was suspended 8 inches away from an aluminum support arm, while the receiver attached 6 inches away from the plexiglas supporting arm pivoted about the surface of the shell (see Figure 5.2).

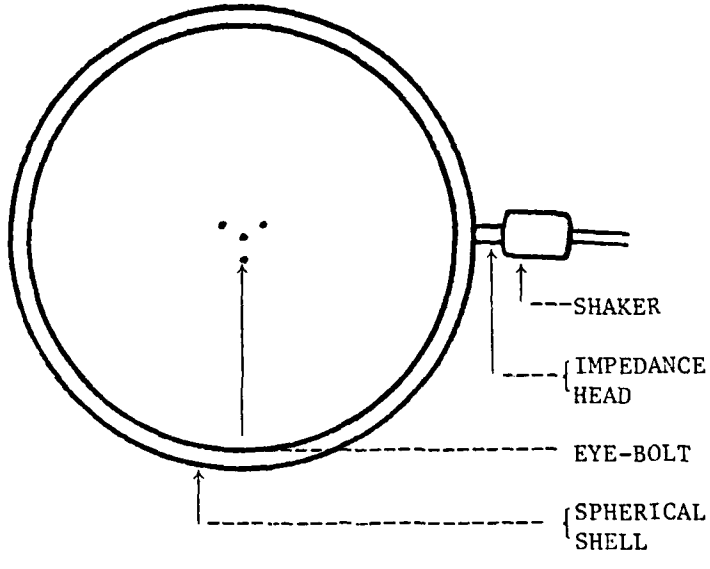

Figure 5.1 Geometrical configuration of a spherical shell and the location of its support system

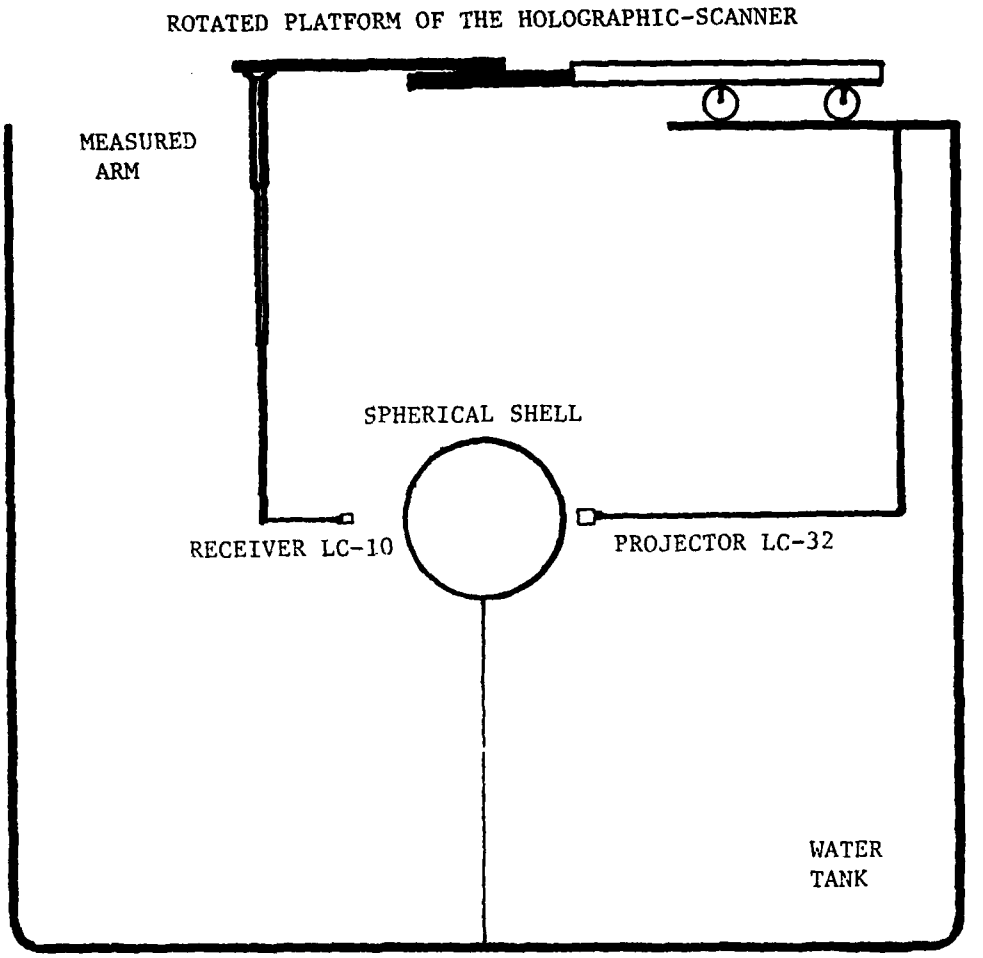

Figure 5.2 Geometrical configuration of the holo-scanner

When the measurements were carried out in the anechoic chamber, a one-inch diameter loudspeaker functioned as a source, and the receiver was the Telectret condenser microphone, Model 5336. It has a dimension of 0.285" x 0.163". The frequency response is flat up to 16 kHz.

For the measurement of the shell's resonance frequencies, a 1/4-lb. Wilcoxon F5B driver was used to vibrate the shell and the Z12 impedance head was used as a force measuring gauge as well as an accelerometer to measure the point acceleration of the vibrating shell. The impedance head was attached to an aluminum adapter (1/2 inch in diameter, 1/4 inch thick) glued to the surface of the shell. In order to use the unit in water, a rubber balloon was used to house the driving unit to prevent wetting. The balloon was glued to the shell and the air inside the balloon was squeezed out.

5.4 Measurement of the Resonance Frequencies

For the measurement of the resonance frequencies of the two spherical shells, two precedures were carried out. First, the measurements of the frequency response of the driving point inertance, defined as the ratio of the acceleration of the shell's surface to the applied force at the driving point, will provide the driving point inertance frequency spectrum. The spectrum's peaks represent the resonant frequencies of a structure within the frequency range. Second, the mode shape is measured when the frequency of excitation is fixed at the frequency corresponding to each peak.

5.4.1 Measurements in Air. In the experiments to measure the driving point admittance, a sinusoidal wave or a random noise was applied to the driver to excite the spherical shell. The shell's

response was received by the attached impedance head and the output was recorded by a two-channel digital signal processor made by Spectrum Dynamics [32]. The result was displayed on a cathode ray screen and/or recorded on an X-Y plotter.

The digital signal processor is a Fast Fourier Transform (FFT) processor. The use of an FFT technique results in measurement of the transfer function which is the ratio of the acceleration of the structural surface to the system forcing function. This transfer function, the inertance, can be measured to a high degree of accuracy by means of a processor. The operational setup is shown in Figure 5.3.

To measure the mode shape of the spherical shell, an accelerometer replaces the impedance head, and the voltage was recorded every 5° around the equator of the shell to measure the response. The measurement sequence was as follows: (1) located the accelerometer at 180° from the driver, and searching for an excited frequency (resonance frequency) around a selected peak frequency of the driving point inertance until a comparable large response was observed on the oscilloscope; and (2) placing the accelerometer every 5° around the equator of the shell to measure the response over 180°.

5.4.2 Measurements in Water. To measure the frequency response of the force excited spherical shell, the experimental setup in air was used except that the LC-10 hydrophone functioned as a receiver located at 180° from the driver instead of the impedance head. In the mode shape measurements, the procedure was the same as that in air. However, the receiver, LC-10 hydrophone, was rotated around the shell to measure the directivity of the pressure field by means of the

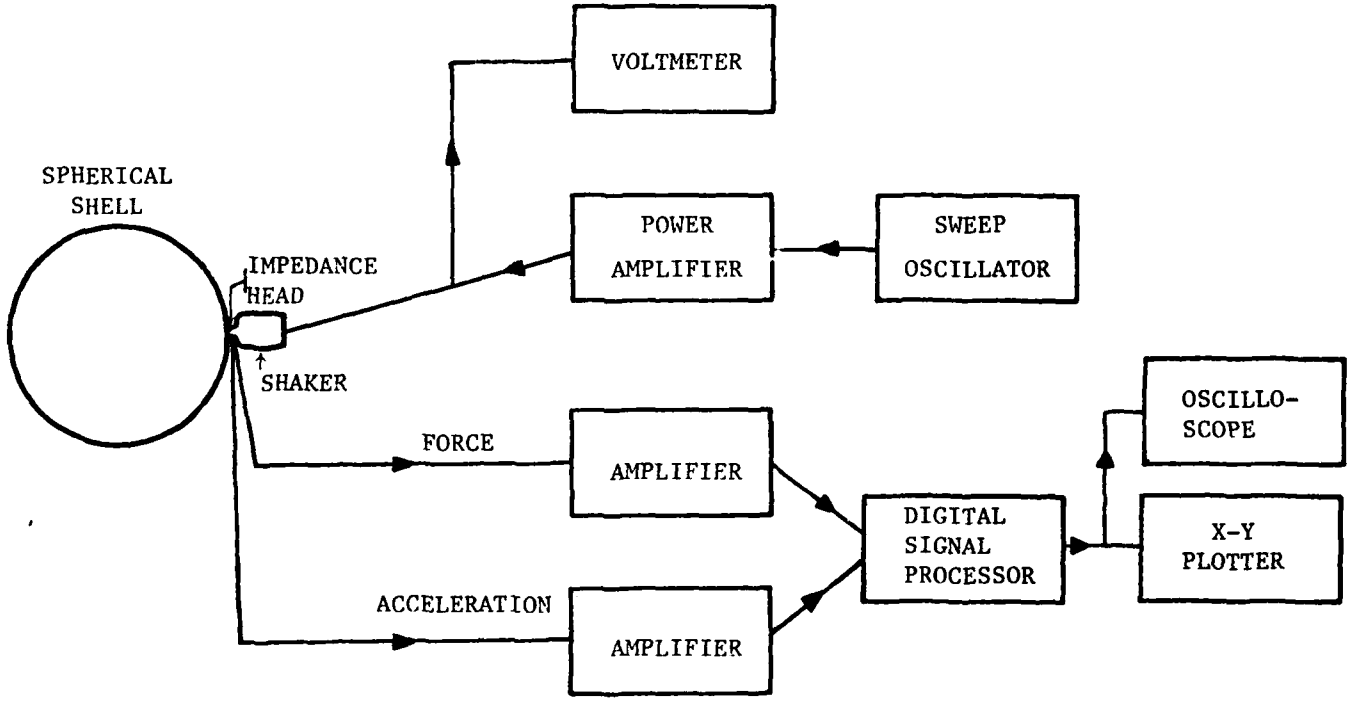

Figure 5.3 Operational set-up of the driving point inertance measurement

holographic scanner. The output of the receiver was recorded on an X-Y plotter. The receiver was located near the shell's surface.

5.5 Measurement of the Directivity Pattern

In this measurement, the near field of a spherical shell insonified by an acoustic spherical source was studied. The source and the receiver were located within one wavelength from the surface of the shell. The source was fixed at one extreme end of the scanner (reference zero degree) while the receiver was rotated about the equator of the shell in the horizontal plane.

5.5.1 Measurement in Water. In the measurement of the acoustic directivity field of a spherical shell, submerged in water and excited by a pulsing spherical source, the received signal was the sum of direct signal and indirect signal (reflected, creeping or diffracted wave). There was a time delay between the received signal and the reference signal. Therefore, the output from the receiver hydrophone was gated to pass the signal that arrived after a time corresponding to the travel time from the source to the surface and then to the receiver.

Technically, the pulse width of a signal is greater than $3/f$, where f is the source frequency. It means that the lower the frequency, the greater the pulse width. The pulse width for the source frequency was varied from 0.2 ms to 0.99 ms to provide a sufficient number of full cycles impinging on the surface. The pulse was repeated every 102 ms to insure that all echoes from the tank boundaries or other surfaces had decayed sufficiently before the next pulse was generated.

The total pressure field was measured by the rotated LC-10 hydrophone continuously, while the LC-32 hydrophone, functioning as a source, was fixed at a reference zero degree. The output from the hydrophone was filtered, amplified, and gated. The measured signal was recorded on an X-Y plotter. The block diagram of the experimental setup is shown in Figure 5.4.

5.5.2 *Measurements in Air*. In the measurement of the directivity pattern in air, a different approach was employed instead of the method mentioned in Section 5.5.1. This technique may be called the sound field visualization technique. By applying this technique, the amplitude and the phase of the pressure field can be recorded on photographic film.

The received signal goes through a monitoring circuit which converts the acoustical signal into a light signal via a light emitted diode (LED). The measurement block diagram is shown in Figure 5.5. The monitoring circuit is a kind of phase circuitry [31]. This circuit provides phase comparison between two signals, the driving signal and the received acoustic signal. The comparison between the phase of the driving signal and the phase of the received signal produces an output pulse of varying width depending on the phase difference between the two signals. A dc voltage ramp corresponding to the pulse width will turn the LED on for a 0° - 90° phase shift (high dc ramp voltages) and off for 90° - 180° phase shift (low dc ramp voltages).

The amplitude circuitry is a comparator circuit [31] which is adjusted to turn the LED on or off when the voltage of the received

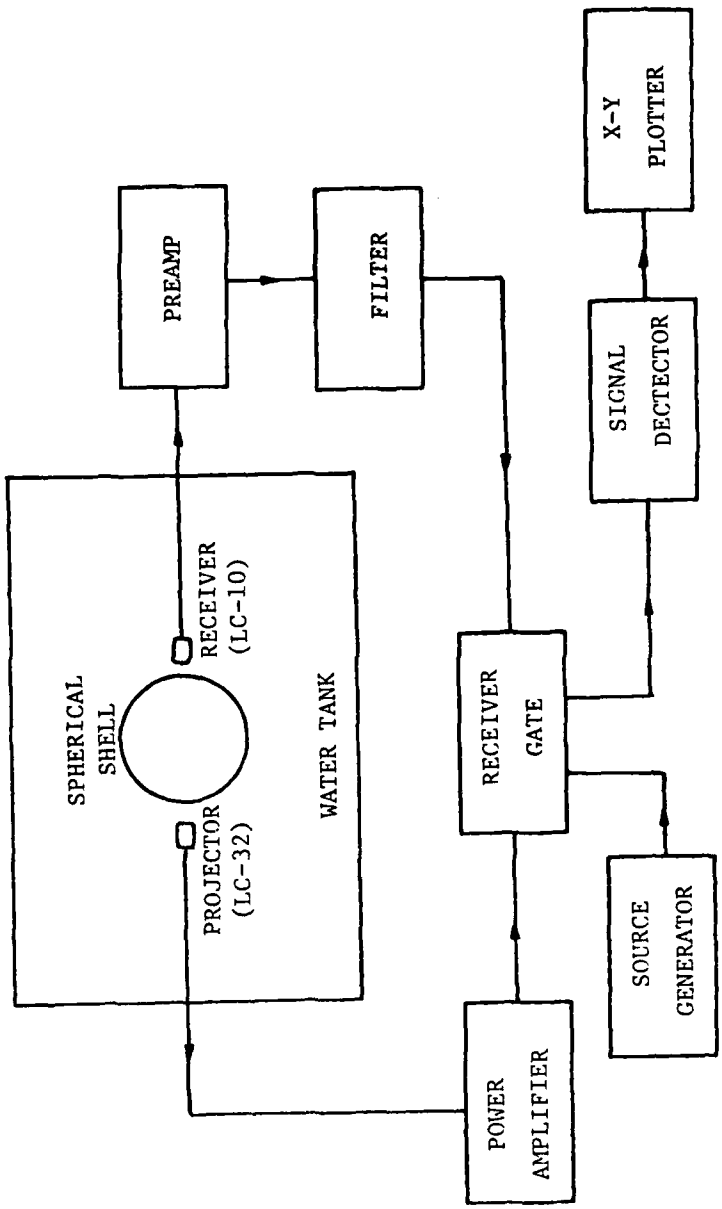

Figure 5.4 Set-up for measuring the sound directivity pattern in water

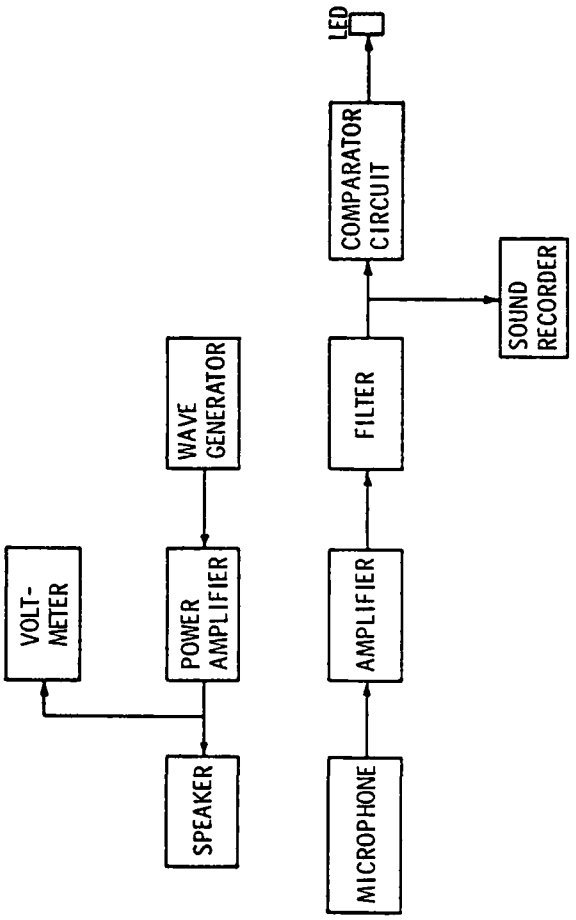

Figure 5.5 Set-up for measuring sound pressure

signal is greater or less than the set upper or lower level of the circuit, respectively.

An overall sketch of the experimental setup is shown in Figure 5.6. The spherical shell, hung in the middle of the anechoic chamber, was insonified by a one-inch diameter speaker. The microphone, attached at the end of a small plastic stick, scanned around the surface of the shell on the equatorial plane. The LED was located right below the measuring boom about 4 inches behind the microphone, whose brightness was calibrated to correspond to the intensity of the sound field. This varying light intensity was recorded by means of a camera set at a long time exposure. The typical measurement time for one picture was about 2 hours for an 8-inch horizontal scanned distance at the stepping rate of 1/8 inch/scan. The resulting photograph was then digitized and processed in three dimensions with relief representing amplitude.

5.6 The Results of the Measurement of Resonance Frequencies

The driving point admittance in air of the thin and thick shells are shown in Figures 5.7a - 5.8b, respectively. Both shells exhibit an antiresonance in the low frequency range as was predicted earlier and shown in Figures 3.5 and 3.6a. In the higher frequency range, the measured resonances are the peaks of the admittance. These resonance frequencies were identified by the measurements of the mode shape and the results are tabulated in Tables 5.1 and 5.2 for the two shells. The difference between the predicted and the measured resonance frequencies is small for most of the measured mode orders. The good agreement occurred in spite of the nonuniformity of

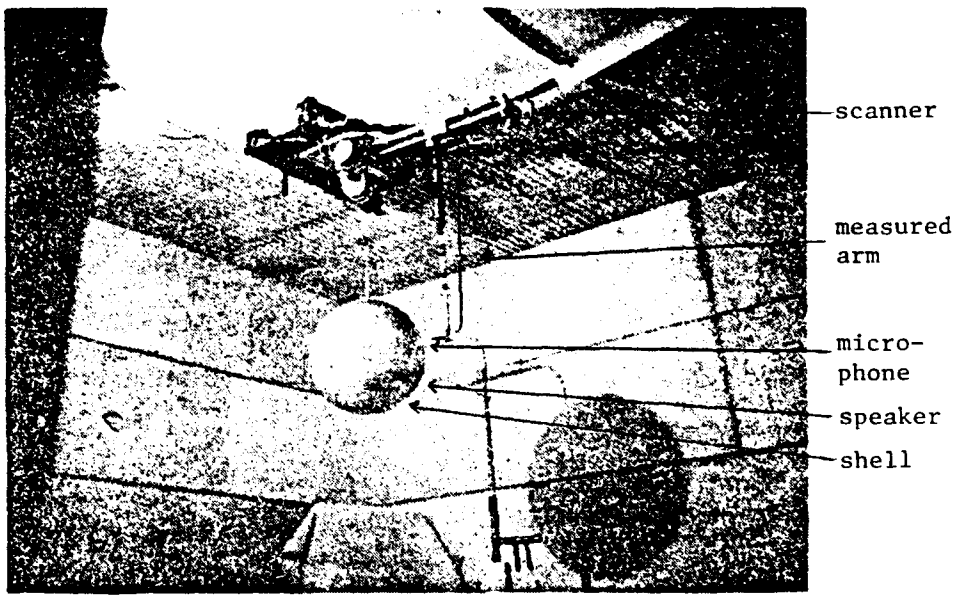

Figure 5.6 Set-up for measuring sound pressure in an anechoic chamber

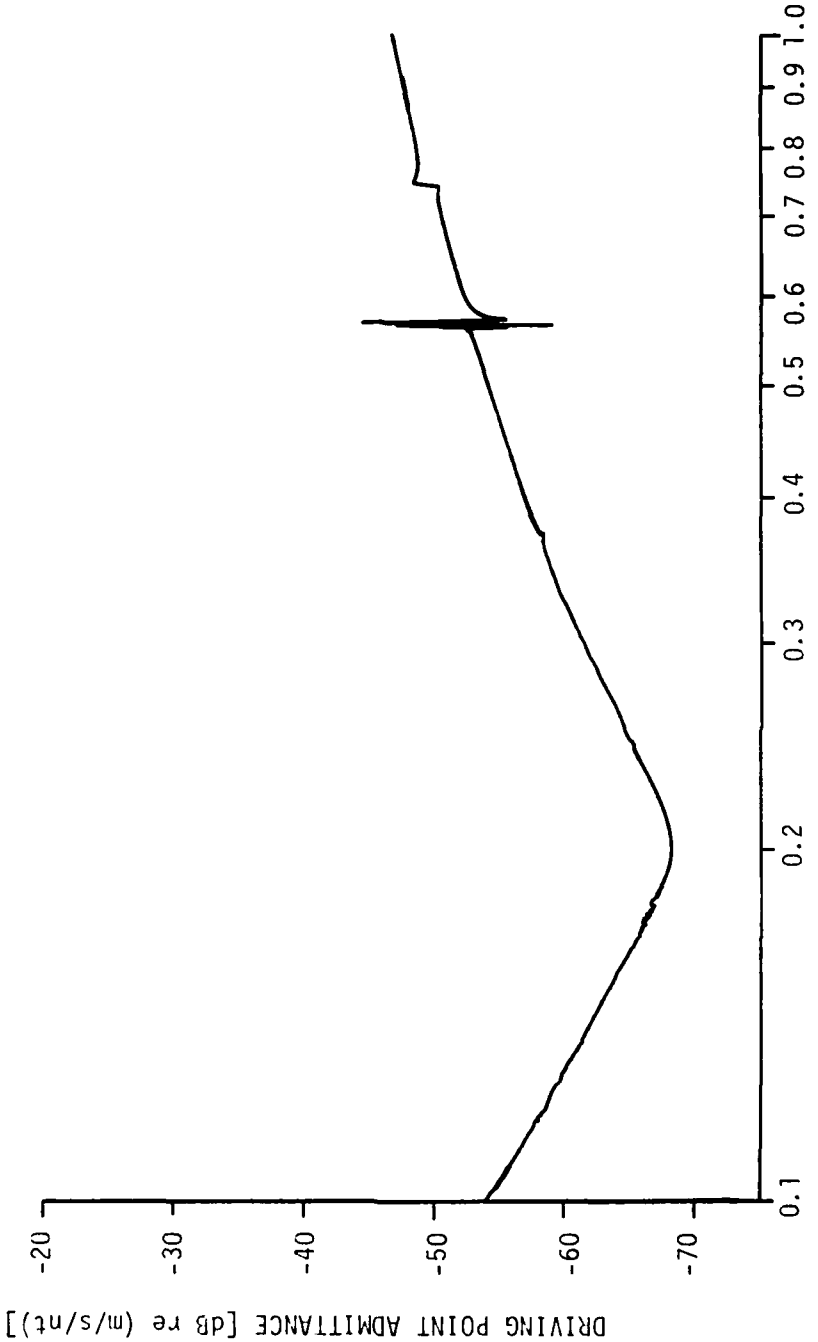

Figure 5.7a Measured driving point inertance of a duralumin spherical shell with thickness h = 0.0514" in air

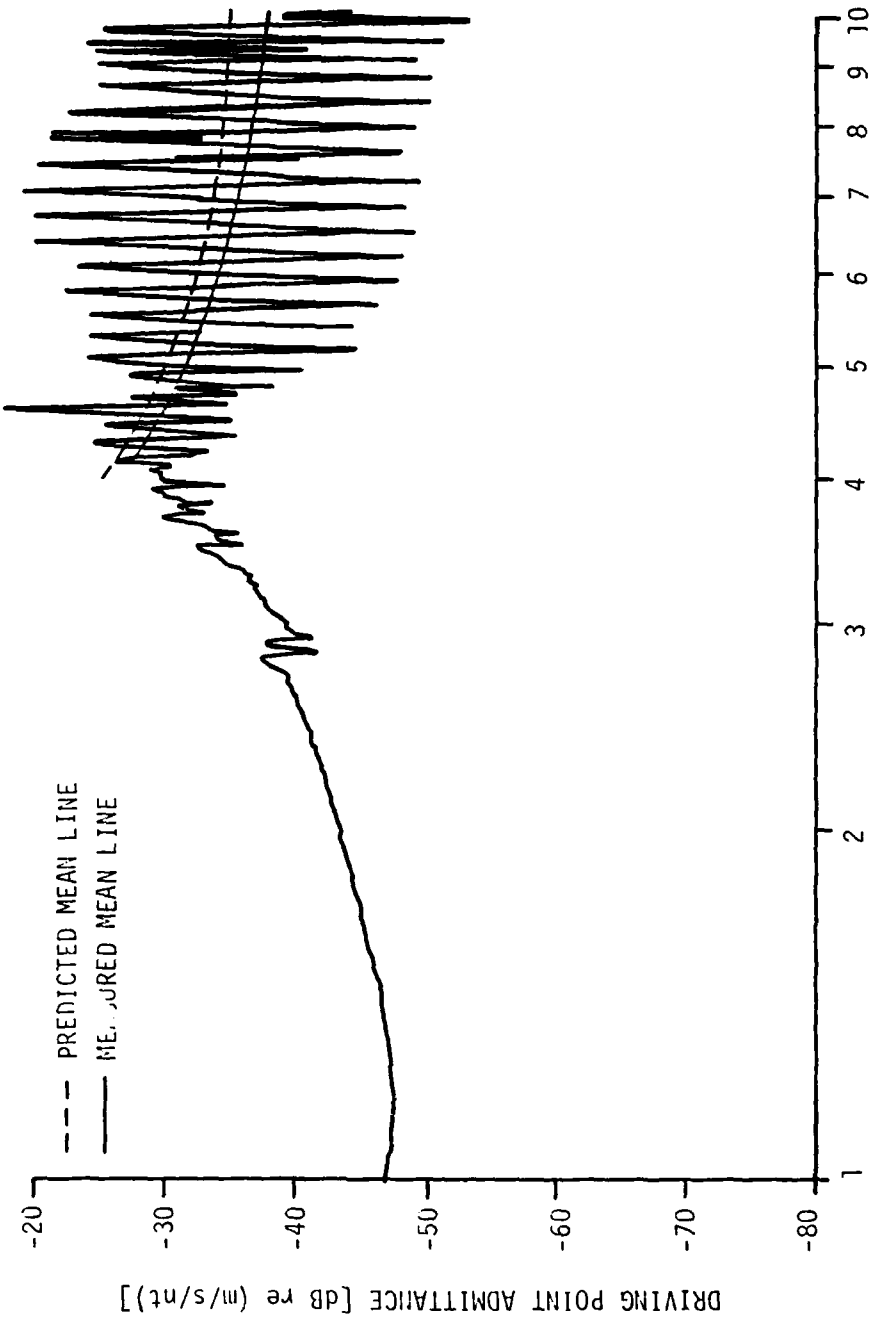

Figure 5.7b Measured driving point inertance of a duralumin spherical shell with thickness h = 0.0514" in air

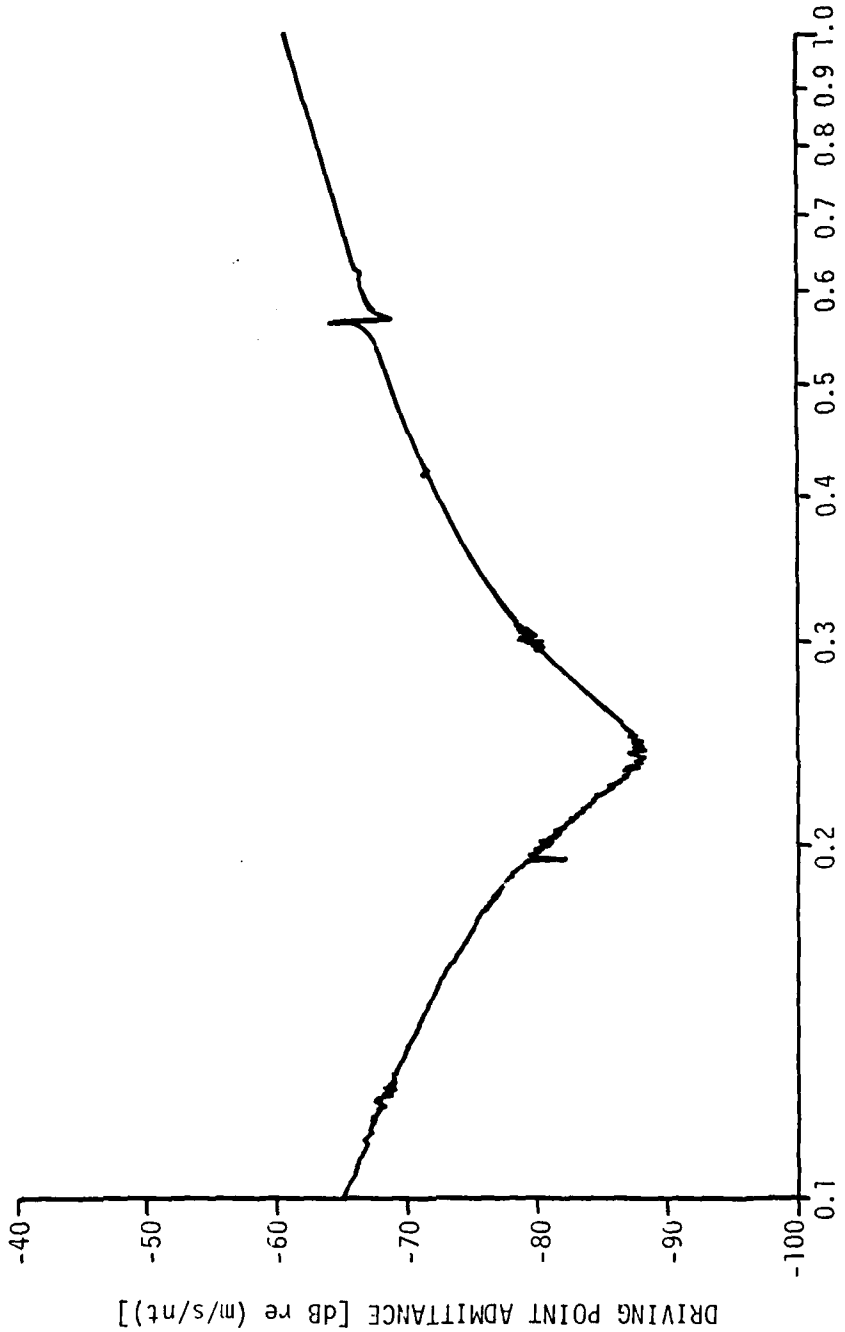

Figure 5.8a Measured driving point inertance of a duralumin spherical shell with thickness h = 0.1069" in air

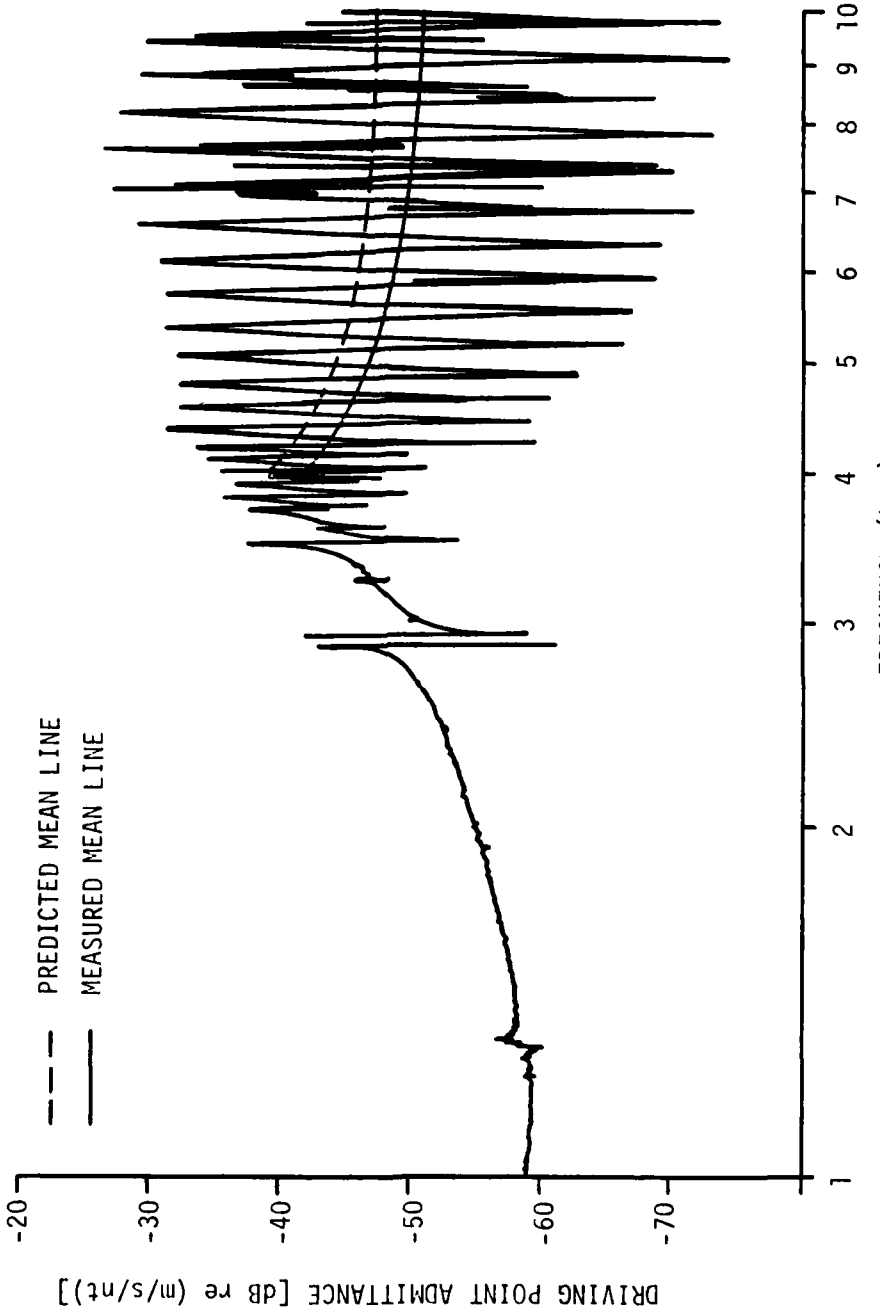

Figure 5.8b Measured driving point inertance of a duralumin spherical shell with thickness h = 0.1069" in air

TABLE 5.1

MEASURED (f'_n) AND CALCULATED (f_n) RESONANCE FREQUENCIES OF A SPHERICAL SHELL (h = 0.0514") SUBMERGED IN AIR AND WATER

	Air		Water	
n	f_n (kHz)	f'_n (kHz)	f_n (kHz)	f'_n (kHz)
2	2.868	2.867	0.732	0.764
3	3.408	3.246	0.927	0.945
4	3.624	3.526	1.065	1.074
5	3.734	3.598	1.177	1.178
6	3.800	3.710	1.276	1.270
7	3.847	3.767	1.365	1.357
8	3.887	3.804	1.448	1.436
9	3.925	3.912	1.567	1.515
10	3.967	3.972	1.605	1.595
11	4.015	4.032	1.682	1.650
12	4.071	4.092	1.761	1.760
13	4.138	4.176	1.844	1.800
14	4.218	4.315	1.931	1.900
15	4.312	4.461	2.024	2.025
16	4.421	4.591	2.124	2.180
17	4.549	4.701	2.234	2.300
18	4.698	4.771	2.354	2.340
19	4.869	4.906	2.486	2.500
20	5.061	5.081	2.630	2.670
21	5.275	5.293	2.788	2.760
22	5.511	5.521	2.958	2.960
23	5.768	5.800	3.143	3.100
24	6.047	6.043	3.341	3.340
25	6.347	6.341	3.554	3.500
26	6.681	6.720	3.782	3.640
27	7.011	7.088	4.025	3.800
28	7.432	7.376	4.283	4.150
29	7.863	7.763	4.558	4.500
30	8.254	8.172	4.848	4.900
31	8.671	8.601	5.154	5.350
32	9.025	9.049	5.475	5.820
33	9.433	9.516	6.160	6.850
34	9.703	10.000	6.160	6.850

TABLE 5.2

MEASURED (f'_n) AND CALCULATED (f_n) RESONANCE FREQUENCIES OF A SPHERICAL SHELL (h = 0.1069") SUBMERGED IN AIR AND WATER

	Air		Water	
n	f_n (kHz)	f'_n (kHz)	f_n (kHz)	f'_n (kHz)
2	2.868	2.877	1.002	1.050
3	3.411	3.460	1.270	1.320
4	3.633	3.601	1.459	1.468
5	3.754	3.758	1.612	1.610
6	3.841	3.855	1.746	1.740
7	3.921	3.943	1.874	1.863
8	4.009	4.059	2.001	1.989
9	4.155	4.092	2.133	2.180
10	4.248	4.192	2.277	2.300
11	4.413	4.343	2.437	2.480
12	4.614	4.548	2.618	2.680
13	4.856	4.737	2.823	2.890
14	5.141	5.007	3.056	3.105
15	5.470	5.308	3.317	3.400
16	5.845	5.681	3.610	3.704
17	6.264	6.053	3.936	4.050
18	6.728	6.501	4.294	4.400
19	7.236	6.970	4.685	4.800
20	7.786	7.538	5.110	5.250
21	8.378	8.103	5.567	5.750
22	9.011	8.722	6.058	6.205
23	9.684	9.422	6.582	6.780
24	10.397	9.900	7.183	7.350
25	11.147	10.692	7.727	7.980
26	11.935	11.412	8.347	8.580
27			9.000	9.220
28			9.684	9.920
29			10.399	10.660
30			11.145	11.400

the shell's thickness and the existence of the weld between the two hemispheres making up each spherical shell.

The measured resonance frequencies for submerged shells in water were obtained from the peaks in the driving point inertance shown in Figures 5.9 and 5.10 for the thin and thick shells, respectively. The measured resonances, as identified by the measured mode shape, are tabulated in Tables 5.1 and 5.2, respectively, for thin and thick shells. The agreement between the measured and predicted resonances again is very good.

It should be noted that the good agreement between the predicted and measured resonance frequencies was attained only after a thorough measurement of the thickness of the shell was made. The manufacturer has supplied us with nominal thicknesses of 8-gauge and 14-gauge for the two shells. However, it has been found that the 8-gauge and the 14-gauge shells actually have thicknesses of 0.1069 inch and 0.0514 inch, respectively. This drop in thickness of two gauges has been confirmed by ultrasonic measurement. In this measurement, a Krautkramer-Branson Ultrasonic Pulse-Echo Thickness Gauge (Model CL 204) [33] was used, with an accuracy of the thickness measurement of $\pm$ 0.01%. The thickness of the shell was obtained by averaging the measured thickness of 120 points of two orthogonal circles on the surface. The corrected resonances using the actual thicknesses are those listed in Tables 5.1 and 5.2. All these data are shown graphically in Figures 5.11, 5.12, 5.13, and 5.14. The decrease in the thickness would have a slight change in the resonance frequencies of shells in air. However, the error is more appreciable

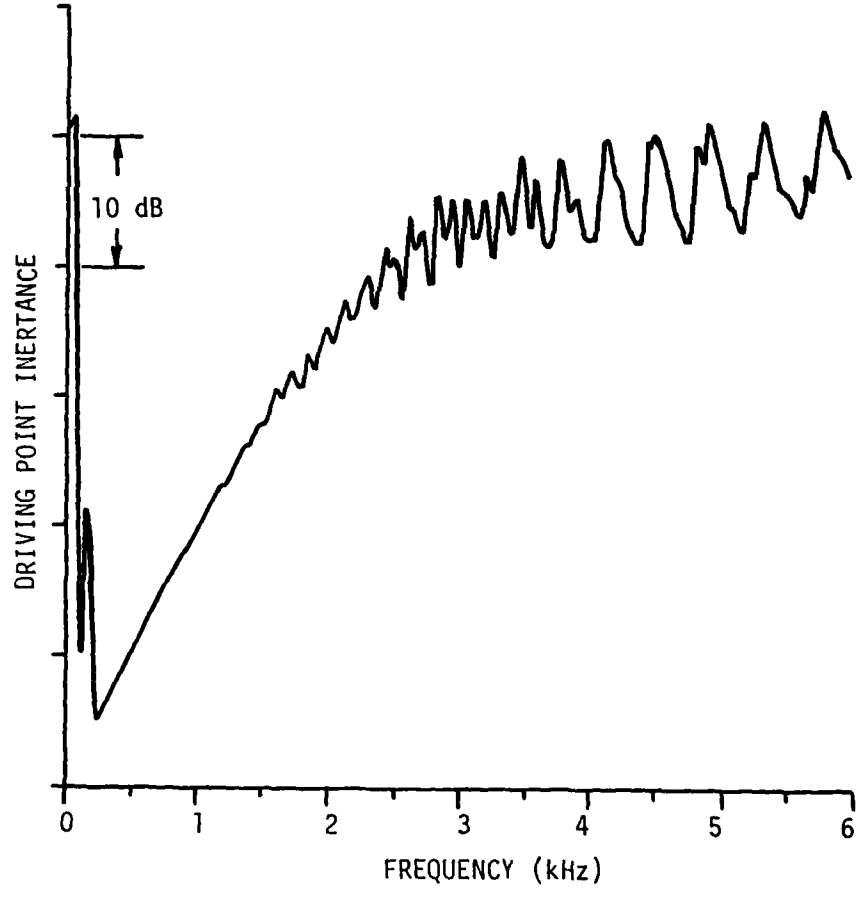

Figure 5.9 Measured driving point inertance of a duralumin spherical shell with thickness h = 0.0514" in water

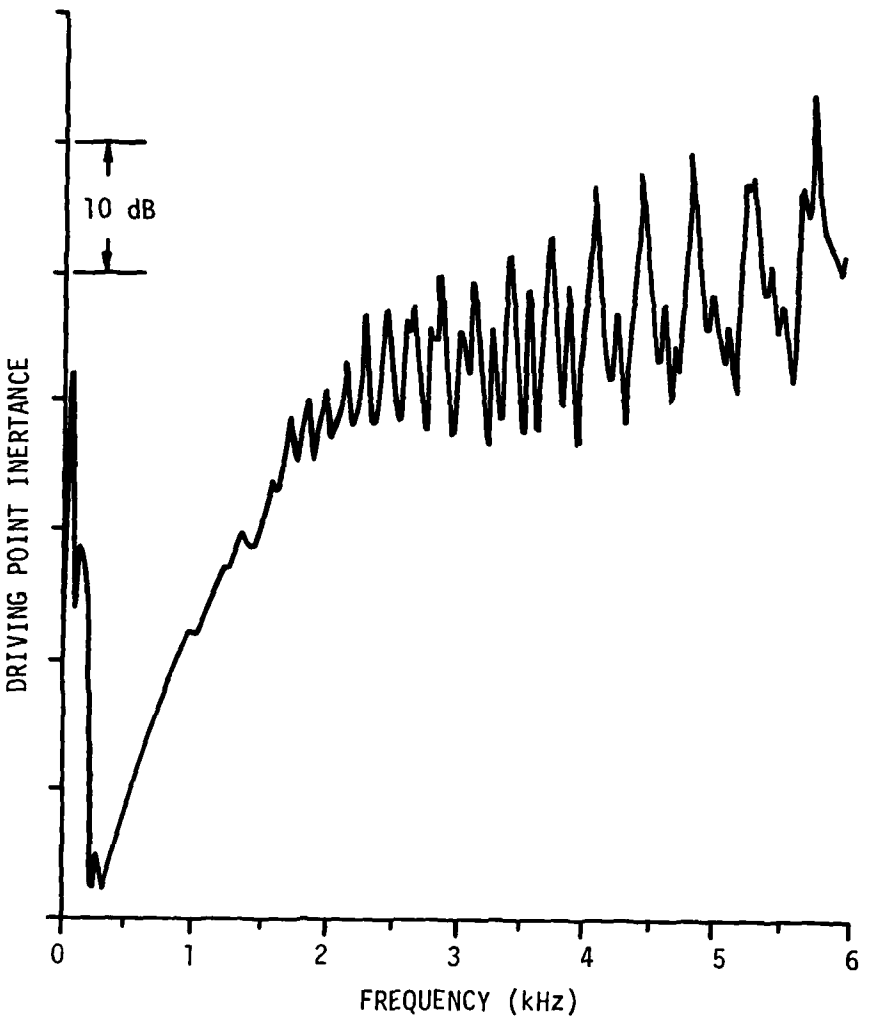

Figure 5.10 Measured driving point inertance of a duralumin apherical shell with thickness h = 0.1069" in water

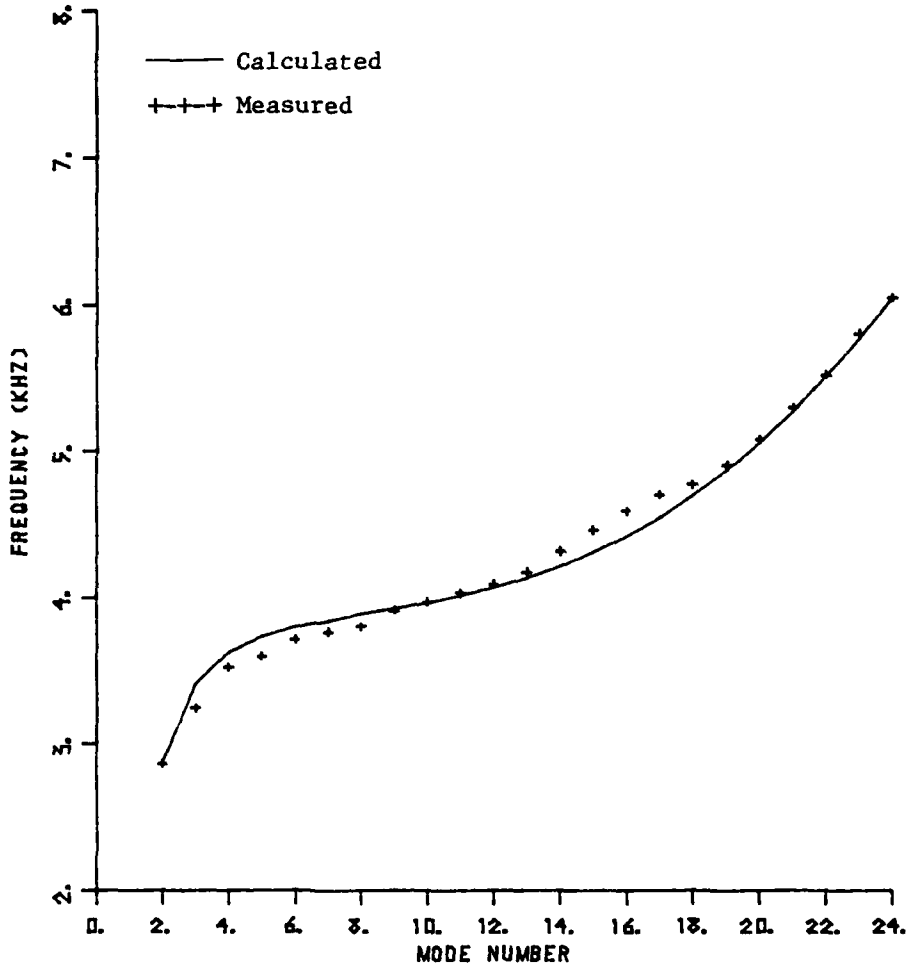

Figure 5.11 Resonant frequencies of a duralumin spherical shell with thickness h = 0.0514" in air

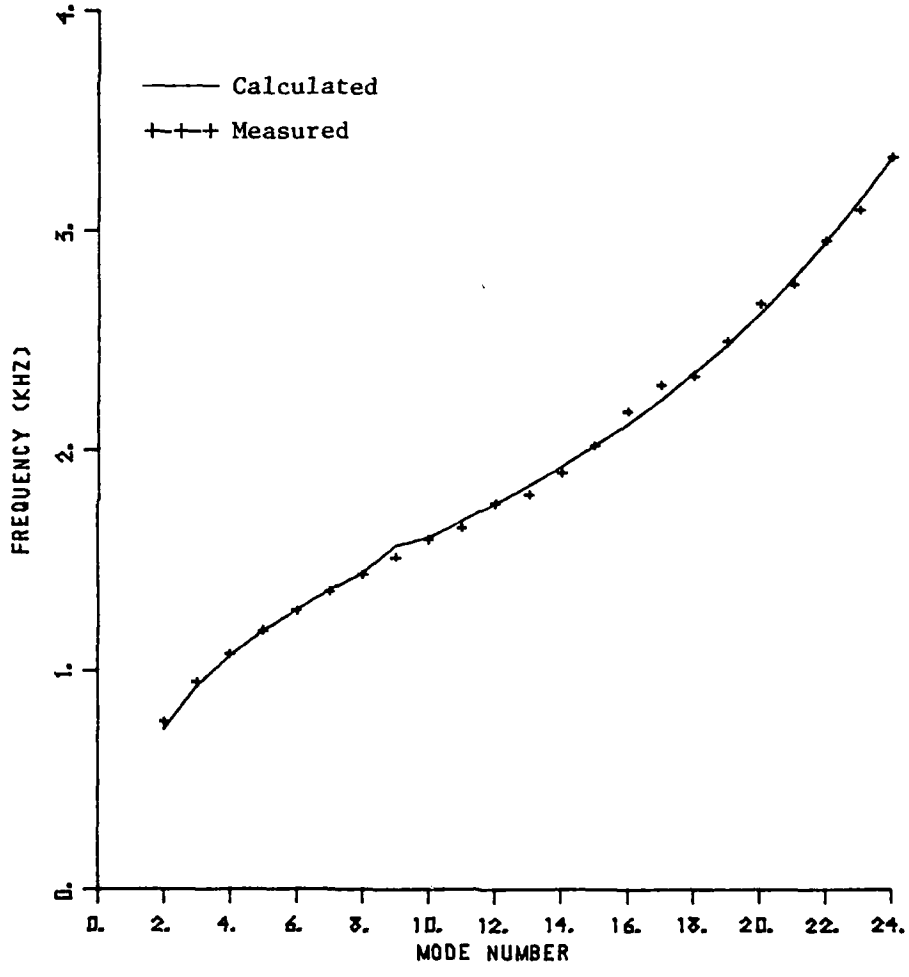
Calculated
Measured
FREQUENCY (KHZ)
0.
1.
2.
3.
4.
0.
2.
4.
6.
8.
10.
12.
14.
16.
18.
20.
22.
24.
MODE NUMBER

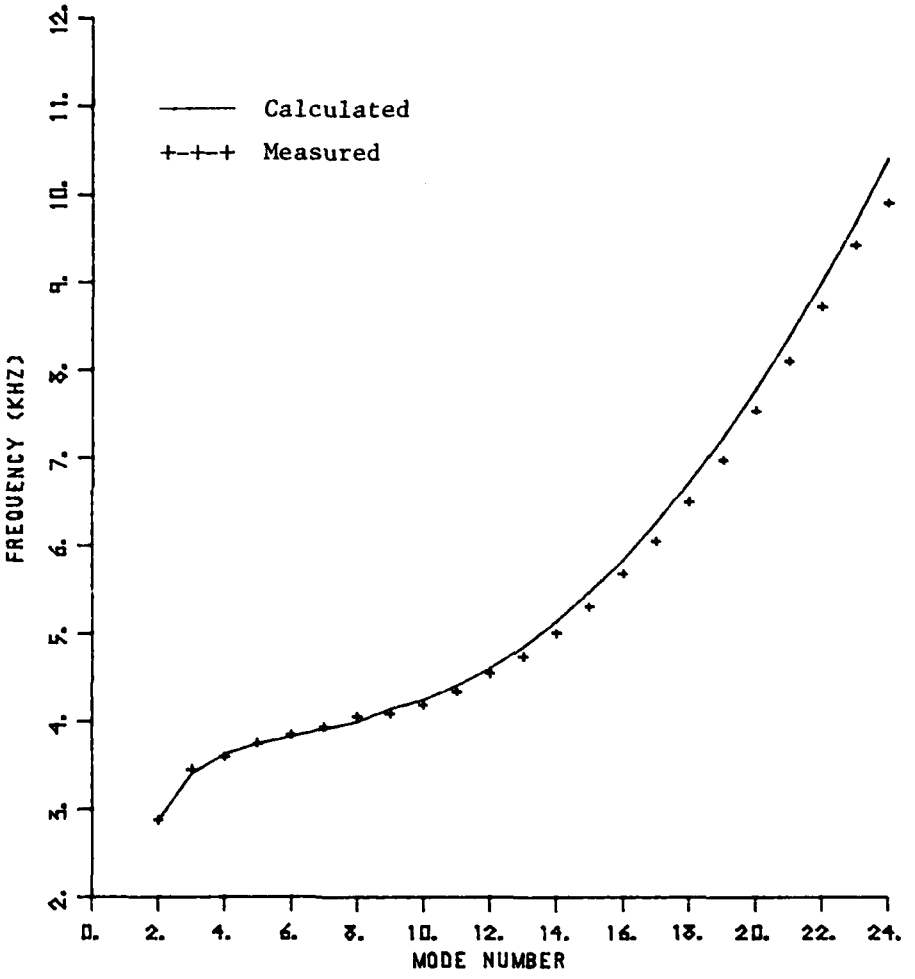

Figure 5.13 Resonant frequencies of a duralumin spherical shell with thickness h = 0.0514" in water

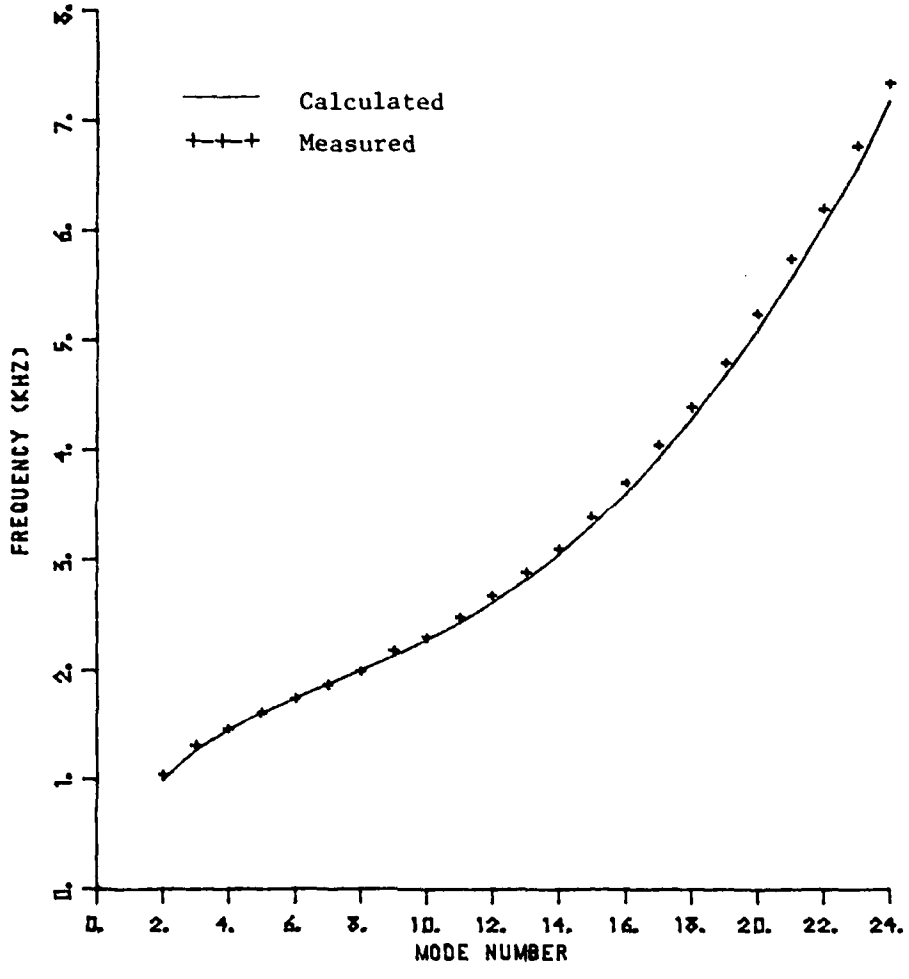

Figure 5.14 Resonant frequencies of a duralumin shperical shell with thickness h = 0.1069" in water

when one uses a thinner wall thickness for the resonance frequencies of shells submerged in water.

5.7 Measured Frequency Spectra of the Shell's Response

The measured driving point admittance of the two shells in air are shown in Figures 5.7 and 5.8 for the thin and thick shells, respectively. These plots were obtained by use of the best available digital mass cancellation scheme. These spectra exhibit high Q's at all the resonances. The mean value of the measured spectra are also shwon vs. the predicted mean value. The predicted mean value was found to be higher than the measured value by approximately 3 dB for both shells. This difference can be attributed to the fact that the measured mean value of shells with low damping or high Q's can fluctuate depending on the support condition of the shells, the dynamic range of the measuring system, and the still inexact mass cancellation scheme for structures with high Q.

The driving point inertance in water is shown in Figures 5.9 and 5.10 for the thin and the thick shells, respectively. Although the mass cancellation scheme was not available for these measurements, the absolute value of the maxima and minima are probably fairly well approximated, since the Q's of the submerged shell were probably lower than those in air.

5.8 The Results of the Directivity Pressure Field Measurement

Figures 5.15, 5.16, 5.17, 5.18, and 5.19 show the directivity pressure field of the shell, h = 0.1069", submerged in water. The pressure field was normalized by the corresponding free field at the

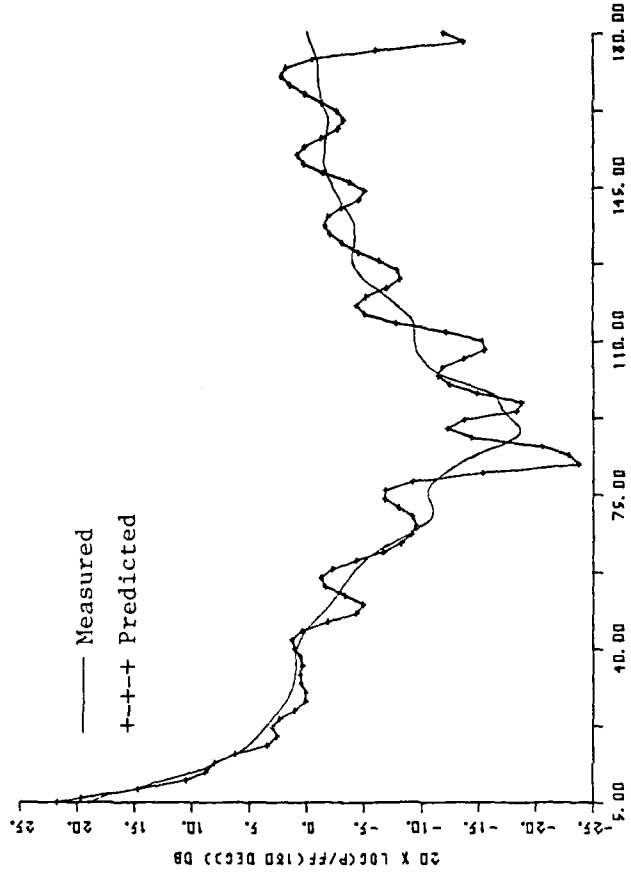

Figure 5.15 Directivity pattern of a shell with thickness h = 0.1069" for ka = 4.4276 in water

AD-A086 008 PENNSYLVANIA STATE UNIV UNIVERSITY PARK APPLIED RESE--ETC F/G 20/1
A STUDY OF THE NEARFIELD OF AN EXCITED SPHERICAL SHELL.(U)
MAR 80 E WONG N00024-79-C-6043
UNCLASSIFIED ARL/PSU/TM-80-30 NL

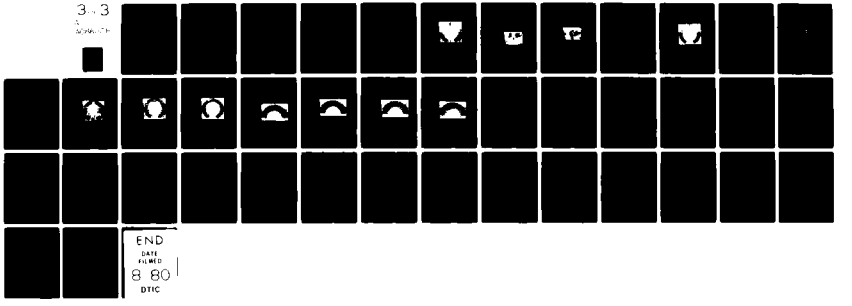

END
DATE FILMED
8 80
DTIC

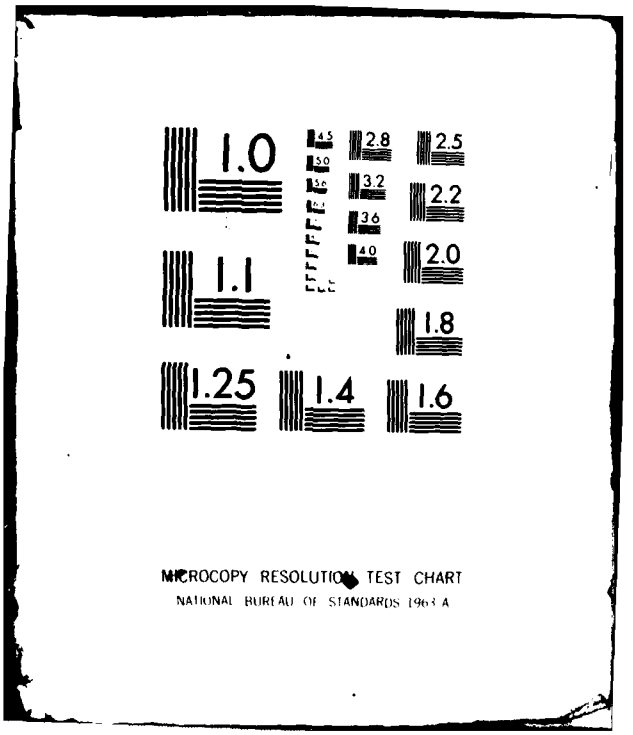
1.0
1.1
1.25
1.4
1.6
1.8
2.0
2.2
2.5
2.8
3.2
3.6
4.0
MICROCOPY RESOLUTION TEST CHART
NATIONAL BUREAU OF STANDARDS 1963 A

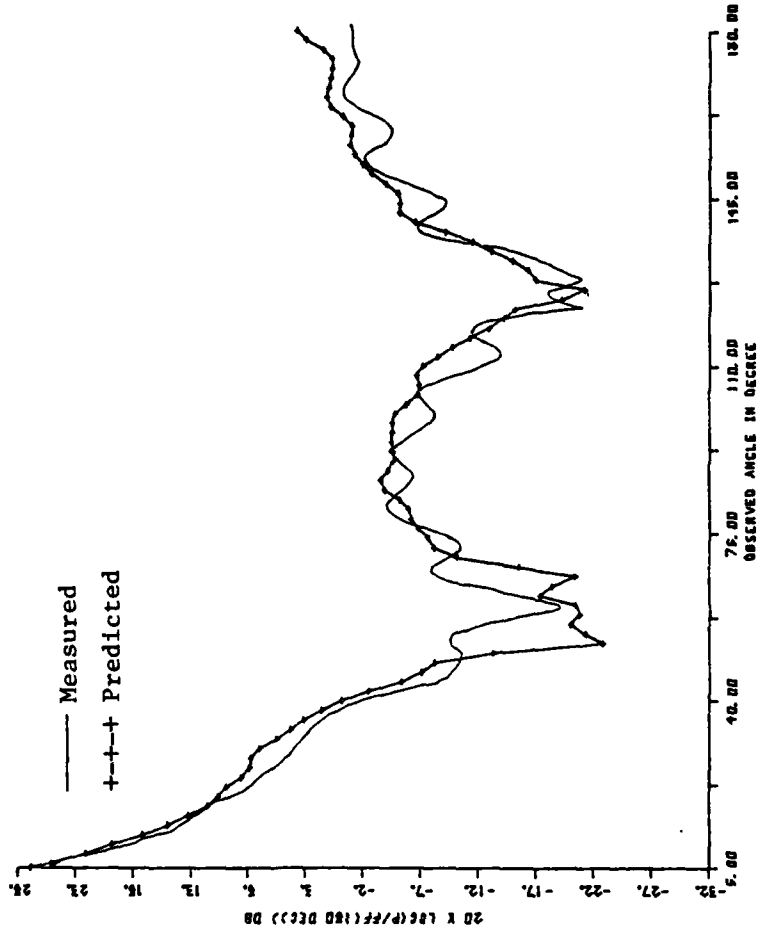

Figure 5.6 Directivity pattern of a shell with thickness h = 0.1069" for ka = 8.398 in water

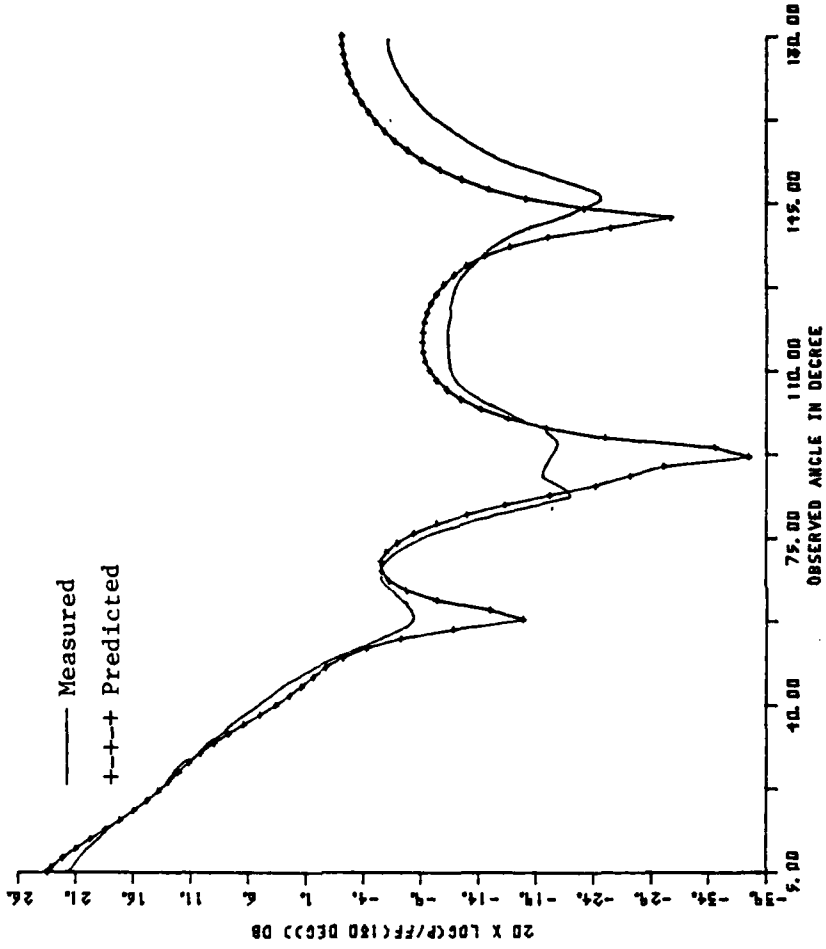

Figure 5.17 Directivity pattern of a shell with thickness h = 0.1069" for ka = 12.235 in water

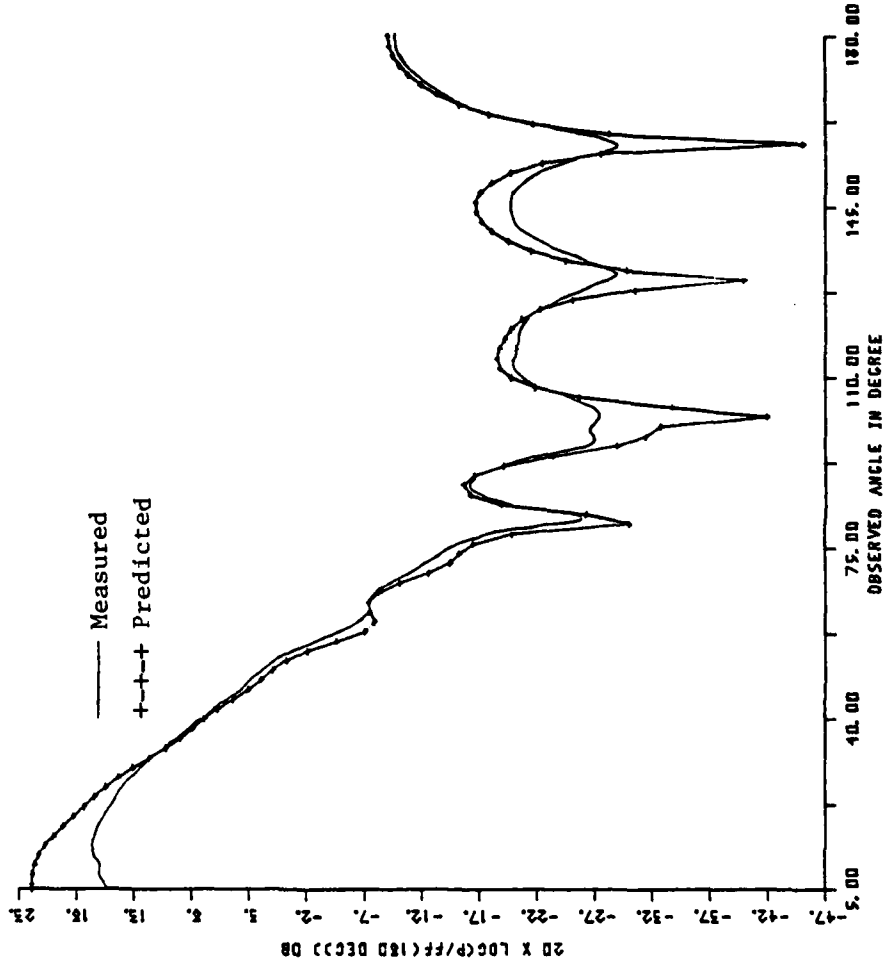

Figure 5.18 Directivity pattern of a shell with thickness h = 0.1069" for ka = 22 in water

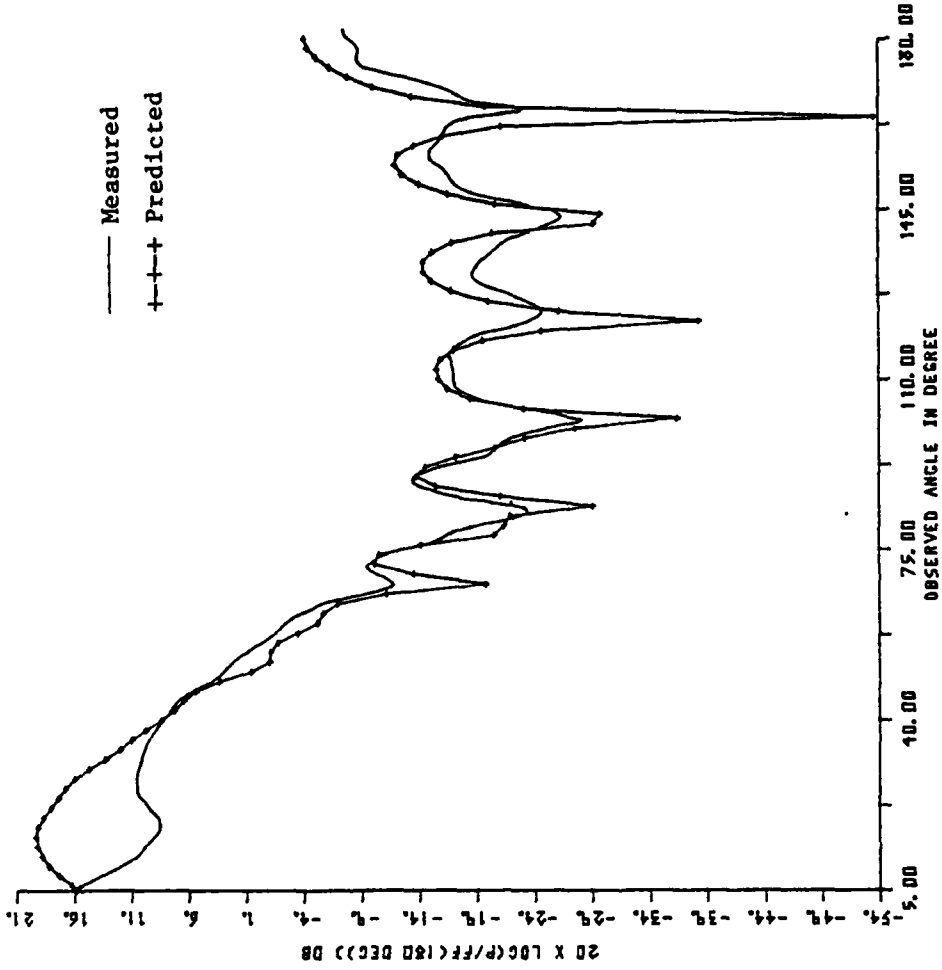

Figure 5.19 Directivity pattern of a shell with thickness h = 0.1069" for ka = 30 in water

receiver located at the antipode, denoted as FF(180°) . The source was located at r_o = 8.945" measured from the acoustic center of the source (LC-32 hydrophone) at the reference zero degree, while the receiver hydrophone, LC-10, was located at r = 8.567" for the measurements shown in Figures 5.15 and 5.16. For Figures 5.17 through 5.19, the distances of the source and the receiver were r_o = 10.195" and r = 8.63" , respectively. The excited frequencies were varied from ka = 4.4276 to 30 . The solid line with asterisks represents the calculated result, and the solid line is the measured data.

Generally, the discrepancy between the measured and calculated pressure fields lies within a few dB. The largest discrepancy occurs at the minima, especially for the near field at the high frequencies patterns (see Figures 5.17 - 5.19).

For the measurement of the directivity pattern in air, the sound visualization technique is used. Figure 5.20 represents the photographic experimental data of sound propagation near the surface of the spherical shell, h = 0.1069", insonified by a 1" diameter speaker located at a distance 1/4" from the surface. The intensity of the lighted area of the photograph represents the amplitude of the sound field for ka = 18 ; scan range, 3/16" to 6". This result is shown in three dimensions with relief representing amplitude in Figure 5.21. Figure 5.22 is a three-dimensional theoretical plot of the predicted directionality field at the same frequency.

As seen in Figures 5.20 and 5.21, there is a bright spot at the antipode as expected from the theory (see Figure 5.22). There

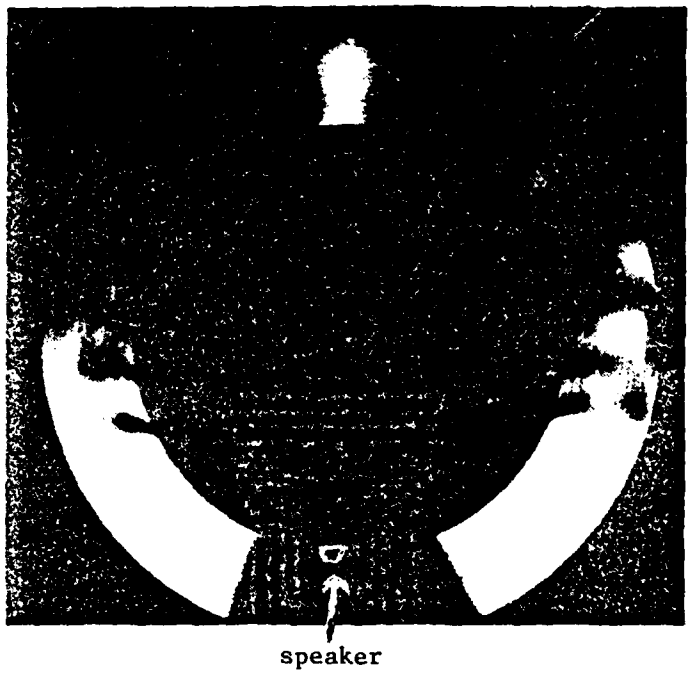

Figure 5.20 2-D photographic experimental data of sound field near a shell with thickness $h = 0.1069"$. insonified by a 1" diameter speaker for $ka = 18$ in air

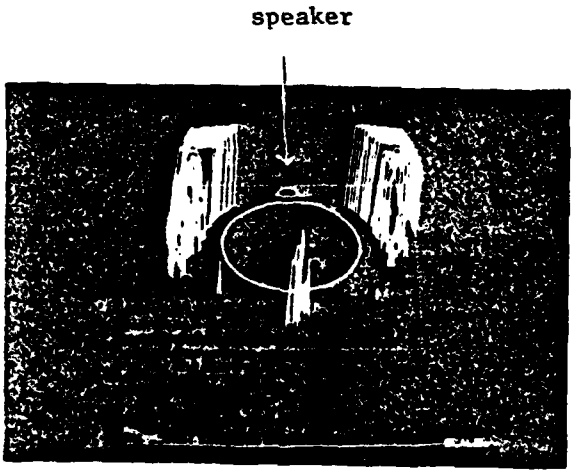

Figure 5.21 3-D measured directivity pattern of a shell with thickness h = 0.1069" for ka = 18 in air

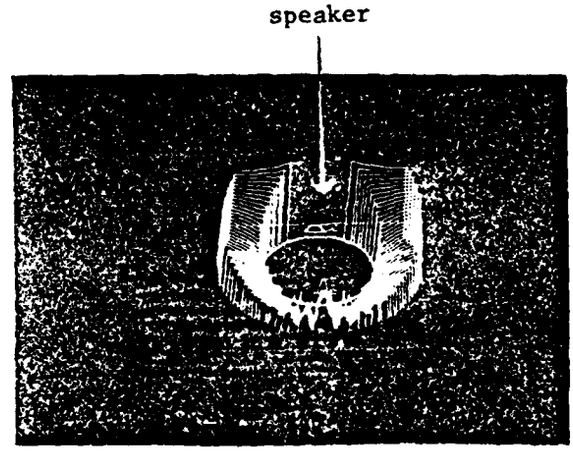

Figure 5.22 3-D predicted directivity pattern of a shell with thickness h = 0.1069" for ka = 18 in air

is a dim zone for angles off the antipode up to about 90°. Actually, it is a weak sound zone (see Figure 5.22) when compared with the bright spot at the antipode and the zone near the source. The voltage level of the comparator circuit has to be adjusted to have a considerably better dynamic range in the picture when compared with the predicted pattern. If the level is set too high, the sound pressure (brightness) in the shadow zone including the antipode area may not show in the picture. On the contrary, if the level is too low, there will result a completely bright annular. It should be recognized that the brightness (the amplitude) is limited by the degree of sensitivity of the film. If the light intensity of the LED exceeds the intensity sensitivity of the film, then all intensity beyond this limitation will have the same intensity. This result causes a flat response in the zone near the source as shown in Figure 5.20.

Figures 5.23 and 5.24 show the photographic recording in two-dimensional cross-section and three-dimensional graphic, respectively, for the same system with $ka = 22$. Figure 5.25 represents the predicted pattern in three-dimensional graphic display. It is clear that the sound field as shown in Figure 5.22 changes rapidly in the zone near the antipode as predicted. The bright spot at the antipode is always there because the sound field is in focus.

Although the sound visualization technique in some ways cannot be as powerful as the method described in the previous section in terms of obtaining detailed data, it is an economic and

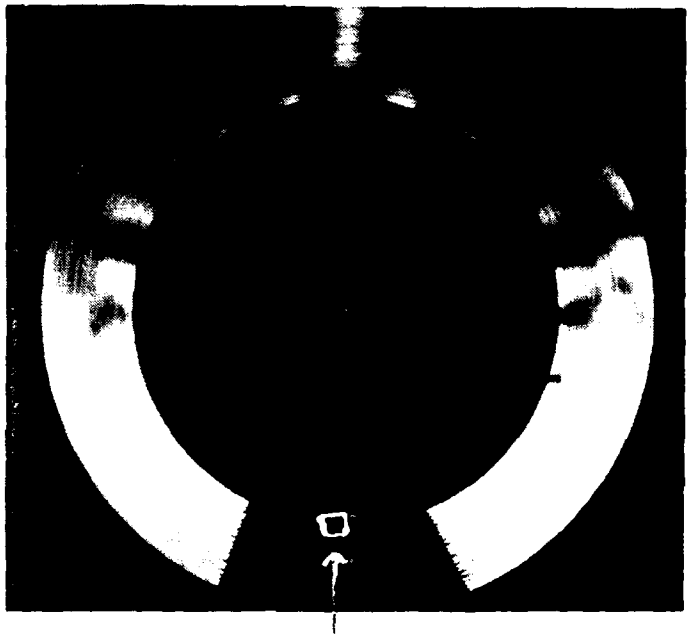

Figure 5.23 2-D measured directivity pattern of a shell with thickness h=0.1069" for ka=22 in air

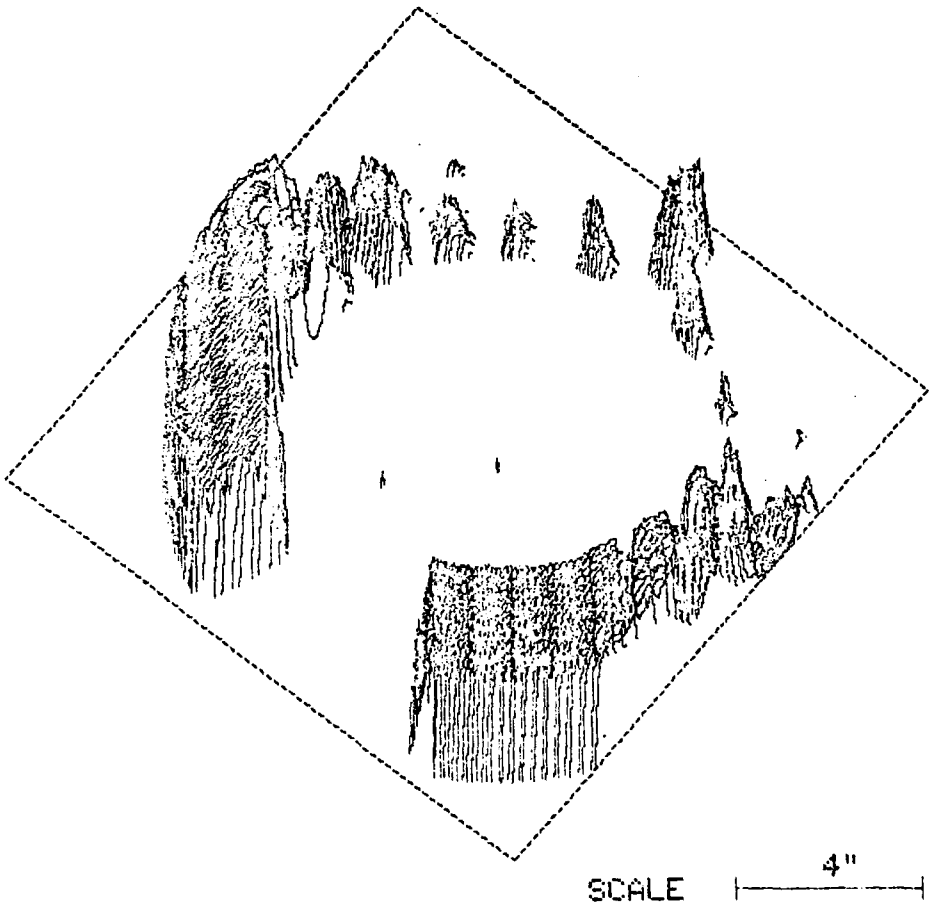

Figure 5.24 3-D measured directivity pattern of a shell with thickness h = 0.1069" for ka = 22 in air

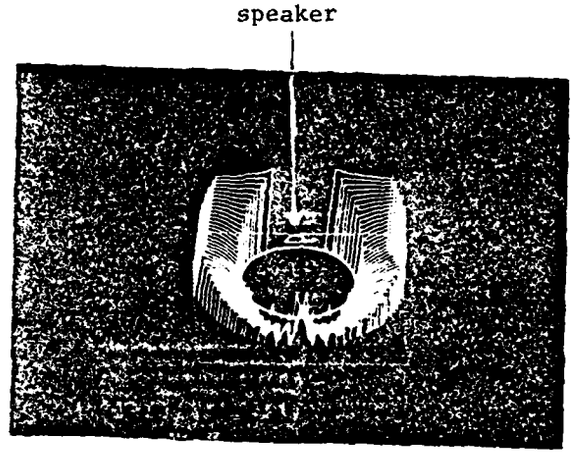

Figure 5.25 3-D predicted directivity pattern of a shell with thickness h = 0.1069" for ka = 22 in air

easy way to map the whole sound field of a spherical shell. And one can visualize the sound field around the shell.

This technique enables the detection of the amplitude and the phase. Figures 5.26, 5.27, and 5.28 show the phase pattern of the acoustic near field of the spherical shell, h = 0.1069", insonified by a 1" diameter speaker located 1/4" from the shell's surface for frequencies ranging from ka = 6 to 30. The scan range is from 1/8" to 5". In viewing these annular phase patterns, the black and white stripes seem to be the creast and trough of a spherical sound wave travelling out from the source. The black stripes are the result of a destructive interference between the incident wave and the indirect wave (received wave), while the white stripes are due to a constructive interference. In the shadow zone, the interference is not as simple as the zone near the source. It has an irregular interference pattern. The irregular area increases with increasing frequency. It is evident that the number of black and white stripes increases and the stripes become narrower as the frequency increases because the interference areas increase in number.

In the following series of pictures, Figures 5.29 through 5.32, the interference phase pattern is shown to be influenced by the source position and its interaction with the shell. Figure 29 shows the phase pattern in the absence of the shell. The speaker, driven with ka = 22.494 , is located at a distance 10" from the surface of the imaginary sphere. The scan range is 0.125" to 8.44". In viewing this result, the wave form is that of a spherical wave spreading outward. In the presence of the shell, the uniform wave form has

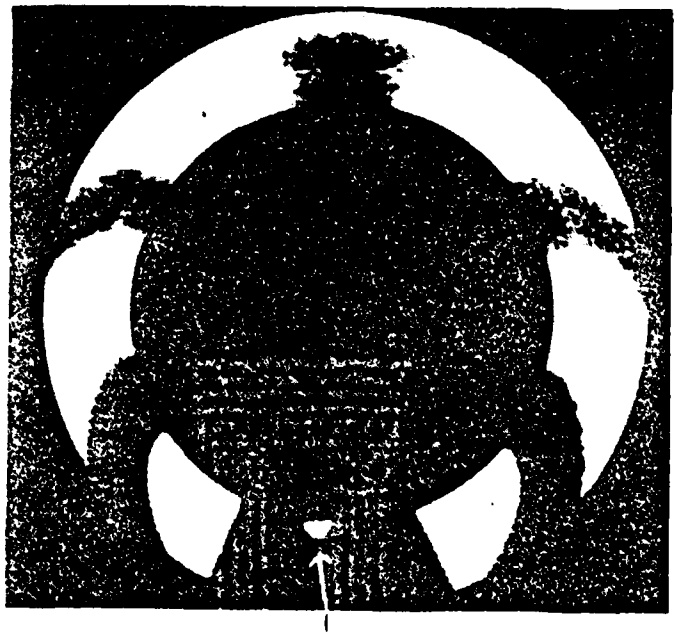

Figure 5.26 Measured phase pattern of a shell with thickness h = 0.1069" for ka = 6 in air

Figure 5.27 Measured phase pattern of a shell with thickness h = 0.1069" for ka = 10 in air

Figure 5.28 Measured phase pattern of a shell with thickness h = 0.1069" for ka = 14 in air

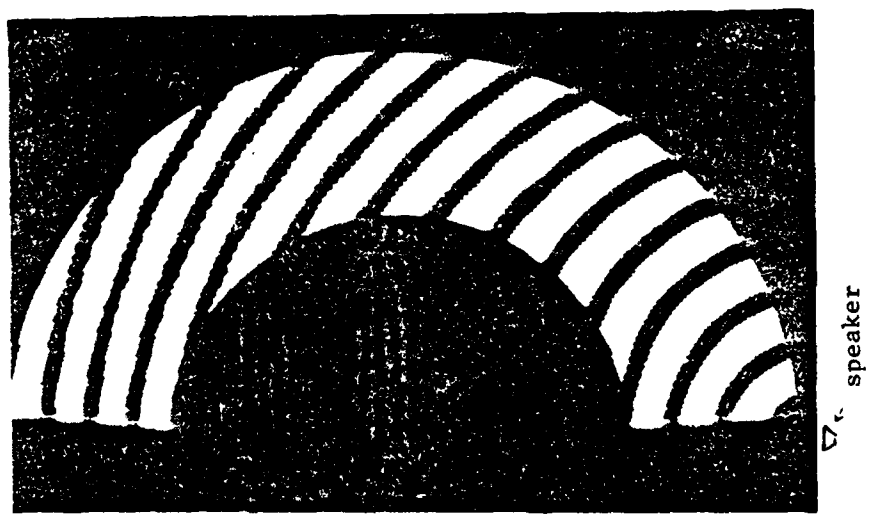

Figure 5.29 Measured phase pattern for a shell with thickness h = 0.1069" for ka = 18 in air

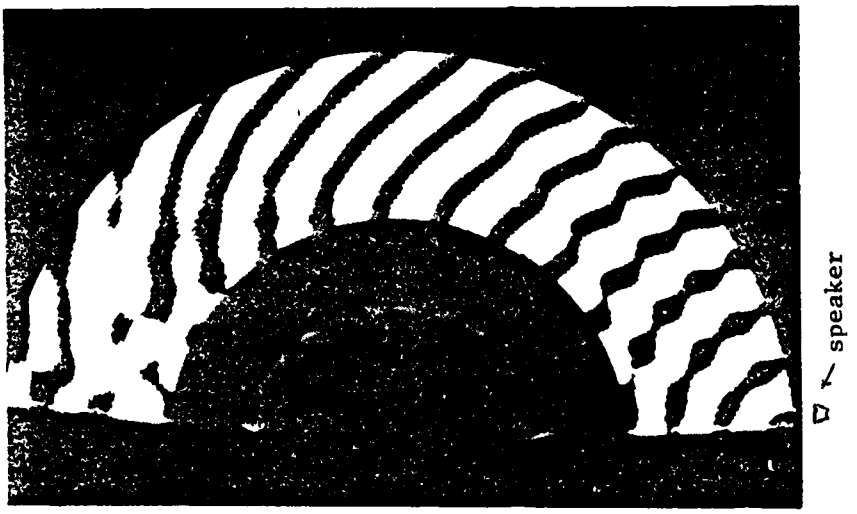

Figure 5.30 Measured phase pattern for a shell with thickness h = 0.1069" for ka = 22 in air

Figure 5.31 Measured phase pattern for a shell with thickness h = 0.1069" for ka = 26 in air

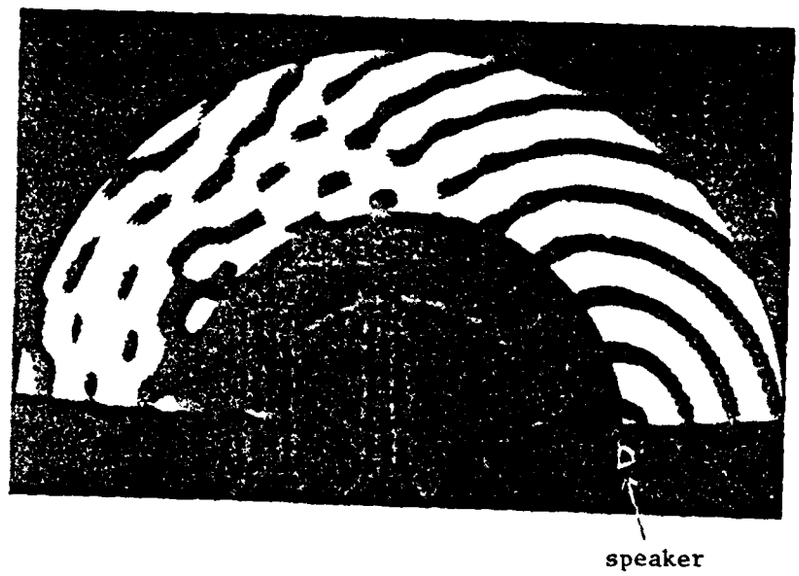

Figure 5.32 Measured phase pattern for a shell with thickness h = 0.1069" for ka = 30 in air

been disturbed due to the presence of the reflected and diffracted waves. In the zone near the source, the distortion of the wave form is low. As the observer point moves away from the source, distortion becomes obvious, especially in the area near the surface because the direct wave no longer reaches there and the diffracted wave dominates that area (shadow zone). Far away from the source in the shadow zone, the wave form of the near field becomes distorted because of strong interference. Figures 5.30, 5.31, and 5.32 show a series of phase patterns for the speaker located at varied distances ranging from 10" to 5/6" away from the shell excited at ka = 22.494 in air. The field in the illuminated zone resembles that of a point source in most of the pictures. However, the field in the shadow zone is primarily due to the weak diffracted (creeping) waves, so that the phase of the pressure is practically unchanged.

From the experimental results and analyses in this chapter, the use of the holographic scanner was shown to give a detailed directivity measurement as well as a sound visualization recording. The detailed measurement only provides a single recording, while the sound visualization technique (SVT) gives a completed image of the phase interference and the diffracted pressure intensity. Also, the SVT supplies information about the location and the driving frequency of the source. The disadvantage of the SVT is that it cannot provide a sufficient dynamic range for use in theoretical verification.

CHAPTER VI

SUMMARY AND CONCLUSIONS

6.1 Introduction

In this study, the vibrational response of submerged spherical shells and the radiated acoustic nearfield of these shells was investigated. An elastic spherical shell was excited to vibration by either a normal point force or an acoustic point source. The equations of motion of an elastic shell was derived by Hamilton's principle, with the excitation force field included in this derivation. The shell's theory used is that for a thin shell with only extensional and bending deformations included.

The solution for the vibrational response of a point excited spherical shell and the resulting acoustic nearfield was predicted by the summation of modal response. These solutions were verified by exciting two duralumin spherical shells to vibration in air and in water and recording the driving point admittance and the resonance frequencies.

In another part of the investigation, the nearfield of an elastic spherical shell due to an acoustic point source was predicted by the wave-harmonic series as well as by the Geometrical Theory of Diffraction (GTD). The nearfield acoustic perssure was measured in air by use of specially constructed apparatus which produced a visual representation of the acoustic field. Measurement of the nearfield in water was also made by use of a specially constructed holographic scanner. These measurements were used to verify the predicted directivity patterns.

6.2 Point Excited Spherical Shells

The vibrational response of point force excited spherical shells was predicted by use of modal summation. The mode shapes of vibration and the resonance frequencies of such shells were then compared to the measured ones. The resonance frequencies in air were measured for mode numbers up to 34 and found to be within 5% of the predicted ones. Since the deformation energy influences the resonance frequencies, this agreement indicates that a deformation theory which includes extensional and bending deformation is adequate for describing the shell's dynamic response. Thus, there is no need to further refine the deformation by including shear deformation and rotatory inertia.

For a point excited shell submerged in water, the resonance frequencies were computed by use of an iterative technique. The iteration starts with the known resonance frequencies of the shells in air. The resonance frequencies of the shells in water are lower than those in air because of the virtual mass of the water being displaced must be added to the mass of the shell. The resonance frequencies and mode shapes of the two shells were measured for mode numbers up to 34. Again, a good agreement was obtained, indicating that the model for the acoustic virtual mass of the water was adequate.

The mean value of the driving point admittance spectra of the vibrating shells in air were also computed exactly by the modal summation and also by Skudrzyk's Mean Value Theorem and found to agree very well. However, when these were compared with the measured mean values, they were found to be 3 dB lower than predicted. This can be attributed to the increase in the modal density by the extra split modes occurring in a spherical shell made of two hemispherical shells

welded at the equator. Such an increase in modal density usually predicts lower mean values, see Equation (2.58).

6.3 Acoustic Nearfield of a Point-Source Excited Spherical Shell

The acoustic nearfield pressure of a spherical shell excited by a point source was computed by use of wave harmonics. The acoustic nearfield includes the direct, the reflected, the diffracted, and most importantly, the radiated field. The weak diffracted waves are due to acoustic-borne waves travelling around the sphere. The radiated waves are due to the vibration of the shell, i.e., the structure-borne waves.

In the illuminated zone of a shell in air, the nearfield looks like that of rigid spheres, because the direct and reflected waves dominate the radiated waves. However, in the shadow zone, only diffracted and radiated waves exist and, hence, the nearfield is dominated by the radiated waves. These were confirmed when the two spherical shells were insonified by an acoustic loudspeaker and a microphone was used to detect the acoustic pressure levels in the neighborhood of the shells in air. The whole test system was located inside an anechoic chamber.

In the illuminated and shadow zones of a spherical shell submerged in water, the radiated waves dominate the other waves. Thus, the structure-borne waves were found to dominate the diffracted waves by as much as 80 dB at low frequencies, and 60 dB at the high frequencies in the shadow zone. The measurements of the nearfield of a spherical shell submerged in water was made in a large water tank. The measured directivity patterns agreed well with the predicted ones up to $ka = 30$.

The GTD method was used to compute the diffracted waves in the shadow zone. The spherical surface was given a real or complex locally reacting impedance. The diffracted rays (creeping waves) were found to be highly attenuated by the absorption of the surface. Thus, the GTD predicted levels which are much lower than those predicted by the exact solution which included radiated waves. Various surface impedances were used in these calculations, such as the characteristic impedance of the shell material, plate wave impedance, etc. The GTD predicted levels for the hardest impedance (ρc of duralumin) which were 60 dB lower than the exactly computed ones.

6.4 Conclusions

The study of the nearfield of spherical shells was carried out to investigate analytically the effect of fluid loading on the response of the shell and to verify these observations by conducting controlled tests in air and in water. Conclusions drawn from the analytical and experimental results include:

a. The vibrational response of the shell in air and water can be modeled by a thin shell theory that includes extensional and bending deformation only.

b. The modes of vibration in air and water are identical, the only difference between them is the resonance frequencies being lower in water than those in air.

c. If the acoustic loading is heavy, such as water, one cannot scale the in-air experiments to those in water.

d. The acoustic nearfield of an elastic structure resembles that of a rigid body in air. However, the nearfield pressure of a shell in water is dominated by the vibrational energy radiating into the nearfield.

e. The GTD method cannot be used to predict the nearfield of an elastic structure in water because the impedance used in the computations must be the exact vibrational impedance of the shell. Otherwise, any other model for the impedance of the shell would predict the weak creeping wave field only.

6.5 Suggested Future Research

There are still more questions that have not been answered in this study. These pertain to the general applicability of analytic methods for the prediction of the nearfield of insonified elastic structures. Specifically, the following areas need further investigations:

1. The modal response of the shell in the higher frequency range. Investigate the need for more exact theory of deformation.
2. The need to use the GTD method for general elastic structures requires further studies into the possibility of including structure-borne vibrational waves in theory.
3. The development of new scaling laws by use of special tests in air, since direct use of scaling from air to water is not feasible.

REFERENCES

1. Junger, M. C., "Sound Scattering by Thin Elastic Shells," J. Acoust. Soc. Amer. 24, 366-373 (1952).

2. Lamb, H., "On the Vibrations of Spherical Shells," Proc. London Math. Soc. 14, 50-56 (1882).

3. Baker, W. E., "Axisymmetric Modes of Vibration of Thin Spherical Shell," J. Acoust. Soc. Amer. 33, 1749-1758 (1961).

4. Kalnins, A., "Effects of Bending on Vibrations of Spherical Shells," J. Acoust. Soc. Amer. 36, 74-81 (1964).

5. Wilkinson, J. P., "Natural Frequencies of Closed Spherical Shells," J. Acoust. Soc. Amer. 38, 367-368 (1965).

6. Junger, M. C., "Vibrations of Elastic Shells in a Fluid Medium and the Associated Radiation of Sound," J. Appl. Mech. 19, 439-445 (1952).

7. Hayek, S., "Vibration of a Spherical Shell in an Acoustic Medium," J. Acoust. Soc. Amer. 40, 342-348 (1966).

8. Lauchle, G. C., "Interaction of a Spherical Acoustical Wave with an Elastic Spherical Shell," J. Sound Vib. 44, 37-46 (1976).

9. Novozhilov, V. V., Thin Shell Theory, P. Noordhoff Ltd., Groningen, The Netherland, 1964.

10. Goldenweizer, A. L., Theory of Elastic Thin Shells, Pergamon Press, Inc., New York, 1961.

11. Hayek, S., "Resonance Frequencies of Submerged Cylindrical Shells," ARL Internal Memorandum, File No. 405.3361-63, October 3, 1969, ARL, The Pennsylvania State University, University Park, PA.

12. Skudrzyk, E. J., Simple and Complex Vibratory System, The Pennsylvania State University Press, University Park, PA, 1968.

13. Levy, B. R. and Keller, J. B., "Diffraction by a Smooth Object," Comm. on Pure and Appl. Math. XII, 159-209 (1959).

14. Keller, J. B., "Diffraction by a Convex Cylinder," IRE Trans. 4, 312-321 (1956).

15. Keller, J. B., Lewis, R. M. and Seckler, B. D., "Asymptotic Solution of Some Diffraction Problems," Comm. on Pure and Appl. Math. IX, 207-265 (1956).

16. Washizu, K., Variational Methods in Elasticity and Plasticity, Pergamon Press, New York, 1968.

17. Fung, Y. C., Foundations of Solid Mechanics, Prentice-Hall, Inc., Englewood Cliffs, NJ, 1965.

18. Feit, D. and Junger, M. C., "High Frequency Response of an Elastic Spherical Shell," J. Appl. Mech. 36, 859-864 (1969).

19. Lazan, B. J., Damping of Material and Members in Structural Mechanics, Pergamon Press, New York, 1968.

20. Morse, P. M. and Feshback, H., Methods of Theoretical Physics, McGraw-Hill Book Co., Inc., New York, 1953.

21. Watson, G. N., "The Diffraction of Electric Waves by the Earth," Proc. Roy. Soc. London A 95, 83-99 (1919).

22. Bremmer, H., Terrestrial Radio Waves, Elsevier Pub. Co., New York, 1949.

23. Nussenzveig, H. M., "High Frequency Scattering by an Impenetrable Sphere," Annals of Physics 34, 23-95 (1965).

24. Franz, W., "Über die Greeschen Funktionen des Zylinders und der Kugel," Z. Naturforschung 99, 705-716 (1954).

25. Magnus, W. and Oberhettinger, F., Function of Mathematical Physics, Chelsea Pub. Co., New York, 1954.

26. Hayek, S. and Stuart, A., "Influence of an Elastic Plate Surface Impedance on Backscattered Sound," ARL Technical Memorandum, File No. TM 74-255, August 16, 1974, ARL, The Pennsylvania State University, University Park, PA.

27. Sacks, D. A., "Diffraction of High Frequency Sound Waves Over Curved Surfaces," Technical Report C-391-210 (1972), Cambridge Acoustical Assoc., Inc., Cambridge, MA.

28. Abramowitz, M. and Stagun, I. S., Handbook of Mathematical Functions, National Bureau of Standards, Washington, DC, 1970.

29. Lauchle, G. C. and Wong, E., "The ARL/FEU Semi-Anechoic Chamber," ARL Internal Memorandum, File No. 75-230 (1975), ARL, The Pennsylvania State University, University Park, PA.

30. Marboe, R. F. and Farwell, R. W., "Absorption and Reflection Characteristics of a Water-Filled Anechoic Tank," File No. TM 6.8830-01, July 15, 1959, Ordnance Research Laboratory, The Pennsylvania State University, University Park, PA.

31. Watson, E. E. and Rishell, J. H., "Acoustical Farfield Holography Scanner and Phase-Only Circuitry," ARL Internal Memorandum, File No. 73-226 (1973), ARL, The Pennsylvania State University, University Park, PA.

32. "Measuring Structural Transfer Functions in Real Time," Application Manual DSP-008 (7/76), Spectral Dynamics Corporation of San Diego.

33. "Krautkramer-Branson Ultrasonic Pulse-Echo Thickness Gauge," Technical Manual, Krautkramer-Branson, Inc., Stratford, CT, November 1975.

BIBLIOGRAPHY

1. Anderson, V. C., "Sound Scattering from a Fluid Sphere," J. Acoust. Soc. Amer. 22, 426-431 (1950).

2. Bolotin, V. V., "On the Density of the Distribution of Natural Frequencies of Thin Elastic Shells," Appl. Math. Mech. 27, 538-543 (1963).

3. Bowman, J. J., Senior, T. B. A. and Uslenghi, P. L. E., Electromagnetic and Acoustic Scattering by Simple Shapes, American Elsevier Publishing Co., New York, 24 (1969).

4. Chree, C., "Forced Vibrations in Isotropic Elastic Solid Spheres and Spherical Shell," Camb. Phil. Soc. Trans. 14 (1889).

5. DeSilva, C. N. and Tersteeg, G. E., "Axisymmetric Vibrations of Thin Elastic Shells," J. Acoust. Soc. Amer. 36, 4, 666-672 (April 1964).

6. Diercks, K. J., "Echoes from Hollow Aluminum Spheres in Water," J. Acoust. Soc. Amer. 41, 380-393 (1967).

7. Dragonette, L. R., Vogt, R. H., Flax, L. and Neubauer, W. G., "Acoustic Reflection from Elastic Spheres and Rigid Spheres and Spheroids. II. Transient Analysis," J. Acoust. Soc. Amer. 55, 1130-1137 (1974).

8. Feit, D. and Junger, M. C., "High Frequency Response of an Elastic Spherical Shell," J. Appl. Mech. 36, 4, 859-864 (December 1969).

9. Flax, L., "High ka Scattering of Elastic Cylinders and Spheres," J. Acoust. Soc. Amer. 62, 1502-1503 (1977).

10. Fock, V. S., "Diffraction of Radio Waves Around the Earth's Surface," J. Phys. USSR 9, 255-266 (1945).

11. Gontkevich, V. S., "Natural Vibrations of Spherical Shells," Issled. po Teorii Sooruzh. 13, 77-63 (1964). (In Russian) (English transl.: N66-16399, Lockheed Missiles and Space Co.)

12. Gontkevich, V. S., "Natural Vibrations of Shells in a Liquid." Published: Kiev, Naukova Dumka, 1964. (In Russian)

13. Hampton, L. D. and McKinney, C. M., "Experimental Study of the Scattering of Acoustic Energy from Solid Metal Spheres in Water," J. Acoust. Soc. Amer. 33, 664-673 (1961).

14. Hickling, R., "Analysis of Echoes from a Solid Elastic Sphere in Water," J. Acoust. Soc. Amer. 34, 1582-1592 (1962).

15. Hickling, R., "Analysis of Echoes from a Hollow Metallic Sphere in Water," J. Acoust. Soc. Amer. 36, 1124-1137 (1964).

16. Hickling, R. and Wang, N. M., "Scattering of Sound by a Rigid Movable Sphere," J. Acoust. Soc. Amer. 39, 276-279 (1966).

17. Hong, S., "Asymptotic Theory of Electromagnetic and Acoustic Diffraction by Smooth Convex Surface of Variable Curvature," J. Math. Phys. 8, 1223-1232 (1967).

18. Hunter, J. L., Layton, M. R. and Fisch, M. R., "Acoustic Backscattering from Thin Air-Filled Spherical Shells," J. Acoust. Soc. Amer. 62, 1139-1143 (1977).

19. Junger, M. C. and Feit, D., "High-Frequency Response of Point-Excited Submerged, Spherical Shells," J. Acoust. Soc. Amer. 45, 630-636 (March 1969).

20. Kalnins, A. and Kraus, H., "Effect of Transverse Shear and Rotary Inertia on Vibration of Spherical Shells," Proc. 5th U. S. Nat. Cong. Appl. Mech. (Minneapolis), 1966, p. 134.

21. Kay, I. and Keller, J. B., "Asymptotic Evaluation of the Field at a Caustic," J. Appl. Phys. 25, 876-883 (1954).

22. Keller, J. B., "Geometric Theory of Diffraction," J. Opt. Soc. Amer. 52, 116-130 (1962).

23. Keller, J. B. and Levy, B. R., "Decay Exponents and Diffraction Coefficients for Surface Waves on Surfaces of Nonconstant Curvature," IRE Trans. on Antennas and Propagation, AP-7, S52-S61 (1959).

24. Keller, J. B., Rubinow, S. I. and Goldstein, M., "Zeros of Hankel Functions and Poles of Scattering Amplitudes," J. Math. Phys. 4, 829-832 (1963).

25. Kock, E. W. and Harvey, F. K., "A Photographic Method for Displaying Sound Wave and Microwave Space Patterns," The Bell System Technical Journal, July 1951.

26. Kouyoumjian, R. G., "Asymptotic High-Frequency Methods," Proc. IEEE 53, 864-876 (1965).

27. Kraus, H. and Kalnins, A., "Transient Vibration of Thin Elastic Shells," J. Acoust. Soc. Amer. 38, 6, 994-1002 (December 1965).

28. McIvor, I. K. and Sonstegard, D. A., "The Axisymmetric Response of a Closed Spherical Shell to a Nearly Uniform Radial Impulse," J. Acoust. Soc. Amer. 40, 6, 1540-1547 (December 1966).

29. Mole, L. A., Hunter, J. L. and Davenport, J. M., "Scattering of Sound by Air Bubbles in Water," J. Acoust. Soc. Amer. 52, 837-842 (1972).

30. Naghdi, P. M. and Kalnins, A., "On Vibrations of Elastic Spherical Shells," J. Appl. Mech. 29, 1, 65-72 (March 1962).

31. Naghieh, M. and Hayek, S. I., "Vibration of Fluid-Filled Fiber-Reinforced Spherical Shells," J. Sound and Vib. 19, 153-166 (1971).

32. Naghieh, M. and Hayek, S. I., "Vibration of Fiber-Reinforced Spherical Shells," J. Sound and Vib. 4, 115-137 (1971).

33. Naghieh, M. and Hayek, S. I., "Transmission of Acoustic Waves Through Submerged Orthotropic Shells," J. Acoust. Soc. Amer. 50, 1334-1342 (1971).

34. Neubauer, W. G., Vogt, R. H. and Dragonette, L. R., "Acoustic Reflection from Elastic Sphere. I. Steady-State Signals," J. Acoust. Soc. Amer. 55, 1123-1129 (1974).

35. Nichols, C. S., Knittle, M. R., Barach, D. and Carlson, M., "A Finite Element Approach to Scattering from Elastic Spherical Shells," NUC TP425, September 1974, Naval Undersea Center, San Diego, California.

36. Pathak, P. H. and Kouyoumjian, R., "An Analysis of the Radiation from Apertures in Curves Surfaces by the Geometrical Theory of Diffraction," Proc. IEEE 62, 1438-1447 (1974).

37. Prasad, C., "On Vibrations of Spherical Shells," J. Acoust. Soc. Amer. 36, 3, 489-494 (March 1964).

38. Rayleigh, Lord, "On the Bending and Vibration of Thin Elastic Shells, Especially of Cylindrical Form," Phil. Trans. Roy. Soc. (London), 105-123 (December 1888).

39. Ross, E. W., Jr., "Membrane Frequencies for Spherical Shell Vibrations," AIAA J., 6, 5, 803-808 (May 1968).

40. Ross, E. W., Jr. and Matthews, W. T., "Frequencies and Mode Shapes for Axisymmetric Vibration of Shells," J. Appl. Mech. 34, 1, 73-80 (March 1967).

41. Seide, P., "Radial Vibrations of Spherical Shells," J. Appl. Mech. 37, 2, 528-530 (June 1970).

42. Shirley, D. J. and Diercks, K. J., "Analysis of the Frequency Response of Simple Geometric Targets," J. Acoust. Soc. Amer. 48, 1275-1282 (1970).

43. Silbiger, A., "Nonaxisymmetric Modes of Vibration of Thin Spherical Shells," J. Acoust. Soc. Amer. 34, 6, 862 (June 1962).

44. Sonstegard, D. A. "Effects of a Surrounding Fluid on the Free, Axisymmetric Vibrations of Thin Elastic Spherical Shells," J. Acoust. Soc. Amer. 45, 2, 506-510 (February 1969).

45. Streifer, W., "Creeping Wave Propagation Constants for Impedance Boundary Conditions," IEEE Trans. AP-12, 764-766 (1964).

46. Strutt, J. W. (Lord Rayleight), "Investigation of the Disturbance Produced by a Spherical Obstacle on the Waves of Sound," Proc. London Math. Soc. 4, 253-283 (1872).

47. Wilkinson, J. P., "Transient Response of Thin Elastic Shells," J. Acoust. Soc. Amer. 39, 5, Pt. 1, 895-898 (May 1966).

48. Wilkinson, J. P. and Kalnins, A., "On Nonsymmetric Dynamic Problems of Elastic Spherical Shells," J. Appl. Mech. 32, 3, 525-532 (September 1965).

49. Workman, G. and Hayek, S. I., "Transmission of Acoustic Waves Through Submerged Viscoelastic Spherical Shells," J. Acoust. Soc. Amer. 5, 1340-1349 (1969).

APPENDIX A

DERIVATION OF THE SHELL'S EQUATIONS OF MOTION

In order to obtain a spherical shell's equations of motion, Equations (2.9) and (2.10), the Hamilton's principle as shown in Equation (2.1) is employed. Let the function

$$F = T - \overline{V} + Q \quad , \tag{A.1}$$

where $F = F(u, u_\theta, \dot{u}, w, w_\theta, w_{\theta\theta}, \dot{w})$. The integral form of the Hamilton's equation can be expressed in a differential form as:

$$\frac{\partial F}{\partial q} - \frac{d}{d\theta}\frac{\partial F}{\partial q_\theta} + \frac{d^2}{d\theta^2}\left(\frac{\partial F}{\partial q_{\theta\theta}}\right) - \frac{d}{dt}\frac{\partial F}{\partial \dot{q}} = 0 \quad , \tag{A.2}$$

where q is a spatial coordinate. Consider a tangential or radial motion, the coordinate u or w replaces q , then:

$$\frac{\partial F}{\partial u} - \frac{d}{d\theta}\frac{\partial F}{\partial u_\theta} - \frac{d}{dt}\frac{\partial F}{\partial \dot{u}} = 0 \tag{A.3}$$

and

$$\frac{\partial F}{\partial w} - \frac{d}{d\theta}\frac{\partial F}{\partial w_\theta} + \frac{d^2}{d\theta^2}\left(\frac{\partial F}{\partial w_{\theta\theta}}\right) - \frac{d}{dt}\frac{\partial F}{\partial \dot{w}} = 0 \quad , \tag{A.4}$$

where $w_\theta = \frac{\partial w}{\partial \theta}$, $w_{\theta\theta} = \frac{\partial^2 w}{\partial \theta^2}$, $\dot{w} = \frac{\partial w}{\partial t}$, $\frac{\partial u}{\partial \theta} = u_\theta$, and $\dot{u} = \frac{\partial u}{\partial t}$.

In regard to the strain energy density, the total kinetic energy, and the potential function as shown in Equations (2.4), (2.7), and (2.8), respectively,

$$\frac{\partial F}{\partial u} = -\frac{\partial \bar{V}}{\partial u}$$

$$= -\frac{2\pi hE}{(1-\nu^2)} \int_o^\pi \left\{ \left[\cot^2\theta u - \cot\theta w - \nu\cot\theta w + \nu\cot\theta \frac{\partial u}{\partial \theta} \right] \right.$$

$$\left. + \beta\left[\cot^2\theta u + \cot^2\theta \frac{\partial w}{\partial \theta} + \nu\cot\theta \frac{\partial^2 w}{\partial \theta^2} + \nu\cot\theta \frac{\partial u}{\partial \theta}\right] \right\} \sin\theta d\theta \quad , \tag{A.5}$$

$$\frac{\partial F}{\partial u_\theta} = -\frac{\partial \bar{V}}{\partial u_\theta}$$

$$= -2\pi a^2 \int_o^\pi \frac{\partial \bar{V}}{\partial u_\theta} \sin\theta d\theta$$

$$= -2\pi a^2 \int_o^\pi \left\{ \frac{Eh}{2(1-\nu^2)} \left[\frac{2\varepsilon_\theta}{a} + \frac{2\nu\rho_\phi}{a}\right] + \frac{Eh^3}{24(1-\nu^2)} \right.$$

$$\left. \times \left[\frac{2K_\theta}{a^2} + \frac{2\nu K_\phi}{a^2}\right] \right\} \sin\theta d\theta \quad ,$$

then:

$$\frac{d}{d\theta}\frac{\partial F}{\partial u_\theta} = -\frac{2\pi Eh}{(1-\nu^2)} \int_o^\pi \left\{ \left[\frac{\partial^2 u}{\partial \theta^2} - \frac{\partial w}{\partial \theta}\right] + \left[\frac{\partial u}{\partial \theta} - w\right] \cot\theta \right.$$

$$+ \nu\left[\frac{\partial u}{\partial \theta}\cot\theta - w\cot\theta - u - \frac{\partial w}{\partial \theta}\right] + \beta\left[\left[\frac{\partial^3 w}{\partial \theta^3} + \frac{\partial^2 u}{\partial \theta^2}\right]\right.$$

$$\left. \left. + \left[\frac{\partial^2 w}{\partial \theta^2} + \frac{\partial u}{\partial \theta}\right]\cot\theta + \nu\left[\cot\theta \frac{\partial u}{\partial \theta} - u + \cot\theta \frac{\partial^2 w}{\partial \theta^2} - \frac{\partial w}{\partial \theta}\right]\right]\right\}$$

$$\times \sin\theta d\theta \quad , \tag{A.6}$$

$$\frac{\partial F}{\partial \dot{u}} = \frac{\partial T}{\partial \dot{u}} = 2\pi\rho_s ha^2 \int_o^\pi \dot{u} \sin\theta d\theta \quad ,$$

and then:

$$\frac{d}{dt}\left(\frac{\partial F}{\partial \dot{u}}\right) = 2\pi\rho_s ha^2 \int_o^\pi \frac{\partial^2 u}{\partial t^2} \sin\theta d\theta \quad . \tag{A.7}$$

Substituting Equations (A.5), (A.6), and (A.7) into Equation (A.3), one obtains:

$$(1 + \beta)\left[(\nu + \cot^2\theta)u - \cot\theta \frac{\partial u}{\partial \theta} - \frac{\partial^2 u}{\partial \theta^2}\right] + [\beta\cot^2\theta + (1 + \nu) + \beta\nu]\frac{\partial w}{\partial \theta}$$

$$- \beta\cot\theta \frac{\partial^2 w}{\partial \theta^2} - \beta \frac{\partial^3 w}{\partial \theta^3} + \frac{1 - \nu^2}{E} \rho_s a^2 \frac{\partial^2 u}{\partial t^2} = 0 \quad . \quad (A.8)$$

Similarly, differentiating the function F with respect to w, one obtains:

$$\frac{\partial F}{\partial w} = - \frac{\partial \bar{V}}{\partial w} + \frac{\partial Q}{\partial w}$$

$$= \frac{2\pi Eh}{(1 - \nu^2)} \int_o^\pi \left\{ \left(\frac{\partial u}{\partial \theta} + u\cot\theta - 2w\right)(1 + \nu)\right\} \sin\theta d\theta$$

$$- 2\pi a^2 \int_o^\pi (p_i + p_r) \sin\theta d\theta \quad , \quad (A.9)$$

$$\frac{\partial F}{\partial w_\theta} = - \frac{\partial \bar{V}}{\partial w_\theta}$$

$$= - 2\pi a^2 \int_o^\pi \frac{Eh^3}{24(1 - \nu^2)} \left[2K_\theta \frac{\partial K_\phi}{\partial w_\theta} + 2\nu K_\theta \frac{\partial K_\phi}{\partial w_\theta}\right] \sin\theta d\theta \quad ,$$

then:

$$\frac{d}{d\theta} \frac{\partial F}{\partial w_\theta} = - \frac{\pi a^2 Eh^3}{12(1 - \nu^2)} \int_o^\pi \left\{\left[2K_\phi \frac{\partial K_\phi}{\partial w_\theta} + 2\nu K_\theta \frac{\partial K_\phi}{\partial w_\theta}\right] \cos\theta \right.$$

$$\left. + \frac{d}{d\theta} \left[2K_\phi \frac{\partial K_\phi}{\partial w_\theta} + 2\nu K_\theta \frac{\partial K_\phi}{\partial w_\theta}\right] \sin\theta\right\} d\theta$$

$$= -\frac{2\pi Eh\beta}{(1-\nu^2)}\int_o^\pi \left\{\nu\cot\theta\,\frac{\partial^3 w}{\partial\theta^3} + (\cot^2\theta - \nu)\,\frac{\partial^2 w}{\partial\theta^2}\right.$$

$$- (2\cot\theta + \cot^3\theta)\,\frac{\partial w}{\partial\theta} + \nu\cot\theta\,\frac{\partial^2 u}{\partial\theta^2}$$

$$\left. + (\cot^2\theta - \nu)\,\frac{\partial u}{\partial\theta} - (2\cot\theta + \cot^3\theta)u\right\}\sin\theta d\theta \quad , \tag{A.10}$$

$$\frac{\partial F}{\partial w_{\theta\theta}} = -\frac{\partial \bar{V}}{\partial w_{\theta\theta}}$$

$$= -\frac{2\pi Eh\beta}{(1-\nu^2)}\int_o^\pi \left\{\left(\frac{\partial^2 w}{\partial\theta^2} + \frac{\partial u}{\partial\theta}\right) + \nu\cot\theta\left(u + \frac{\partial w}{\partial\theta}\right)\right\}\sin\theta d\theta \quad ,$$

then,

$$\frac{d^2}{d\theta^2}\left(\frac{\partial F}{\partial w_{\theta\theta}}\right) = -\frac{2\pi Eh\beta}{(1-\nu^2)}\int_o^\pi \left\{\frac{\partial^4 w}{\partial\theta^4} + (2+\nu)\,\frac{\partial^3 w}{\partial\theta^3} - (1+2\nu)\,\frac{\partial^2 w}{\partial\theta^2}\right.$$

$$- \nu\cot\theta\,\frac{\partial w}{\partial\theta} + \frac{\partial^3 u}{\partial\theta^3} + (2+\nu)\cot\theta\,\frac{\partial^2 u}{\partial\theta^2}$$

$$\left. - (1+2\nu)\,\frac{\partial u}{\partial\theta} - \nu\cot\theta u\right\}\sin\theta d\theta \quad , \tag{A.11}$$

and

$$\frac{\partial F}{\partial \dot{w}} = \frac{\partial T}{\partial \dot{w}} = 2\pi\rho_s h a^2\int_o^\pi \dot{w}\,\sin\theta d\theta \quad ,$$

then,

$$\frac{d}{dt}\left(\frac{\partial F}{\partial w}\right) = 2\pi\rho_s h a^2\int_o^\pi \frac{\partial^2 w}{\partial t^2}\,\sin\theta d\theta \quad . \tag{A.12}$$

Substituting Equations (A.9), (A.10), (A.11), and (A.12) into Equation (A.4), one obtains:

$$\beta \frac{\partial^3 u}{\partial \theta^3} + 2\beta\cot\theta \frac{\partial^2 u}{\partial \theta^2} - [(1 + \nu)(1 + \beta) + \beta\cot^2\theta] \frac{\partial u}{\partial \theta}$$

$$+ [\beta\cot^3\theta + 3\beta\cot\theta - (1 + \beta)(1 + \nu)\cot\theta]u$$

$$+ \beta\left\{\frac{\partial^4 w}{\partial \theta^4} + 2\cot\theta \frac{\partial^3 w}{\partial \theta^3} - (1 + \nu + \cot^2\theta) \frac{\partial^2 w}{\partial \theta^2}\right.$$

$$\left. + (2\cot\theta + \cot^3\theta - \nu\cot\theta) \frac{\partial w}{\partial \theta}\right\} + 2(1 + \nu)w$$

$$+ \frac{1 - \nu^2}{E} \rho_s a^2 \frac{\partial^2 w}{\partial t^2} + \frac{1 - \nu^2}{Eh} a^2(p_i + p_r) = 0 \quad , \quad (A.13)$$

where $\beta = (h/a)^2/12$.

APPENDIX B

DERIVATION OF THE DIFFRACTION FACTOR

The derivation of the term $\Omega h_{s_n}^{(2)}(ka) \,/\, \frac{\partial}{\partial s}\left[\Omega h_s^{(1)}(ka)\right]_{s=s_n}$ and the boundary condition of an impedance shell is outlined in this appendix.

The boundary condition of the spherical shell is presented in Equation (4.9) as:

$$\frac{h_{s_n}^{(1)}(ka)}{h_{s_n}^{(1)'}(ka)} = iZ_a \quad . \tag{B.1}$$

By making use of the properties:

$$h_n^{(1)}(x) = \sqrt{\frac{\pi}{2x}}\, H_{n+1/2}^{(1)}(x)$$

and

$$h_n^{(1)'}(x) = \sqrt{\frac{\pi}{2x}}\left[H_{n+1/2}^{(1)'}(x) - \frac{1}{2x} H_{n+1/2}^{(1)}(x)\right]$$

$$\approx \sqrt{\frac{\pi}{2x}}\, H_{n+1/2}^{(1)'}(x) \quad , \quad x >> 1 \, , \tag{B.2}$$

Equation (B.1) can be expressed in terms of the cylindrical Hankel function as:

$$\frac{H_{s_n}^{(1)}(ka)}{H_{s_n}^{(1)'}(ka)} = iZ_a \quad , \tag{B.3}$$

where $s_n = \mu_n - 1/2$. Furthermore, the cylindrical Hankel function can be presented in terms of the Airy function [24, 25, 28] as $x \approx n$ for large x:

$$H_n^{(1)}(x) \sim \frac{2}{\pi} e^{-i\pi/3} \left(\frac{6}{x}\right)^{1/3} A(q_n) \quad , \tag{B.4}$$

where $A(q_n)$ is the Airy function,

$$A(q) = \int_o^\infty \cos(t^3 - q_t)dt \tag{B.5}$$

and

$$q = \left(\frac{6}{x}\right)^{1/3} e^{-i\pi/3} (n - x) \quad . \tag{B.6}$$

For the poles of the Hankel function in Equation (B.3):

$$s_n = ka + q_n \left(\frac{ka}{6}\right)^{1/3} e^{i\pi/3} \quad . \tag{B.7}$$

The derivative of the Hankel function with respect to the argument is obtained by taking a differentiation of $H_n^{(1)}(x)$ in Equation (B.4):

$$H_n^{(1)'}(x) \approx \frac{2}{\pi} \left(\frac{6}{x}\right)^{1/3} e^{-i\pi/3} [A'(q)q' - \frac{1}{3x} A(q)]$$

and

$$q' \approx - e^{-i\pi/3} \left(\frac{6}{x}\right)^{1/3} [1 + \frac{1}{3}\left(\frac{1}{x}\right)(n - x)]$$

$$\approx - e^{-i\pi/3} \left(\frac{6}{x}\right)$$

For large x, and $n \sim x$,

$$H_n^{(1)'}(x) \sim \frac{2}{\pi}\left(\frac{6}{x}\right)^{2/3} e^{-i2\pi/3} A'(q) \quad . \tag{B.8}$$

Substituting Equations (B.5) and (B.8) into Equation (B.3), one obtains the boundary condition in the form of the Airy function:

$$\frac{A'(q_n)}{A(q_n)} = e^{i5\pi/6} \left(\frac{ka}{6}\right)^{1/3} Z_a^{-1} \quad . \tag{B.9}$$

For large x, $s_n \sim \mu_n$, where $\mu_n = s_n + 1/2$, and by using the relationship in Equation (B.2), one can reduce

$$\frac{\Omega h_{s_n}^{(2)}(x)}{\frac{\partial}{\partial s}\left[\Omega h_{s_n}^{(1)}(x)\right]_{s=s_n}} \sim \frac{\Omega H_{\mu_n}^{(2)}(x)}{\frac{\partial}{\partial \mu}\left[\Omega H_{\mu}^{(1)}\right]_{\mu=\mu_n}} \quad , \tag{B.10}$$

where $\Omega h_{s_n}(x) = h_{s_n}(x) - iZa\, h'_{s_n}(x)$. Taking a differentiation of Equations (B.4) and (B.8) with respect to the order of n , one has:

$$\frac{\partial}{\partial n} H_n^{(1)}(x) \approx \frac{2}{\pi} e^{-i2\pi/3} \left(\frac{6}{x}\right)^{2/3} A'(q) \tag{B.11}$$

and

$$\frac{\partial}{\partial n} H_n^{(1)'}(x) \approx \frac{2}{\pi} \left(\frac{6}{x}\right) A''(q)$$

$$= -\frac{4q}{\pi x} A(q) \quad , \tag{B.12}$$

where $A''(q) = -q/3A(q)$. Using the relationship in Equations (B.4), (B.8), (B.11), (B.12), and

$$H_{s_n}^{(1)}(x)\, H_{s_n}^{(2)'}(x) - H_{s_n}^{(1)'}(x) H_{s_n}^{(2)}(x) = \frac{4}{i\pi ka} \quad ,$$

Equation (B.10) can, therefore, be reduced in terms of the Airy functions:

$$\frac{\Omega H_{s_n}^{(2)}(ka)}{\frac{\partial}{\partial s}\left[\Omega H_s^{(1)}(ka)\right]_{s=s_n}} = \frac{\pi e^{i5\pi/6}}{6} \left(\frac{ka}{6}\right)^{1/3} \left[\left\{A'(q_n)\right\}^2 + \frac{q_n}{3} A^2(q_n)\right]^{-1} . \tag{B.13}$$

DISTRIBUTION

Commander (NSEA 09G32)
Naval Sea Systems Command
Department of the Navy
Washington, DC 20362 — Copies 1 and 2

Commander (NSEA 0342)
Naval Sea Systems Command
Department of the Navy
Washington, DC 20362 — Copies 3 and 4

Defense Technical Information Center
5010 Duke Street
Cameron Station
Alexandria, VA 22314 — Copies 5 through 16

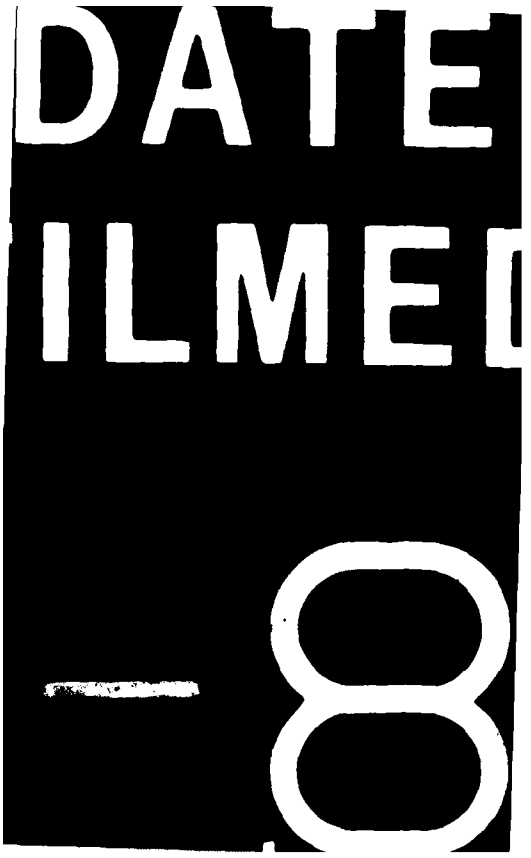
DATE
ILME
8